

University of Strathclyde  
Department of Pure and Applied Chemistry

Extending the scope of mid-infrared spectrometry  
for *in situ* process analysis through ATR  
immersion probes

Allyson Christine McIntyre

A thesis submitted to the Department of Pure and Applied  
Chemistry, University of Strathclyde, Glasgow, in part  
fulfilment of the regulations for the degree of Doctor of  
Philosophy

December 2011

## **Copyright**

This thesis is the result of the author's original research. It has been composed by the author and has not been previously submitted for examination which has led to the award of a degree.

The copyright of this thesis belongs to the author under the terms of the United Kingdom Copyright Acts as qualified by University of Strathclyde Regulation 3.50. Due acknowledgement must always be made of the use of any material contained in, or derived from, this thesis.

Signed:

Date:

To my family, *per asepera ad astra!*

## **Acknowledgements**

Firstly, I would like to thank my supervisor Professor David Littlejohn for his expertise, advice and all of his encouragement. I would also like to show my appreciation to Dr. Alison Nordon for her continuous help with the chemometric analysis and use of the Matlab software and associated toolboxes, not to mention those fantastic scripts. I will always be grateful to you both for the generous help and support you have given to me throughout my studies.

I would like to acknowledge Gary Colquhoun and members of Fibre Photonics for their help with all aspects of the ATR probes. I would also like to extend my thanks to the members of the CPACT consortium for taking the time to listen to my research presentations and giving me advice and suggestions to fulfill some of my research goals. Zengping Chen, I am grateful for you always answering my questions on calibration transfer algorithms and improvements to the SST algorithm.

Thank you to Megan Holden for the work completed on your summer placement, your samples that I also used for my calibration transfer work and acquiring the data on the FTLA series instrument; this work was invaluable to my studies. In addition I would also like to thank Madeleine Bilyk, a final year project student involved with the whisky analysis work. Furthermore, I would like to thank Mariana Fazenda for all her help completing the fermentation process and reference assays.

This research has been made possible through the SPIRIT scheme created by ScotCHEM and Chemical Sciences Scotland with joint funding from the Scottish Funding Council, WestChem and Fibre Photonics.

Finally, I would like to give special thanks to colleagues, friends and family who have been there through it all, good and bad. Pamela Allan, thank you for listening, you really did help me stay on track. To my boyfriend (David), you are a star for putting up with me throughout.

## Abstract

This study concerned developments and applications of attenuated total reflection (ATR) mid-infrared (MIR) insertion probes featuring novel polycrystalline silver halide fibres. Improvements in probe performance from the original design to the newer designs were observed; although some changes provided manufacturing benefits rather than performance improvements. Detailed evaluation of two 12 mm diameter probes and a 2.7 mm diameter single fibre probe was performed for analysis of mixtures of acetone, ethanol and ethyl acetate. Calibration transfer was attempted for situations when either the ATR probe or MIR spectrometer were changed. Direct transfer introduced severe calibration errors, so two standard calibration methods, direct standardisation (DS) and piecewise direct standardisation (PDS), and a new method spectral space standardisation (SST), were compared. The SST procedure incorporating a scaling factor demonstrated advantages over DS and PDS giving lower errors of prediction and simpler implementation over PDS. Two other application areas were also investigated: identification of counterfeit Scotch whisky and study of a fermentation reaction. The identification of counterfeit Scotch whiskies was based on the determination of ethanol concentration and the spectra of the dried residues of the suspect samples. The latter measurement also proved successful as a procedure to gain a greater understanding of the impact of manufacturing variables on the generation of the colour of whisky. Near-infrared (NIR) and MIR spectrometry were used to study a fermentation reaction; selected spectral regions of the NIR or MIR data can be used to monitor three properties of the fermentation process: optical density, glycerol and ammonium concentrations. PLS models built with NIR data produced better results than those using MIR data for the prediction of optical density and ammonium. However, the results for the predictions of glycerol were comparable; indications of the potential benefits of data fusion were apparent when the MIR and NIR data were combined.

# Contents

<b>Copyright</b> .....	i
<b>Dedication</b> .....	ii
<b>Acknowledgements</b> .....	iii
<b>Abstract</b> .....	iv
<b>Contents</b> .....	v
<b>1 INTRODUCTION</b> .....	1
1.1 An overview of process analysis .....	1
1.2 Sampling and analytical approaches in process analysis .....	5
1.3 Collaboration with Fibre Photonics and scope of thesis .....	8
1.4 References .....	10
<b>2 BACKGROUND AND THEORY</b> .....	12
2.1 Principles of infrared spectrometry .....	12
2.2 Optical fibres for use in infrared spectrometry .....	16
2.3 Probe designs in infrared spectrometry .....	21
2.4 Overview of chemometrics and multivariate regression .....	25
2.4.1 <i>Principal component analysis (PCA)</i> .....	25
2.4.2 <i>Partial Least Squares (PLS) regression</i> .....	26
2.4.3 <i>Design of Experiment manager software (DoEman)</i> .....	27
2.5 References .....	30
<b>3 USE OF MIR AND NIR SPECTROMETRY FOR PROCESS ANALYSIS</b> ...	32
3.1 Introduction .....	32
3.2 An assessment of the applications of infrared spectrometry .....	35
3.3 Conclusions .....	47
3.4 References .....	50
<b>4 ATR MIR PROBE DEVELOPMENT</b> .....	55
4.1 Introduction .....	55
4.1.1 <i>ATR MIR probes for in situ analysis</i> .....	55
4.1.2 <i>Design features</i> .....	57
4.1.2.1 Fibre selection .....	58

4.1.2.2	Seals .....	58
4.1.2.3	Geometry and size of crystal .....	59
4.1.2.4	Alignment .....	62
4.1.2.5	Use of modular components for manufacture .....	64
4.1.2.6	Mono fibre design.....	64
4.1.3	<i>Basis of this study</i> .....	65
4.2	Experimental.....	66
4.2.1	<i>Samples</i> .....	66
4.2.2	<i>MIR spectrometry</i> .....	67
4.2.3	<i>Probes assessed</i> .....	68
4.2.4	<i>Methods of analysis</i> .....	69
4.2.4.1	Probe performance.....	69
4.2.4.2	Pathlength determination .....	69
4.2.5	<i>Data analysis</i> .....	71
4.3	Results .....	73
4.3.1	<i>Probe performance</i> .....	73
4.3.1.1	Spectral interpretation.....	73
4.3.1.2	Predictions of concentrations of acetone, ethanol and ethyl acetate in ternary mixtures .....	82
4.3.2	<i>Pathlength investigation</i> .....	85
4.4	Conclusions .....	95
4.5	References .....	98
<b>5</b>	<b>CALIBRATION MODELS FOR ANALYTE PREDICTION</b> .....	<b>99</b>
5.1	Introduction .....	99
5.1.1	<i>The use of calibration models</i> .....	99
5.1.2	<i>Calibration transfer methods in infrared spectrometry</i> .....	100
5.1.3	<i>Basis of this study</i> .....	113
5.2	Experimental.....	114
5.2.1	<i>Solvent mixture sample preparation</i> .....	114
5.2.2	<i>MIR spectrometry</i> .....	115
5.2.3	<i>Data analysis</i> .....	116
5.2.4	<i>Calibration transfer algorithms</i> .....	117

5.3	Results .....	121
5.3.1	<i>Analysis of solvent mixtures</i> .....	121
5.3.1.1	Determination of trends in data .....	121
5.3.1.2	Calibration model optimisation using DoEman software.....	128
5.3.2	<i>Comparison of calibration transfer algorithms</i> .....	138
5.3.2.1	Multiplexing of two probes – transfer of calibration model.....	138
5.3.2.2	Transfer of all multivariate calibration models with all calibration samples .	143
5.3.3	<i>Investigation using a subset of calibration samples</i> .....	153
5.3.3.1	Improvement to SST algorithm .....	153
5.3.3.2	Leverage – sample selection.....	157
5.3.3.3	Process scale-up – calibration transfer example .....	157
5.4	Conclusions .....	165
5.5	References .....	166
<b>6</b>	<b>WHISKY ANALYSIS</b> .....	<b>170</b>
6.1	Introduction .....	170
6.1.1	<i>Scotch whisky</i> .....	170
6.1.2	<i>Manufacturing of Scotch whisky</i> .....	171
6.1.3	<i>Counterfeiting of Scotch whisky</i> .....	175
6.1.4	<i>Identification of counterfeit whisky</i> .....	176
6.1.4.1	Ethanol determination.....	177
6.1.4.2	Congener determination.....	178
6.1.4.3	Colorant analysis .....	178
6.1.4.4	Miscellaneous methods of counterfeit identification.....	180
6.1.5	<i>Basis of this study</i> .....	181
6.2	Experimental.....	183
6.2.1	<i>Samples</i> .....	183
6.2.1.1	Blend authenticity .....	183
6.2.1.2	Cask investigation.....	183
6.2.2	<i>Mid-infrared spectrometry</i> .....	185
6.2.3	<i>Methods of analysis</i> .....	186
6.2.3.1	Ethanol content determination.....	186
6.2.3.2	Colorant determination .....	187

6.2.4	<i>Data analysis</i> .....	187
6.2.4.1	Blend authenticity.....	188
6.2.4.2	Cask investigation.....	187
6.3	Results .....	190
6.3.1	<i>Blend authenticity</i> .....	190
6.3.1.1	Determination of ethanol concentration .....	190
6.3.1.2	Analysis of dried residues.....	193
6.3.1.3	Identification of counterfeit whisky.....	196
6.3.2	<i>Cask analysis investigation</i> .....	199
6.4	Conclusions .....	239
6.5	References .....	243
<b>7</b>	<b>MIR AND NIR SPECTROMETRY FOR FERMENTATION ANALYSIS..</b>	<b>245</b>
7.1	Introduction .....	245
7.1.1	<i>Monitoring fermentation processes</i> .....	245
7.1.2	<i>Use of combined data</i> .....	250
7.1.3	<i>Basis of this study</i> .....	251
7.2	Experimental.....	253
7.2.1	<i>Samples</i> .....	253
7.2.2	<i>NIR spectrometry</i> .....	254
7.2.3	<i>MIR spectrometry</i> .....	255
7.2.4	<i>Data analysis</i> .....	255
7.3	Results .....	256
7.3.1	<i>Optical density prediction</i> .....	257
7.3.2	<i>Glycerol concentration prediction</i> .....	262
7.3.3	<i>Ammonium ion concentration prediction</i> .....	270
7.3.4	<i>Combination of MIR and NIR data for the prediction of glycerol</i> .....	275
7.4	Conclusions .....	281
7.5	References .....	284
<b>8</b>	<b>CONCLUSIONS AND SUGGESTIONS FOR FUTURE WORK.....</b>	<b>287</b>
8.1	Conclusions .....	287
8.2	Suggestions for future work .....	290

<b>Publications and external presentations .....</b>	<b>292</b>
<b>Appendices .....</b>	<b>294</b>

# 1 Introduction

## 1.1 An overview of process analysis

The control of manufacturing processes in industry has become increasingly important in recent times. The product quality depends on two main aspects; raw material properties and the manufacturing process. The chemical industry is dependent on the development of analytical techniques that are capable of providing a route to cost-effective and consistent manufacture that will result in a higher quality product. The major challenge in controlling consistent manufacturing of batches is being able to identify the origin of any variations in the raw material, or process, and being able to take the necessary corrective action as early as possible.<sup>1-5</sup>

Process analytical chemistry (PAC) can be described as the application of analytical skills and instrumentation to monitor and control manufacturing processes.<sup>6, 7</sup> Initial work in PAC involved sampling the processes and transporting these samples to a central laboratory which could have safety implications and cause time delays. However, the ideal situation would be real-time *in situ* measurements with the ability of closed loop control and optimisation.<sup>8, 9</sup> Utilising chemometric techniques, the relationship between measured values and the real properties could be modelled for control and optimisation. Process analytical technology (PAT) is a more recent term that is widely adopted in the pharmaceutical industry and is promoted by the Food and Drug Administration (FDA) as “A system for designing, analysing and controlling manufacturing through timely measurements of critical quality and performance attributes of raw and in-process materials and processes with the goal of ensuring final product quality”.<sup>10</sup> PAT is fast becoming a key way to monitor and control the manufacturing process in the pharmaceutical industry where the specifications on drug manufacture are becoming tighter for final drug products. It allows the rapid detection of potential problems preventing the loss of time, money and precious feedstock during manufacture.

There are many instrumental techniques used in process analytical systems, but spectroscopic methods are prevalent in many industries. Optical spectroscopic

techniques currently used in process analysis are mid-infrared (MIR), near-infrared (NIR), and ultra violet-visible (UV-visible) absorption spectrometries and Raman scattering spectrometry, each with their advantages and disadvantages for use in process analytical systems.

The spectroscopic technique that will be used in a process analytical system is chosen ultimately because of the properties of the process to be monitored. The technique used will be the one that can give the most useful, reliable and reproducible data whilst encountering the least amount of problems for that specific process, at best cost. For example, if the process has a significant aqueous content, NIR spectrometry would not be as suitable as some of the signals may be obscured; although water can affect MIR spectra. The nature of the spectra and the opportunity to use e.g. ATR probes means that MIR spectrometry is less affected by the presence of significant amounts of water.

NIR spectrometry is already acknowledged as an established technique for process analysis and, with increasing efforts being made to turn MIR spectrometry into a reliable process instrument, a wide range of applications can be monitored by at least one, if not both, of these techniques.

The chemical industry is increasingly considering process analytical applications of at-, on- and in-line spectroscopic techniques to monitor chemical processes. These allow for the careful monitoring of parts of the process or in some cases, the whole process. Spectroscopic absorption techniques such as NIR and MIR are being used more often as they can be coupled to fibre optics. This allows e.g. a reaction to be monitored in real time quickly and easily. Additionally, the instrument can be isolated to minimise vibrational and electrical interferences from the process environment. Due to the ease and speed of spectroscopic measurements, these are viewed as a more efficient choice over traditional chromatographic techniques for process analysis, although the calibration models required are more complex. Being able to monitor chemical processes in real time with the use of spectroscopic

techniques allows the chemistry of the process to be monitored and understood, which can be of great benefit during process optimisation.<sup>1-5</sup>

The objective of PAC is to generate reliable and timely quantitative and qualitative information about the process. This information can provide benefits in raw material analyses, in-process testing, monitoring of process streams, control of crystallisation processes, validation of vessel cleaning, as well as for process control and optimisation of drying and blending processes and product quality. With the use of spectroscopic techniques, industry can have a greater understanding of the chemical processes and can locate potential problems easier. PAC is applicable to and widely used in many fields, including, but not limited to the petrochemicals, food and pharmaceutical industries, as the following examples illustrate. NIR and MIR spectrometry have been successfully used for the monitoring and control of various processes in the food industry,<sup>11</sup> including wine and cheese analysis.<sup>12-14</sup> Karoui *et al.* completed a feasibility study on the use of NIR and MIR spectra to determine different properties of soft cheeses such as fat content and pH.<sup>12</sup> Both techniques were used successfully to analyse some of the properties of the soft cheese samples, however, more samples would be required to improve the accuracy of the methods for process control. The application of MIR spectrometry in wine analysis was investigated by Patz *et al.*<sup>14</sup> MIR spectrometry was used to analyse several properties of the wine samples with short analysis times, generating good information about the quality of sample. With the exception of degassing of sparkling samples, the method required no preparation for the samples and provided reproducible results. PAC is also well established in the pharmaceuticals industry, known as PAT, and is used to help keep drug products within specification throughout the manufacture.<sup>15, 16</sup> Spectroscopy has been used by the petrochemicals industry for process control including examples of NIR for monitoring and characterisation of crude petroleum.<sup>17</sup> Falla *et al.*<sup>17</sup> proposed a method to estimate from NIR spectra the properties of crude petroleum with simulated distillation. The simulated distillation approach has an advantage in speed of analysis over traditional true boiling point determination for the control and characterisation of the crude product; also, it requires no sample preparation before analysis. Applications of MIR spectrometry are also being

considered; Andrade *et al.*<sup>18</sup> used MIR spectroscopy to analyse the total aromaticity to characterise the weathering process of oil spillages.

Due to the increase in implementation of PAC, it is vital that in-process instrumentation is robust, reliable and can withstand a variety of extreme process conditions, as well as still maintaining the ability to produce fast, reproducible and reliable data. This will allow the stages in the process to proceed more efficiently, while maintaining confidence in the results obtained.

## 1.2 Sampling and analytical approaches in process analysis

There are many approaches to sampling and monitoring of a chemical process and these can be split into six main categories.<sup>7-9, 19-24</sup> Some sampling approaches appear better than others for the use of process control in manufacturing, but each have advantages and disadvantages:

Off-line analysis – involves the manual collection of a sample from the process stream. The sample is then transported to a remote or centralised laboratory for analysis. Typical examples of this type of analysis include gas chromatography - mass spectrometry (GC-MS) and high performance liquid chromatography (HPLC). This is often a laborious and time consuming type of analysis. However, it can allow for complex sample preparation to be carried out if required and can have economic benefits from the use of shared facilities.

At-line analysis – also involves the manual collection of a sample from the process stream, however, the sample is then transported to a dedicated instrument usually located in the manufacturing area. Typical examples here are gas chromatography (GC) and visible spectrometry. Having a dedicated system nearby allows for quicker analysis to be carried out, but often requires simpler sample preparations as the operators are not usually skilled analysts. As the instrument is dedicated to the manufacturing area it has to be robust and reliable. This is a faster method than off-line analysis, although it is not as flexible in the use of instrumentation.

On-line analysis – involves automated sampling techniques where the sample is collected by an automated system and transported through a sample line to the automated analyser. A typical example of this type of analysis is on-line GC. Again as the analyser is near the process line, it has to be robust and reliable. The signal can be intermittent or continuous depending on the analyser process or if there is a requirement for any sample preparation; although this is not normally completed for on-line analysis. On-line analysis can give fast turnaround times, but the infrastructure for sampling and sample transfer can be very expensive.

Process analytical systems can be very useful in the chemicals and chemistry-using industries, but they are not without their problems. It has been noted that about 90% of process analyser failures are ultimately attributable to problems with the sampling system.<sup>19</sup> Sampling is the most critical stage in the analysis of the process; a poorly collected sample will lead to poor quality in the results obtained, and it may lead to the wrong decision being made about a specific operation. It is vital that any sample taken is representative of the bulk to ensure that the information derived is appropriate for decisions that are to be made about the status of the process.

In-line analysis – involves an analyser located close enough to the process to allow the use of an *in situ* probe to take measurements of the processes. As the probe is *in situ* no sample collection is required with this type of analysis, also there is no need for a separate sampling line, making this a faster and potentially less expensive type of analysis over on-line. Typical examples of in-line analysis are NIR and MIR spectrometry. The in-line analyser has to be very robust and reliable as it sits near to the manufacturing process. A known disadvantage of in-line analysis is fouling of the probe, which can affect the results obtained.

Non-invasive analysis – can be viewed as the ideal situation in process analysis as it requires no sample collection and there is no requirement for probe insertion to the process being monitored, avoiding possible contamination problems. The aim of this type of analysis is to take non-contact measurements; therefore, there is no physical contact with the sample, although there may be contact with the vessel/reactor containing the sample. An example of this type of analysis is the use of a NIR spectrometer that can be operated through a sight glass in the manufacturing equipment. A disadvantage of non-invasive analysis such as NIR spectrometry is that the sight glass window may become fouled.

Inferential analysis – the analysis can be inferred through measurements such as temperature, flow rate and viscosity, or spectral measurements if they are affected by the parameter for which information is required, e.g. monitoring the viscosity of a

process, if the viscosity of the liquid increases this indicates there is a greater number of higher boiling components present in the sample.

Every process analysis system needs to be designed in a way that will allow the most meaningful results to be obtained in the most efficient way. During the design process both the advantages and the disadvantages of the different types of analysis must be considered along with some other important points.<sup>25</sup>

The reactor type: is it going to be a batch or continuous process?

The scale of the operation.

The sampling required: how and where will the samples be measured and how frequent will the measurements be taken?

The design of the analyser: the analyser has to be right for the process and ensure it produces results which are meaningful and reproducible.

Any calibration requirements.

Data interpretation: what information will be required and how long will it take?

Diagnostics, e.g. fault indications and analysis.

Use of data: will there be a feedback loop to control the process?

All of the above points are important in the design and must be considered in the development of each process analytical system, in order to optimise the conditions and obtain the best results. For example, if you compare the sampling points needed for a batch or a continuous process, a batch process will require one or two sampling points, whereas a continuous process may require numerous sampling points and at different times. This shows that PAC is a useful way to achieve process control. However, it requires a great deal of time and cost to design and implement. Consequently, in-process measurement systems are used for process control only if it can be shown that the information gained and the benefits derived will outweigh the cost of design and implementation. PAC can help to understand the process more thoroughly allowing for more efficient step changes in process manufacture, as well as allowing the earlier detection of potential manufacturing problems. This can aid in time saving by achieving more efficient processes with less wastage.

### 1.3 Collaboration with Fibre Photonics and scope of thesis

The research described in this thesis was funded under the Scottish Funding Council's SPIRIT scheme. The SPIRIT scheme promotes collaboration between a university group and a small to medium enterprise (SME) in Scotland, with the specific target of underpinning the research of that SME. Fibre Photonics, an SME based in Livingston, Scotland, manufacture and supply fibre optic probe technology and have developed MIR transmitting materials such as polycrystalline silver halide for fibre-optic immersion probes. Whereas spectroscopic techniques that use silica based fibres are commonly used for *in situ* process measurements, there have been fewer applications of MIR spectrometry, owing to problems in finding suitably robust fibres that transmit in this region. However, the advent of robust silver halide fibres for use with attenuated total reflection (ATR) probes has opened up new opportunities for *in situ* and rapid analysis by MIR spectrometry. To determine specific application areas where MIR immersion probes could be useful for process control, an assessment of the literature was carried out. The assessment reviewed the use of in-line MIR and NIR spectrometry in different application areas to determine where in-line probes could be beneficial for analysis and determine application areas where the development of future combined probes may provide greater information about the processes being monitored. Using the information from the assessment, an indication of where the development of in-line probes could best suit the needs of the users in different industrial sectors could be passed on to the SME to aid their research and development. Since the introduction of MIR materials for fibre-optic immersion probes, the company has focused on the development of ATR MIR probes, implementing design changes to improve the performance and robustness of the probes. A selection of probes were investigated to determine how the design changes altered the performance and predictive ability of the probes. The results of this study should help the company with future work in the design and development of fibre optic based probes.

With the increased use of in-line probes for process control, there is a need for robust calibration models and the ability to transfer these between instruments or when probes are replaced. Many examples of NIR calibration transfer exist in the

literature; however, minimal research has been completed for the use of calibration transfer for MIR calibration models. Fibre Photonics not only needs to produce high quality products, but needs to make sure there is a use for these products in industry. For this reason, an investigation into the use of a selection of calibration transfer algorithms for the transfer of calibration models between ATR MIR probes and spectrometers has been completed. The ability to use calibration model transfer algorithms with the ATR MIR probes can increase the implementation of these probes for process control, for example when multiplexing multiple probes for one process.

As Fibre Photonics is interested in determining the possible application areas where in-line MIR probes could potentially be used in process analysis, part of this research investigated two application areas. Firstly, ATR MIR spectrometry was assessed for the analysis of whisky, in particular for the determination of authenticity. The second application area was in fermentation monitoring; MIR and NIR spectroscopy were used to analyse samples at different stages throughout a reaction using off-line methods to investigate the potential benefits of the combination of MIR and NIR regions for monitoring fermentation reactions. If the combination of MIR and NIR spectra can provide advantages for the analysis of fermentation reactions it will indicate the potential future benefit in the development of a combined MIR-NIR probe for process analysis.

The aims of the research described in this thesis can, therefore, be summarised as follows:

- Research the design, development and application of MIR probes for *in situ* process analysis.
- Study the use of calibration models for analyte prediction and specifically the use of calibration transfer algorithms for MIR analysis with *in situ* probes.
- Apply MIR spectroscopy for the analysis of Scotch whisky including the determination of authenticity.
- Complete initial studies into the combined use of MIR and NIR *in situ* measurements for synergistic benefit in process analysis.

## 1.4 References

1. K. R. Beebe, W. W. Blaser, R. A. Bredeweg, J. P. Chauvel, R. S. Harner, M. Lapack, A. Leugers, D. P. Martin, L. G. Wright and E. D. Yalvac, *Anal. Chem.*, 1993, **65**, R199-R216.
2. N. S. Sahni, T. Isaksson and T. Naes, *Chemom. Intell. Lab. Syst.*, 2001, **56**, 105-121.
3. J. A. Westerhuis, S. P. Gurden and A. K. Smilde, *Anal. Chem.*, 2000, **72**, 5322-5330.
4. T. Amari and Y. Ozaki, *Macromolecules*, 2001, **34**, 7459-7462.
5. C. Coffey, B. E. Cooley and D. S. Walker, *Anal. Chim. Acta*, 1999, **395**, 335-341.
6. F. McLennan, in *Process analytical chemistry*, eds. B. R. Kowalski and F. McLennan, Blackie Academic & Professional, London, 1995, pp. 1-13.
7. J. B. Callis, D. L. Illman and B. R. Kowalski, *Anal. Chem.*, 1987, **59**, 624-637.
8. J. Workman, M. Koch, B. Lavine and R. Chrisman, *Anal. Chem.*, 2009, **81**, 4623-4643.
9. J. Workman, B. Lavine, R. Chrisman and M. Koch, *Anal. Chem.*, 2011, **83**, 4557-4578.
10. *Guidance for Industry PAT — A Framework for Innovative Pharmaceutical Development, Manufacturing, and Quality Assurance*, <http://www.fda.gov/downloads/Drugs/GuidanceComplianceRegulatoryInformation/Guidances/UCM070305.pdf>, Accessed 04/08/2011, 2011.
11. H. Huang, H. Yu, H. Xu and Y. Ying, *J. Food Eng.*, 2008, **87**, 303-313.
12. R. Karoui, A. M. Mouazen, E. Dufour, R. Schoonheydt and J. De Baerdemaeker, *Eur. Food Res. Technol.*, 2006, **223**, 363-371.
13. D. Cozzolino, M. Parker, R. G. Damberg, M. Herderich and M. Gishen, *Biotechnol. Bioeng.*, 2006, **95**, 1101-1107.
14. C. D. Patz, A. Blicke, R. Ristow and H. Dietrich, *Anal. Chim. Acta*, 2004, **513**, 81-89.
15. *Drug application regulatory compliance*, <http://www.fda.gov/Drugs/DevelopmentApprovalProcess/HowDrugsareDevelopedandApproved/ApprovalApplications/AbbreviatedNewDrugApplicationANDAGenerics/ucm154098.htm#Guidance Documents>, Accessed 04/08/2011, 2011.
16. L. X. Yu, *Pharm. Res.*, 2008, **25**, 781-791.
17. F. S. Falla, C. Larini, G. A. C. Le Roux, F. H. Quina, L. F. L. Moro and C. A. O. Nascimento, *J Petrol Sci Eng*, 2006, **51**, 127-137.
18. J. M. Andrade, P. Fresco, S. Muniategui and D. Prada, *Talanta*, 2008, **77**, 863-869.
19. D. C. Hassell and E. M. Bow, *Appl. Spectrosc.*, 1998, **52**, 18A.
20. J. Workman, D. J. Veltkamp, S. Doherty, B. B. Anderson, K. E. Creasy, M. Koch, J. F. Tatera, A. L. Robinson, L. Bond, L. W. Burgess, G. N. Bokerman, A. H. Ullman, G. P. Darsey, F. Mozayeni, J. A. Bamberger and M. S. Greenwood, *Anal. Chem.*, 1999, **71**, 121R-180R.
21. D. C. Cornish, G. J. Epton and M. J. Smurthwaite, *Sampling Systems for Process Analysers*, Butterworth, London, 1981.

22. J. R. P. Clarke, *Anal. Chim. Acta*, 1986, **190**, 1.
23. K. J. Clevett, *Process Analyser Technology*, John Wiley and Sons, New York, 1986.
24. K. J. Clevett, in *Process analytical chemistry*, eds. B. R. Kowalski and F. McLennan, Blackie Academic & Professional, London, 1995, pp. 39-105.
25. M. J. Roberts, A. A. Garrison, S. W. Kerchel and E. C. Muly, *Process Control Qual.*, 1991, **1**, 281-291.

## 2 Background and Theory

### 2.1 Principles of infrared spectrometry<sup>1-5</sup>

Infrared spectroscopy can be used to gather information about the structure of a compound by examining its vibrational properties. The sample will absorb energy from the incident radiation causing vibrations to occur; when a molecule vibrates, all of the bonds will stretch and relax in combination. The difference in the incident and detected energy at each frequency will lead to absorption bands. The strongest absorptions occur in the mid-infrared (MIR) range caused by fundamental vibrations. Weaker absorptions occur in the near-infrared (NIR) range which are caused by overtones and combinations of fundamental vibrations. Table 2.1 details the characteristic transitions in the MIR and NIR infrared regions.

**Table 2.1: MIR and NIR infrared radiation characteristic transitions.**

<b>Radiation</b>	<b>Wavenumber range (cm<sup>-1</sup>)</b>	<b>Wavelength range (nm)</b>	<b>Characteristic transitions</b>
Near-infrared	14300 – 4000	700 – 2500	Overtones and combinations mostly due to X-H, where X = C, O and N.
Mid-infrared	4000 – 500	2500 – 5 x10 <sup>4</sup>	Fundamental vibrations, overtones and combinations.

The bond vibrations that occur in a molecule can be compared to a simple diatomic molecule and the potential energy ( $V$ ) of this molecule can be described by the harmonic oscillator model (Equation 2.1); where  $k$  is the force constant,  $r$  is the inter-nuclear distance,  $r_e$  is the equilibrium distance and  $x$  is the displacement coordinate.

$$V = \frac{1}{2}k(r - r_e)^2 = \frac{1}{2}kx^2 \quad \text{Equation 2.1}$$

The potential energy curve for the compression and extension of the bond is a parabola (Figure 2.1); the minimum is observed when the bond is at the equilibrium

distance ( $r_e$ ). The equilibrium is established between the repulsive and attractive forces of the two atoms. If the bond is compressed or extended away from the equilibrium point, a sharp increase in the potential energy will occur.

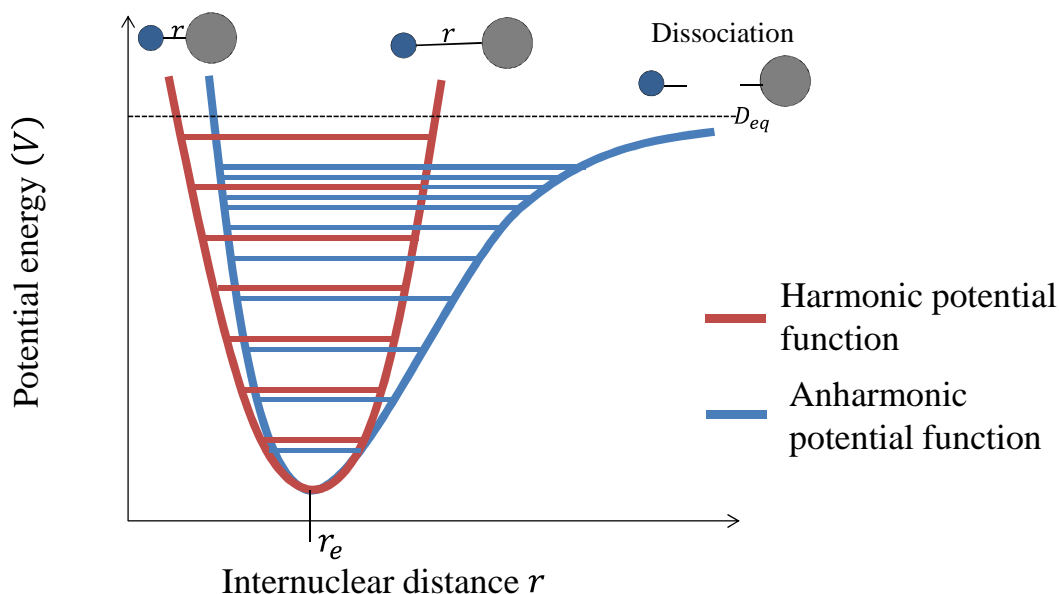


**Figure 2.1:** Potential energy diagram for a diatomic molecule.  $D_{eq}$  is the energy of dissociation of the atoms and  $r_e$  is the equilibrium bond length.

When there is an increase in the potential energy the diatomic molecule will oscillate and the frequency of vibration ( $\nu$ ) is described by Equation 2.2. The frequency is dependent on the reduced mass of the diatomic molecule ( $\mu$ ) and the force constant ( $k$ ).

$$\nu = \frac{1}{2\pi} \sqrt{\frac{k}{\mu}} \quad \text{Where } \mu = \frac{m_1 m_2}{m_1 + m_2} \quad \text{Equation 2.2}$$

$m_1$  and  $m_2$  correspond to the mass of the individual atoms in the diatomic molecule. Equally spaced energy levels exist and are given by Equation 2.3: where  $h$  is Planck's constant,  $\nu$  is the vibration frequency defined above and  $v$  is the vibrational quantum number, which can only have positive integer values.

$$E_{vib} = h\nu \left( v + \frac{1}{2} \right) \quad \text{Equation 2.3}$$

Diatomic molecules, therefore, can never have zero vibrational energy; as when  $v = 0$ ,  $E_{vib} = \frac{1}{2}h\nu$ , implying that the atoms present in a diatomic molecule are never completely at rest relative to one another. The energy levels,  $G(v)$ , can be expressed in wavenumber units ( $\text{cm}^{-1}$ ) by Equation 2.4, where  $\bar{\nu}$  is the wavenumber vibrational transition.

$$G(v) = \frac{E_{vib}}{hc} = \bar{\nu} \left( v + \frac{1}{2} \right) \quad \text{Equation 2.4}$$

The vibrational energy levels corresponding to different values of  $v$  are represented in Figure 2.2 as equally spaced horizontal lines. The selection rules for transitions between energy levels indicate that transitions are allowed for non-zero values of the transition moment. This occurs if the vibration is accompanied by a net change in dipole moment; therefore, a vibrational-spectral transition can only occur in heteronuclear diatomic molecules.

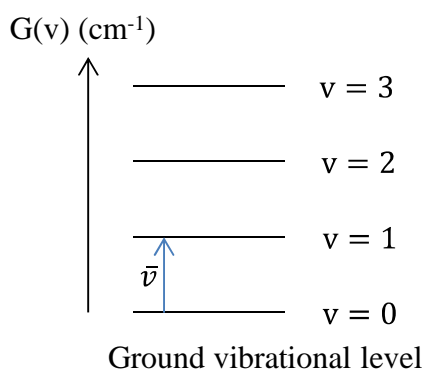


**Figure 2.2: Vibrational energy levels of the harmonic oscillator.**

A further restriction can be imposed from the quantum mechanical harmonic oscillator where the vibrational quantum number ( $v$ ) can only change by a single unit. So, allowed transitions can only occur across one energy level for example,  $v = 0 \rightarrow v = 1$  is allowed but  $v = 0 \rightarrow v = 2$  is forbidden. The first transition  $v = 0 \rightarrow v = 1$  is called the fundamental transition which is the strongest transition. Boltzman distribution dictates that at room temperature most molecules will exist in the ground vibrational level ( $v = 0$ ). Therefore, transitions occurring from levels greater than zero will be much weaker as there will be a lower population of molecules occupying those vibrational levels.

In reality all molecules do not follow this simple harmonic motion; they are known as anharmonic oscillators. There are two reasons for the occurrence of anharmonic oscillators: the first is due to an accumulation of the repulsive forces that arise as the bonds in the molecule compress; the second is due to the weakening of the bonds as they stretch. On compression the electron clouds of the two atoms limit the approach of the nuclei, resulting in the potential energy rising rapidly. During extension the bond between the atoms will eventually break when the vibrational energy level reaches the dissociation energy, the potential energy levels off, see Figure 2.1. Therefore, the relationship between the potential energy and displacement is not as simple as that for simple harmonic motion. Experimentally there are two effects that indicate that molecules are not ideal oscillators: the vibrational energy levels are not equally spaced, and the overtone transitions are observed. Equation 2.5 can be used to describe the energy levels of the allowed states of the anharmonic oscillator.

$$G(v) = \frac{E_{vib}}{hc} = \bar{\nu} \left( v + \frac{1}{2} \right) - x_e \bar{\nu} \left( v + \frac{1}{2} \right) - X \left( v + \frac{1}{2} \right)^2 \quad \text{Equation 2.5}$$

Where  $x_e$  is the anharmonicity constant and  $X = x_e \bar{\nu}$ . The energy levels are no longer evenly spaced as they were in the harmonic oscillator (see figure X); the space gradually decreases as the energy increases. The allowed change in vibrational quantum number for an anharmonic oscillation is not limited to  $\pm 1$ .

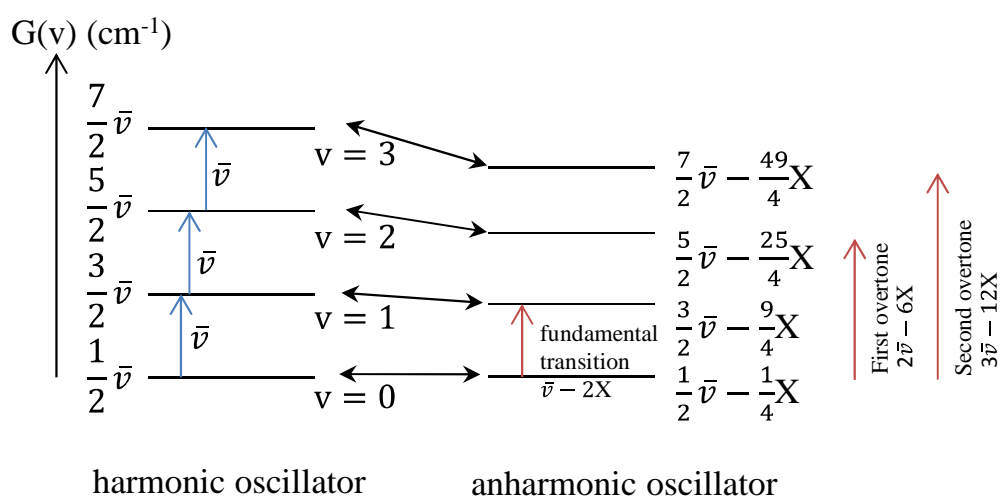


Figure 2.3: Energy levels and transitions for harmonic and anharmonic oscillator.

## 2.2 Optical fibres for use in infrared spectrometry

The optical fibres allow data acquisition from otherwise inaccessible locations in the process as well as removing the need for any form of extractive sampling. Although optical fibres are very useful in spectroscopic analysers the employment of these fibres has some difficulties. Spectroscopic fibre optics require a high transmittance to polychromatic radiation, whilst ensuring that there are no interactions in the form of absorbance or scattering. Care must always be taken in the use of optical fibres to prevent physical shocking and overstressing of the fibres, as it can lead to long term damage of the optical fibres.<sup>6</sup>

An optical fibre is made up of a cylindrical core with a refractive index,  $n_1$ , which is higher than the refractive index of the annular outer cladding,  $n_2$ . These types of fibres are referred to as step-index optical fibres as the refractive index in each of the core and cladding regions are uniform. See Figure 2.4 for a cross section of a step index optical fibre.<sup>6,7</sup>

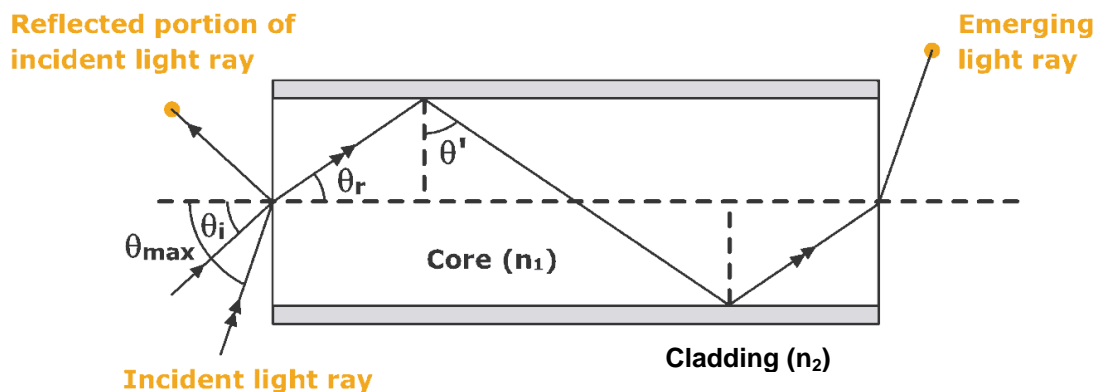


Figure 2.4: A cross section through a step index optical fibre.<sup>6</sup>

The angle of refraction,  $\theta_r$ , of the ray can be related to the angle of incidence,  $\theta_i$ , at the air/core interface by:

$$\sin \theta_i = n_1 \sin \theta_r \quad \text{Equation 2.6}$$

The refracted ray will strike the core/cladding interface at an angle of incidence  $\theta$ , this will be equal to  $90 - \theta_r$ . In order for the ray to continue propagating along the

fibre, the ray must be totally reflected at the core/cladding interface. For total internal reflectance to occur the minimum value of  $\theta$  is given by:

$$n_1 \sin \theta_{min} = n_2 \quad \text{Equation 2.7}$$

In the years since fibre optics were first constructed to transmit infrared radiation, a range of different types of optical fibre exist. Each optical fibre has its advantages and disadvantages and so they are chosen for their suitability for a particular application. The different core materials have different transmission performances and so the fibres are chosen to give the optimum transmission at the wavelengths required for each application, Table 2.2 details some examples of fibre optic materials and their properties.<sup>6, 8-11</sup>

**Table 2.2: Properties of fibre optic materials.<sup>6</sup>**

Wavelength range	Fibre material	Maximum length	Comments
MIR 550 - 6500 cm <sup>-1</sup> (18 – 1.5 μm)	As <sub>2</sub> S <sub>3</sub>	A few m	The fibres have a low frequency cut-off at 1000 cm <sup>-1</sup> and absorb at 3300 and 2500 cm <sup>-1</sup> . Also these fibres can be quite expensive and fragile.
	Silver halide	< 10 m	These are visible light sensitive; however, their robustness has been greatly improved.
NIR 3850 – 28500 cm <sup>-1</sup> (2.6 – 0.35 μm)	Low OH silica	> 1000 m	Low cost fibres with excellent transmission. The silica must be “dry” to avoid strong OH absorption.

Table 2.2 shows that silica based fibres are suitable for use in the NIR region, however, silica fibres are not transparent in the MIR region and so special materials are required. Figure 2.5 shows the spectral attenuation increasing towards 2600 nm (3850 cm<sup>-1</sup>) for NIR silica fibres.

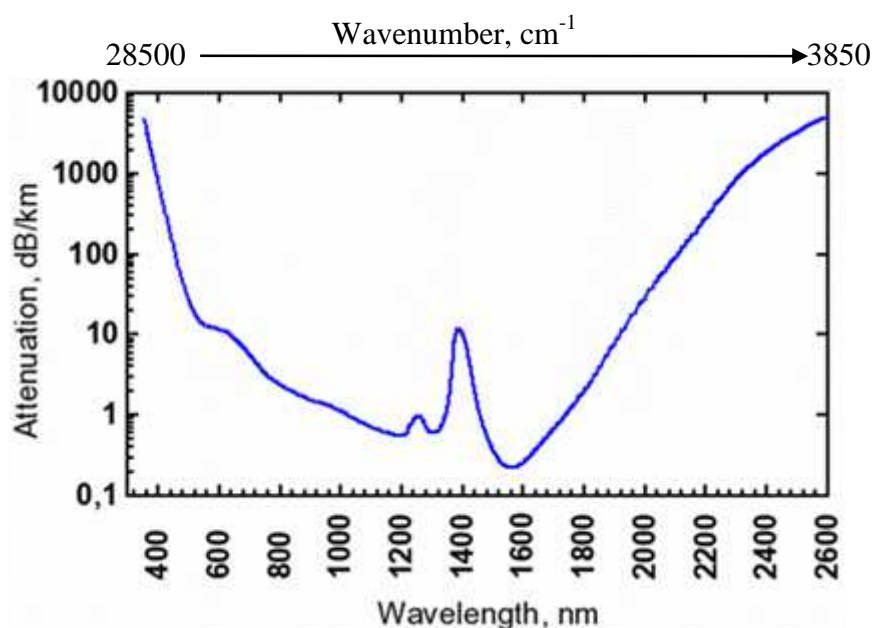


**Figure 2.5: Typical spectral attenuation of NIR fibres from Fibre Photonics.<sup>12</sup>**

Studies on the applications of MIR optical fibres have been on-going since the 1980s.<sup>13-15</sup> Optical fibres using materials such as chalcogenide and silver halide have been shown to have some applications, but they both have disadvantages. Fibre optics constructed of chalcogenide have been commercially available for a number of years, but their applications are limited as chalcogenide fibres are fragile and toxic, and show limited transparency beyond  $8 \mu\text{m}$  ( $<1250 \text{ cm}^{-1}$ ). Other fibres consisting of silver halide material are non-toxic and are transparent in the wavelength range from  $3$  to  $18 \mu\text{m}$  ( $3300 - 550 \text{ cm}^{-1}$ ). This advancement has allowed the construction of flexible silver halide fibre optics that can be coupled with attenuated total reflection probes.<sup>13</sup>

Although silver halide based fibres have advantages over chalcogenide fibres, developments are still on going in an attempt to increase the length of fibres to allow greater use of MIR spectrometry for *in situ* measurements. Polycrystalline silver halide infrared fibres (PIR) and chalcogenide infrared fibres (CIR) are both currently being used in MIR spectroscopy. The features of PIR and CIR fibres are compared with NIR silica fibres in Table 2.3.<sup>12</sup>

**Table 2.3: Details of key properties of chalcogenide (CIR), polycrystalline silver halide (PIR) and silica fibres (from Fibre Photonics).<sup>12</sup>**

Parameter	CIR Fibre	PIR Fibre	Silica fibre (NIR)
Core/clad structure materials	Chalcogenide As <sub>2</sub> S <sub>3</sub> glasses	AgCl:AgBr solid solution crystals	Pure fused silica (low OH <sup>-</sup> ) / fluorine doped fused silica
Typical transmission range	1.5 – 6.0 μm (~ 6650– 1650 cm <sup>-1</sup> )	3 – 18 μm (~ 3300 – 550 cm <sup>-1</sup> )	0.35 – 2.6 μm (~ 28500 – 3850 cm <sup>-1</sup> )
Specific features	Toxic, fragile and non-hygroscopic.	Non-toxic, non-hygroscopic, very flexible and UV sensitive	Radiation resistant, flexible, laser damage resistant and operate in high vacuum
Temperature range	270 K – 370 K	Up to 420 K	83K – 658K <sup>a</sup>

<sup>a</sup> depending on coating used

Table 2.3 shows a difference in the typical transmission ranges between the two MIR fibres; the typical transmission spectra of PIR and CIR fibres in Fibre Photonics probes are given in Figure 2.6.<sup>12</sup>

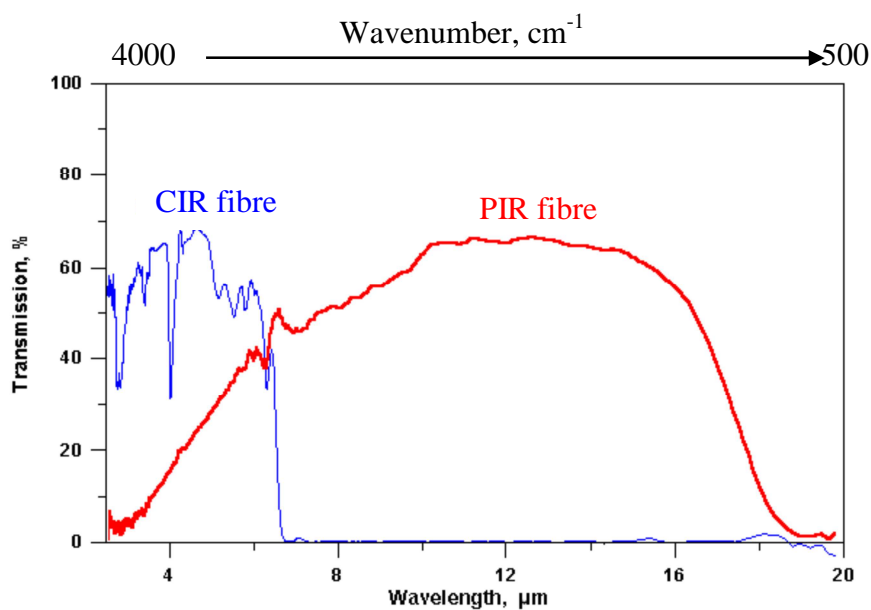


**Figure 2.6: Typical transmission spectra of 1.5 m long PIR and CIR fibres in Fibre Photonics probes.<sup>12</sup>**

Although the typical transmission range for CIR fibres from Fibre Photonics is in the range  $1650\text{ cm}^{-1}$  to  $6650\text{ cm}^{-1}$ , there are examples of CIR fibres which can transmit beyond this range. The SpectraProbe system consists of CIR fibres which transmit in the range  $1000\text{ cm}^{-1}$  to  $2000\text{ cm}^{-1}$ , although the upper range was determined by the design of the spectrometer rather than the fibre.<sup>16</sup>

### 2.3 Probe designs in infrared spectrometry

There are four main optical probe designs available for *in situ* monitoring: transmission probes, transfection probes, reflectance probes and attenuated total reflection (ATR) probes.<sup>17, 18</sup>

A transmission probe (Figure 2.7)<sup>6, 17</sup> allows radiation to pass down the length of the probe through the excitation fibre before being bent through 180° by a retroreflector. The radiation passes through a small sample gap filled with sample, and then will pass through the collection fibre back to the spectrometer. Typical pathlengths for these probes are around 1-2 mm for the NIR, however due to the small pathlengths required by MIR the sample gap would normally be too small to allow a sample flow.

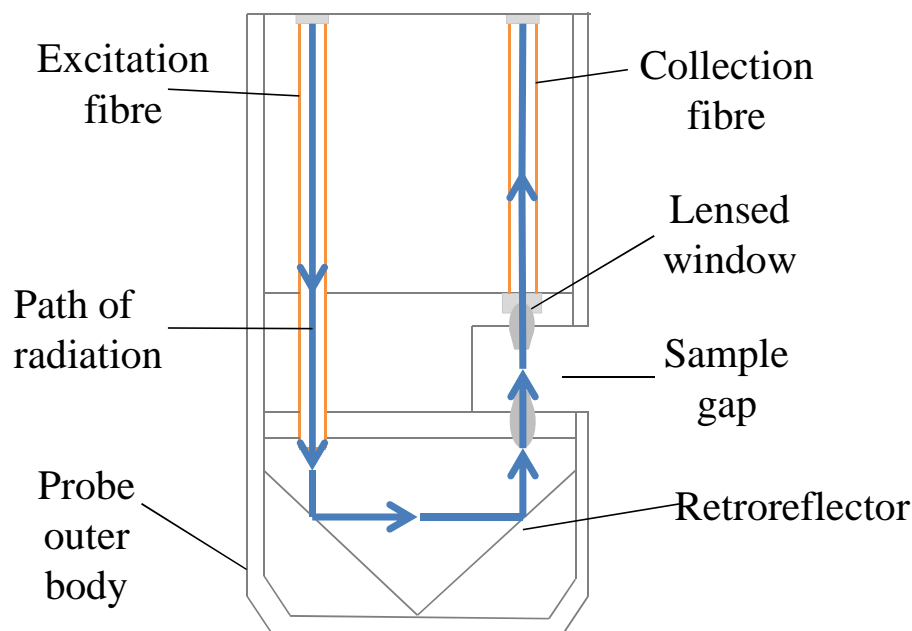


**Figure 2.7: Schematic of a transmission probe adapted from references 6 and 17.**

The transfection probe (Figure 2.8)<sup>6, 17</sup> operates slightly differently from the transmission probe. The radiation from the excitation fibre passes through the sample and is then reflected back via a mirror through the sample again and then into the collection fibre. These probes are easy to manufacture and the simple design allows changes of the optical pathlength.

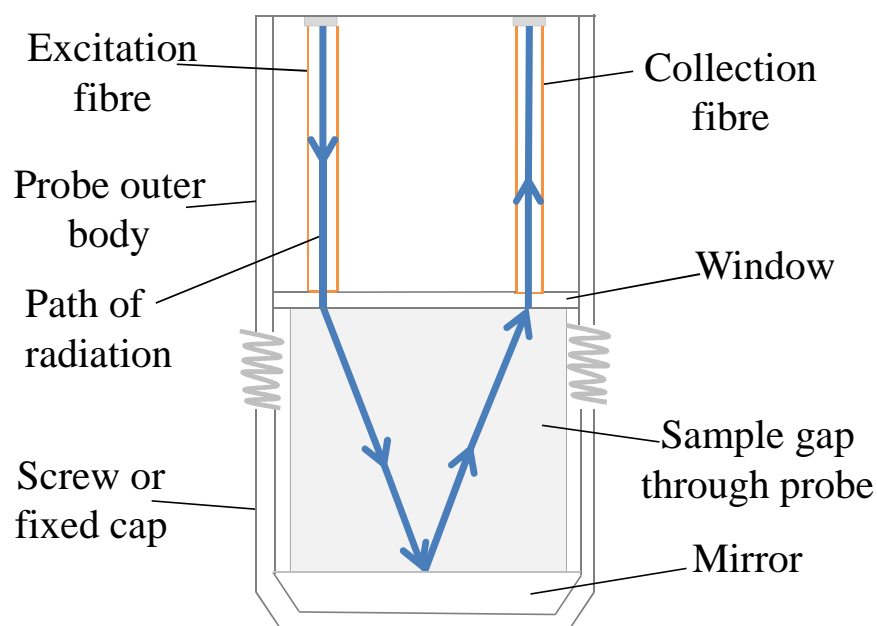


**Figure 2.8: Schematic of a transflection probe adapted from references 6 and 17.**

Reflectance probes (Figure 2.9)<sup>17</sup> are generally used for powders and slurries or any samples that have significant diffuse reflectance. The amount of radiation returned by this diffuse reflectance is much less than for transmission. Therefore, it is usual for larger core diameter fibres (600 – 1000  $\mu\text{m}$ ) or multiple fibres to be used to collect the maximum amount of diffusely reflected radiation. The radiation travels down the probe *via* the excitation fibre or fibres in the bundle to the tip of the probe where the radiation is focussed onto the sample. The back-scattered radiation is focussed onto the collection fibre or fibres in the bundle for transmission to the spectrometer. Figure 2.9 shows an example of a six excitation fibre, one collection fibre reflection probe; however, different arrangements and numbers of fibres can be used.

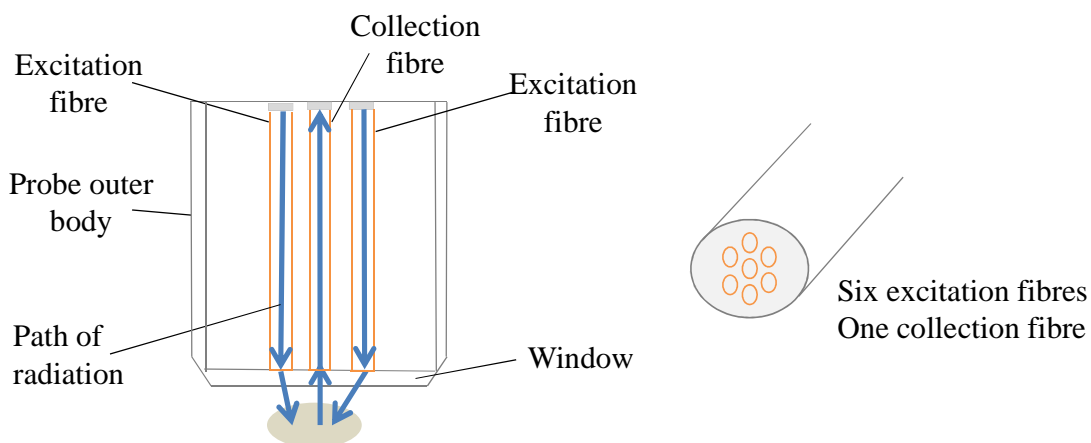


**Figure 2.9: Schematic of a reflectance probe adapted from reference 17.**

A newer development in *in situ* probe design is the ATR probe used in MIR spectrometry. A schematic of an ATR probe can be viewed in Figure 2.10.<sup>6, 7, 17</sup> The radiation in an ATR probe is sent through a transmitting crystal at the end of the probe where the spectroscopic information will be collected from the sample/crystal interface.

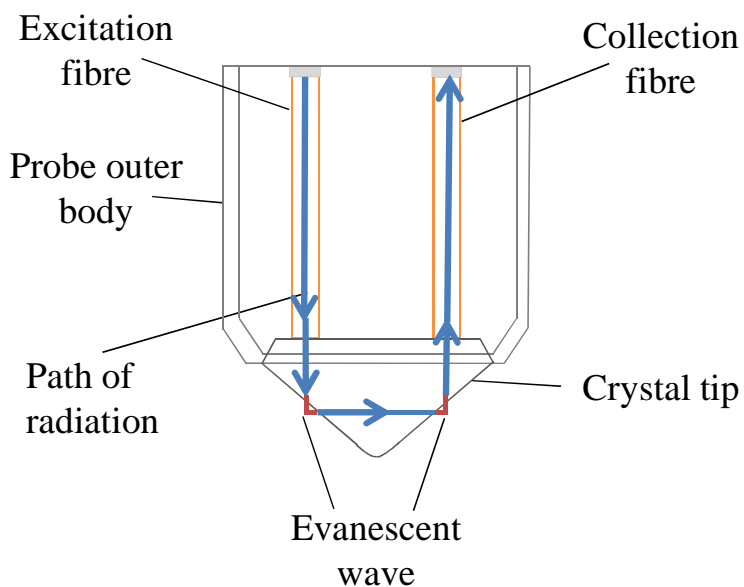


**Figure 2.10: Schematic of an ATR probe adapted from references 6, 7 and 17.**

Under certain conditions the radiation passing through a prism of high refractive index material will be totally internally reflected. The radiation passed down the fibres of the ATR probe does not physically leave the probe, but instead interacts

with the sample via an evanescent wave at the sample/crystal interface. The angle at which total internal reflection occurs is called the critical angle ( $\theta_c$ ) and is calculated by Equation 2.8, where  $n_1$  is the refractive index of the ATR crystal and  $n_2$  is the refractive index of the sample.

$$\theta_c = \sin^{-1}n_2/n_1 \quad \text{Equation 2.8}$$

When the sample solution is brought into contact with the crystal the evanescent wave will be attenuated in the regions of the spectrum at which the sample absorbs. The depth of penetration ( $d_p$ ) for a single reflection is given by Equation 2.9, where  $\theta$  is the angle of incidence and  $\lambda$  is the wavelength of the incident light.

$$d_p = \lambda / 2\pi n_1 [\sin^2\theta - (n_2/n_1)^2]^{0.5} \quad \text{Equation 2.9}$$

A relationship also exists between the number of reflections, the penetration depth and the pathlength, given in Equation 2.10, where  $b$  is the pathlength.

$$b = d_p \times \text{No. reflections at the crystal} \quad \text{Equation 2.10}$$

In MIR spectrometry, a ZnSe element (refractive index about 2.4) is often used and depending on the number of internal reflections, provides a pathlength of 1 – 10  $\mu\text{m}$ . For many process applications, however, more robust materials such as diamond (refractive index 2.42) are used for the ATR crystal as they can cope with harsher conditions and have a similar refractive index to ZnSe.<sup>19</sup> ATR probes can be useful for analysing strongly absorbing compounds owing to the small pathlength, which can be varied through different numbers of reflections within the crystal. Consequently, ATR probes are becoming more useful for *in situ* analysis by MIR (and also UV-visible) spectrometry.

## 2.4 Overview of chemometrics and multivariate regression

Chemometrics was defined by B. M. Wise and B. R. Kowalski as;

“..the science of relating measurements made on a chemical system to the state of the system via application of mathematical or statistical methods.”<sup>20</sup>

Chemometrics is being used more extensively to understand the data produced by spectroscopic techniques in process monitoring. Although infrared spectra can show a lot of structural information of a pure material, usually this involves the analysis of fully resolved peaks and measurement of their absorbances. For process monitoring, this usually involves more complex mixtures and requires quantitative multi-component analysis. Often the spectra of individual components of the complex mixtures overlap and so the individual analytes cannot be easily identified. Using chemometric applications such as multivariate calibration allows the correlation between the sample spectra and the known analyte values to be determined.<sup>20</sup>

### 2.4.1 Principal component analysis (PCA)

PCA is one of the main chemometric applications used when analysing complex process control spectra. PCA is used to find the combination of variables or factors that describe any major trends in the data.<sup>20</sup> The basic concept is to describe the data set using a small number of abstract variables that are known as principal components (PC). These principal components are generally referred to as ‘latent’ variables. The PCs obtained from the original data set must describe the underlying structure, in terms of the relationships between different samples and between different measurement variables.

Looking at PCA mathematically, a given data set can be represented as a matrix  $\mathbf{X}$  with  $m$  rows and  $n$  columns, where each variable is in a column and each sample in a row. The data matrix is considered as being made up of two separate components: the underlying structure (systematic variation) in the data and random fluctuations, or “noise”, due to the measurement process. The data matrix  $\mathbf{X}$  can then be represented as:

$$\mathbf{X} = \mathbf{M} + \mathbf{E}$$

where the  $\mathbf{M}$  matrix represents the underlying structure or ‘model’ of the data and  $\mathbf{E}$  is the random fluctuations (‘noise’) matrix.

As a result of PCA, the model matrix  $\mathbf{M}$  is further divided into two smaller matrices,  $\mathbf{T}$  and  $\mathbf{P}$ , represented as:

$$\mathbf{M} = \mathbf{T} \mathbf{P}$$

Therefore,

$$\mathbf{X} = \mathbf{T} \mathbf{P} + \mathbf{E}$$

$\mathbf{T}$  is known as the scores matrix and will indicate any similarities or dissimilarities between samples.  $\mathbf{P}$  is known as the loadings matrix and it describes the relationships between the individual measurement variables. If  $\mathbf{E}$  contains only ‘noise’ the score matrix,  $\mathbf{T}$  and the loadings matrix,  $\mathbf{P}$  will describe all of the structure of the original data matrix. PCA therefore allows the data produced from chemical process monitoring to be described by less factors than the original number of variables, with no significant loss of information.<sup>20</sup>

#### **2.4.2 Partial Least Squares (PLS) regression**

PLS was developed by H. Wold;<sup>21</sup> the method involves PCA decomposition and inverse least squares regression (ILS) in one stage. PLS is related to both principal component regression (PCR) and ILS-multiple linear regression (ILS-MLR) and is seen as the procedure that combines the two. PCR is a two stage process and is primarily used to find factors that describe the greatest amount of variance in the predictor variables, e.g. the spectra. PCR assumes that the concentration estimates are error free. Whereas ILS-MLR is designed to seek out a single factor that can best correlate the predictor variables (spectra) with the predicted variables (concentrations).<sup>20</sup> FOR ILS-MLR, the user chooses which variable contains the error. The purpose of PLS regression is to establish a linear model that links the spectral data and the reference values. The technique will model both the spectral data and the reference values to determine the variable in the spectral data that will best describe the reference values. PLS assumes that the error is equally distributed in both the spectral data and the reference values.<sup>22, 23</sup>

In PLS regression, the matrices containing the spectral data,  $\mathbf{X}$ , and the known concentrations,  $\mathbf{Y}$ , are decomposed in a manner similar to PCA resulting in two model matrices which are further divided into smaller matrices:

$\mathbf{X} = \mathbf{TP}$  where  $\mathbf{T}$  and  $\mathbf{P}$  are the scores and loadings, respectively for  $\mathbf{X}$

$\mathbf{Y} = \mathbf{UQ}$  where  $\mathbf{U}$  and  $\mathbf{Q}$  are the scores and loadings, respectively for  $\mathbf{Y}$

The scores from the decomposition of each starting matrix,  $\mathbf{T}$  and  $\mathbf{U}$ , are related. During an iterative calculation process, the scores matrices from the  $\mathbf{T}$  and  $\mathbf{U}$  are exchanged to improve the relationship between the principal components for each dataset; the  $\mathbf{X}$  matrix information is used to adjust the  $\mathbf{Y}$  matrix principal components and vice versa. The PLS algorithm defines a relationship between the scores of the two starting matrices from the decomposition and ILS-MLR. This relationship can be defined as:

$$\mathbf{U} = \mathbf{TB}$$

Where  $\mathbf{T}$  and  $\mathbf{U}$  are the scores for  $\mathbf{X}$  and  $\mathbf{Y}$ , respectively and  $\mathbf{B}$  represents the regression coefficients. In the PLS model, it is assumed that the model error is in both the concentrations and the spectral responses. The regression coefficients,  $\mathbf{B}$ , are determined in the PLS model by measurement of the spectra of a set of calibration solutions. Once the regression coefficients have been calculated, they can then be used to determine the concentrations of analytes in the 'unknown' samples.

### 2.4.3 Design of Experiment manager software (DoEman)

In chemometric analysis of spectral data, good calibration models are essential in order to achieve accurate predictive results. Reviewing the regression methods such as PLS regressions, explained in section 2.4.2, the number of possible calibration models that can be built with all the possible factors is very high. The major challenge is to identify the best model that will give accurate and reliable predictions. Generally two methods of approach can be adopted, one being good fitting abilities and the other being good prediction abilities, but these can sometimes be referred to as contradictory methods.<sup>24</sup> An example defining this could be a model with a precise fit to the calibration samples although it would not be able to predict any

samples that differ from the calibration samples; this is a case of over-fitting. Therefore, for calibration model applications, it is necessary to have a balance between good fit and good predictive ability. The issue surrounding the best calibration model can be attributed in part to the optimisation of many input factors and one or more response factors. To review these many factors and to aid optimal calibration model building, a design of experiment approach was described by Flåten and Walmsley.<sup>24</sup> This approach starts with identifying the significant factors for the data set and then determining their levels. The factors can include different kinds of pre-treatment, type of regression method and number of principal components. With the significant factors and their levels identified, the experimental design can be set up. This information can be used with the CPACT, DoEman graphical user interface software<sup>25</sup> where information about the factors and their levels are input along with the spectral data for analysis. The software is designed to look at the main factors included in the experimental design as well as the interaction effects between factors. The software produces plots with respect to the root mean square error of calibration (RMSEC) and root mean square error of prediction (RMSEP) values; the information contained within the plots can help identify the optimal settings for the factors selected. These plots can be analysed and the parameters that minimise the RMSEC and RMSEP selected to build the calibration model.

RMSEC is used to determine how well the model fits the data and RMSEP is used to determine how well the model predicts data that was not present in the original model. Both RMSEC and RMSEP can be calculated using the same equation, see below.

$$\text{RMSE (C or V)} = \sqrt{\frac{\sum_{i=1}^n (\hat{y}_i - y_i)^2}{n}} \quad \text{Equation 2.11}$$

Where in Equation 2.11,

$\hat{y}_i$  = predicted value

$y_i$  = known value

$n$  = number of samples

For RMSEC,  $\hat{y}_i$  are the predicted values of all the samples that were used in the model formation and  $y_i$  are the known values of these samples. Whereas for RMSEP,  $\hat{y}_i$  are the predicted values of a new set of samples that were not included in the original model formation and  $y_i$  are the known values of the new data that is being predicted.

## 2.5 References

1. J. H. van der Maas, *Basic Infrared Spectroscopy*, 1st edn., Heyden & Son Ltd., London, 1969.
2. P. R. Griffiths, in *Handbook of vibrational spectroscopy* eds. J. M. Chalmers and P. R. Griffiths, J. Wiley, New York, 2002, vol. 1, pp. 33-43.
3. D. Steele, in *Handbook of vibrational spectroscopy* eds. J. M. Chalmers and P. R. Griffiths, J. Wiley, New York, 2002, vol. 1, pp. 44-70.
4. H. W. Siesler, in *Near-Infrared Spectroscopy*, Wiley-VCH, 2007, pp. 1-10.
5. L. Bokobza, in *Near-Infrared Spectroscopy*, Wiley-VCH Verlag GmbH, 2007, pp. 11-41.
6. D. Littlejohn, *Process Analysis* <http://video.strath.ac.uk/processanalysis/>, Accessed 23/07/2009.
7. Y. Raichlin and A. Katzir, *Appl. Spectrosc.*, 2008, **62**, 55A-72A.
8. P. Lucas, A. A. Wilhelm, M. Videia, C. Boussard-Pledel and B. Bureau, *Corros. Sci.*, 2008, **50**, 2047-2052.
9. H. M. Heise, A. Bittner, L. Kupper and L. N. Butvina, *J. Mol. Struct.*, 1997, **410**, 521-525.
10. V. Artyushenko, A. Bocharnikov, G. Colquhoun, C. Leach, V. Lobache, T. Sakharova and D. Savitsky, *Vib. Spectrosc.*, 2008, **48**, 168-171.
11. V. Artyushenko, C. Wojciechowski, J. Ingram, V. Kononenko, V. Lobachev, T. Sakharova, J. Ludczak, A. Grzebieniak and Z. Wojciechowski, Warsaw, Poland, SPIE, 5951, 595103-595108, 2005.
12. *Fibre Photonics*, <http://www.fibrephotonics.com>, Accessed 04/08/2011, 2011.
13. L. Kupper, H. M. Heise and L. N. Butvina, *J. Mol. Struct.*, 2001, **563**, 173-181.
14. M. R. Taghizadeh, P. J. Melling, F. A. P. Tooley, S. D. Smith and R. Arieli, *Optica Acta*, 1984, **31**, 371-377.
15. A. Bornstein, N. Croitoru, A. S. M. Radiation and Electromagnetic, *Appl. Phys. Lett.*, 1985, **46**, 705.
16. C. McGill, R. Ferguson, K. Donoghue, A. Nordon and D. Littlejohn, *Analyst*, 2003, **128**, 1467-1470.
17. J. Andrews and P. Dallin, in *Process Column, Spectroscopy Europe*, J Wiley & IM Publications, 2003, vol. 15, Issue 4 <http://www.clairret.co.uk/downloads/PSC03.pdf>, Accessed 23/09/2011.
18. P. J. Melling and M. Thomson, in *Handbook of vibrational spectroscopy* eds. J. M. Chalmers and P. R. Griffiths, J. Wiley, New York, 2002, vol. 2, pp. 1551-1559.
19. H. M. Heise, L. Kupper and L. N. Butvina, *Spectroc. Acta Pt. B-Atom. Spectr.*, 2002, **57**, 1649-1663.
20. B. M. Wise and B. R. Kowalski, in *Process analytical chemistry*, eds. B. R. Kowalski and F. McLennan, Blackie Academic & Professional, London, 1995, pp. 259-312.
21. M. J. Adams, *Chemometrics in analytical spectroscopy* Royal Society of Chemistry, Cambridge, 2004.
22. T. Salomonsen, H. M. Jensen, D. Stenbæk and S. B. Engelsen, *Carbohydr. Polym.*, 2008, **72**, 730-739.

23. Y. Roggo, P. Chalus, L. Maurer, C. Lema-Martinez, A. Edmond and N. Jent, *J. Pharmaceut. Biomed.*, 2007, **44**, 683-700.
24. G. R. Flåten and A. D. Walmsley, *Analyst*, 2003, **128**, 935-943.
25. A. Owen, PhD thesis, University of Strathclyde., 2006.

### 3 Use of MIR and NIR spectrometry for process analysis

#### 3.1 Introduction

Infrared spectrometry is one of the most widely used spectroscopic techniques because of its ability to not only identify, but quantify chemical species regardless of their state. Infrared spectrometry has been widely used in laboratories for many years, but recent developments have seen this technique being applied increasingly for process control in chemical manufacturing and in industrial plants.

NIR spectrometry is known for its ease of use and is well established in PAC, with numerous reviews<sup>1, 2</sup> and publications<sup>3-5</sup> on its application for on/in – line monitoring. The reason for the establishment of NIR spectroscopy over MIR spectroscopy in PAC is not because of NIR spectroscopy being any better for process control, but more because of the ability to use cheap silica fibres that allow the spectrometer to be placed up to hundreds of meters away from the process. These silica fibres have also been available for use with optical probes, such as transmittance and reflection probes, to allow *in situ* monitoring of processes. Although MIR spectroscopy is generally harder to interface than NIR spectroscopy, it can offer more information on the chemical species. The interfacing issues of MIR spectrometry are due to the fibre limitations, whereby cheap silica fibres cannot be used for MIR spectrometry, as discussed in chapter 2. Therefore, MIR spectrometry has been less commonly used in PAC than NIR spectrometry.

In recent years, there has been an increase in the use of infrared spectroscopic techniques for monitoring and control in a range of applications such as bio-analytical applications,<sup>6-9</sup> fermentation processes,<sup>10-13</sup> esterification reactions,<sup>14, 15</sup> powder blending,<sup>16</sup> polymerisation reactions<sup>17, 18</sup> and also raw material testing.<sup>9, 19</sup> The following examples give an indication of the types of analysis that have been reported.

Petersen *et al.*<sup>20</sup> described the use of *in situ* NIR spectrometry to monitor glucose and ammonium in *Streptomyces coelicolor* fermentations. Off-line NIR measurements

were also carried out to compare and highlight the issues of *in situ* monitoring of fermentations. Petersen *et al.*<sup>20</sup> were able to make suitable predictions for glucose; however, the results for ammonium were not satisfactory. The main reason for the poor ammonium prediction was due to the signal attenuation of the optical fibres above 2000 nm. *In situ* NIR spectrometry has also been applied for the quantification of microcarrier animal cell cultures, Petiot *et al.*<sup>13</sup> were able to monitor the concentrations of glucose and lactate during the process. As well as *in situ* immersion probe measurements, NIR spectroscopy has been used non-invasively; Yang *et al.*<sup>21</sup> described the use of a portable fibre optic visible-NIR reflectance system to determine the growth stages of tomato fruits. Hassan Refat<sup>22</sup> used non-invasive NIR spectroscopy to identify drugs such as diazepam and methadone hydrochloride. Using non-invasive NIR measurements reduced the time required for drug analysis and required no sample pre-treatment. Recently advances have also been made in NIR imaging and Suda *et al.*<sup>23</sup> described the use of NIR imaging to monitor the brain activation in subjects when involved in face to face conversation.

Applications of MIR spectrometry in PAC have been more limited, although there have been notable successes in monitoring process streams; for example MIR spectrometry was used as an on-line technique for the real-time monitoring of analytes in gas phase effluent streams,<sup>24</sup> where a low resolution MIR spectrometer (Bomem MB-155 FT-IR spectrometer) was used with a quartz gas cell to analyse organic containing effluents from an industrial process. With the use of PLS a region of spectral data was selected that removed the effect of CO<sub>2</sub> on the quantitative analysis. Another example involved a study of the kinetics of nitrile biotransformation reactions by real-time MIR spectroscopy.<sup>7</sup> The biocatalysis of whole cell suspensions of the bacterium *Rhodococcus rhodochrous* LL100-21 was monitored in real-time using a React IR spectrophotometer. Due to the absorption of nitrile arising in the region where diamond is cut-off (1900 – 2200 cm<sup>-1</sup>) a silicon ATR probe was used instead of a diamond probe. ATR MIR spectrometric techniques are also becoming increasingly important in the control of crystallisation processes, aiding a reduction in the process time for manufacture of batches.<sup>25</sup> In this study it was found that monitoring the liquid phase concentration and hence the

supersaturation level in production can indicate the starting point and the potential yield of the process, as well as areas where problems may occur. MIR spectrometry has also been observed in applications for the rapid determination of several coal properties.<sup>26</sup> A sample set consisting of 142 raw coals from different suppliers were analysed by ATR MIR spectrometry by applying a close contact between the surface of the coal and the diamond crystal using a Golden Gate-Specac ATR accessory connected to the interferometer. The ATR MIR system was able to provide relative error determination similar to the reference transmission mode with the advantage of no sample preparation. Here fast classification of coal samples based on mineral matter composition and kaolinite content were achieved with the prospect of future on-line methods apparent.

## **3.2 An assessment of the applications of infrared spectrometry**

With NIR spectrometry well established in PAC and applications of MIR spectrometry increasing, a wide range of processes could now be monitored by at least one if not both of these techniques. John Coates provides a table of example applications for process infrared spectroscopy<sup>27</sup> which has been used in this research as the basis for an evaluation of the different process application areas, where MIR and NIR spectrometry could be used for analysis. The main focus of this evaluation was on in-line applications; however there are some references to other methods. Some processes may only be monitored by one of the techniques, but there are some application areas that might have the potential for analysis by a combination of both MIR and NIR spectroscopy, with benefit achieved by fusing the data. As well as evaluating the potential techniques for each application area, an assessment has been made regarding the most appropriate mode of measurement (transmission, reflectance and ATR) for each application. The evaluation of MIR and NIR spectrometry for the different process application areas is summarised in Table 3.1. The notes given after Table 3.1 discuss the measurement mode options and where appropriate suggest applications where in-line spectrometry may be beneficial.

**Table 3.1: Evaluation of potential applications of process MIR and NIR spectrometry**

Application	Sample type	Wavenumber range (cm <sup>-1</sup> )	
		500 → 4000	4000 → 14300
Refinery production	Gases	Transmission	Transmission
Fuels	Gases	Transmission	Transmission
Speciality gas products	Gases	Transmission	
Combustion gases	Gases	Transmission	Transmission
Ambient air monitoring	Gases	Transmission	Transmission
Aerosol products	Gases	Transmission	Transmission
Refrigeration	Gases	Transmission	Transmission
Semiconductors	Gases	Transmission cell	
Refinery production	Liquids (very viscous)	ATR	Transmission or reflectance
Plastics & polymers	Liquids (very viscous)	Reflectance	Reflectance
Polymer products	Liquids (very viscous)	Reflectance	Transmission or reflectance
Food products	Liquids (very viscous)	Reflectance	Reflectance
Fuels	Liquids (viscous)	ATR	Transmission or reflectance
Oil & lubricants	Liquids (viscous)	ATR	Transmission or reflectance
Solvents	Liquids	ATR	Transmission
General chemicals	Liquids	ATR (impurities)	Transmission (bulk)
Chemical reaction monitoring	Liquid processes	ATR (specific compounds)	Transmission (general reaction monitoring)

Application	Sample type	Wavenumber range (cm <sup>-1</sup> )	
		500 → 4000	4000 → 14300
Consumer products	Liquids	ATR or reflectance (additives & impurities)	Reflectance or transmission (bulk & specialist group monitoring)
Specialised products	Liquids	ATR (trace)	Reflectance (bulk)
Environmental	Liquids	ATR	
Food products	Liquids	ATR or reflectance	Transmission or reflectance
Pharmaceutical products & development	Liquids	ATR	Transmission
Food products	Fermentations	ATR	Transmission or reflectance
General chemicals	Powders	Reflectance	Reflectance
Specialised products	Powders	Reflectance	Reflectance
General chemicals	Solids	Reflectance	Reflectance
Plastics & polymers	Solids	Reflectance	Reflectance
Polymer products	Solids	Reflectance	Reflectance
Specialised products	Solids	Reflectance	Reflectance
Environmental	Solids	Reflectance	
Pharmaceutical products & development	Solids	Reflectance	Reflectance
Packaging	Solids	Reflectance	Reflectance

Refinery production - Separate examples of the use of immersion MIR<sup>28</sup> and NIR<sup>5</sup> probes for the analysis and characterisation of crude products are given in the literature. Dearing *et al.*<sup>28</sup> described the use of ATR MIR immersion probes to characterise crude oil products using data fusion of process techniques. Although ATR MIR spectrometry was successfully used in the characterisation by data fusion, errors were introduced into the model due to the inability of IR to capture the variations for the higher boiling fractions. Falla *et al.*<sup>5</sup> used a NIR transmission immersion probe for the rapid estimation of the simulated distillation properties of crude petroleum. In refinery production the general sample types are gases and liquids; transmission infrared spectrometry would be the appropriate technique for gas sample analysis, while the possibility of transmission or ATR techniques could be used for any liquid samples. This application area has some potential for either MIR or NIR spectrometry, each useful in different ways. As the NIR spectra would be dominated by CH components in the samples it would be useful for high concentration analysis. For some samples, e.g. blending, MIR analysis could be beneficial by providing additional functional group capability when monitoring specific compounds. In-line probes seem to have potential scope for the analysis of refinery production samples. There are, however, some issues with compatibility of the probes with the physical form of the samples as some material may be very viscous. Also, probe fouling could be an issue.

Fuels - A comparative study of diesel analysis by FTIR, FTNIR and FT-Raman spectroscopy completed by Santos *et al.*<sup>29</sup> explained the use of an immersion transmittance accessory for FTNIR analysis and an ATR cell and ATR immersion probe for FTIR analysis. The results indicated that the use of a conventional ATR cell, instead of an immersion probe, was preferable even though it was more time consuming due to cell cleaning and sample exchanges. One reason was due to the spectral regions selected for the modelling: the region below 1000 cm<sup>-1</sup> was shown to be significant for modelling diesel, but was only accessible using the conventional ATR cell and not the ATR probe, because of fibre limitations. Santos *et al.*<sup>29</sup> discussed the issues surrounding MIR spectroscopy as an analysis tool for fuels, however, examples for fuel quality control have been reported. A study on the

prediction of the properties of diesel/biodiesel blends by NIR and MIR spectroscopy was completed by de Fátima Bezerra de Lira *et al.*;<sup>30</sup> spectra were acquired in the NIR region using a quartz flow cell and in the MIR region using an ATR probe. The results indicated that each of the NIR and MIR models could be used individually to predict the distillation temperatures and sulfur content, while NIR spectroscopy was favoured for the prediction of density in the blend samples.

Speciality gas products - Generally most applications involve the use of a gas cell for the IR measurement.<sup>31, 32</sup> However, there is an example, described by Laviolette *et al.*,<sup>33</sup> where an *in situ* MIR transmission probe was used to measure simultaneously the solids volume fraction and gaseous species composition in a gas – solid system. In this study, the *in situ* probe was inserted into a fluidized bed, where absorbance spectra were acquired to analyse the molar fraction of a tracer gas in the emulsion and bubble phases of gas tracer experiments. Several limitations of the use of the MIR fibre-optic probe were discussed by the authors: the fibre probe was limited to ambient temperature due to the nature of fluoride glass used in the fibre optics; the measurement was limited by the modulation frequency; and the IR beam must be of the highest possible signal-to-noise ratio. Although there were limitations, many of these could possibly be overcome with the use of more modern spectrometers and fibre-optic probes other than the ones used in the study. The research discussed by Laviolette *et al.* has shown the possibility for MIR transmission spectrometry for gas phase monitoring *in situ*.

Combustion gases – An example by Stec *et al.*<sup>34</sup> described the use of an FTIR spectrometer - gas cell set up for the on-line quantification of gaseous fire effluents that contain mixtures of components, where different procedures for calibrating the system were investigated. FTIR was investigated for the analysis of fire gases as it had the potential to identify and quantify a large number of chemical species over short time periods, which was not easily attainable with other measurements which are made off-line on standard physical fire models, known as fire tests. There is no real application for the use of probe analysis in this area; multi-pass gas cell monitoring in the transmission mode will give better results.

Ambient air monitoring – Most commonly, samples taken in this application area are analysed using multi-pass gas cells in the MIR region;<sup>35-37</sup> either through use of static gas fills where the cell is filled with sample, analysed and then the cell is emptied before the new sample fills the cell, or through a continuous flow of sample passed through the cell. Transmission NIR spectroscopy could be used for monitoring major components in the sample; however, there is little use for *in situ* infrared measurements.

Aerosol products - The propellant gas consists of two different sample types, namely droplets and particles. Analysis of the direct composition of the aerosol samples would be difficult. Nasibulin *et al.*<sup>38</sup> described the use of FTIR using an on-line gas analyser and other techniques to analyse the aerosol products and decomposition of ferrocene vapour that are used in the formation of carbon nanotubes. However, FTIR was only used to analyse gaseous products in a gas analyser after the aerosol particles had first been removed.

Refrigeration - This application area would give rise mainly to gaseous samples with measurement being made in the transmission mode for the NIR and MIR regions, with perhaps more application being seen for the MIR region. There is not much scope here for *in situ* infrared analysis.

Semiconductors - Semiconductor applications will require gas composition analysis, so MIR spectrometry using a gas transmission cell may be useful. Specialist cells would be required to give multiple paths for gases unless the sample was a concentrated gas and the analyte was the main component rather than the trace component. Substrate analysis for contaminants by reflectance NIR could be difficult depending on the levels that are required to be quantified.

Plastics and polymers – Several studies of plastics and polymer samples analysed by infrared spectrometry have been reported.<sup>39-42</sup> However, some of the research, for example by Ghebremeskel<sup>40</sup> has been completed off-line when analysing cast

polymer films to study the interactions of polymer blends. Conversely, Fischer *et al.*<sup>39</sup> described the use of NIR spectroscopy for the continuous monitoring of extrusion processes of polymers. The study included the use of both transmission and diffuse reflection NIR spectroscopy to quantify the composition of polymer blends and the content of filler in polymer matrices. In-line NIR transmission spectrometry was used to monitor the transparent systems to measure the copolymer in the melt and off-line NIR reflectance spectroscopy was used for the quantification of the non-transparent filler chalk samples. NIR spectroscopy was chosen by Fischer *et al.* as it allowed in-line real-time quantitative analysis; the lack of stability and high energy losses of MIR optical fibre probes at the time of this research meant that this technique was discounted. The authors touched on previous work with an in-line ATR MIR system; however, they stated that careful consideration of the wetting and adhesion processes between the polymer melt and the ATR crystal is needed for accurate quantification. Shield and Ghebremeskel<sup>41</sup> illustrated the use of MIR and NIR spectroscopy to study and characterise blends of copolymers. In this research, NIR measurements were made *in situ* with a diffuse reflectance fibre optic probe, however, the MIR measurements, used to monitor the absorbance of the characteristic components as a function of concentration, were acquired off-line by either pressing thin films of material and mounting them on an IR card for analysis or placing some material directly on the ATR crystal and applying some pressure. The combination of off-line ATR-FTIR and in-line NIR spectrometry was used to determine accurately the polymer composition of the elastoblends, however, due to the viscosity of the samples it would be difficult to use in-line measurements of MIR. Even so, there have been some applications of in-line ATR MIR spectrometry for monitoring of copolymerization reactions.<sup>43-45</sup> In these studies the resultant copolymer was analysed off-line.

Polymer products - Dumitrescu *et al.*<sup>46</sup> described a set up of two NIR optical fibre probes which were attached to the injection moulding machine and connected to a FTIR spectrometer. The set up allowed the in-line process monitoring of the material as it was passing through the injection moulder. The preliminary results indicated the potential to detect different materials and the moisture of the materials. Other

examples of spectrometric analysis of polymer products have been reported. For example, Mirschel *et al.*<sup>47</sup> described the use of NIR reflection spectroscopy to analyse the coating thickness of UV-cured acrylate coatings. Witschnigg *et al.*<sup>48</sup> discussed the use of NIR spectroscopy for the in-line characterisation of nanocomposite materials. This research indicated good correlation between the Young's Modulus, the layer distance and the drawing force with the NIR spectra and PLS algorithms.

Food products – This is an application area where NIR measurements have been well used,<sup>1, 49</sup> and there may be some analysis where MIR spectrometry may be applicable. An area that has seen extensive research using off-line NIR measurements is the analysis of wine products and fermentations by Cozzolino *et al.*<sup>50-56</sup> This area is also being researched for analysis by MIR spectrometry, with reports on the analysis of wines by off-line<sup>57</sup> and flow-through cell<sup>58</sup> absorption measurements. The research into the analysis of beverages using MIR and NIR spectrometry is widespread and as such Cozzolino and Damberg<sup>59</sup> presented a chapter detailing the application of the techniques at different steps in the production of beer and wine. Research has also progressed in the analysis of whisky by NIR and MIR spectrometry; a review of the literature in this area can be found in chapter 6. A feasibility study of off-line NIR and MIR analysis of soft cheeses was completed by Karoui *et al.*,<sup>60</sup> showing the possible use of NIR spectrometry for bulk content analysis of total nitrogen and MIR spectrometry for the determination of fat content. This shows there are some applications where a probe that features a combination of the two techniques could be useful. Examples of in-line diffuse reflectance NIR probes for analysis of solid food products occur in the literature: Collell *et al.*<sup>61</sup> described the use of a diffuse reflectance NIR probe to predict the moisture and salt content of fermented pork sausages and Berardinelli *et al.*<sup>62</sup> characterised apricots using a NIR diffuse reflectance probe. Kupper *et al.*<sup>63</sup> described the use of an in-line ATR MIR immersion probe for the authentication and quantification of extra virgin olive oils. Flavours, fragrances and fermentation processes have the potential to be analysed using a combination of NIR and MIR spectrometry. Fermentation samples can originate from food product applications<sup>52, 64</sup> as well as other bioprocess

reactions<sup>10, 65-67</sup> and bioethanol production.<sup>68</sup> There are many examples in the literature where NIR<sup>4, 52, 65, 68, 69</sup> and MIR<sup>7, 8, 10, 66, 70-73</sup> spectrometry have been used successfully for in-line fermentation analysis.

Oils and lubricants – Many examples of this application area in the literature are off-line measurements of oil and lubricant products. Both NIR and MIR spectrometry have been used to quantify the moisture levels in samples;<sup>74-76</sup> MIR spectrometry has also been routinely used for the analysis of oils and lubricants to determine service condition<sup>77-81</sup> and oxidation products.<sup>82, 83</sup>

Solvents - Solvent analysis by MIR spectrometry can be used for compositional monitoring especially of mixtures and for detecting impurities. Some regions can potentially be identified for specific measurements using limited range customised instruments. It is concluded, however, that there would be limited applicability for a combined NIR – MIR probe in this application area.

General chemicals – Solid sample analysis would be hard to achieve using ATR MIR or transmission NIR probes. However reflectance probes for each of the wavelength regions have greater potential for analysis of solid materials. The use of non-invasive or in some cases insertion probes would be suitable for powder samples.

Chemical reaction monitoring - Currently there are many examples in the literature of the use of *in situ* MIR<sup>14, 17, 84-88</sup> or NIR<sup>15, 69, 89-91</sup> spectrometry for the monitoring of chemical reactions. An example where both MIR and NIR spectrometry have been used *in situ* to monitor the same reaction was described by Amari and Ozaki.<sup>92</sup> In their study, an ATR MIR probe and a NIR transmission probe were immersed into the solution in the reaction vessel to monitor the initial oligomerization of Bis(hydroxyethyl terephthalate). ATR MIR spectrometry was used to monitor the OH end groups and the free ethylene glycol, parameters that can aid the understanding of polymerisation. NIR spectrometry was also used with some success to predict the OH end groups and free ethylene glycol. Acquiring data with MIR and NIR spectrometry simultaneously and using 2D correlations, information relating to

the polymerisation and the amount of water in the reaction could be determined. As water has the potential for side reactions such as hydrolysis in an oligomerization reaction and the understanding of the polymerisation of the reaction is important, the combination of MIR and NIR spectrometry could be valuable in reaction monitoring of this kind. MIR spectrometry has advantages over NIR spectrometry for analysing functional groups of liquid processes.

Consumer products - There are currently measurements to determine surfactants and chelating agents of liquid detergents and soaps by off-line MIR spectrometry, incorporating ATR cells.<sup>93-95</sup> Ventura-Gayete *et al.*<sup>93</sup> developed a fully mechanised procedure implementing an ATR MIR flow through accessory for the determination of sodium alpha-olefin sulfonate, an ionic surfactant widely used in liquid detergent formulations. Utilisation of this procedure allowed the analysis to be less expensive with greater flexibility for the determination of surfactants. Ventura-Gayete *et al.*<sup>94</sup> also assessed the use of ATR MIR spectrometry for the determination of chelating agents in liquid detergents. In this study they described the possibility of ATR MIR probes for quality control measurements. The use of an in-line ATR MIR immersion probe has the potential to improve this analysis further by allowing simpler analysis and cleaning procedures.

Specialised products – This application area includes water treatment products, dyes and pigments, textiles, pulp and paper and also agrochemicals. Samples for this application area are mainly solids and liquids taken during production. Barton *et al.*<sup>96</sup> described the use of off-line NIR reflectance measurements to analyse the fibre content in flax stems; in contrast to previous research, the authors analysed the flax stems when they were intact allowing the analysis process to be more efficient. Canals *et al.*<sup>97</sup> determined the practicality of using in-line NIR and off-line MIR measurements in the characterisation of paper finishes. The samples were successfully classified using either the NIR or MIR spectra. However, as the NIR radiation penetrates deeper into the paper surface than does MIR radiation, information about the paper matrix interferes with information about the paper finish, therefore extra care needs to be taken when processing the spectra and building

models with the NIR data. Moros *et al.*<sup>98</sup> discussed the applicability of MIR and NIR spectrometry for the quality control of agrochemical formulations and noted that NIR spectrometry has been used to a lesser degree. Therefore, they developed and compared an off-line transmission NIR method to a procedure that used flow-through transmission MIR measurements for the quality control of pesticides in agrochemicals. Both procedures were able to generate comparable results to those obtained with the HPLC reference method. The spectrometric procedures had advantages over the HPLC method in increasing the sample throughput and reducing the volume of organic solvent required for the analysis.

Environmental - There are examples describing the use of MIR spectrometry for the analysis of soil samples.<sup>99-103</sup> For solid samples, such as soils, reflectance measurements are widely used. Vohra *et al.*<sup>102</sup> describe a remote MIR reflection detection method for measuring organic contaminants in soil samples; the method was able to detect trace amounts of the chlorinated hydrocarbon trichloroethylene. Reeves<sup>103</sup> compares the use of NIR and MIR reflectance methods in a review of the routine analysis of soil samples in the laboratory and on-site. For liquid samples, ATR MIR measurements are more useful and many applications have been reported. Pejcic *et al.*<sup>104</sup> reviewed the use of MIR spectrometry for analysis of organic pollutants in aqueous environments and found that ATR MIR spectrometry had greater selectivity over other technologies and could be routinely used to screen a wide range of compounds and contaminants. A novel ATR-FTIR sensor was developed by Acha *et al.*<sup>105</sup> to measure non-invasively the concentration of chlorinated species in the aqueous effluent of a de-chlorinating bioreactor. NIR analysis will not contribute a lot of information to sample analysis. There may be sensitivity issues around ATR MIR spectrometry which could limit opportunities for certain sample types.

Pharmaceutical products and development – NIR spectrometry has been widely used to analyse development samples and products for a number of years, leading to a number of reviews of the application of NIR spectrometry in the pharmaceutical industry.<sup>2, 19, 106</sup> NIR spectrometry has been used successfully in the monitoring of

powder blending processes,<sup>16, 107</sup> to gain understanding of high shear granulation processes,<sup>108</sup> and to monitor content uniformity of pharmaceutical tablets.<sup>109, 110</sup> MIR analysis is also widely used in pharmaceutical product and development applications with examples arising for the on-line monitoring of batch cooling crystallisations<sup>85</sup> and chemical imaging of pharmaceutical tablets.<sup>111</sup> Druy<sup>112</sup> described some of the applications for MIR spectrometry for the pharmaceutical process environment. Also, Févotte<sup>113</sup> outlined the use of MIR and NIR spectrometry for *in situ* monitoring of pharmaceutical crystallisation processes.

Packaging - Identification of plastics and films using MIR and NIR<sup>114</sup> spectrometry is possible. An example of ATR-FTIR imaging was described by van Dalen *et al.*<sup>115</sup> to identify and locate different layers in multilayer plastic packaging material. NIR reflectance measurements were used by Feldhoff *et al.*<sup>116</sup> for the on-line monitoring and identification of waste consumer packaging. The NIR reflectance set up allowed the collection of NIR spectra of waste packaging materials located on an industrial conveyer belt when the belt is moving at 1 m/s. With the use of a decision algorithm a distinction could be made between packaging of polyethyleneterephthalate (PET), polystyrene (PS) or polyvinylchloride (PVC) and cardboard beverage containers; although, some misclassifications were observed for products of polyethelene (PE) and polypropylene (PP). Improvements suggested by the authors could allow on-line monitoring by NIR spectrometry of waste consumer packaging with the conveyer belt at a speed of 2 m/s.

### 3.3 Conclusions

The review of the literature has demonstrated that there are numerous examples where in-line MIR or NIR probes have been implemented or could provide benefits if used for process analysis. However, some applications are more suited to using gas cells for process monitoring, for example analyses involving combustion gases, speciality gas products, ambient air monitoring and semiconductors. Aerosol products could potentially be analysed by transmission infrared spectrometry, however, the possibility of reflection and lots of scattering at the particle interface could lead to complicated measurements. Analysis is best completed after the aerosol particles are first removed. The issues surrounding the analysis of direct samples, suggests that in-line analysis would be difficult.

There are some areas where use of combined probes could be beneficial such as the combination of ATR MIR and transmission NIR spectrometry. For refinery production there is potential scope for a combination probe where the NIR transmission mode is used for major component analysis and the ATR MIR mode for minor component analysis. There are, however, some issues with compatibility of the probes with the physical form of the samples as some material may be very viscous. Fuel samples in general tend to be less viscous and therefore insertion probes may be more compatible. NIR transmission spectrometry would be useful for the calculation of octane numbers for the bulk components and MIR spectrometry may have some potential in limited wavenumber ranges for analysis of additives present in the samples. The application area of food products (including fermentation processes) already utilises in-line NIR and MIR spectrometry a great deal, however, there could be some benefits from the use of a combined ATR MIR and transmission NIR probe for the analysis of liquid samples. There may even be some advantages in combining (fusing) the MIR and NIR data as well, especially for fermentation samples. The combination of NIR spectrometry for the analysis of bulk components and MIR spectrometry to analyse additives or impurities could also be beneficial within the oil and lubricants area, similarly, there is also an opportunity for the analysis of liquid samples in the general chemical area. Another area where this type of combined probe could have some benefits is in chemical reaction monitoring. A combined

probe could allow the product formation to be monitored by NIR spectrometry and use MIR spectrometry to monitor specific compounds (e.g. intermediates or by-products) to allow more information about reaction mechanisms. For monitoring of heterogeneous reactions where the liquid contains small amounts of particulate material, measurements using a combined probe could be useful. For example, MIR spectra could be useful for the de-convolution of contributions of scattering and absorption while NIR spectrometry could be used for the analysis of bulk samples. In the area of consumer products, in-line MIR spectrometry may be useful for the analysis of complex blends of liquid samples. However, there may be some applications for use of a combined probe; where NIR spectrometry could analyse the bulk components and MIR spectrometry could monitor trace components. Pharmaceutical products and development and speciality products could also be areas where the use of a combined ATR MIR – transmission NIR probe could be of benefit in process monitoring.

Another type of combined probe that may provide some potential benefit is a MIR – NIR reflectance probe, which would be particularly useful for analysing viscous liquids and solids samples. Production samples of plastics and polymers tend to be very viscous or even solid materials, so insertion probes will be of limited use for analysis. Some assessment would be required to determine if a combination of non-invasive reflection measurements of NIR and MIR spectra, over NIR measurements alone, gives some benefits in the analysis of copolymer samples, polymer melts and polymer blends. Some of the comments on monitoring of plastic and polymer applications are also appropriate to polymer products. Solid polymer production would be best studied through reflection measurements, whereas NIR transmission measurements could possibly be used for flow-through measurements of molten material. A combined reflectance probe may be more appropriate for the analysis of viscous liquids and solids samples from the food products area, such as dairy products, oils and fats. There may also be some opportunity for a combined probe in reflectance mode for solid or powder general chemical samples. Solid samples of speciality products are most likely to be monitored using non-invasive reflectance measurements; however, in this area the majority of analysis would be

made using NIR spectrometry rather than MIR spectrometry. Conversely, the area of pharmaceutical products and development could be beneficial for composition monitoring; NIR spectrometry would be useful for blend control and major component analysis of tablets and powders and MIR spectrometry would be used for monitoring minor components. Packaging samples are essentially solid materials which require reflection measurements, with specific compounds and additives being analysed by MIR spectrometry and NIR spectrometry being used to monitor the process.

From the assessment of the literature and evaluation of application opportunities, it is apparent that development in probe technology would be beneficial in many areas of process analysis. The research described in this project focussed mainly on developments in ATR-MIR probe design and opportunities. However, the analysis of application areas has provided Fibre Photonics with incentives to develop combined NIR – MIR probes that could extend their product range. One of the areas where a combined probe could be useful is in fermentation monitoring and a preliminary evaluation of the possible benefits in this area has been included in the research programme.

### 3.4 References

1. H. Huang, H. Yu, H. Xu and Y. Ying, *J. Food Eng.*, 2008, **87**, 303-313.
2. Y. Roggo, P. Chalus, L. Maurer, C. Lema-Martinez, A. Edmond and N. Jent, *J. Pharmaceut. Biomed.*, 2007, **44**, 683-700.
3. M. Andre, *Anal. Chem.*, 2003, **75**, 3460-3467.
4. S. A. Arnold, R. Gaensakoo, L. M. Harvey and B. McNeil, *Biotechnol. Bioeng.*, 2002, **80**, 405-413.
5. F. S. Falla, C. Larini, G. A. C. Le Roux, F. H. Quina, L. F. L. Moro and C. A. O. Nascimento, *J Petrol Sci Eng*, 2006, **51**, 127-137.
6. A. Ring, V. Schreiner, H. Wenck, K. P. Wittern, L. Kupper and R. Keyhani, *Skin Res. Technol.*, 2006, **12**, 18-23.
7. M. R. Dadd, D. C. A. Sharp, A. J. Pettman and C. J. Knowles, *J. Microbiol. Methods*, 2000, **41**, 69-75.
8. H. M. Heise, L. Kupper and L. N. Butvina, *Spectroc. Acta Pt. B-Atom. Spectr.*, 2002, **57**, 1649-1663.
9. W. Plugge and C. van der Vlies, *J. Pharmaceut. Biomed.*, 1996, **14**, 891-898.
10. J. Schenk, I. W. Marison and U. von Stockar, *J. Biotechnol.*, 2007, **128**, 344-353.
11. N. Petersen, P. Ödman, A. Cervera, S. Stocks, A. E. Lantz and K. Gernaey, *New Biotechnol.*, 2009, **25S**, S208.
12. A. González-Vara y R., G. Vaccari, E. Dosi, A. Trilli, M. Rossi and D. Matteuzzi, *Biotechnol. Bioeng.*, 2000, **67**, 147-156.
13. E. Petiot, P. Bernard-Moulin, T. Magadoux, C. Gény, H. Pinton and A. Marc, *Process Biochem.*, 2010, **45**, 1832-1836.
14. C. McGill, R. Ferguson, K. Donoghue, A. Nordon and D. Littlejohn, *Analyst*, 2003, **128**, 1467-1470.
15. C. A. McGill, A. Nordon and D. Littlejohn, *Analyst*, 2002, **127**, 287-292.
16. D. J. Wargo and J. K. Drennen, *J. Pharmaceut. Biomed.*, 1996, **14**, 1415-1423.
17. T. Amari and Y. Ozaki, *Macromolecules*, 2001, **34**, 7459-7462.
18. M. Blanco, M. Sánchez and M. Alcalà, *Anal. Bioanal. Chem.*, 2010, **397**, 3575-3579.
19. B. Swarbrick, *Vib. Spectrosc*, 2007, **44**, 171-178.
20. N. Petersen, P. Ödman, A. E. C. Padrell, S. Stocks, A. E. Lantz and K. V. Gernaey, *Biotechnol. Progr.*, 2010, **26**, 263-271.
21. H. Yang, B. Kuang and A. M. Mouazen, *Appl. Spectrosc.*, 2011, **65**, 931-938.
22. H. A. Hassan Refat, *Forensic Sci. Int.*, 2011, **206**, 87-91.
23. M. Suda, Y. Takei, Y. Aoyama, K. Narita, T. Sato, M. Fukuda and M. Mikuni, *Neuropsychologia*, 2010, **48**, 441-447.
24. D. Qin and G. Cadet, *Anal. Chem.*, 1997, **69**, 1942-1945.
25. P. Barrett, B. Smith, J. Worlitschek, V. Bracken, B. O'Sullivan and D. O'Grady, *Org. Process Res. Dev.*, 2005, **9**, 348-355.
26. M. T. Bona and J. M. Andres, *Talanta*, 2008, **74**, 998-1007.
27. J. P. Coates, in *Process Analytical Technology*, ed. K. A. Bakeev, Blackwell Publishing, Oxford, 2005.
28. T. I. Dearing, W. J. Thompson, C. E. Rechsteiner and B. J. Marquardt, *Appl. Spectrosc.*, 2011, **65**, 181-186.

29. V. O. Santos, F. C. C. Oliveira, D. G. Lima, A. C. Petry, E. Garcia, P. A. Z. Suarez and J. C. Rubim, *Anal. Chim. Acta*, 2005, **547**, 188-196.
30. L. de Fátima Bezerra de Lira, F. V. C. de Vasconcelos, C. F. Pereira, A. P. S. Paim, L. Stragevitch and M. F. Pimentel, *Fuel*, 2010, **89**, 405-409.
31. A. McFarlane, L. McMillan, I. Silverwood, N. G. Hamilton, D. Siegel, S. F. Parker, D. T. Lundie and D. Lennon, *Catal. Today*, 2010, **155**, 206-213.
32. M. Hundt, P. Sadler, I. Levchenko, M. Wolter, H. Kersten and K. Ostrikov, *J. Appl. Phys.*, 2011, **109**.
33. J.-P. Laviolette, G. S. Patience and J. Chaouki, *AIChE J.*, 2010, **56**, 2850-2859.
34. A. A. Stec, P. Fardell, P. Blomqvist, L. Bustamante-Valencia, L. Saragoza and E. Guillaume, *Fire Safety J.*, 2011, **46**, 225-233.
35. P. Maddaloni, P. Malara, G. Gagliardi and P. De Natale, *Appl. Phys. B-Lasers Opt.*, 2006, **85**, 219-222.
36. M. Grutter, *Atmosfera*, 2003, **16**, 1-13.
37. A. Cantu, G. Pophal, S. Hall and C. T. Laush, *Appl. Phys. B-Lasers Opt.*, 1998, **67**, 493-496.
38. A. G. Nasibulin, S. D. Shandakov, A. S. Anisimov, D. Gonzalez, H. Jiang, M. Pudas, P. Queipo and E. I. Kauppinen, *J. Phys. Chem. C*, 2008, **112**, 5762-5769.
39. D. Fischer, T. Bayer, K. J. Eichhorn and M. Otto, *Fresenius J. Anal. Chem.*, 1997, **359**, 74-77.
40. Y. Ghebremeskel, J. Fields and A. Garton, *J. Polym. Sci. Pol. Phys.*, 1994, **32**, 383-386.
41. S. R. Shield and G. N. Ghebremeskel, *J. Appl. Polym. Sci.*, 2003, **88**, 1653-1658.
42. G. George, N. Hynard, G. Cash, L. Rintoul and M. O'Shea, *Comptes Rendus Chimie*, **9**, 1433-1443.
43. Y. Stavropoulos, O. Kammona, E. G. Chatzi and C. Kiparissides, *J. Appl. Polym. Sci.*, 2001, **82**, 1776-1787.
44. J.-w. Zhao, H. Zhu, Y.-x. Wu, R. Jian and G.-y. Wu, *Chin. J. Polym. Sci.*, 2010, **28**, 385-393.
45. E. G. Chatzi, O. Kammona and C. Kiparissides, *J. Appl. Polym. Sci.*, 1997, **63**, 799-809.
46. O. R. Dumitrescu, D. C. Baker, G. M. Foster and K. E. Evans, *Polym. Test.*, 2005, **24**, 367-375.
47. G. Mirschel, K. Heymann and T. Scherzer, *Anal. Chem.*, 2010, **82**, 8088-8094.
48. A. Witschnigg, S. Laske, M. Kracalik, M. Feuchter, G. Pinter, G. Maier, W. Märzinger, M. Haberkorn, G. R. Langecker and C. Holzer, *J. Appl. Polym. Sci.*, 2010, **117**, 3047-3053.
49. I. González-Martín and J. M. Hernández-Hierro, *Talanta*, 2008, **76**, 1130-1135.
50. D. Cozzolino, W. Cynkar, N. Shah and P. Smith, *Comput. Electron. Agr.*, 2011, **77**, 81-85.
51. D. Cozzolino, M. J. Kwiatkowski, M. Parker, W. U. Cynkar, R. G. Dambergs, M. Gishen and M. J. Herderich, *Anal. Chim. Acta*, 2004, **513**, 73-80.

52. D. Cozzolino, M. Parker, R. G. Damberg, M. Herderich and M. Gishen, *Biotechnol. Bioeng.*, 2006, **95**, 1101-1107.
53. D. Cozzolino, H. E. Smyth and M. Gishen, *J. Agric. Food. Chem.*, 2003, **51**, 7703-7708.
54. D. Cozzolino, H. E. Smyth, K. A. Lattey, W. Cynkar, L. Janik, R. G. Damberg, I. L. Francis and M. Gishen, *Anal. Chim. Acta*, 2005, **539**, 341-348.
55. L. Liu, D. Cozzolino, W. U. Cynkar, R. G. Damberg, L. Janik, B. K. O'Neill, C. B. Colby and M. Gishen, *Food Chem.*, 2008, **106**, 781-786.
56. L. Liu, D. Cozzolino, W. U. Cynkar, M. Gishen and C. B. Colby, *J. Agric. Food. Chem.*, 2006, **54**, 6754-6759.
57. D. Cozzolino, M. Holdstock, R. Damberg, W. Cynkar and P. Smith, *Food Chem.*, 2009, **116**, 761-765.
58. C. D. Patz, A. Blicke, R. Ristow and H. Dietrich, *Anal. Chim. Acta*, 2004, **513**, 81-89.
59. D. Cozzolino and R. G. Damberg, in *Infrared Spectroscopy for Food Quality Analysis and Control*, Academic Press, San Diego, 2009, pp. 377-397.
60. R. Karoui, A. M. Mouazen, E. Dufour, R. Schoonheydt and J. De Baerdemaeker, *Eur. Food Res. Technol.*, 2006, **223**, 363-371.
61. C. Collell, P. Gou, P. Picouet, J. Arnau and J. Comaposada, *Meat Sci.*, 2010, **85**, 325-330.
62. A. Berardinelli, C. Cevoli, F. A. Silaghi, A. Fabbri, L. Ragni, A. Giunchi and D. Bassi, *J. Food Sci.*, 2010, **75**, E462-E468.
63. L. Küpper, H. M. Heise, P. Lampen, A. N. Davies and P. McIntyre, *Appl. Spectrosc.*, 2001, **55**, 563-570.
64. T. Yano, T. Aimi, Y. Nakano and M. Tamai, *J. Ferment. Bioeng.*, 1997, **84**, 461-465.
65. P. Roychoudhury, R. O'Kennedy, B. McNeil and L. M. Harvey, *Anal. Chim. Acta*, 2007, **590**, 110-117.
66. J. Schenk, I. W. Marison and U. von Stockar, *Anal. Chim. Acta*, 2007, **591**, 132-140.
67. S. Sivakesava, J. Irudayaraj and A. Demirci, *J. Ind. Microbiol. Biotechnol.*, 2001, **26**, 185-190.
68. B. Liebmann, A. Friedl and K. Varmuza, *Anal. Chim. Acta*, 2009, **642**, 171-178.
69. A. Nordon, D. Littlejohn, A. S. Dann, P. A. Jeffkins, M. D. Richardson and S. L. Stimpson, *Analyst*, 2008, **133**, 660-666.
70. G. Mazarevica, J. Diewok, J. R. Baena, E. Rosenberg and B. Lendl, *Appl. Spectrosc.*, 2004, **58**, 804-810.
71. D. L. Doak and J. A. Phillips, *Biotechnol. Progr.*, 1999, **15**, 529-539.
72. J. Schenk, C. Viscasillas, I. W. Marison and U. von Stockar, *J. Biotechnol.*, 2008, **134**, 93-102.
73. P. Roychoudhury, L. M. Harvey and B. McNeil, *Anal. Chim. Acta*, 2006, **571**, 159-166.
74. F. R. van de Voort, J. Sedman, R. Cocciardi and S. Juneau, *Talanta*, 2007, **72**, 289-295.
75. M. Blanco, J. Coello, H. Iturriaga, S. MasPOCH and R. González, *Mikrochim. Acta*, 1998, **128**, 235-239.

76. E.-P. Ng and S. Mintova, *Microchem. J.*, 2011, **98**, 177-185.
77. M. P. Zakharich, I. I. Zaitsev, V. P. Komar, F. N. Nikonovich, M. P. Ryzhkov and I. V. Skorniyakov, *J. Appl. Spectrosc.*, 2001, **68**, 61-65.
78. F. R. Van De Voort, J. Sedman, R. A. Cocciardi and D. Pinchuk, *Tribol. T.*, 2006, **49**, 410-418.
79. M. J. Adams, M. J. Romeo and P. Rawson, *Talanta*, 2007, **73**, 629-634.
80. A. R. Caneca, M. F. Pimentel, R. K. H. Galvão, C. E. da Matta, F. R. de Carvalho, I. M. Raimundo Jr, C. Pasquini and J. J. R. Rohwedder, *Talanta*, 2006, **70**, 344-352.
81. M. A. Al-Ghouti and L. Al-Atoum, *J. Environ. Manage.*, 2009, **90**, 187-195.
82. N. Gracia, S. Thomas, P. Bazin, L. Duponchel, F. Thibault-Starzyk and O. Lerasle, *Catal. Today*, 2010, **155**, 255-260.
83. A. Georgiev, I. Karamancheva and L. Topalova, *J. Mol. Struct.*, 2008, **872**, 18-23.
84. M. Hofmann, J. E. Puskas and K. Weiss, *Eur. Polym. J.*, 2002, **38**, 19-24.
85. Z.-P. Chen, J. Morris, A. Borissova, S. Khan, T. Mahmud, R. Penchev and K. J. Roberts, *Chemom. Intell. Lab. Syst.*, 2009, **96**, 49-58.
86. L. Kupper, H. M. Heise and L. N. Butvina, *J. Mol. Struct.*, 2001, **563**, 173-181.
87. W. R. Moser, J. R. Berard, P. J. Melling and R. J. Burger, *Appl. Spectrosc.*, 1992, **46**, 1105-1112.
88. P. MacLaurin, N. C. Crabb, I. Wells, P. J. Worsfold and D. Coombs, *Anal. Chem.*, 1996, **68**, 1116-1123.
89. P. A. Bird, D. C. A. Sharp and J. M. Woodley, *Org. Process Res. Dev.*, 2002, **6**, 569-576.
90. C. Coffey, B. E. Cooley and D. S. Walker, *Anal. Chim. Acta*, 1999, **395**, 335-341.
91. C. P. Beyers, H. F. M. Boelens, L. Klumperman and J. A. Westerhuis, *Appl. Spectrosc.*, 2004, **58**, 863-869.
92. T. Amari and Y. Ozaki, *Macromolecules*, 2002, **35**, 8020-8028.
93. J. F. Ventura-Gayete, B. F. Reis, S. Garrigues, Á. Morales-Rubio and M. de la Guardia, *Microchem. J.*, 2004, **78**, 47-54.
94. J. F. Ventura-Gayete, M. de la Guardia and S. Garrigues, *Talanta*, 2006, **70**, 870-875.
95. L. Carolei and I. G. R. Gutz, *Talanta*, 2005, **66**, 118-124.
96. F. E. Barton, D. E. Akin, W. H. Morrison, A. Ulrich and D. D. Archibald, *J. Agric. Food. Chem.*, 2002, **50**, 7576-7580.
97. T. Canals, J. R. Riba, R. Cantero, J. Cansino, D. Domingo and H. Iturriaga, *Talanta*, 2008, **77**, 751-757.
98. J. Moros, S. Armenta, S. Garrigues and M. de la Guardia, *Anal. Chim. Acta*, 2006, **565**, 255-260.
99. L. J. Janik, R. H. Merry, S. T. Forrester, D. M. Lanyon and A. Rawson, *Soil Sci Soc Am J*, 2007, **71**, 507-514.
100. M. Forouzangohar, R. S. Kookana, S. T. Forrester, R. J. Smernik and D. J. Chittleborough, *Environ. Sci. Technol.*, 2008, **42**, 3283-3288.
101. M. I. Ali, Q. Perveen, B. Ahmad, I. Javed, R. Razi-Ul-Hussnain, S. Andleeb, N. Atique, P. B. Ghumro, S. Ahmed and A. Hameed, *Int. J. Agric. Biol.*, 2009, **11**, 577-580.

102. S. T. Vohra, F. Bucholtz, G. M. Nau, K. J. Ewing and I. D. Aggarwal, *Appl. Spectrosc.*, 1996, **50**, 985-990.
103. J. B. Reeves Iii, *Geoderma*, 2010, **158**, 3-14.
104. B. Pejicic, M. Myers and A. Ross, *Sensors*, 2009, **9**, 6232-6253.
105. V. Acha, M. Meurens, H. Naveau and S. N. Agathos, *Biotechnol. Bioeng.*, 2000, **68**, 473-487.
106. M. Blanco, J. Coello, H. Iturriaga, S. Maspoch and C. de la Pezuela, *Analyst*, 1998, **123**, 135R-150R.
107. P. A. Hailey, P. Doherty, P. Tapsell, T. Oliver and P. K. Aldridge, *J. Pharmaceut. Biomed.*, 1996, **14**, 551-559.
108. J. Rantanen, H. Wikstrom, R. Turner and L. S. Taylor, *Anal. Chem.*, 2005, **77**, 556-563.
109. Y. Sulub, R. LoBrutto, R. Vivilecchia and B. Wabuyeale, *Vib. Spectrosc.*, 2008, **46**, 128-134.
110. Y. Sulub, R. LoBrutto, R. Vivilecchia and B. W. Wabuyeale, *Anal. Chim. Acta*, 2008, **611**, 143-150.
111. K. L. A. Chan, S. V. Hammond and S. G. Kazarian, *Anal. Chem.*, 2003, **75**, 2140-2146.
112. M. A. Druy, *Spectroscopy*, 2004, **19**, 60-63.
113. G. Févotte, *Int. J. Pharm.*, 2002, **241**, 263-278.
114. D. Garcia and M. Cibulsky, *J. Vinyl. Addit. Techn.*, 2005, **11**, 39-46.
115. G. van Dalen, P. C. M. Heussen, R. den Adel and R. B. J. Hoeve, *Appl. Spectrosc.*, 2007, **61**, 593-602.
116. R. Feldhoff, D. Wienke, K. Cammann and H. Fuchs, *Appl. Spectrosc.*, 1997, **51**, 362-368.

## 4 ATR MIR probe development

### 4.1 Introduction

#### 4.1.1 ATR MIR probes for *in situ* analysis

The advancements in *in situ* MIR spectrometry over the years have been significant and have seen this technique being successfully implemented in industry. MIR spectroscopy has not been as commonly employed as an *in situ* technique due to the limitations in optical fibres; more often NIR spectroscopy is implemented as it uses cheap silica fibres which allow a process to be monitored up to hundreds of meters away. However, MIR spectroscopy cannot make use of silica fibres as they do not transmit in this region and so special materials are required. Due to this limitation a large amount of research has been devoted to the development of both optical fibres and probe designs to increase the use of *in situ* MIR spectrometry. Chapter 2 details the different optical fibres that can be used for *in situ* infrared spectrometry and the improvements that have been made to allow greater use of MIR for *in situ* measurements. Different probe designs can be used to allow *in situ* measurements by infrared spectrometry; this research looks at the development of ATR MIR probes that couple with polycrystalline silver halide fibres.

Since the implementation of ATR probes for *in situ* analysis, various developments have been made and currently there are many manufacturers of *in situ* ATR probes for MIR spectrometry with slight differences in their design. The ATR probe design used by Fibre Photonics<sup>1, 2</sup> is adapted from a patent by Day and Poulter<sup>3</sup> which described an optical fibre probe for ATR measurements, see Figure 4.1 for a schematic of the Fibre Photonics ATR probe. The design consists of two parallel polycrystalline silver halide fibres that run from a diamond crystal tip to the end of the assembly at the sma connectors. A hastelloy bodied shaft protects the fibres and allows the fibres to be positioned at the edge of the crystal tip. The shaft is completely sealed allowing immersion into the samples for analysis. The rest of the fibre from the end of the shaft to the sma connectors is sealed in a protective conduit material. There is a split introduced to separate each fibre which allows one fibre to be attached to the source and the other to the detector. The radiation passes through

the excitation fibre connected to the source by total internal reflection to the diamond crystal tip; at the crystal the evanescent wave will interact with the sample at the sample/crystal interface where the wave will be attenuated in the regions of the spectrum at which the sample absorbs.

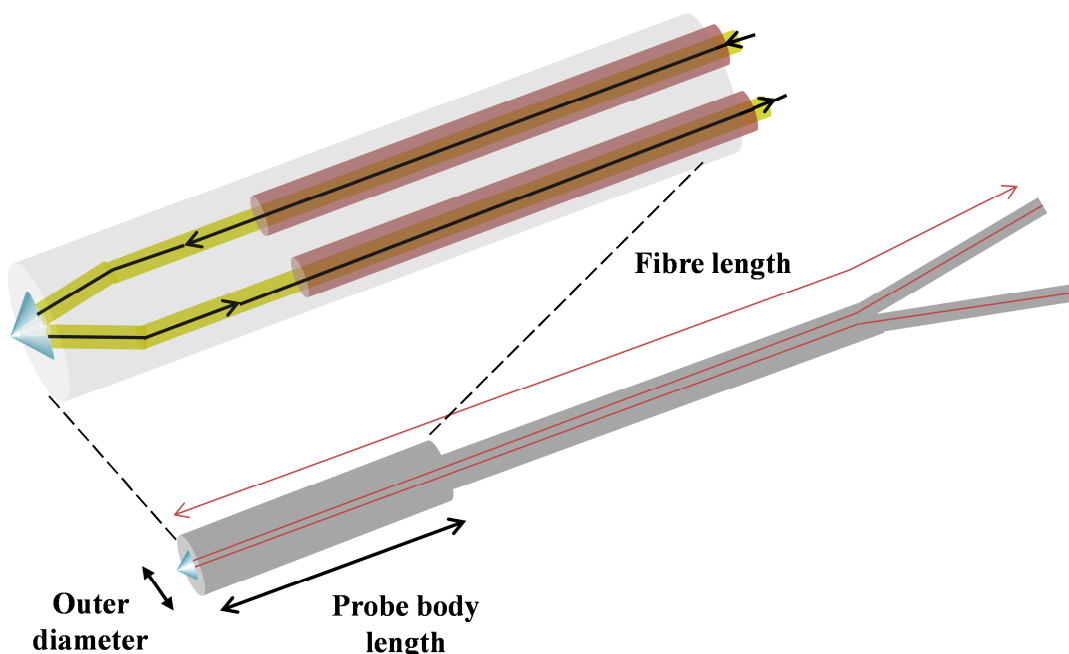
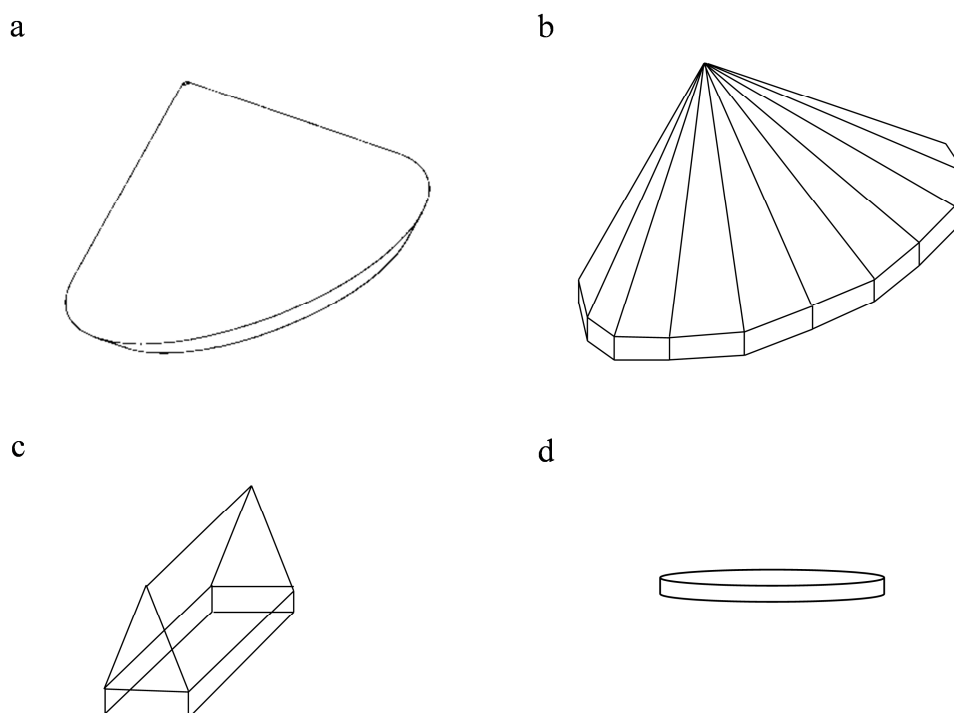


Figure 4.1: Schematic of ATR probe design adapted from information supplied by Fibre Photonics.<sup>1</sup>

Other manufacturers of ATR probes include Remspec Corporation<sup>4, 5</sup>, Bruker Optics<sup>6, 7</sup> and Mettler Toledo<sup>8</sup> and with the exception of the probe from Remspec Corporation, they appear to use a dual fibre design similar to that of Fibre Photonics. The Remspec Corporation probes differ from the other manufacturers by using fibre optic bundles in their ATR probes, detailed in a patent by Berard *et al.*<sup>5</sup> The bundle of infrared transmitting fibres is fitted next to the ATR crystal, where the radiation enters the ATR crystal from one or more excitation fibres and is reflected in the crystal and transferred to the detector through multiple collection fibres.

Each manufacturer incorporates different geometries of ATR crystal in the design of their ATR probes; Fibre Photonics uses a single face cone geometry (Figure 4.2a), Remspec Corporation uses a multiple face cone geometry (Figure 4.2b), Bruker

Optics uses a prism geometry (Figure 4.2c) and Mettler Toledo uses a disk geometry (Figure 4.2d).



**Figure 4.2: Schematics of diamond crystal geometries used in (a) Fibre Photonics, (b) Remspec Corporation, (c) Bruker Optics and (d) Mettler Toledo ATR probe designs.**

The different crystal geometries permit different numbers of reflections at the crystal interface, which will affect the pathlength and the performance of the probes. In addition, other design features can affect the performance and robustness of ATR probes and as such, there is a constant effort by probe manufacturing companies to improve their design and manufacturing procedures to produce better quality and more robust probes.

#### **4.1.2 Design features**

Design alterations can have two main impacts, firstly, to deliver better performance for the end user and secondly, to improve the cost and efficiency to manufacture the probes for the company. The make-up of the fibre optic probe is complex and there are many design features associated with the manufacture that can be altered in an attempt to improve the overall performance of the probe. Some of the design features that have been addressed by Fibre Photonics include: the fibre selection, the

geometry and size of the diamond crystal tip, the alignment of the fibres within the probe shaft, the use of modular components for manufacture of the probes, and also the implementation of a mono fibre design for smaller diameter probes. These design features are discussed in more detail below.

#### **4.1.2.1 Fibre selection**

The fibre selection can have a large impact on the performance of the final manufactured probe, where both the length of the fibre and the quality of the fibre can affect the attenuation. In general, the longer the length of the fibre the greater the potential losses of radiation will be as it travels along the length of the fibre; small losses will occur at each internal reflection within the probe. Due to the standard dual fibre design of Fibre Photonics probes, any change in the fibre length will affect both the excitation and collection fibres. For example, the difference in the total amount of fibre between a 1 m probe and a 1.5 m probe is 1 m. The quality of the fibre can also affect the performance of the probe; polycrystalline silver halide fibres are produced through an extrusion process and the spectral quality of the fibres can vary during production. In recent years, Fibre Photonics has introduced an extra step in their manufacturing process to test for the spectral quality of the output fibre from the extrusion process to determine the most suitable fibres for use in probe manufacture. The fibres can be divided into two classes, standard grade fibre and spectral grade fibre; it is spectral grade fibre which is used for the manufacture of the ATR probes. The main difference in quality between the two classes is in the attenuation characteristics; the spectral grade fibre has lower attenuation at the edges of the MIR region and, therefore, is better suited for use in ATR probes to allow better performance across the whole operating region.

#### **4.1.2.2 Seals**

Seals are inserted around the diamond crystal tip and are used to seal the probe end when the probe is fully manufactured. If the seal is fitted correctly it will create a complete seal around the diamond crystal, preventing any liquids or substances infiltrating into the inside of the probe and damaging the fibres. Different materials can be used to make the seal, however, care must be taken to ensure the quality and

ruggedness of the seal is not compromised when the entire probe is fitted together; as elevated pressures are used at this stage. Fibre Photonics found that their original seals made of polytetrafluoroethylene (PTFE) could occasionally crack under this pressure, therefore, allowing leaks to occur in the probes. In addition, a PTFE peak could be seen in the spectra of all probes manufactured with the PTFE seal. The company currently use polyether ether ketone (PEEK) seals in their manufacturing production, which have been found to be more robust and can withstand the higher pressures required during manufacture. The main advantage of this design feature change is to aid the production of more robust probes rather than increasing performance, however, it is still important to the manufacture of these probes.

#### **4.1.2.3 Geometry and size of crystal**

The design of the diamond crystal can impact on the overall performance of the probes as well as manufacturing costs. The diamond crystal tip is an expensive part of the manufacture of these ATR probes, therefore, a reduction in size can provide cost saving benefits to the company. In addition, if the geometry and size of the diamond crystal is optimised, improvements to the performance can be made. The size and geometry of the crystal tip are important in the manufacture of ATR probes as they can impact on both the angle of incidence of the radiation as well as the number of internal reflections at the crystal. When these two properties are altered it can affect the pathlength of the probe and hence the overall performance. It is, therefore, critical that when changes are made to the size and geometry of the diamond crystal tip, that they do not have a detrimental effect on the path length of the probe. Fibre Photonics originally produced probes with a 3 mm diamond cone crystal, but have since moved to a 2.4 mm diamond cone with a slight change in geometry, a schematic of the two diamond cones are given in Figure 4.3 a and b, respectively.

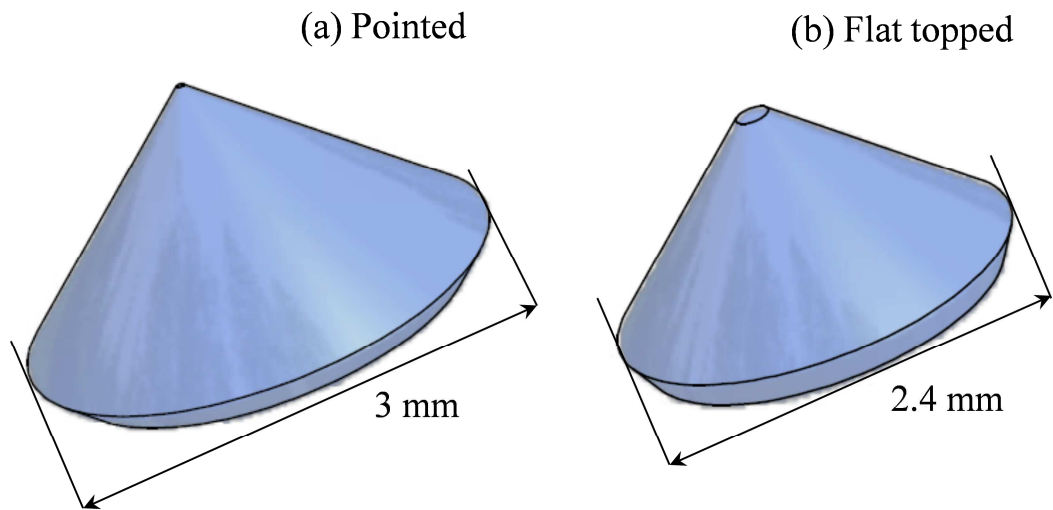


**Figure 4.3: Schematic of two diamond crystal geometries used by Fibre Photonics, supplied by Fibre Photonics.<sup>1</sup>**

The reduction in size and alteration in geometry are thought to reduce the cost of manufacturing, whilst maintaining the overall performance of the ATR probes. The geometry of the crystal used with the mono fibre probe is the same as Figure 4.3a, however, it is only 1.2 mm in size.

Fibre Photonics completed an investigation of diamond sizes using a ray tracing program to determine the optimal dimensions to obtain the highest transmission output; Figure 4.4, gives an schematic of the diamond cone and fibres with the ray tracing lines.

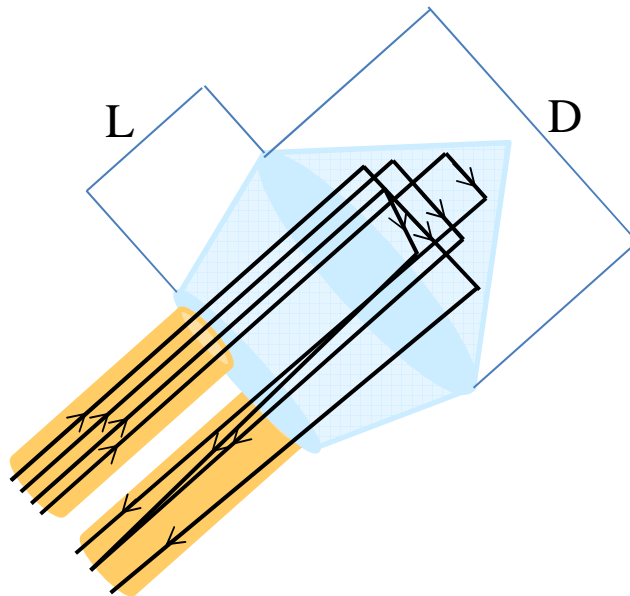


**Figure 4.4: Schematic of ray tracing lines exiting one fibre, reflecting off the diamond crystal twice back into the collecting fibre; where the diameter (D) and length (L) were investigated, adapted from figure supplied by Fibre Photonics.<sup>1</sup>**

Figure 4.4 shows the radiation having two points of contact with the diamond crystal, but due to the cone shape the incident radiation, which will diverge as it exits the fibre, will actually reflect off the curve of the crystal at many points; some of the radiation will be reflected as shown in Figure 4.4, however, some will also be reflected around the cone in a helical manner with some radiation being lost and some transferred to the detector through the collection fibre. Therefore, Fibre Photonics estimate their diamond cones as being 2 – 3 reflections. The two dimensions that have been investigated are the diameter (D) of the widest point of the crystal cone and the length (L) of the angled base section of the diamond crystal. The ray tracing program simulated the effect on the radiation trace when the two dimensions were altered. Many different combinations were analysed and the % transmission was plotted against the dimensions D and L in mm; the plotted results supplied by Fibre Photonics are given in Figure 4.5.

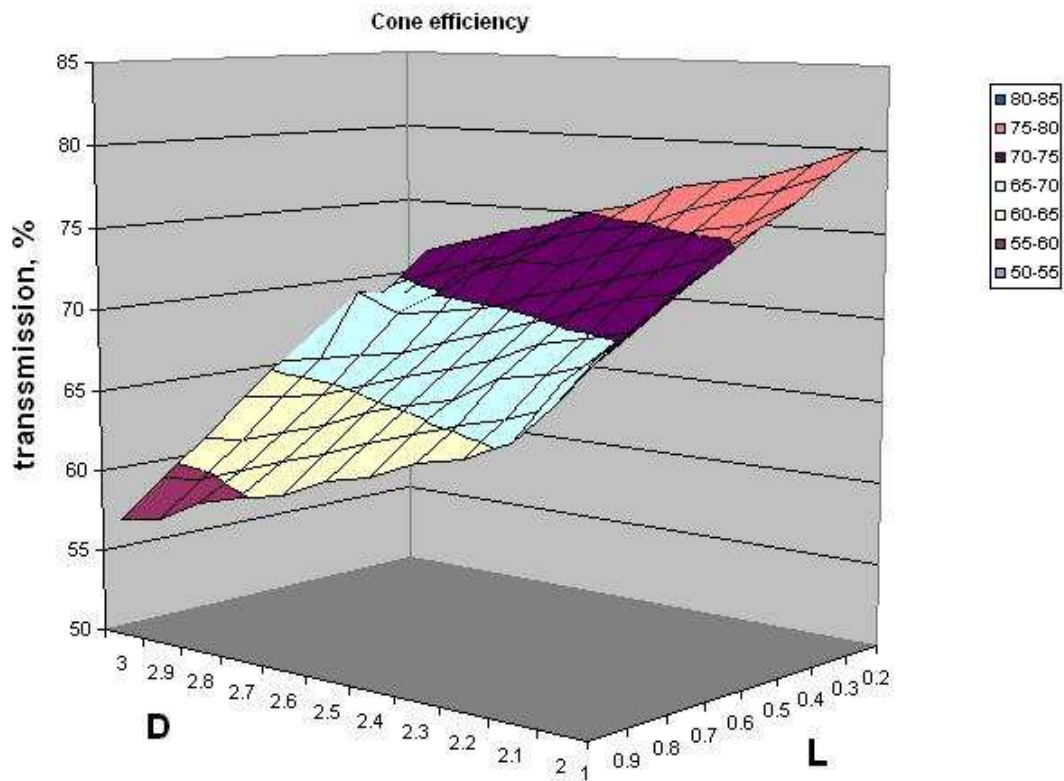


**Figure 4.5: Plot of % transmission vs. diamond crystal diameter (D) and length (L) as depicted in Figure 4.4, supplied by Fibre Photonics.<sup>1</sup>**

The results indicated that a higher transmission was reached as the dimensions of both D and L were reduced. Using this information and the ray tracing images similar to Figure 4.4, the dimensions of the current diamond crystal, given in Figure 4.3b were derived: D was set at 2.4 mm and L at 0.2 mm. This investigation only highlighted the perceived advantages of the probe design in terms of optical throughput rather than the effect on pathlength.

#### **4.1.2.4 Alignment**

The alignment of the fibres is a crucial step in the manufacturing of ATR probes. If the fibres are out of alignment, total internal reflection may not occur in the crystal as the radiation may not be guided into the crystal at an appropriate angle or position for total internal reflection to occur, therefore, no signal will be produced. Another possibility is that the collection fibre is out of alignment and much of the reflected radiation will not be detected by the collection fibre. To prevent misalignment and provide a more repeatable manufacturing process, the fibres are placed in a titanium

ferrule and then pushed up against the base of the diamond crystal. The ferrule is designed with channels for the precise alignment required for the fibres and the diamond cone selected. Another effect occurs when the fibres are not correctly lined up against the crystal, known as fringing. The main cause is from incorrect cutting of the fibre ends; if there is an angled gap between the end of the fibre and the crystal base, fringing will occur. Ensuring that the fibres are cut straight can minimize the effect of fringing. In addition, a malleable non-IR active material can be placed at the end of the crystal between the crystal base and the ends of the fibres. Therefore, when the fibres are pressed up against this material it will mould around the fibre end preventing any gaps and, therefore, impeding the fringing effect, see Figure 4.6.

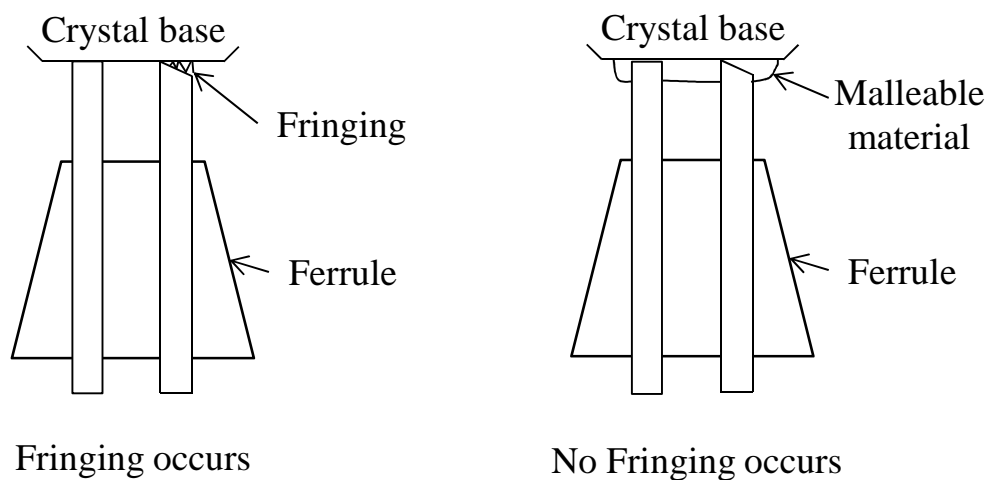


**Figure 4.6: Schematic diagram of fibres placed in ferrule and pressed up against the crystal base, showing the effect of fringing when no malleable material is used and no fringing when material is used.**

To ensure good performance, it is still important to have straight fibre ends and to keep the amount of the softer material to a minimum. Care must also be taken when using this extra material as refraction of the light will occur at the interface between each different material and so, the probe must be designed in a way that total internal reflection in the crystal is still possible. Fibre Photonics used AgCl as the soft malleable material for earlier manufactured probes, however, during the manufacturing process when the parts were pushed together to gain good contact, fibre breakage or seal breakage could occur. For that reason, Fibre Photonics opted to remove the AgCl material from production and instead have improved the cutting of the fibre ends to minimise the fringing, while preventing seal and fibre breakage.

#### **4.1.2.5 Use of modular components for manufacture**

One of the major challenges to the manufacturing of probes is achieving a consistently robust product. A way to improve the manufacturing process is the use of modular components, where the aim is to standardise the opto-mechanical parts. The modular components consist of standardised parts that have been fitted together before assembly of the probe. Each modular component is designed to fit together using simple connections. Through the standardisation of the different parts of the probes, assembly should be more repeatable, providing robust probes with consistent performance. An added advantage of the use of modular components is faster assembly of the probes without loss of quality. Before the use of modular components, the probes consisted of several parts that required fitting and welding together in specific ways to produce the final product. This process can affect the repeatability and robustness of the probes, as the parts may be fitted together by different people leading to slight differences in the final product. In addition, the process of fitting together the individual parts could lead to twisting or breakage of the fibres inside the probe. The use of modular components should help standardise the manufacturing process and minimise the occurrence of twisting or breakage of fibres. A potential limitation to using this universal design approach is that small adjustments are difficult to make, however, the requirement to make any adjustments should be minimal and the overall repeatability and robustness of the probes should be improved.

#### **4.1.2.6 Mono fibre design**

Sometimes there may be a requirement to analyse a very small amount of sample or insert a probe into a small vessel, therefore standard sized probes may be too large. Due to the dual fibre design of Fibre Photonics' standard probes, it is difficult to reduce the probe dimensions to less than 6 mm outside diameter. Fibre Photonics have, therefore, implemented a design change to produce smaller diameter probes, by using a single fibre for both the excitation and collection of radiation. The mono fibre design incorporates a 2.7 mm outside diameter probe with a 1.2 mm diamond crystal tip. The design has the advantages of using a smaller diamond crystal tip, less optical fibre and less material for the probe shaft, reducing the cost of manufacture, whilst

maintaining good spectral performance and allowing sample monitoring in small vessels and samples.

#### **4.1.3 Basis of study**

Many probe design features can be altered to improve the product quality and performance and the above review details some of the changes in design features that have been implemented by Fibre Photonics when manufacturing their probes. In this study, six probes were selected, where changes had been made to the design of the probe, to investigate the performance of the ATR MIR probes. The probes were used to acquire spectra of a set of ternary mixtures and calibration models were built to predict the concentration of the three analytes present in the mixtures. The root mean square error of prediction (RMSEP) statistic and percentage relative standard deviation (%RSD) were used to assess if the performance of the probes was altered when changes to the probe design were made. Furthermore, an investigation into the determination of the pathlength of the six probes was completed. A better understanding of how the pathlengths of the probes changed over the spectral range may help in understanding any differences in the spectra when modifications were made to the design of the probe.

## 4.2 Experimental

### 4.2.1 Samples

A set of mixtures of acetone, ethanol and ethyl acetate were prepared to assess the performance of the ATR MIR probes. The mixtures were prepared using the method described by Holden,<sup>9</sup> outlined below.

- Each mixture was prepared in a glass vial that had been rinsed in acetone and allowed to dry before use.
- The weights of each component were measured out using a balance with an accuracy of 4 decimal places; readings were recorded to 2 decimal places. Appendix 4.1 contains a table representing the weights of each of the three components for each of the 16 mixtures prepared.
- All weights were recorded with the lid on the sample bottles, so as to help prevent evaporation of the liquids. Pasteur pipettes were used to fill the vials to reduce the error and maintain weight values accurate to 2 decimal places. All measurements were taken using the tare button and the total weight calculated using a difference by weight approach (see Appendix 4.1 for an example calculation).

The concentrations of each component in the mixtures were then calculated as a weight percentage; these values can be viewed in Table 4.1. Mixtures 1 – 10 represent the calibration samples and mixtures 11 – 16 represent the test samples.

**Table 4.1: Concentrations of acetone, ethanol and ethyl acetate present in each mixture.**

Mixture number	Concentrations as weight percentage (% w/w)		
	Acetone	Ethanol	Ethyl acetate
1 – calibration 1	0.0	100.0	0.0
2 – calibration 2	100.0	0.0	0.0
3 – calibration 3	0.0	0.0	100
4 – calibration 4	51.3	48.7	0.0
5 – calibration 5	49.8	0.0	50.2
6 – calibration 6	0.0	49.9	50.1
7 – calibration 7	34.1	33.9	32.0
8 – calibration 8	65.5	17.2	17.3
9 – calibration 9	18.0	65.7	16.3
10 – calibration 10	17.2	18.0	64.8
11 –test 1	6.1	84.6	9.3
12 –test 2	28.4	58.1	13.5
13 –test 3	42.5	32.2	25.3
14 –test 4	82.6	10.6	6.8
15 –test 5	47.4	6.9	45.7
16 –test 6	10.8	18.3	70.9

#### 4.2.2 MIR spectrometry

MIR spectra were acquired with a resolution of  $16\text{ cm}^{-1}$  in the  $400 - 4000\text{ cm}^{-1}$  range using an ABB MB3000 FTIR spectrometer, coupled with polycrystalline silver halide fibres to hastelloy bodied probes with diamond cone crystals (Fibre Photonics Ltd, Livingston, UK) of different design features (see section 4.2.3 for details of the different probes assessed in this study). The spectrometer was fitted with a fibre optic interface to allow the attachment of the different ATR probes. Spectra were acquired using Horizon MB<sup>TM</sup> FTIR software version 3.0.13.1 (ABB, Canada) and GRAMS (Graphic Relational Array Management System) /AI software version 7.00 (Galactic Industries Corporation, Salem, USA). The spectra were exported as text files from Horizon software and as SPC files from GRAMS software and imported into Matlab data analysis software.

### 4.2.3 Probes assessed

Six ATR MIR probes were selected where alterations had been made to the design features. Table 4.2 lists the six probes assessed in this study; details of the differences in design and the change in manufacturing process are provided in the table.

**Table 4.2: Details of Fibre Photonics ATR probes assessed in this study; the major change to the design feature during manufacture is listed.**

Probe	Outer diameter (mm)	Probe body length (cm)	Fibre length (m) <sup>o</sup>	Diamond size (mm)
1	12	30	1.8	3
	New diamond cone sealing introduced, other features remained the same as the original design. AgCl used between the optical fibres and crystal base.			
2	12	15	2.8	3
	Fibre alignment altered; also incorporates new diamond cone sealing. AgCl used between the optical fibres and crystal base.			
3	12	30	1.0	2.4
	Different diamond cone size and geometry with the altered fibre alignment and the new diamond cone sealing. No AgCl used.			
4	6	50	1.5	2.4
	Use of modular components, incorporates the change in design features made to probes 1 – 3. No AgCl used.			
5	2.7	10	1.1	1.2
	Reduction of probe size including a mono fibre design.* No AgCl used.			
6	12	30	2.0	3
	Original design features. AgCl used between the optical fibres and crystal base.			

<sup>o</sup>This is the length of the fibre when measured from diamond tip to sma connectors; the actual length of polycrystalline fibre within the probe and connected cable will be double, see section 4.1.1 and 4.1.2.1.

\*Different design to other 5 dual fibre probes, see section 4.1.2.6.

## **4.2.4 Methods of analysis**

### **4.2.4.1 Probe performance**

The probe was inserted into each solvent mixture in a vial and sealed with sealing film before analysis; when not in use, the sample vials were sealed to prevent any evaporation. The probe was washed and cleaned with water and acetone and allowed to dry prior to each analysis. An air background reference single beam spectrum was collected and the sample single beam spectrum ratioed against this to produce a transmission spectrum, which was then converted to an absorbance spectrum. 51 scans were accumulated for each measurement (acquisition time of 51 s), with six repeat measurements made for each sample.

### **4.2.4.2 Pathlength determination**

To understand the pathlength differences of the six probes and how the pathlength changes over the spectral range, an investigation was carried out to determine the pathlengths of the probes at a selection of wavenumbers in the range 560 – 1790  $\text{cm}^{-1}$ . The data used for calculation of the molar absorptivity coefficient was provided for the investigation, but for confidentiality reasons, the identity of the source cannot be disclosed. The first part of this investigation involved the determination of the molar absorptivity coefficient of a solvent at a range of wavenumbers across the spectral range of interest. To do this, measurements were taken of an empty cell (Specac variable pathlength liquid cell with ZnSe windows, 32 scans at 4  $\text{cm}^{-1}$ ) to obtain a sine wave pattern, which is a result of interference phenomena within the cell, see Figure 4.7.<sup>10</sup>

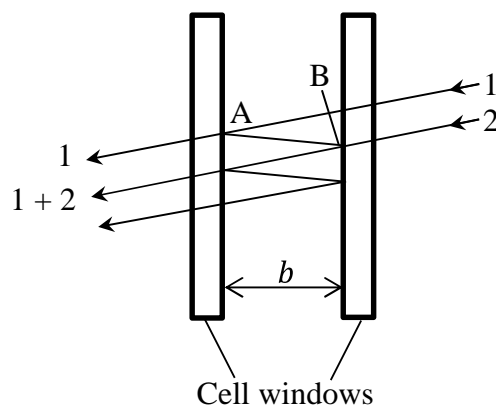


**Figure 4.7: The formation of the spectral interference pattern. The conditions are easier to explain with the slanted incident beam, however, are identical to a perpendicular incident beam. A part of beam 1 is reflected at point A and, again, a fraction of this is reflected at point B. At position B, this fraction of beam will interfere with beam 2 resulting in constructive or destructive interferences; figure reproduced from IR Spectroscopy.<sup>10</sup>**

The difference in refractive index between the air and window material was great enough to reflect the radiation back and forth. Constructive and destructive interference occurred and the spectrum indicates at which wavelengths this occurred. The spectral interference depended on the pathlength,  $b$ , between the cell windows. Using the maxima or minima of the interference in the spectrum, the pathlength,  $b$ , could be calculated using Equation 4.1.<sup>10</sup>

$$b = \frac{m}{2} \frac{1}{\bar{\nu}_1 - \bar{\nu}_2} \quad \text{Equation 4.1}$$

The number of maxima (or minima) between the selected wavenumbers  $\bar{\nu}_1$  and  $\bar{\nu}_2$  is denoted by  $m$ . The units of  $b$  from Equation 4.1 are cm. This procedure was used to calculate the pathlengths of the variable pathlength cell when set at six nominal pathlengths (80, 90, 100, 110, 120 and 150  $\mu\text{m}$ ) to determine the actual pathlength of the cell at these settings. When the cell was in each of the six settings it was also filled with acetone and a spectrum acquired (32 scans at  $16 \text{ cm}^{-1}$ ) for calculation of the molar absorptivity coefficient of this solvent. The calculated pathlengths for the six settings were plotted against the absorbance values of the acetone spectrum acquired at the same pathlength. The gradient of the trendline constrained through zero is equivalent to the molar absorptivity coefficient,  $\epsilon$ , multiplied by the

concentration,  $c$ , of the solvent, from the Lambert-Beer-Bouguer law in Equation 4.2, where  $A$  is the absorbance and  $b$  is the pathlength.

$$A = \epsilon bc \quad \text{Equation 4.2}$$

The equation of the trendline is  $y = mx$ , where  $y$  is the absorbance and  $x$  is the pathlength, therefore  $m = \epsilon c$ .

The second part of the investigation was to use the calculated molar absorptivity coefficient to determine the pathlength of the six ATR MIR probes at the same selection of wavenumbers used for part 1. To do this the absorbance spectra of acetone acquired with each of the six probes as per section 4.2.4.1 were used with the calculated molar absorptivity coefficient at the selection of wavenumbers to calculate the pathlength of the probes at that specific wavenumber.

#### 4.2.5 Data analysis

Data were imported into Matlab versions 7.5.0.342 (R2007b) and 7.11.0.584 (R2010b) (Mathworks Inc., Natick, MA, USA) with PLS\_Toolbox version 4.1 (Eigenvector Research Inc., WA, USA). Spectra were analysed and regions in the data that would provide information about the samples were used to construct calibration models. The spectra from the calibration solutions and their concentration values were used to produce multivariate partial least squares (PLS) calibration models. All models were constructed using the spectral region 560 to 1790  $\text{cm}^{-1}$  and mean centred absorbance data. The average predicted concentrations from the models were compared with the expected concentrations of the three analytes and the root mean square error of prediction (RMSEP) values were calculated within Excel 2007/2010 (Microsoft Corporation) using the function given in Equation 4.3 (replicate of Equation 2.11 in chapter 2, for convenience) to determine numerically the level of error associated with each of the predictions.

$$RMSEP = \sqrt{\frac{\sum_{i=1}^n (\hat{y}_i - y_i)^2}{n}} \quad \text{Equation 4.3}$$

Where,

$\hat{y}_i$  = predicted value

$y_i$  = known value

$n$  = number of samples

The relative standard deviation (%RSD) was calculated for the prediction of each test mixture for each analyte using Equation 4.4, where  $\sigma$  is the standard deviation and  $\bar{x}$  is the average of the six repeat measurements.

$$\%RSD = \frac{\sigma}{\bar{x}} \times 100 \quad \text{Equation 4.4}$$

The average %RSD was then calculated for the predicted concentration of the six test samples for each analyte. The RMSEP value and %RSD were compared and used to determine if the performance of the probes had been improved when design changes were implemented.

## **4.3 Results**

### **4.3.1 Probe performance**

#### **4.3.1.1 Spectral interpretation**

To investigate the performance of the six probes the spectra acquired were compared to determine any changes or improvements when different probes were used to analyse the samples. The acquired pure component spectra of ethanol, acetone and ethyl acetate from the six probes were compared to determine if there were any differences present. The overlaid average absorbance spectra for ethanol (calibration 1) acquired using the six ATR MIR probes are given in Figure 4.8. The most notable difference is the change in absorbance between the spectra; this can be seen clearly in Figure 4.9 in the range 950-1200  $\text{cm}^{-1}$ . The differences in the absorbance between the six probes change with wavenumber over the spectral range; the greatest difference is observed for the peak around 1040  $\text{cm}^{-1}$ . Apart from the differences in absorbance, the six ATR MIR probes produce similar spectra.

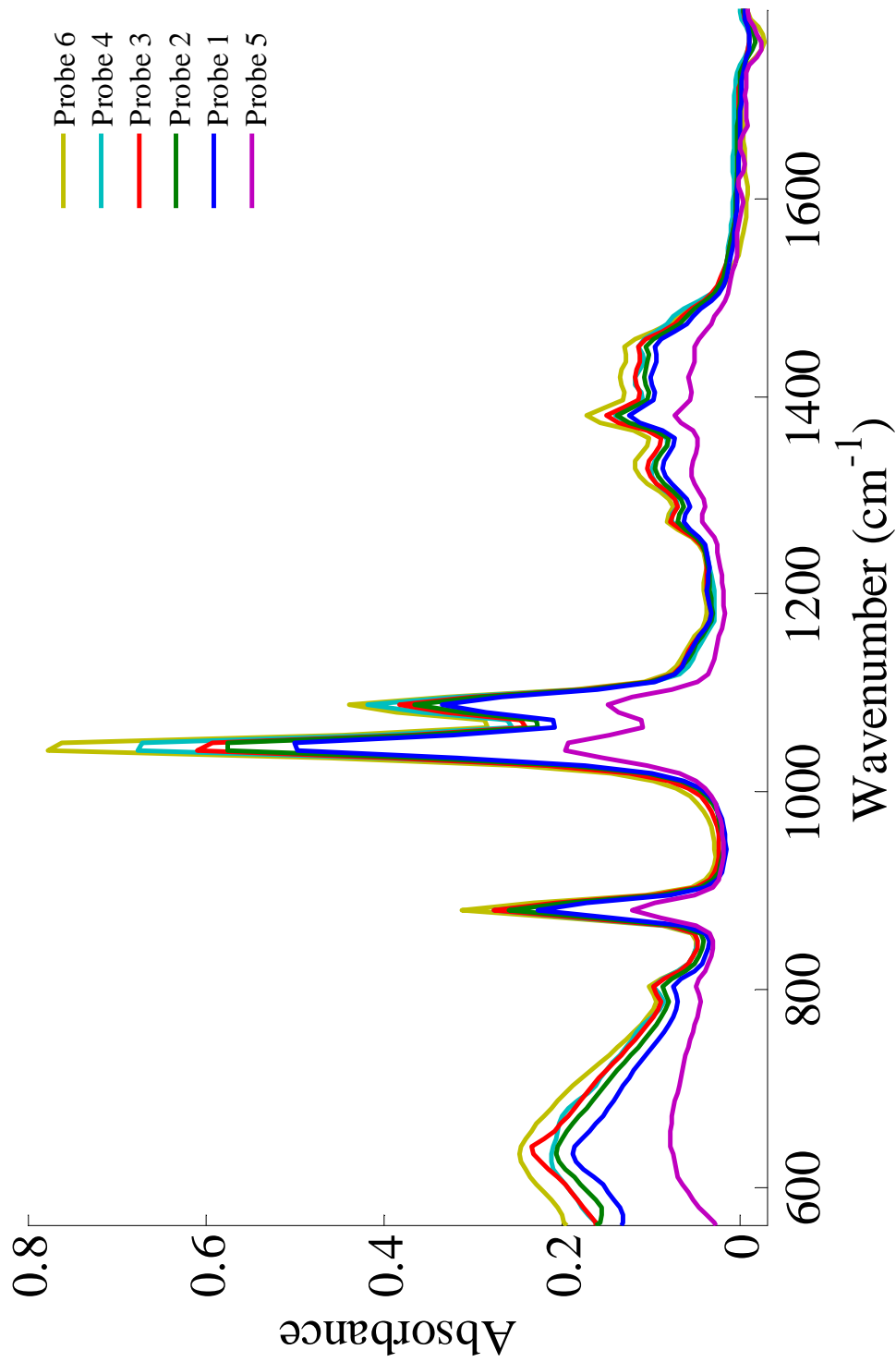
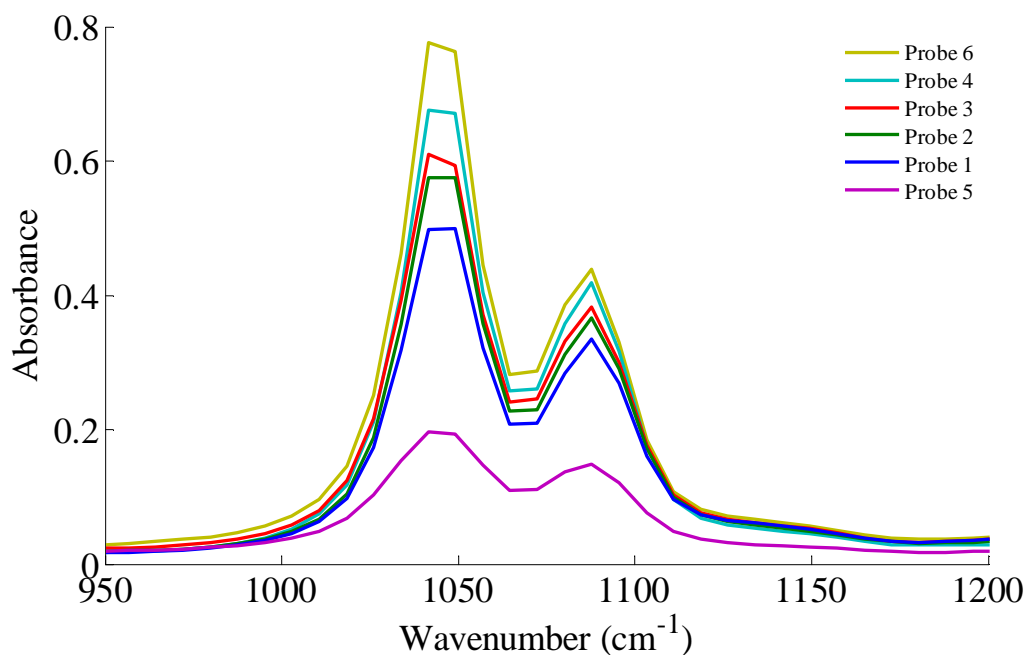


Figure 4.8: Overlaid average (n=6) ATR MIR absorbance spectra of ethanol (Calibration 1) acquired in the range 560 – 1790 cm<sup>-1</sup> using probes 1 – 6.



**Figure 4.9: Overlaid average (n=6) ATR MIR absorbance spectra of ethanol (Calibration 1) acquired in the range 950 – 1200  $\text{cm}^{-1}$  using probes 1 – 6.**

The overlaid average absorbance spectra for acetone (calibration 2) acquired using the six ATR MIR probes are given in Figure 4.10. As for ethanol, a difference in the absorbance between the spectra of acetone from the six probes can be observed. The difference in absorbance is larger at higher wavenumbers than at lower wavenumbers; this is easily observed when comparing the change in absorbance for peaks around 900  $\text{cm}^{-1}$  and 1700  $\text{cm}^{-1}$ . In addition, there appears to be a change in the ratio of the larger peaks, as illustrated for two peaks in the range 1190 – 1400  $\text{cm}^{-1}$  in Figure 4.11. The ratio of the three larger peaks of the acetone spectrum (1219  $\text{cm}^{-1}$ , 1358  $\text{cm}^{-1}$  and 1713  $\text{cm}^{-1}$ ) were calculated and compared, see Table 4.3. The peak at 1219  $\text{cm}^{-1}$  was assigned a value of one and the relative ratio of the other peaks was determined.

**Table 4.3: Table of calculated ratio of the three largest peaks present in the acetone spectra (Calibration 2) acquired with the six ATR MIR probes.**

	Wavenumber (cm <sup>-1</sup> )		
	1219	1358	1713
Probe 1	1.0	0.8	1.1
Probe 2	1.0	0.9	1.3
Probe 3	1.0	0.9	1.2
Probe 4	1.0	0.8	1.1
Probe 5	1.0	1.0	0.4
Probe 6	1.0	1.1	1.9

In general for probes 1 – 4 the absorbance of the peak at 1358 cm<sup>-1</sup> is the smallest, then it is the peak at 1219 cm<sup>-1</sup> and finally the largest absorbance is observed for the peak at 1713 cm<sup>-1</sup>. Probes 5 and 6 do not follow this pattern; for probe 5 the two peaks at 1219 cm<sup>-1</sup> and 1358 cm<sup>-1</sup> are equivalent and the absorbance of the peak observed at 1713 cm<sup>-1</sup> is considerably smaller. For probe 6, the absorbance of the peak at 1358 cm<sup>-1</sup> is larger than that of the peak at 1219 cm<sup>-1</sup>. These results indicate that there is a difference between the six probes; the reason for the difference in probe 5 is most likely due to the change in the design of the probe as this is a mono fibre design with a smaller diamond cone size than the other probes. Probe 6 was the original manufacturing design; therefore the changes incorporated in probes 1 – 5 appear to have altered the spectrum of acetone.

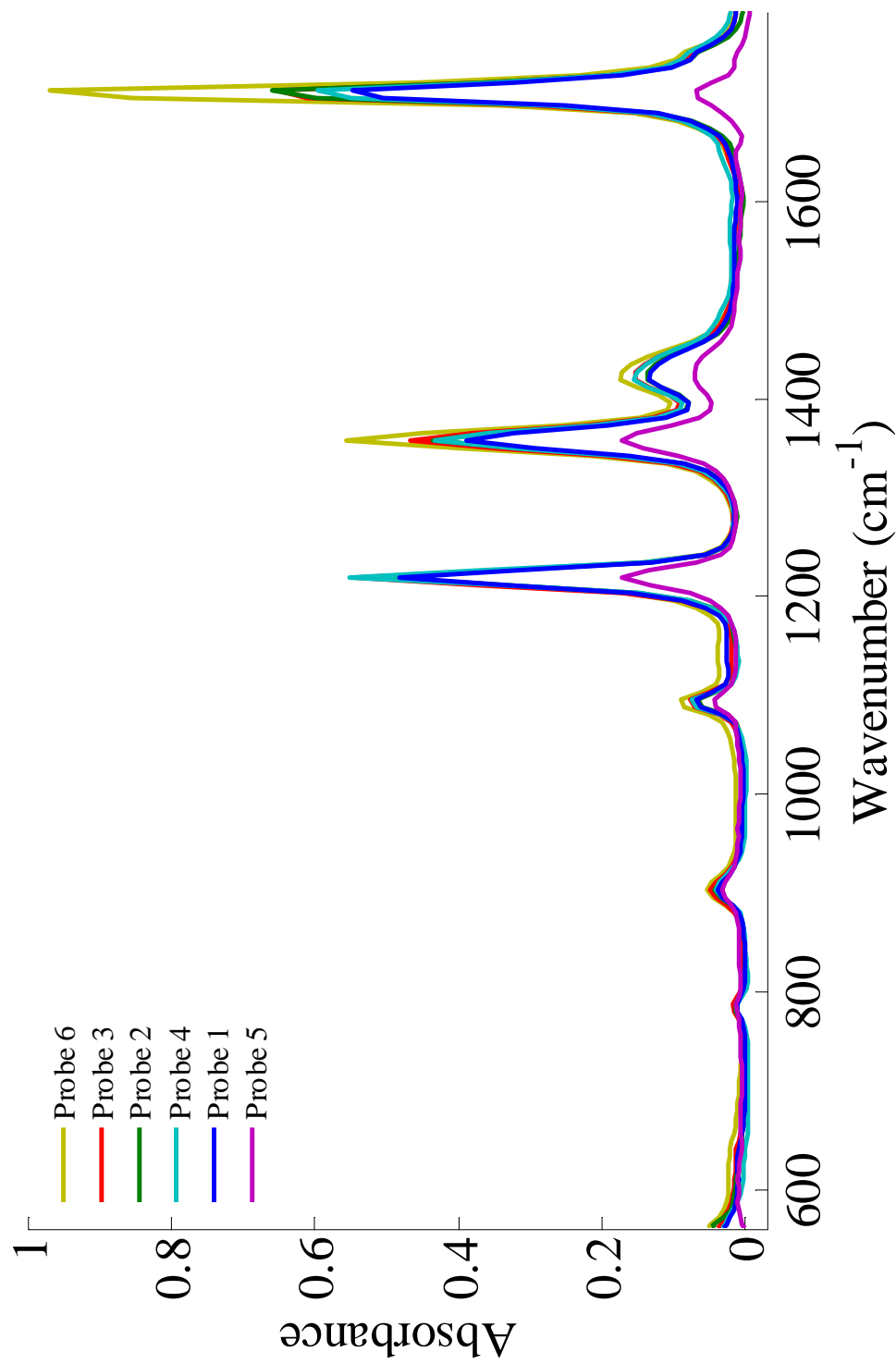


**Figure 4.10:** Overlaid average (n=6) ATR MIR absorbance spectra of acetone (Calibration 2) acquired in the range 560 – 1790 cm<sup>-1</sup> using probes 1 – 6.

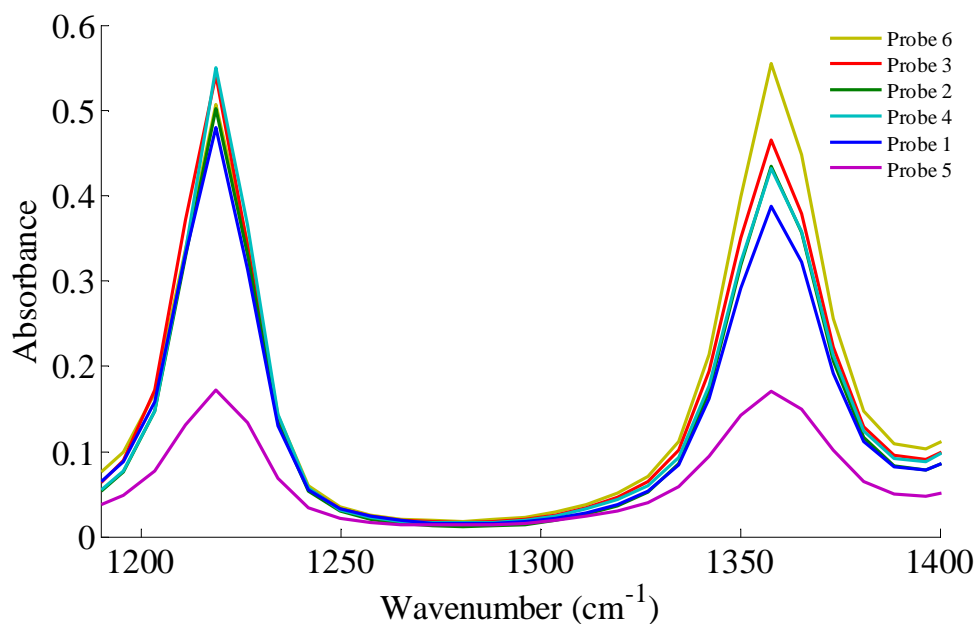


**Figure 4.11: Overlaid average (n=6) ATR MIR absorbance spectra of acetone (Calibration 2) acquired in the range 1190 – 1400  $\text{cm}^{-1}$  using probes 1 – 6.**

The overlaid average absorbance spectra for ethyl acetate (calibration 3) acquired using the six ATR MIR probes are given in Figure 4.12. As for ethanol and acetone, the main observation is the difference in the absorbance with wavenumber over the spectral range. However, in the spectral range 560 – 1000  $\text{cm}^{-1}$ , there is a smaller difference in the absorbance values of approximately 0.1 or less for the six ATR MIR probes, as illustrated in Figure 4.13. From 1000 – 1790  $\text{cm}^{-1}$  larger differences occur with the largest absorbance difference observed for the peak at 1735  $\text{cm}^{-1}$ , as shown in Figure 4.14, where a difference in absorbance greater than 0.8 is observed. For all three analytes, probes 1 – 4 give more similar absorbances when compared with probes 5 and 6.

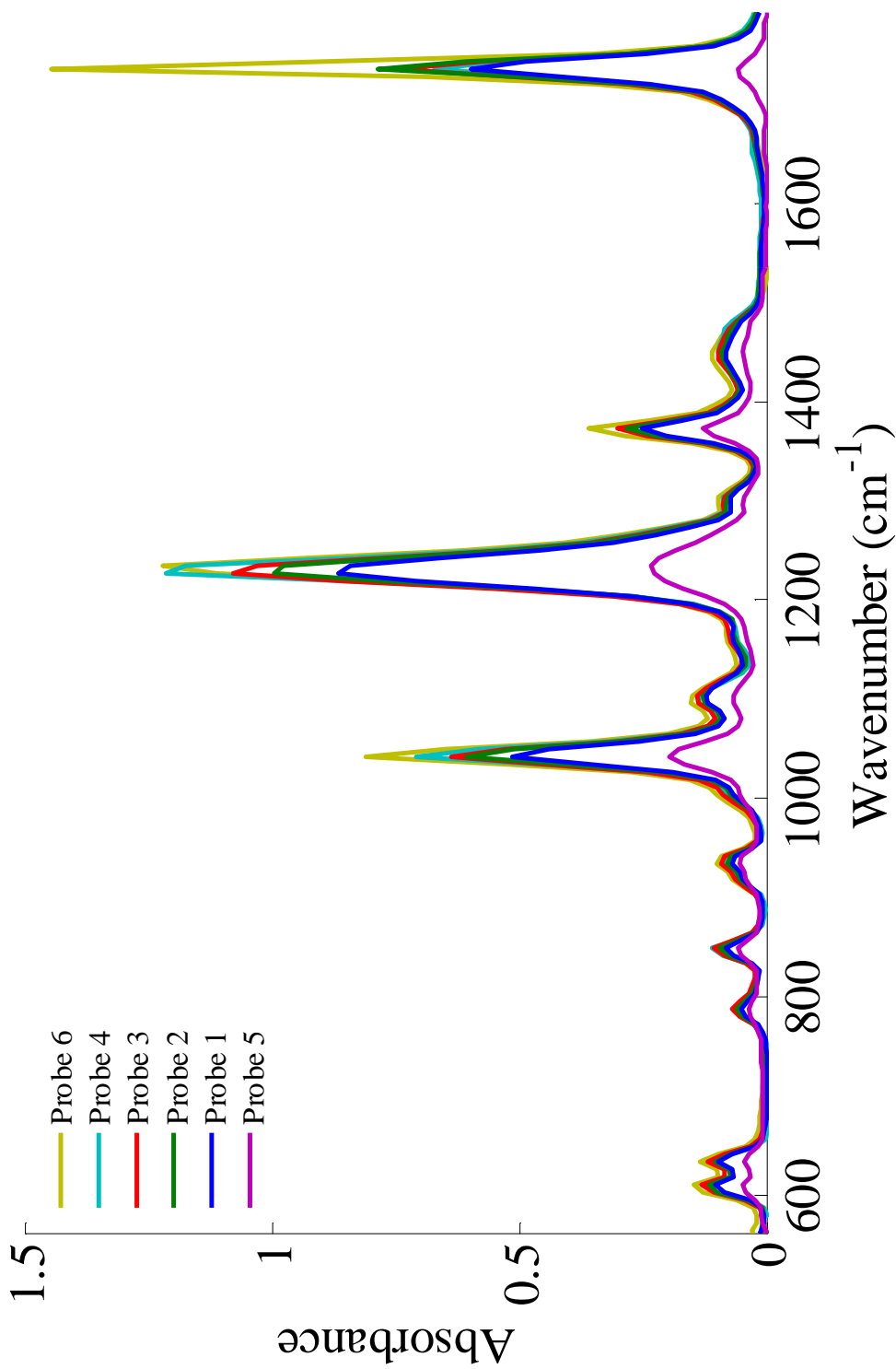
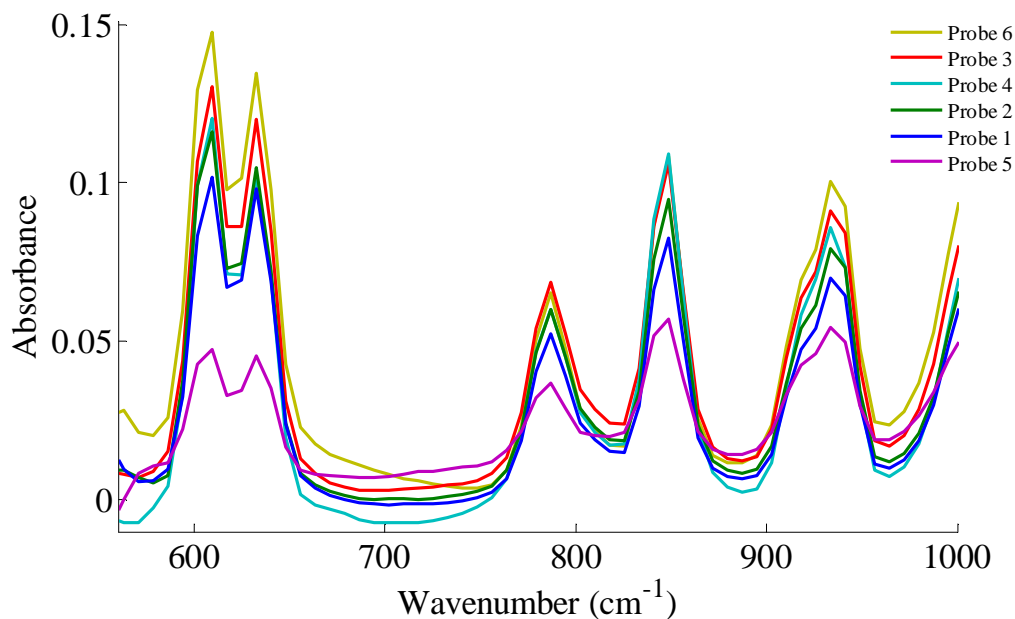
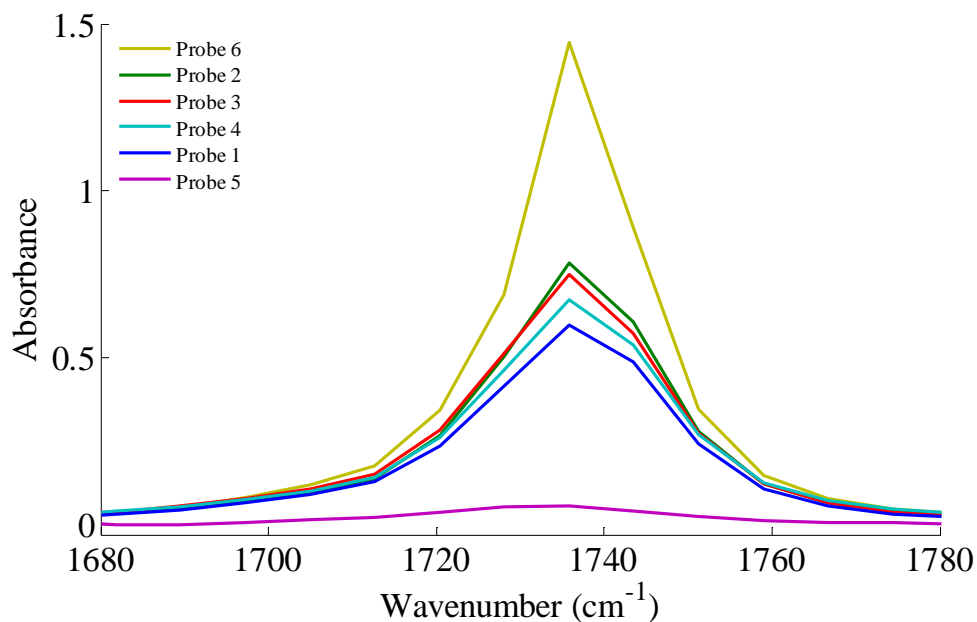


Figure 4.12: Overlaid average (n=6) ATR-MIR absorbance spectra of ethyl acetate (Calibration 3) acquired in the range 560 – 1790 cm<sup>-1</sup> using probes 1 – 6.



**Figure 4.13: Overlaid average (n=6) ATR MIR absorbance spectra of ethyl acetate (Calibration 3) acquired in the range 560 – 1000  $\text{cm}^{-1}$  using probes 1 – 6.**



**Figure 4.14: Overlaid average (n=6) ATR MIR absorbance spectra of ethyl acetate (Calibration 3) acquired in the range 1680 – 1780  $\text{cm}^{-1}$  using probes 1 – 6.**

Reviewing the spectra acquired using the six ATR MIR probes; the design changes to the probes have not altered the general quality of the spectra. However, absorbance differences occur between the spectra of the probes, and in the case of acetone there are also some peak ratio differences. According to the Lambert-Beer-

Bouguer law (Equation 4.2) there is a linear relationship between the absorbance, and the concentration and pathlength. In this research, the sample mixtures remained the same, therefore, the concentration and molar absorptivity coefficient are constant. In this instance, any change in absorbance is dependent on a change in pathlength. So, there must be pathlength differences between the six probes, see section 4.3.2 for the investigation into the pathlength of these probes. There is a further relationship between the pathlength and the number of reflections, given in Equation 4.5, where  $d_p$  is the penetration depth.

$$b = d_p \times \text{No. reflections at the crystal} \quad \text{Equation 4.5}$$

Therefore, the change in pathlength can be associated with a change in the number of reflections at the crystal and/or a change in penetration depth. The penetration depth for a single reflection is related to the wavelength of the incident light,  $\lambda$ , and the angle of incidence at the crystal surface,  $\theta$ , through Equation 4.6, where  $n_1$  is the refractive index of the ATR crystal and  $n_2$  is the refractive index of the sample.

$$d_p = \lambda / 2\pi n_1 [\sin^2 \theta - (n_2/n_1)^2]^{0.5} \quad \text{Equation 4.6}$$

So, a change in absorbance can be associated with a change in the angle of incidence at a specific wavelength, through the influence on  $d_p$ .

A change in  $\theta$  and the number of reflections at the crystal could occur when the size and geometry of the diamond crystal are changed. A change in  $\theta$  will also be caused by differences in the alignment of the optical fibre to the crystal surface. Probes 1, 2 and 6 have the original size and geometry of diamond, see Figure 4.3a. Probes 3 and 4 incorporate a different diamond crystal shape and design (Figure 4.3b), Probe 5 contains a smaller diamond crystal size, but uses the original geometry given in Figure 4.3a.

Due to the helical nature of these cone designs discussed in section 4.1.2.3, it is difficult to determine what the number of reflections are and, therefore, it is possible that there is a difference between the two cone geometries. In addition, the dimensions of the two diamond crystals have different angles, therefore, the angle of incidence at the crystal will be different and a change in the penetration depth will

occur between the two crystals. As the manufacturing process consisted of manually fitting together many different parts, differences in alignment can be expected. However, with the use of modular components and mechanically stable clamp arrangements to hold the fibres in place to maintain their accurate position, fewer variations will occur in more recently manufactured probes.

The differences in absorbance observed between the six probes are, therefore, most likely a combination of effects caused by the change in fibre alignment and diamond cone size and geometry. From this assessment, it is unclear why there is such a large change in absorbance between the original manufacturing process for probe 6 to the production of probe 1, where the design change was a new cone sealing, as it is unlikely that this will have an effect on the performance of the probe.

#### **4.3.1.2 Predictions of concentrations of acetone, ethanol and ethyl acetate in ternary mixtures**

PLS calibration models were built using the acquired spectra for the calibration samples in the region  $560 - 1790 \text{ cm}^{-1}$ ; the data were mean centered with no derivation. The number of latent variables required was determined from the model that produced the minimum value of the root mean square error of cross-validation (RMSECV) obtained using leave-one-out cross validation. Separate calibration models were built using the spectra acquired from each probe; the models were then applied to predict the concentrations of the three analytes in the test samples acquired on the same system as the data used for the calibration model.

The accuracy of the concentration predictions of each component obtained with each probe were then compared to indicate any advantages of the design changes implemented in the probe manufacture. The expected and predicted concentrations of the three analytes were tabulated and the RMSEP and %RSD values were calculated to determine numerically the level of error associated with each of the predictions. The results for ethanol, acetone and ethyl acetate are given in Table 4.4, Table 4.5 and Table 4.6, respectively.

**Table 4.4: Expected and predicted concentrations for ethanol from PLS calibration models for probes 1 – 6.**

<b>Mixture number</b>	<b>Expected concentration (% w/w)</b>	<b>Concentration predictions (% w/w)</b>					
		Probe 1	Probe 2	Probe 3	Probe 4	Probe 5	Probe 6
<b>Test 1</b>	84.6	84.7	84.9	84.9	83.8	82.2	83.5
<b>Test 2</b>	58.1	58.0	57.4	57.8	58.1	57.4	58.7
<b>Test 3</b>	32.2	31.5	30.7	31.1	30.2	30.1	32.4
<b>Test 4</b>	10.6	10.4	9.6	10.5	10.5	9.9	9.2
<b>Test 5</b>	6.9	5.2	4.0	4.7	4.4	5.0	5.7
<b>Test 6</b>	18.3	18.1	17.6	17.6	17.8	17.9	17.7
	RMSEP	0.7	1.4	1.1	1.4	1.6	1.0
	%RSD	0.3	0.7	0.2	0.9	1.5	4.5

**Table 4.5: Expected and predicted concentrations for acetone from PLS calibration models for probes 1 – 6.**

<b>Mixture number</b>	<b>Expected concentration (% w/w)</b>	<b>Concentration predictions (% w/w)</b>					
		Probe 1	Probe 2	Probe 3	Probe 4	Probe 5	Probe 6
<b>Test 1</b>	6.1	6.0	6.4	6.0	7.1	7.9	6.2
<b>Test 2</b>	28.4	28.6	28.8	28.3	27.4	28.2	27.8
<b>Test 3</b>	42.5	42.8	43.1	42.9	43.5	43.0	43.5
<b>Test 4</b>	82.6	83.2	83.4	83.1	82.9	82.5	83.7
<b>Test 5</b>	47.4	47.8	48.0	48.0	48.1	46.5	48.8
<b>Test 6</b>	10.8	11.4	11.8	11.6	10.8	11.8	12.6
	RMSEP	0.4	0.7	0.5	0.8	0.9	1.1
	%RSD	0.2	0.3	0.1	0.8	2.2	1.8

**Table 4.6: Expected and predicted concentrations for ethyl acetate from PLS calibration models for probes 1 – 6.**

Mixture number	Expected concentration (% w/w)	Concentration predictions (% w/w)					
		Probe 1	Probe 2	Probe 3	Probe 4	Probe 5	Probe 6
<b>Test 1</b>	9.3	9.3	8.7	9.1	9.1	9.9	10.3
<b>Test 2</b>	13.5	13.4	13.8	13.9	14.5	14.4	13.5
<b>Test 3</b>	25.8	25.8	26.2	26.0	26.3	26.9	24.1
<b>Test 4</b>	6.4	6.4	7.0	6.4	6.6	7.5	7.2
<b>Test 5</b>	46.9	46.9	47.9	47.3	47.4	48.5	45.6
<b>Test 6</b>	70.5	70.5	70.7	70.8	71.4	70.3	69.7
	RMSEP	0.6	1.0	0.8	0.9	1.4	0.8
	%RSD	0.2	0.4	0.1	0.2	2.7	1.2

On assessing the results for the concentration predictions achieved with the six ATR MIR probes, several conclusions can be made:

- Low RMSEP values were determined for probes 1 – 4 for the three analytes, with values less than 1.5% w/w. Small differences in the RMSEP values were observed, however, when considering the magnitude of the errors these differences are relatively insignificant.
- Good %RSD values were also observed for probe 1 – 4 for the three analytes, with values less than 1%.
- The RMSEP results for probe 5 were slightly greater than observed for probes 1 – 4, with values between 0.9 and 1.6% w/w.
- The %RSD values were also greater for probe 5 than probes 1 – 4, with values between 1.5 and 2.7%.
- The RMSEP results for probe 6 were similar to those observed for probes 1 – 4, however, the %RSD values were greater than those observed for all the other probes.
- Overall probes 1 and 3 give the best performance when the results for RMSEP and %RSD are considered.

Probe 5 implements a different probe design where a single fibre is used instead of a dual fibre design and also incorporates a smaller diamond crystal giving a smaller pathlength in comparison to the other probes. The signal to noise of this probe will, therefore, be smaller than achieved with the other probes and so more variation in the acquired spectra can be expected, which will result in larger %RSD results. However, even though probe 5 has a reduced sensitivity it can still be used successfully to analyse samples in combination with the MB3000 spectrometer, with RMSEP values less than 2% w/w and %RSD values less than 3%. Probe 6 has higher %RSD values in comparison to the other dual fibre probes, especially for the prediction of ethanol; this is most likely caused by the poor predictions for the low % w/w concentrations of this analyte. Probe 6 was the original manufacturing design, therefore, the results obtained with probes 1 – 4 suggest that the manufacturing alterations adopted had improved the performance of the probes.

#### **4.3.2 Pathlength investigation**

The spectrum of an empty variable pathlength cell was acquired and used to determine the actual pathlength of the cell at six settings. Figure 4.15 gives an example of the sine wave generated from this acquisition when the pathlength was set at 150  $\mu\text{m}$ . The number of maxima was counted between the two points indicated in Figure 4.15 and used in Equation 4.1, given in section 4.2.4.2 to calculate the actual pathlength.

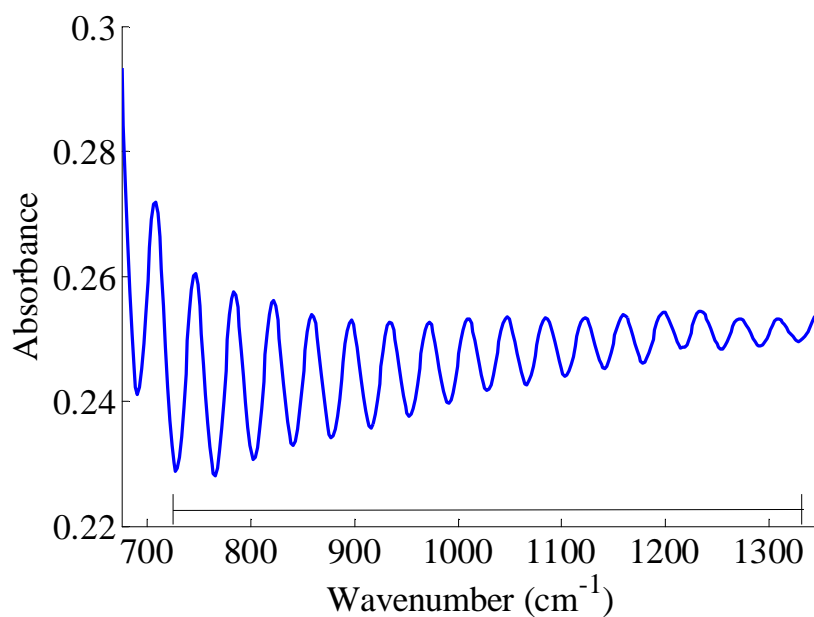


**Figure 4.15: Spectral interference sine wave acquired when measurement of an empty variable pathlength cell set at 150  $\mu\text{m}$  was made.**

The spectral interference sine waves were analysed for six set pathlength values: 80, 90, 100, 110, 120 and 150  $\mu\text{m}$  and the results are given in Table 4.7. The pathlength values are given here in cm as it allowed for a more accurate determination of the gradient of the trendline and so further calculations of the molar absorptivity would also be more accurate.

**Table 4.7: Tabulated results for the calculation of the pathlength of the variable cell at six settings and the absorbance values for acetone at 1095 cm<sup>-1</sup> at the same six settings.**

Set pathlength value (cm)	$\bar{\nu}_1$ (cm <sup>-1</sup> )	$\bar{\nu}_2$ (cm <sup>-1</sup> )	$m$	$\bar{\nu}_1 - \bar{\nu}_2$ (cm <sup>-1</sup> )	Calculated pathlength (cm)	Absorbance at peak 1095 cm <sup>-1</sup>
0.008	1188	700	7	488	0.007	0.770
0.009	1182	739	7	444	0.008	0.874
0.01	1175	717	8	457	0.009	0.967
0.011	1178	708	9	471	0.010	1.050
0.012	1175	696	10	478	0.010	1.136
0.015	1327	727	16	600	0.013	1.423

The calculated pathlengths for the six settings were then plotted against the absorbance values at a range of wavenumbers across the spectral range analysed using the same settings. Nine wavenumbers were selected in total across the range 787 – 1767 cm<sup>-1</sup>, as indicated in Figure 4.16. As many of the acetone peaks were off scale using the transmission cell, points were selected near to where the acetone peaks arise, where absorbance values could be detected. Ideally, points would be selected that give absorbance values less than 1.0, however, for this data, it would not have been possible to calculate the pathlengths of the *in situ* probes as the absorbance values would be too low at these wavenumber points. Therefore, the R<sup>2</sup> value for the trendline was evaluated to determine the closeness of fit of the data points to the trendline that had been constrained through zero. Table 4.7 and Figure 4.17 show the results for the peak at 1095 cm<sup>-1</sup> as an example. The absorbance vs. pathlength plots for the other eight wavenumbers selected are given in Appendix 4.2, where the equation of the straight line and R<sup>2</sup> value were calculated and are tabulated in Table 4.8.

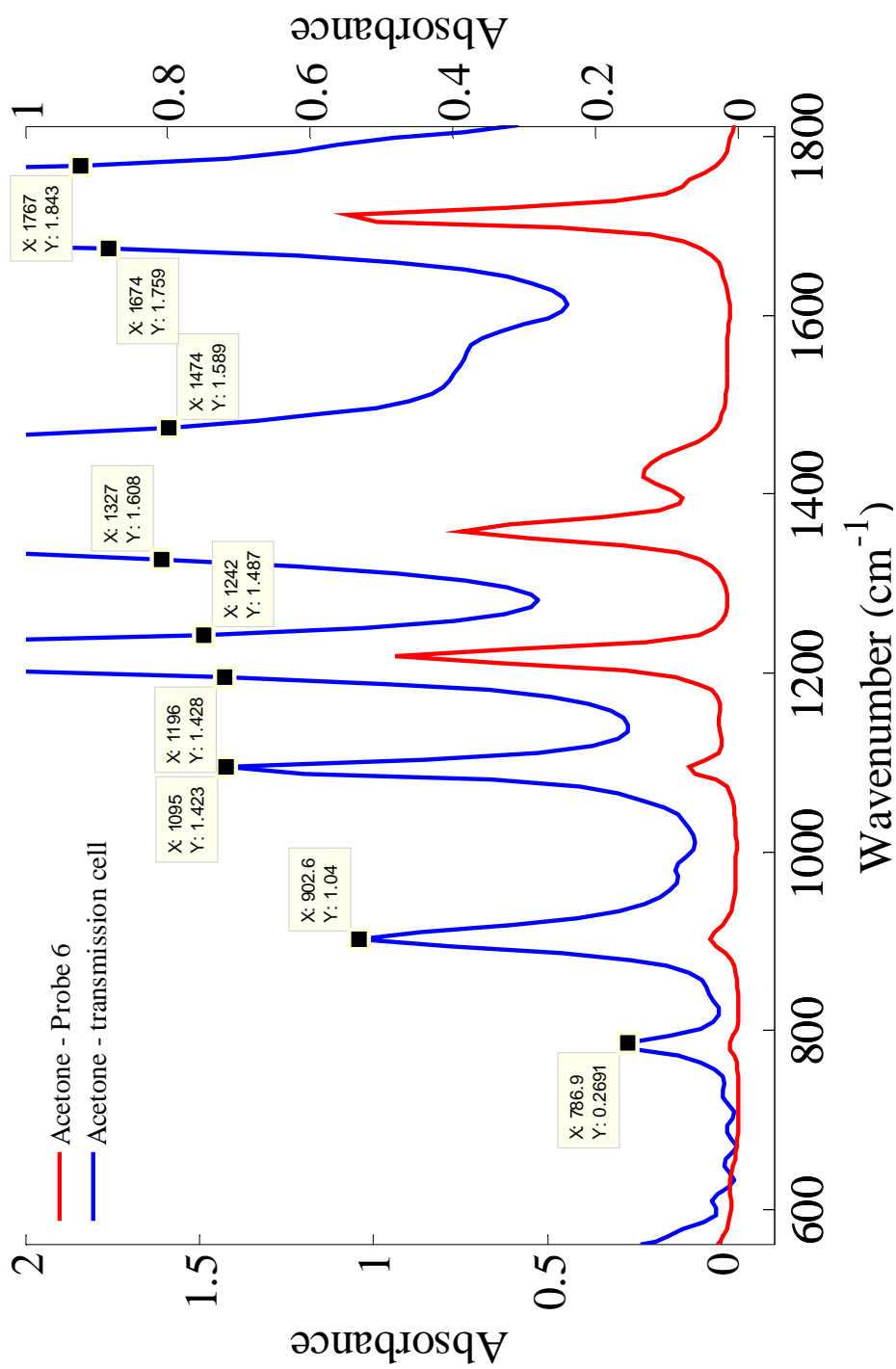
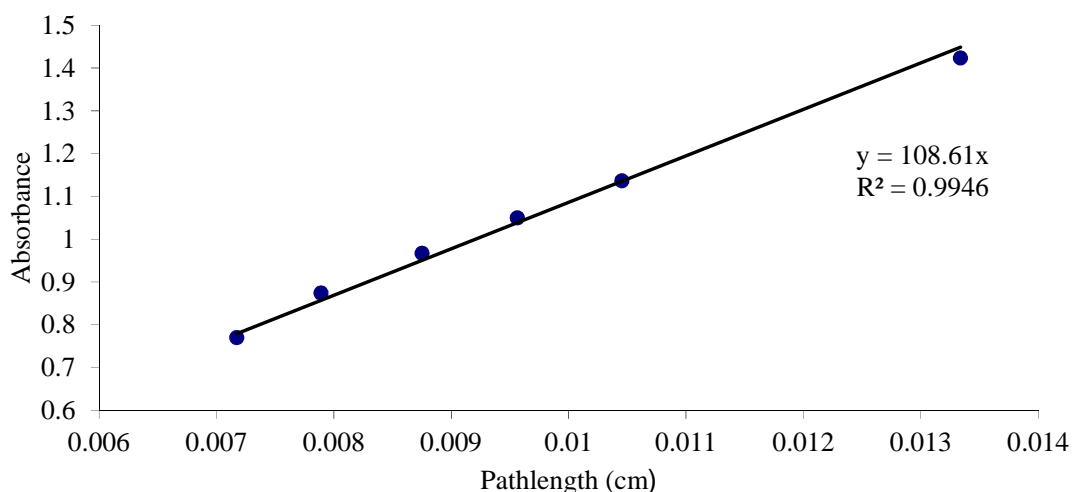


Figure 4.16: Overlaid absorbance spectra of acetone (calibration 2) acquired in the range  $560 - 1810 \text{ cm}^{-1}$  using probe 6 and with the variable transmission cell. Labels indicate the nine wavenumbers selected for the determination of the molar absorptivity coefficient of acetone. Left hand absorbance scale is for the transmission cell acetone spectra and the right hand absorbance scale is for probe 6 acetone spectra.



**Figure 4.17:** Absorbance values for a peak at  $1095\text{ cm}^{-1}$  acquired using the variable pathlength cell vs. the calculated pathlength of the cell. The trendline indicates the linear relationship and the equation of the line can be used to determine the molar absorptivity coefficient.

**Table 4.8:** Equation of the trendline and  $R^2$  values for nine selected wavenumbers in the acetone spectrum.

Wavenumber ( $\text{cm}^{-1}$ )	Equation of line	$R^2$ value
787	$y = 18.689x$	0.9112
903	$y = 75.285x$	0.9816
1095	$y = 108.61x$	0.9946
1196	$y = 108.28x$	0.9953
1242	$y = 113.79x$	0.9932
1327	$y = 119.32x$	0.9938
1474	$y = 117.25x$	0.9923
1674	$y = 132.95x$	0.9967
1767	$y = 138.79x$	0.9976

As defined earlier in section 4.2.4.2, the gradient of the line in Figure 4.17 is equivalent to  $\epsilon c$ . Therefore, the molar absorptivity coefficient at  $1095\text{ cm}^{-1}$  is calculated as follows:

$$\varepsilon = \frac{m}{c}$$

$$\varepsilon = \frac{108.61}{c}$$

For acetone, the concentration is 13.619 mol/L, so,  $\varepsilon = 7.97 \text{ L mol}^{-1} \text{ cm}^{-1}$ . This calculation was carried out for nine selected wavenumbers and the results are given in Table 4.9.

**Table 4.9: Calculated molar absorptivity coefficient for nine selected wavenumbers in the acetone spectrum.**

Wavenumber (cm <sup>-1</sup> )	Molar absorptivity coefficient (L mol <sup>-1</sup> cm <sup>-1</sup> )
787	1.37
903	5.53
1095	7.97
1196	7.95
1242	8.36
1327	8.76
1474	8.61
1674	9.76
1767	10.19

The calculated molar absorptivity values were then used with the acquired absorbance values for acetone for the six ATR MIR probes to determine the pathlength for each probe at the nine selected wavenumbers. Six replicate measurements of acetone were acquired using all six *in situ* ATR MIR probes, the pathlength was determined for each measurement and then the average was calculated. An example calculation for one measurement acquired using probe 1 at 1095 cm<sup>-1</sup> is given below:

$$b = \frac{A}{\varepsilon c}$$

$$b = \frac{0.0695}{7.97 \times 13.619}$$

Therefore the pathlength is  $6.399 \times 10^{-4}$  cm or  $6.399 \mu\text{m}$  at  $1095 \text{ cm}^{-1}$ . The average pathlength results for the six probes at the nine wavenumbers in the acetone spectrum, indicated in Figure 4.18, are given in Table 4.10 after conversion to  $\mu\text{m}$ .

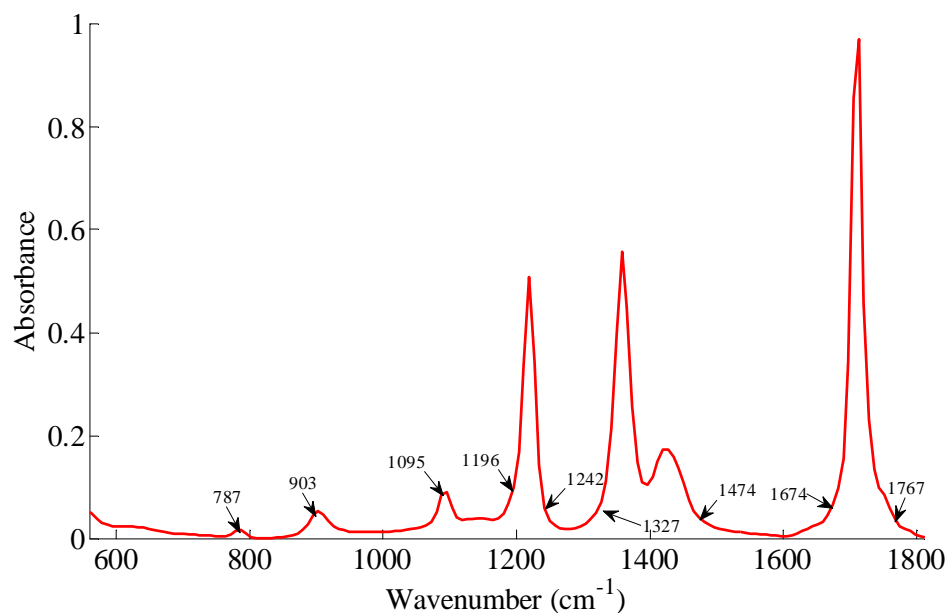


**Figure 4.18: Average (n=6) ATR MIR absorbance spectra of acetone (calibration 2) in the range 560 – 1810  $\text{cm}^{-1}$  using probe 6.**

**Table 4.10: Calculated average pathlengths for six ATR MIR probes at nine selected wavenumbers.**

Wavenumber ( $\text{cm}^{-1}$ )	Probe 1	Probe 2	Probe 3	Probe 4	Probe 5	Probe 6
	Pathlength ( $\mu\text{m}$ )					
787	6.6	7.6	9.6	5.9	6.7	8.7
903	5.1	5.6	6.6	5.5	4.3	7.2
1095	6.4	6.2	7.2	6.8	4.0	8.3
1196	8.1	7.0	8.3	7.1	4.5	9.2
1242	4.9	4.7	5.0	5.0	3.0	5.2
1327	4.5	4.4	5.4	5.0	3.4	5.9
1474	2.7	2.5	3.1	3.8	1.7	3.5
1674	4.0	3.7	4.6	4.9	0.8	5.0
1767	2.2	1.8	2.3	3.0	*	2.7

\*Absorbance values too low to calculate pathlength.

Variations in the pathlength over the spectral range can be observed for the ATR probes and the trends for probes 1 and 5 are given in Figure 4.19; the points relate to the actual calculated pathlengths and the lines between the points are there only to make the general trend easier to view. The trends for probes 2 and 6, and 3 and 4 are given in Figure 4.20 and Figure 4.21, respectively.

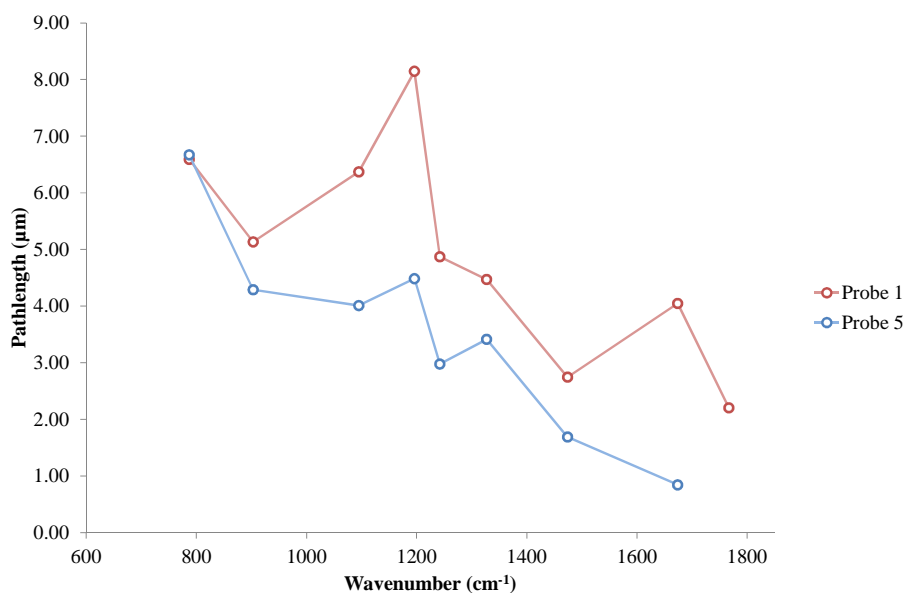


**Figure 4.19: Pathlength vs. selected wavenumber for probes 1 and 5 with lines between points to highlight the increasing and decreasing trend in the pathlength of the probes.**

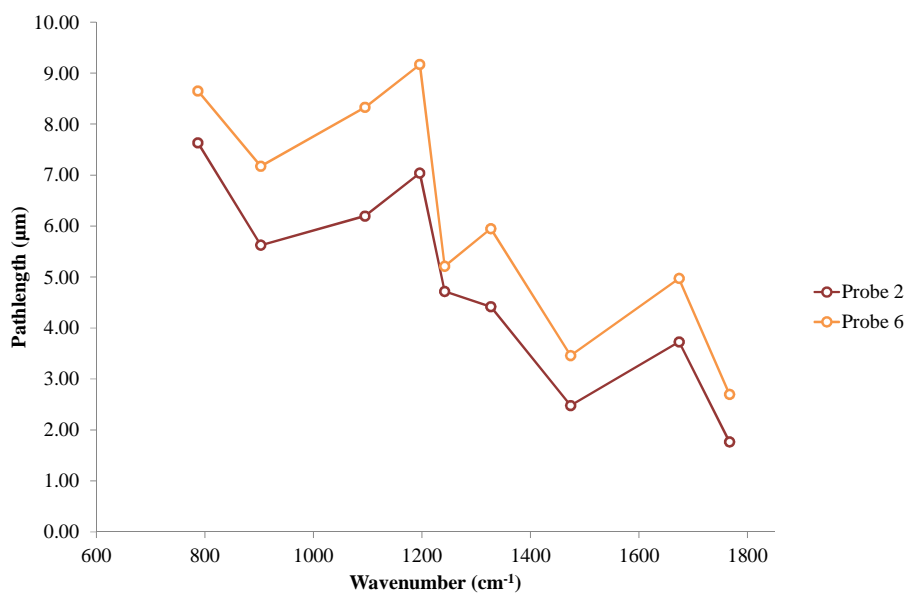


**Figure 4.20: Pathlength vs. selected wavenumber for probes 2 and 6 with lines between points to indicate the increasing and decreasing trend in the pathlength of the probes.**

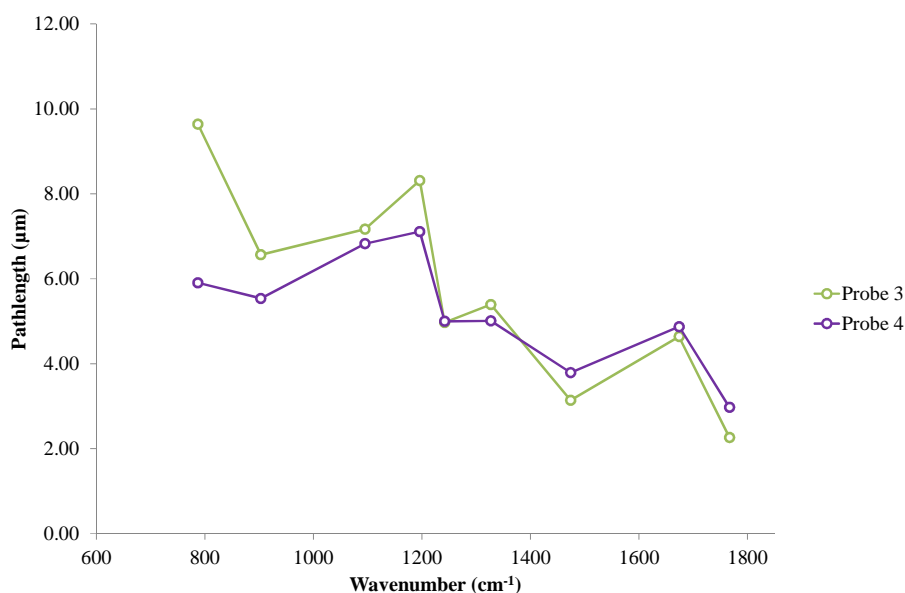


**Figure 4.21: Pathlength vs. selected wavenumber for probes 3 and 4 with lines between points to indicate the increasing and decreasing trend in the pathlength of the probes.**

Reviewing the results of the pathlength determinations for the six ATR probes, several conclusions can be made:

- Probes 1 – 3 and 6 follow similar trends where there are large pathlengths at  $787\text{ cm}^{-1}$ , these decrease at  $903\text{ cm}^{-1}$  before increasing again to the maximum pathlength observed at  $1196\text{ cm}^{-1}$ . From this point the pathlength decreases considerably to  $1474\text{ cm}^{-1}$  and remains small with the exception of a minor increase at  $1674\text{ cm}^{-1}$ .
- It is difficult to determine if the pathlength increases at  $1196$  and  $1674\text{ cm}^{-1}$  are anomalies in the data, however as the trend is similar between 4 of the dual fibre probes, it is likely that these increases are real. Comparing the trends in pathlength to Figure 4.18, the increase in pathlength occurs when there is an increase in absorbance, where an acetone peak arises; therefore the increase may be due to acetone absorbing more strongly in these regions.
- A slight difference in trend is observed for probe 4, higher pathlengths at  $1196$  and  $1674\text{ cm}^{-1}$  still occur, however, lower pathlengths are observed at lower wavenumbers for this probe.
- Probes 3 and 6 have larger pathlengths at lower wavenumbers in comparison to the other probes.

- At higher wavenumbers, probe 4 and 6 have longer pathlengths, however, probe 3 is not that much lower.
- The single fibre probe, probe 5, follows a different trend to the dual fibre probes, with a steady decrease from the maximum pathlength at  $787\text{ cm}^{-1}$  to its lowest pathlength at  $1674\text{ cm}^{-1}$ . No pathlength was determined at  $1767\text{ cm}^{-1}$  as the absorbance values were too low.
- Considering the pathlength results, probe 6 provides the largest pathlength, with probe 3 providing similar results.

## 4.4 Conclusions

The six ATR MIR probes were all able to be used to analyse and produce good quality spectra for the sample mixtures. The most prominent difference observed between the spectra of the different probes was the change in absorbance, which can be related to a change in pathlength caused by differences in the angle of incidence at the crystal surface, causing changes in the penetration depth, or by the number of reflections within the diamond crystal. Due to the design of the probes it is difficult to determine exactly where these changes originated from and it is most likely that a few factors in the design of the probe affect both the angle of incidence and the number of reflections in the crystal. A difference in peak ratios was observed for acetone for the original probe design, probe 6, and the mono fibre design, probe 5. The difference in the ratios of the peaks in probe 5 can be explained by the change in the pathlength, as the investigation revealed that the pathlength steadily decreases from  $787 - 1674 \text{ cm}^{-1}$ , so this probe has small pathlengths of less than  $1 \mu\text{m}$  around  $1700 \text{ cm}^{-1}$  in comparison to the dual fibre probes which see an increase in pathlength around the same region. The decrease in pathlength for the single fibre probe 5 is most likely due to the implementation of a smaller diamond cone crystal when the smaller diameter design was incorporated. It is more difficult to explain the absorbance differences observed with probe 6 at different wavenumbers; higher pathlengths are observed around wavenumbers where acetone peaks occur, however, when comparing the spectra of all the probes, these results do not reflect the results of the pathlength determination study. The main reason for this, is because the pathlengths were not determined for the actual acetone peaks for reasons discussed previously, therefore, for example, the acetone peak at  $1219 \text{ cm}^{-1}$  has the largest absorbance with probe 4. However, the pathlength results for  $1196 \text{ cm}^{-1}$  suggest that probe 6 has the largest pathlength and, therefore, the higher absorbance; observing the overlaid spectra of all the probes at  $1196 \text{ cm}^{-1}$ , there is a higher absorbance for probe 6 at this wavenumber, but not for the acetone peak at  $1219 \text{ cm}^{-1}$ . The difference in the peak ratios of probe 6 versus the other dual fibre designs, suggests that the design changes implemented have had an effect on the spectra. However, the trends observed for the pathlength determinations show different results; the trends

for the dual fibre probes are similar, indicating similarities between the probes. The ratio differences observed in the spectra for probe 6 cannot, therefore, be explained with the results from the pathlength determinations. It is likely that more information could be deduced if pathlengths could be determined for the wavenumbers where acetone peaks occur.

The predictions of analyte concentrations indicated that all six probes could be used to successfully predict the concentrations of the analytes. Probes 1 and 3 have the best performance when RMSEP and %RSD are considered. Probe 1 introduced a new diamond cone sealing; it is clear that the design change from the original probe, probe 6, has made an improvement, however, it may be possible that other design differences that may have been incorporated, such as fibre selection may have caused the change in performance rather than the use of new diamond cone seals. Probe 3 incorporated the new diamond cone sealing and fibre alignments, as well as the new size and geometry of diamond crystal. From the increased performance and good pathlength results obtained with probe 3, it is evident that the changes have made an improvement, as probe 3 provided better overall performance than probe 1 and 2. The results observed for probe 2 were very similar to those of probes 1, 3 and 4 indicating that the fibre alignment had provided an improvement over the original manufactured design and allowed good performance to be maintained between the other dual fibre probes. The spectra acquired using probe 4 were very similar to those measured with probes 1, 2 and 3, as was the performance for predicting the concentration of analytes; it seems, therefore, that the use of modular components for the manufacture of the probes did not adversely affect performance. However, there was a pathlength decrease observed at lower wavenumbers for this probe when compared to the other dual fibre probes.

Overall, the design changes implemented have improved the performance of the probes in comparison to the original design with the best results being obtained by probe 3. The observations indicate that the size and geometry of the diamond crystal have a large impact on the probe performance. It was also interesting to note that the

modular component design approach to probe manufacturing, with its production advantages, did not adversely affect probe performance.

The results of this study have indicated that changing the size and geometry of the diamond crystal in the probe have made improvements to the overall performance of the ATR MIR probes, therefore, future recommendations to Fibre Photonics would be to implement the newer diamond cone design and to ensure repeatable manufacture of the crystal, to increase the consistency between probes. In addition, the use of modular components was shown not to adversely affect the performance of the probes; if Fibre Photonics adopt this manufacturing procedure they should be able to efficiently produce robust ATR MIR probes that give consistently good performance. The removal of the non-IR active malleable material, AgCl, and improvement of the fibre end cutting and fibre alignment procedures appears to have also improved the overall performance of the probes, indicating that the AgCl material is no longer required; therefore, the number of seal breakages and leakages should be minimised, consequently improving the robustness of the probes.

## 4.5 References

1. *Personal communication*, G. Colquhoun, Fibre Photonics, Livingston, 2011.
2. *Fibre Photonics*, <http://www.fibrephotonics.com>, Accessed 04/08/2011, 2011.
3. *Optical fibre probe for attenuated total reflectance measurements*, *United States Pat.*, 5218656, 1993.
4. *REMSPEC Corporation*, [www.remspec.com](http://www.remspec.com), Accessed 12/10/2011, 2011.
5. *Optical fibre coupled devices for remote spectroscopy in the infrared*, *United States Pat.*, 5170056, 1992.
6. *Bruker Optics*, [www.brukeroptics.com](http://www.brukeroptics.com), Accessed 12/10/2011, 2011.
7. *Temperature resistant IR measurement probe*, *Germany Pat.*, DE 102005052223, 2007.
8. *Mettler Toledo*, [uk.mt.com](http://uk.mt.com), Accessed 12/10/2011, 2011.
9. *Personal communication*, M. Holden, University of Strathclyde, Glasgow, 2008.
10. H. Günzler and H.-U. Gremlich, *IR Spectroscopy: An Introduction*, Wiley-VCH, Weinheim, 2002.

## 5 Calibration models for analyte prediction

### 5.1 Introduction

#### 5.1.1 The use of calibration models

Multivariate calibration models are widely used in industry for a variety of techniques, especially for spectroscopic measurements. They are used successfully to determine quantitative information from complex analytical data and, therefore, widely used in optical spectroscopy. In particular, NIR spectroscopy is dependent upon multivariate calibration for quantitative analysis and advances have been made in the applications of NIR spectrometry due to the capability of the multivariate calibration models. A multivariate calibration can take a lot of effort to build and, therefore, it is intended for use over a long time period; in comparison, univariate calibration can be simpler to implement, but may require recalibration on a day-to-day basis. Generally, multivariate models are based on a large number of real samples collected over a period of time and hence it is time intensive to develop robust calibration models.

Although calibration models are designed primarily to be used for an extended period of time, if any changes to the initial process conditions or equipment are introduced, the robustness of the model may be affected, reducing the accuracy of the results obtained. A number of situations can arise where the multivariate calibration model may become invalid: if the instrument used for development of the original calibration has been replaced; if there have been temperature fluctuations and measurements have been taken at an altered temperature; if there has been instrumental drift in the instrument over time; if there has been a shift in the instrumental response; or if there has been a physical change to the composition of the samples under analysis.<sup>1</sup> In these circumstances a full recalibration would normally be required, incurring extra costs and downtime while this is completed. To avoid preparing completely new multivariate models from scratch, various calibration transfer methods have been devised to reduce the likelihood of erroneous measurements or limit the number of additional experiments that need to be carried out to allow the model to still be appropriate.

### 5.1.2 Calibration transfer methods in infrared spectrometry

The transfer of calibration models is seen as a major challenge in industry as the models can be very sensitive to small variations in both the wavelength and absorbance in the spectrum.<sup>2</sup> These small variations can cause a calibration model to become invalid for prediction of concentrations based on spectra taken with e.g. a new analyser system. The direct transfer of calibration models does not usually provide satisfactory results owing to minor differences between instruments and changes in performance characteristics over time. For this reason, instrument standardisation methods were developed to deal with the problem and aid the transfer of calibration models.<sup>2</sup>

Since the implementation of PAC and chemometric analysis, there have been a range of articles relating to the use of calibration transfer and instrument standardisation in NIR spectrometry. As MIR spectrometry has been used less frequently in process analysis than NIR spectrometry (owing to the aforementioned problems with optical fibres), there are fewer examples of MIR calibration model transfer. However, many of the advancements made in the NIR model transfer could be applicable to MIR analysis.

De Noord,<sup>1</sup> Feudale *et al.*,<sup>3</sup> and van den Berg *et al.*<sup>4</sup> have discussed the issues surrounding calibration transfer and the various methods in place for instrument standardisation. Different strategies that can be used before a given calibration model is implemented were discussed and the main ideas that have been brought forward from these reviews are outlined below.

Instrument matching involves the careful control of the experimental parameters in order to keep the two instruments as similar as possible. To achieve this, the analyst is required to identify the parameters which are most critical for the transferability of the model. Adhihetty *et al.*<sup>5</sup> described a method for the matching of two FTIR spectrometers through the control of experimentally dependant variables. It was expressed that the experimental variables that can affect the model transfer must be identified. Therefore, there is high importance on the control of these variables to

allow the model to be transferred successfully. The major caveat to this strategy is that the analyst is required to have simultaneous access to both instruments. De Noord<sup>1</sup> also noted that instrument matching could only be used if two instruments of the same manufacturer and type were being used. Instrument matching does have merit in some applications; however, the inherent restrictions make this method impractical in every day industrial applications.

Robust calibration models are designed to withstand changes between instruments, temperatures etc., and different approaches have been developed. The first approach, referred to as global models, seeks to include the different sources of variation in the design to develop a universal model. Global models contain the expected variation for a wide range of experimental conditions and, therefore, will have less sources of variation that need to be strictly controlled in future data. To develop an accurate global model, the analyst must be able to anticipate any new sources of variance and also the full degree of the variability within the data. Ozdemir *et al.*<sup>6</sup> discussed the performance of genetic regression (GR) for optimum wavelength selection to correct for instrumental drift. GR has been shown to compensate for wavelength shifts of up to 4 nm for multi-instrument calibration. The predictions of the models improved when the shifted data was incorporated in the model. Global models can be very complicated; however, they have been shown to provide reliable predictions. Despagne and Massart<sup>7</sup> indicated that the predictions from a global model were not as accurate as from a local model if there were non-modelled variations present in the data. It is clear that if there is a possibility of any future variability in the experimental conditions, it should be reduced where possible to ensure better predictions.

A second approach discussed for the development of robust calibration models is based upon the variables used for model building. Robust models can be built when variables that are insensitive or have reduced sensitivity to the variations in instrumental changes or experimental conditions are incorporated in the model.<sup>8</sup> Therefore, when variations do occur in the spectra, because of changes to experimental conditions or a change in instrument, then the variables will present

little change in the regression coefficients. There are a number of examples of this approach in the literature<sup>9-12</sup> and some involve the use of orthogonal methods.<sup>13-15</sup> Ozdemir *et al.*<sup>16</sup> described a procedure for the calibration of multiple instruments where the spectra from each were used during the construction of the calibration models. Genetic algorithms enabled the discovery of the variables that allowed the calibration model to be used for two near-infrared systems. Robust models were built which required minimal data collection from the second instrument, providing time saving benefits for calibration transfer. No pre-treatment was required for implementation; also the method did not require the same resolution for both instruments. The success of this approach is undoubtedly dependent on finding suitable variables that are insensitive to variation, but sensitive to quantifying the analyte.

Model updating accounts for new variations by rebuilding the model with the addition of a small number of test samples to the existing calibration set. The samples that are added must accurately describe the variability of the new instrument in a way that the model is applicable to both the new and the old instrument and is valid for both. The addition of these new samples will make the model more robust to the new measurement conditions and so will lead to better predictions. Some different approaches have been explored including sample selection,<sup>17, 18</sup> weighting,<sup>19, 20</sup> the blank augmentation protocol<sup>21</sup> and Tikhonov regularisation.<sup>22-24</sup> Greensill *et al.*<sup>17</sup> completed an assessment of a number of chemometric techniques for calibration transfer between spectrometers including model updating. The selected spectra, determined by the Kennard-Stone method, were used to successfully transfer calibration models between the spectrometers providing good predictions and in some cases better RMSEP results. A problem exists with model updating in that only a few new samples are added to the original model and so there may be a large difference noted between the new and old samples, causing an increase in the error of the model. Setarehdan *et al.*<sup>18</sup> addressed this issue by developing a strategy, based on PCA and PLS multivariate techniques, to help decide which new samples should be added to the calibration set. With the use of these multivariate techniques, a new sample can be defined by how “similar” it is to the samples that were currently

used in the calibration dataset. This is completed by residual analysis after PCA is performed. If the sample under consideration has a spectrum “similar” to the spectra of the calibration samples in the dataset, then an assumption is made that the current model can predict the analyte concentration of that sample. However, if the sample under consideration is defined as being “dissimilar”, it indicates that this sample contains new information that is not modelled by the current calibration dataset. This sample is then added to the calibration data set to improve the model. Stork and Kowalski<sup>19</sup> investigated the theoretical weighting scheme for updating regression models. They discussed the issue around the calibration set being dominated by samples collected from the original model before any changes arose. By implementing a weighting scheme and hence increasing the contribution of the new component to the model, the error can be reduced; this will result in a decrease in the prediction error. Model updating has the advantage of not requiring the measurement of standardisation samples on both spectrometers. Although, it has the inherent disadvantage that for complex systems a considerable number of samples are required to capture the new variance and so the model updating method tends towards full recalibration.<sup>3</sup>

As well as the strategies mentioned above, de Noord<sup>1</sup> and Feudale *et al.*<sup>3</sup> also discussed the different standardisation methods that are available for the transfer of calibration models after they have been built. In the standardisation methods reviewed, the response function of a secondary system is modified to match the response function of the primary system. In general, there are three ways to achieve this: standardise the regression coefficients,<sup>25-27</sup> the spectral responses<sup>25, 28</sup> or the predicted values using mathematical manipulation.<sup>29</sup>

#### Standardisation of the regression coefficients

The standardisation of the regression coefficients for the model can be completed by a method that was proposed by Wang *et al.*<sup>25</sup> The transfer method involves the transformation of the original model into a new model that will be suitable for the new system. This method can be defined for both classical and inverse calibration

models. The classical method is expressed with two main assumptions being implied throughout:

- the linear relationship of the response of the instruments;
- the concentrations for all of the analytes that contribute to the response are known.

The inverse calibration models differ from classical model standardisation as only the concentration of the analyte of interest needs to be known. Wang *et al.*<sup>25</sup> noted that inverse model standardisation worked well when applied to comparatively large sample sets. Also, it was observed that classical model standardisation can be restricted in its modelling ability, nevertheless it has the ability to work with fewer samples than that of the full calibration set.

#### Standardisation of the spectral responses

Standardisation of the spectral responses models the instrumental differences using regression of the spectral responses of a set of samples measured on the primary instrument against the same set of samples measured on the secondary instrument. As a result, any changes in the response between the two instruments can be corrected for, and then the initial model can be used for prediction on the secondary instrument without the need to formulate new regression coefficients. In the literature, there have been examples of both univariate and multivariate methods which have been proposed to standardise spectral responses from a secondary instrument.

Feudale *et al.*<sup>3</sup> discussed the univariate standardisation approach that was developed by Shenk and Westerhaus,<sup>28</sup> which comprises a single correction factor at every wavelength channel to correct for the intensity differences between spectra. The Shenk and Westerhaus algorithm has been utilised for calibration transfer across NIR instruments in a number of examples.<sup>25, 30-33</sup> Bouveresse *et al.*<sup>30</sup> employed the algorithm for calibration transfer across NIR instruments where different standardisation samples were used. Using this algorithm they were able to determine the best standardisation sample set that would gain the best predictions. They discovered that the best results were achieved when using samples that covered the

same range as the prediction samples, or at least a subset of this range. The algorithm provides poorer results if the standardisation samples employed are of a different nature to those samples being analysed. Bouveresse and Massart<sup>31</sup> investigated different alterations to the spectral intensity correction step of the Shenk and Westerhaus algorithm in an attempt to improve the results when the nature of the samples is different; applying locally weighted regression in the spectral intensity correction step produced better results in comparison to simple linear regression. The modified algorithm allows standardisation with samples of a different nature to those being analysed and does not require analysis of the standardisation samples on both instruments.

As the majority of spectral data requires the use of multivariate analysis there has been some important developments made in this area. Two well-known and commonly used standardisation methods that were developed by Wang *et al.*<sup>25</sup> are direct standardisation (DS) and piecewise direct standardisation (PDS). Since their introduction for calibration transfer, a considerable amount of effort has been extended to improve their application.<sup>8, 17, 29, 34-55</sup> The DS method corrects the spectra acquired on the second instrument to match the spectra that were collected on the primary instrument, while the original calibration model remains unchanged. The responses from the two instruments are related to one another by a transform function. The spectra measured on the second instrument are then standardised to match the spectra collected on the primary instrument using the transform function. The standardised spectra can then be used along with the original unchanged calibration model to predict the unknown concentrations of the samples from the secondary instrument. A problem with this approach and with PDS is around the additive background. When this additive background term is unaccounted for, incomplete transfer of calibration models between instruments can be seen. Wang *et al.*<sup>37</sup> addressed this issue and proposed additive background correction measures. The correction consisted of mean-centring each set of transfer samples to remove any constant baseline differences present. Another difficulty is the number of standardisation samples chosen for the transform is usually smaller than the number of variables. Therefore, if the selected subset of standardisation samples does not

cover the whole experimental space, not all of the spectral information contained in the spectrum of the test sample measured on the secondary instrument will be transferred by DS. The spectral information that is orthogonal to the space spanned by the spectra of the standardisation samples measured on the secondary instrument will be lost during transformation leading to poor results. A large number of standardisation samples are needed to avoid this problem. Other solutions to this issue include estimation of the transform function by means of PLS regression or a reduction in the number of variables involved in the regression; this lays the foundation for PDS. PDS is similar to DS, however, it aims to recreate each spectral point on the primary instrument from several measurements in small channel windows on the secondary instrument. The calculation of the transform function in PDS differs from DS in that it does not use the entire spectrum of the transfer samples to correct each wavelength on the secondary instrument. Instead PDS uses variables in the local window around the channel of interest; this is because when the responses on one instrument are shifted to the other, information about the shift is most likely to be found in restrictive local regions in the second instrument.<sup>34</sup> This window size can be varied and should be optimised before use for calibration model building. As PDS uses a moving window, edge effects can occur where there is insufficient data to be able to form a complete window. In these cases, the ends of the spectra are either removed or estimated by extrapolation.<sup>8, 35</sup> PDS is one of the most widely used transfer methods due to its capability at enabling the simultaneous correction of intensity differences and wavelength shifts. Wang *et al.* described a study where transfer results with PDS were better than those of the full set recalibration.<sup>36</sup> Although PDS is commonly used for calibration transfer it is not without problems. One of the main issues associated with PDS has been the observation of artefacts in the transferred spectra. Bouveresse *et al.*<sup>38</sup> described the occurrence of artefacts when subsets of samples which are not representative of the entire experimental domain are used. If the subset of samples are selected using algorithms such as the Kennard and Stone algorithm or leverage algorithm, which aim to select samples which are representative of the entire experimental domain, then a reduction in the artefacts present in the transferred spectra were observed.

Newer standardisation procedures have now been developed and their performance compared to that of other standardisation methods.<sup>56-59</sup> Chen *et al.*<sup>56</sup> implemented a procedure that could correct for temperature-induced spectral variations, named loading space standardisation (LSS). The main feature of LSS is a correction procedure which standardises the loading space. To build the LSS correction model, two parameters must be known: the degree of the polynomials and the number of factors that describe the information in the spectra. The degree of the polynomials is dependent on the non-linearity of the temperature effects and it is this that allows this standardisation method to correct for temperature-induced variations. The number of factors should be no less than the number of chemical components contained in the samples. As well as the two parameters required to build the LSS correction model, another parameter must be optimised during the process to allow this procedure to effectively model the temperature effects. This parameter is the number of standardisation samples included in the procedure. Chen *et al.* were able to show the LSS standardisation method successfully corrected the effects of temperature variations in NIR spectra of ternary mixtures of ethanol, water, and 2-propanol. If the calibration model is built on the temperature closest to that of the test samples then more accurate predictions will result. Limitations of LSS are the requirement to measure the temperature for every spectrum and that the same training samples must be used to acquire the spectra at the different training temperatures. Chen and Morris<sup>57</sup> further developed the LSS procedure to incorporate an optical path-length estimation and correction method (OPLEC) to address the problems of multiplicative influential mode and composition-related influential mode, which can jointly affect spectral measurements. This new procedure, termed extended loading space standardisation (ELSS) proposed to linearize spectroscopic data which had changes in external variables. ELSS was able to monitor both the temperature-induced spectral variations as well as the multiplicative effects from the variations in the measurement conditions. The ELSS procedure outperformed both the original LSS and global PLS procedures providing better predictive performance. ELSS has been implemented in the on-line monitoring of batch cooling crystallisation of organic compounds using ATR-FTIR spectroscopy,<sup>60</sup> providing enhanced predictive ability over the other models assessed.

Papers by Chen *et al.*<sup>59</sup> and Du *et al.*<sup>58</sup> highlight the need for methods which are easier to implement and at the same time can handle complex situations and provide better performance. Each set of authors has proposed a new strategy for calibration standardisation. Chen *et al.*<sup>59</sup> offered the systematic prediction error correction (SPEC) method; this includes a transformation which is a special case of LSS. The concentration of the target analyte in the test samples can be predicted from its standardisation spectrum by a multivariate linear calibration model built using the spectra of the calibration samples measured at the calibration conditions. The standardisation includes the systematic prediction error of the multivariate linear calibration model caused by spectral differences due to variations in the measurement conditions or changes in instrument. Chen *et al.* compared their SPEC method to other calibration standardisation procedures for two different data sets and found that SPEC improved the predictive results when changes in instrument and experimental conditions occurred. A benefit of SPEC is that implementation is relatively uncomplicated, with only one model parameter requiring optimisation. The number of chemical variation sources in the spectral data must be known; this can be set to the number of significant singular values of the spectral data. The simple implementation of SPEC has advantages over procedures like PDS which require multiple parameters to be optimised to gain the best prediction results. The proposed method by Du *et al.*<sup>58</sup> involves the spectral standardisation by spectral space transformation (SST). SST follows on from previous methods whereby spectra that are measured on a secondary instrument are corrected to match the spectra acquired by the primary instrument while the model remains unchanged. The SST procedure eliminates, where possible, any spectral differences caused by the change in instrument or experimental conditions, by a transformation between two spectral spaces spanned by the related spectra of a subset of standardisation samples measured on both instruments. SST was tested with a set of NIR and MIR data and the results were compared with other standardisation methods. In both the NIR and MIR examples, SST produced better predictions than PDS, univariate slope and bias correction (SBC), and global PLS, providing evidence that SST can be used to correct for spectral variations caused by changes in instrumental or experimental

conditions maintaining the predictive ability of the original model. SST does require the analysis of the standardisation samples to be analysed with both sets of conditions, as with PDS. However, SST is easier to implement requiring the optimisation of only one parameter, the number of principal components that represent the spectral information in the data of the standardisation samples. Du *et al.* have shown that in practice this can be set equal to or slightly larger than the number of significant singular values of the combined data. SST can provide better predictive results than the other standardisation methods with the advantage of its simple implementation.

#### Standardisation of the predicted variables

Standardisation of the predicted variables is commonly achieved by using univariate slope and bias correction (SBC).<sup>29</sup> In this method the spectra of a calibration sample set measured on the primary instrument are predicted with the calibration model that was developed using the secondary instrument, which allows a univariate linear model to be developed to correct the predicted values.<sup>29</sup> SBC thereby assumes that there is a linear relationship between the predictions measured on the secondary instrument to those predictions that would have been attained if the samples were measured on the primary instrument. The test spectra measured on the primary instrument were then predicted using the calibration model developed on the secondary instrument and the predictions were then corrected using the univariate linear slope and bias correction model developed in the previous step. Bouveresse *et al.*<sup>29, 61</sup> were able to demonstrate that for simple univariate corrections of the predicted values, the SBC method was a success when identical instrumentation was used. However, if unrelated instruments were used the differences between the instrumental responses are more complex and SBC will be less likely to obtain satisfactory corrections with non-standardised spectra. Furthermore, de Noord<sup>1</sup> does not recommend this approach if the calibration models that are to be used are more complex than univariate or simple multiple linear regression (MLR). Pereira *et al.*<sup>52</sup> completed a study comparing seven transfer methods and two pre-treatment procedures for calibration transfer between three NIR spectrometers, for the determination of compounds in a broad set of gasoline samples. SBC was found to

provide the worst results of the seven transfer methods investigated when a transfer was made between two instruments of the same or different manufacturer and type. This work supports the idea of SBC being difficult to use successfully for the transfer of models other than those that involve simple univariate corrections. Bergman *et al.*<sup>47</sup> described a comparison of standardisation methods for model transfers, indicating for their models that SBC has the ability to be used for transfer of calibration models between instruments of similar type, e.g. from one dispersive instrument to another and between instruments of different types, e.g. from a dispersive instrument to a FT instrument. For the SBC method, the individual concentrations of active ingredient within the samples used for the transfer had to have a variance of at least 2.5% to achieve acceptable results. To obtain the best results, the samples used for the correction were required to have individual concentration variances between 5-8% in the active material content. This method also required a larger number of samples to be involved in the correction to generate good results. In this study by Bergman *et al.*,<sup>47</sup> although SBC was used successfully in the transfer between different instrument types, the other methods investigated had perceivable advantages over SBC for the calibration transfer.

#### Other standardisation methods

The calibration transfer methods described thus far have been used successfully for a variety of applications in industry, however in addition to these there has been some literature on other methods for standardisation and calibration transfer.<sup>62-67</sup> For the most part, standardisation methods are used to model the relationship between the spectra in the original measurement space. However, these models can also be used to model the differences between spectra that have been transformed to another domain. It was Walczak *et al.*<sup>62</sup> that proposed that standardisation be done in the wavelet domain (WD) and compared the performance to that of the PDS and SBC methods for two different data sets. This method relates the wavelet transform coefficients of a small subset of standard samples, which have been acquired on two instruments, with univariate linear models. These models are then used to transfer the wavelet coefficients of the new spectra, after which conversion back to the wavelength domain is completed.<sup>42, 62</sup> Standardisation can also be completed in

principal component (PC) space, whereby the PC scores for the samples are transferred from the secondary to the primary instrument and then converted back to the original variable space. For both methods, any spectral variation is compressed and, therefore, can lead to greater stability when the transfer is taking place. As a consequence of this compression along the wavelength axis, any window-based standardisation methods such as PDS cannot be used as the local information is not retained and, therefore, compression is difficult. For that reason the transfer in these domains is limited only to univariate models or to direct standardisation methods.<sup>68</sup> <sup>69</sup> Further discussions by Liu *et al.*<sup>70</sup> described the use of wavelet regression in multivariate calibration and calibration transfer for data fusion detailing the advantages and disadvantages.

There has been work in the area of artificial neural networks (ANNs) for standardisation.<sup>66, 67, 71-73</sup> The major caveats to ANNs for standardisation are around the fact that ANNs generally experience over-fitting problems; this is because a reasonably sized ANN will have far more parameters to be estimated than there will be transfer samples available. Also, ANN models are optimised on the ability of the network to produce a spectrum instead of the ability to minimise prediction errors. Consequently, ANNs are still not commonly used as standardisation methods, although work completed by Fei *et al.*<sup>67</sup> has shown some possibility that ANNs combined with genetic algorithms can provide smaller prediction errors than PLS models.

In addition to the ongoing work into ANNs standardisation and wavelet hybrid standardisation methods, there has been work published in the area of non standardisation methods such as Gaussian process regression for multivariate spectroscopic calibration.<sup>74</sup> Gaussian process regression is a different method for the development of a calibration model derived from the perspective of Bayesian regression analysis. It was shown that this method could achieve reliable and acceptable results for both linear and non-linear data sets. Gaussian process regression looks promising to the future work of calibration transfer although there are still some issues present: the multiple component calibration requires separate

models for each response variable and at the time of publication the solution involved significant computational power. Further work developed possibilities in the use of Gaussian process regression for calibration transfer with multivariate regression.<sup>75-77</sup> Another method, that has been about for a number of years, is orthogonal signal correction (OSC), which is a procedure used in the pre-processing stages of modelling.<sup>78, 79</sup> Sjöblom *et al.*<sup>78</sup> evaluated the use of orthogonal signal correction when applied to calibration transfers of NIR spectra. It was shown that OSC gave comparable results when compared with PDS methods. Canonical correlation analysis (CCA) was discussed and compared with traditional PDS methods by Fan *et al.*<sup>80</sup> The results showed that the method based on CCA could be used successfully to correct for the differences noted between the spectra measured on different instruments. When compared with PDS, it can be observed that when there is a great deal of information known about the variability between the instruments, then the CCA method can outperform PDS. However, in some instances, gaining enough knowledge about the between-instrument variations is not always possible, and in the cases where the information is limited and the sample subset is small, PDS is superior.

The majority of the methods discussed have been successfully applied to various calibration transfer problems. No one method can be selected as being able to provide the best results for calibration transfer of complex systems, however some standardisation methods such as PDS are, by and large, the accepted method. Some positive results have also been shown in the areas of ANNs and non standardisation methods. In spite of all of this, the choice of calibration transfer methodology will ultimately depend upon the application for which it is required, as no method is successful in all situations.

### 5.1.3 Basis of this study

The above review has indicated that since the introduction of direct standardisation and piecewise direct standardisation by Wang *et al.*,<sup>25</sup> procedures such as LSS, SPEC and SST have been developed that provide advantages in easier implementation and the ability to obtain equal or better predictive results than some of the commonly used methods. The majority of applications have been directed at NIR calibration transfers owing to the routine use of this technique in industry. However, with advances in fibre and probe technology more applications involving MIR spectrometry can now be found.

In this study, the widely used standardisation methods DS and PDS have been investigated for their use in calibration transfer of MIR calibration models where the spectrometer, probe or both have been altered. The newer procedure SST has also been investigated and compared to the predictive results of DS and PDS to assess the claims of Du *et al.*<sup>58</sup> that SST is easier to implement and has the ability to complete calibration transfers using a reduced number of standardisation samples. In process analysis, it is often necessary to scale up systems when moving from development to manufacturing. This can involve a change in the size of *in situ* probes used for spectral measurements. So, an additional part of this study involved the building of a calibration model using spectra acquired with a smaller probe (imitating a laboratory set-up) with transfer to predict the concentrations of analytes from the spectra analysed with a larger probe (imitating scale-up). The performance of DS, PDS and SST based on the root mean square error of prediction (RMSEP), was compared when different numbers of standardisation samples were used in the standardisation procedures.

## 5.2 Experimental

### 5.2.1 Solvent mixture sample preparation

Previous work carried out by M. Holden<sup>81</sup> selected mixtures of acetone, ethyl acetate and ethanol as model systems to assess the MIR ATR probes and spectrometers. A solvent mixture design was created to determine the concentrations of the three components that should be present in each of the calibration and test samples (Figure 5.1). This mixture design was used for comparison with PCA scores plots to determine the similarities and differences in the data obtained.

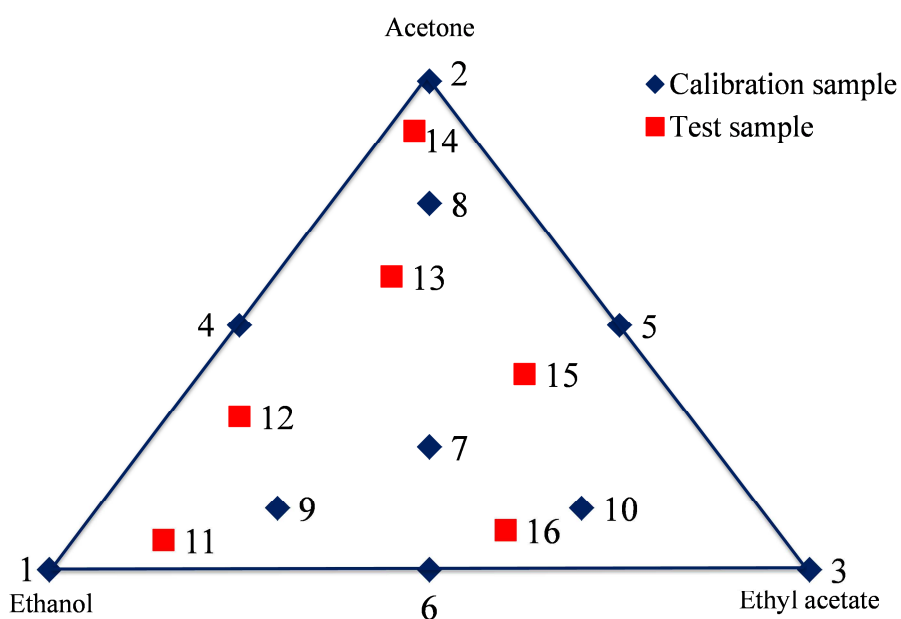


Figure 5.1: Schematic of the sample mixture design for acetone, ethanol and ethyl acetate.

Mixtures for this study had been prepared beforehand by Megan Holden using the method described in section 4.2.1. The weights of each of the three components for the 16 mixtures prepared are tabulated in Appendix 5.1. The concentrations of each component in the mixtures were calculated as a weight percentage; these values can be viewed in Table 5.1.

**Table 5.1: Concentrations of acetone, ethanol and ethyl acetate present in each mixture.**

Mixture number	Concentrations as weight percentage (% w/w)		
	Acetone	Ethanol	Ethyl acetate
1 – calibration 1	0.0	100.0	0.0
2 – calibration 2	100.0	0.0	0.0
3 – calibration 3	0.0	0.0	100.0
4 – calibration 4	50.0	50.0	0.0
5 – calibration 5	50.0	0.0	50.0
6 – calibration 6	0.0	49.9	50.1
7 – calibration 7	33.3	33.4	33.3
8 – calibration 8	65.6	17.4	17.0
9 – calibration 9	17.1	66.0	17.0
10 – calibration 10	17.0	17.0	66.0
11 –test 1	6.0	85.0	9.0
12 –test 2	26.0	61.0	13.0
13 –test 3	42.0	33.0	25.0
14 –test 4	83.0	10.0	7.0
15 –test 5	47.0	7.0	46.0
16 –test 6	11.0	18.0	71.0

### 5.2.2 MIR spectrometry

MIR spectra were acquired with a resolution of  $16\text{ cm}^{-1}$  in the  $400 - 4000\text{ cm}^{-1}$  range using three infrared spectrometer systems (ABB MB3000 FTIR, ABB BOMEM MB155 in MIR mode, and an ABB FTLA2000 series FTIR). The MB3000 spectrometer system incorporated a 2 port high-throughput double pivot Michelson fully jacketed interferometer mechanism with a ZnSe beamsplitter and a deuterium triglycine sulphate (DTGS) detector and redesigned electronics. The MB155 system

incorporates a different interferometer design, namely a 4 port patented double pendulum interferometer design with a KCl beamsplitter and a DTGS detector. The FTLA 2000 series spectrometer was on loan to the department for a short period of time and therefore, the exact specifications are not available. However, this series incorporated a 4 port patented Michelson-type design with 2 corner-cube retroreflectors mounted on a wish-bone scan arm with either KBr or ZnSe optics and a DTGS detector. The data from the FTLA2000 series instrument was acquired by Megan Holden prior to the start of this study. Each spectrometer was coupled with polycrystalline silver halide fibres to hastelloy bodied probes with diamond cone crystals (Fibre Photonics Ltd, Livingston, UK) of different diameters (see Table 5.2 for details of the three probes investigated in this study).

**Table 5.2: Details of three Fibre Photonics probes investigated.**

Probe	Outer diameter of probe shaft (mm)	Silver halide fibre length (m)*	Diamond crystal size (mm)
Probe 1	12	1.5	3
Probe 2	12	1.7	3
Probe 3	2.7	1.1	1.2

\*This is the length of the fibre when measured from diamond tip to sma connectors; the actual length of polycrystalline fibre within the probe will be double, see chapter 4.

Each spectrometer was fitted with a fibre optic interface to allow the attachment of the ATR probes. Spectra were acquired using Horizon MB<sup>TM</sup> FTIR software version 2.1.9.0 (produced by ABB, analytical business unit, Canada) and GRAMS (Graphical Relational Array Management System) /AI software version 4.04 (produced by Galactic Industries Corporation, Salem, USA). The spectra were exported as text files from Horizon software and as SPC files from GRAMS software and imported into Matlab data analysis software.

### 5.2.3 Data analysis

Data were imported into Matlab versions 7.5.0.342 (R2007b) and 7.11.0.584 (R2010b) (Mathworks Inc., Natick, MA, USA) with PLS\_Toolbox version 4.1

(Eigenvector Research Inc., WA, USA). Spectra were plotted and analysed to identify regions in the data that would provide information about the samples and remove the regions that only contribute noise to the measurements.

Principal component analysis (PCA) was used to find the combination of variables that described any major trends in the data. The principal components obtained from the spectra described the underlying structure and allowed any trends between samples, spectrometers or probes to be determined.

The spectra from the calibration solutions and their concentration values were used to produce multivariate partial least squares (PLS) calibration models. All models were constructed using the spectral region 579 to 1844  $\text{cm}^{-1}$ . As an aid in the determination of the optimal PLS calibration models, DoEman analysis was completed using the DoEman toolbox (DoEmanGUI, produced by University of Strathclyde, UK, 2004) integrated within the Matlab software.<sup>82, 83</sup> The predicted concentrations from the models were compared with the expected concentrations of the three analytes and the root mean square error of prediction (RMSEP) values were calculated within Excel 2007/2010 (Microsoft Corporation) using the function given in Equation 5.1 (replicate of Equation 2.11 in chapter 2, for convenience) to determine numerically the level of error associated with each of the predictions.

$$RMSEP = \sqrt{\frac{\sum_{i=1}^n (\hat{y}_i - y_i)^2}{n}} \quad \text{Equation 5.1}$$

Where,

$\hat{y}_i$  = predicted value

$y_i$  = known value

$n$  = number of samples

#### 5.2.4 Calibration transfer algorithms

In the direct standardisation (DS) method,<sup>25</sup> the spectra measured on the secondary instrument are corrected to match the spectra collected on the primary instrument while the calibration model remains unchanged. The response matrices of the two

instruments are related to one another by a transformation matrix  $\mathbf{F}$  as described in Equation 5.2.

$$\mathbf{S}_1 = \mathbf{S}_2 \mathbf{F} \quad \text{Equation 5.2}$$

Where  $\mathbf{S}_1$  and  $\mathbf{S}_2$  are the response matrices of the standardisation samples acquired from the primary and secondary instruments, respectively. Rearranging Equation 5.2 for  $\mathbf{F}$  gives the following expression;

$$\mathbf{F} = \mathbf{S}_2^+ \mathbf{S}_1 \quad \text{Equation 5.3}$$

Where  $\mathbf{S}_2^+$  is the pseudo-inverse of  $\mathbf{S}_2$ . The response of an unknown sample measured on the secondary instrument,  $\mathbf{r}_2^T$  is standardised to the response  $\hat{\mathbf{r}}_1^T$  expected from the primary instrument, as shown in Equation 5.4.

$$\hat{\mathbf{r}}_1^T = \mathbf{r}_2^T \mathbf{F} \quad \text{Equation 5.4}$$

The model constructed using  $\mathbf{S}_1$ , along with the concentrations on the primary instrument, are used for the prediction of the unknown concentrations on the secondary instrument. It is assumed in direct standardisation that the relationship between the responses is linear, although some non-linearity can be endured in the multivariate regression.

Piecewise direct standardisation (PDS)<sup>25, 36</sup> recreates each spectral point on the primary instrument from several measurements in small channel windows on the secondary instrument. The calculation of the transfer matrix,  $\mathbf{F}$ , in PDS differs from DS in that it does not use the entire spectrum of all the transfer samples to correct each wavelength on the secondary instrument. Instead PDS uses variables in the local window around the channel of interest; this is because when the responses on one instrument are shifted to the other, information about the shift is most likely to be found in restrictive local regions in the second instrument.<sup>34</sup> This window size can be varied and should be optimised before use for calibration model building. In PDS, a subset of calibration transfer samples are measured on the primary and secondary instruments, producing two response matrices related to each other by a transformation matrix,  $\mathbf{F}$ , which is assembled from a set of calculated regression vectors. For a subset measurement  $\mathbf{r}_{1,i}$ , at a wavelength,  $i$ , on the primary instrument,

subset measurements on the secondary instrument  $\mathbf{r}_{2,i-j} \dots \mathbf{r}_{2,i+k}$  at wavelengths surrounding  $i$  from wavelengths  $i-j$  to  $i+k$  are chosen to put into a matrix,  $\mathbf{X}_i$ . A multivariate regression equation can be calculated as

$$\mathbf{r}_{1,i} = \mathbf{X}_i \mathbf{b}_i \quad \text{Equation 5.5}$$

This multivariate regression can be used to determine a reasonable approximation for the non-linearity intensity change. The regression vector,  $\mathbf{b}_i$  can be calculated *via* various multivariate calibration methods such as PLS and then subsequently used to transfer the unknown sample measured on the secondary instrument,  $\mathbf{r}_2^T$ , piece by piece into the spectrum, as if it were analysed on the primary instrument.

SST follows on from DS and PDS whereby the spectra measured on a secondary instrument are corrected to match the spectra on the primary instrument while the original calibration model remains unchanged. The rows of the spectral matrices  $\mathbf{X}_1$  and  $\mathbf{X}_2$  correspond to the spectra of the subset of standardisation samples measured on both the primary and secondary instruments, which are used for the standardisation procedure. The combined spectral matrix then becomes  $\mathbf{X}_{\text{comb}} = [\mathbf{X}_1, \mathbf{X}_2]$ . Completing singular value decomposition of  $\mathbf{X}_{\text{comb}}$  will provide the expression detailed in Equation 5.6,

$$\mathbf{X}_{\text{comb}} = [\mathbf{U}_s, \mathbf{U}_n] \begin{bmatrix} \Sigma_s & 0 \\ 0 & \Sigma_n \end{bmatrix} [\mathbf{V}_s, \mathbf{V}_n]^T = \mathbf{T}_s \mathbf{P}_s^T + \mathbf{E} = \mathbf{T}_s [\mathbf{P}_1^T, \mathbf{P}_2^T] + \mathbf{E} \quad \text{Equation 5.6}$$

where,  $\mathbf{T}_s = \mathbf{U}_s \Sigma_s$ ;  $\mathbf{P}_s = \mathbf{V}_s$ ;  $\mathbf{E} = \mathbf{U}_n \Sigma_n \mathbf{V}_n^T$ . The superscript 'T' indicates the transpose and the subscripts 's' and 'n' correspond to the spectral information and noise, respectively. If the actual number of spectroscopically active chemical components in the spectra is  $r$ , then  $\mathbf{P}_s$  will have  $r$  columns. The sub-matrices of  $\mathbf{P}_s^T$  ( $\mathbf{P}_s^T = [\mathbf{P}_1^T, \mathbf{P}_2^T]$ ) will have the same number of columns as in  $\mathbf{X}_1$  and  $\mathbf{X}_2$ , respectively. Allowing for the Beer-Lambert law,  $\mathbf{X}_{\text{comb}}$  can also be expressed as follows:

$$\mathbf{X}_{\text{comb}} = [\mathbf{X}_1, \mathbf{X}_2] = \mathbf{C} [\mathbf{S}_1^T, \mathbf{S}_2^T] + \mathbf{E} \quad \text{Equation 5.7}$$

where  $\mathbf{C}$  is the concentration and  $\mathbf{S}_1$  and  $\mathbf{S}_2$  are the pure spectral matrices. The columns of  $\mathbf{S}_1$  and  $\mathbf{S}_2$  contain the pure spectra of the chemical components in the

standardisation samples on the primary and secondary instruments, respectively. When Equation 5.6 and Equation 5.7 are combined the following equations will result:

$$\mathbf{CS}_1^T = \mathbf{T}_s \mathbf{P}_1^T, \quad \mathbf{CS}_2^T = \mathbf{T}_s \mathbf{P}_2^T \quad \text{Equation 5.8}$$

$$\mathbf{S}_1^T = (\mathbf{C}^T \mathbf{C})^{-1} \mathbf{C}^T \mathbf{T}_s \mathbf{P}_1^T = \mathbf{R} \mathbf{P}_1^T, \quad \mathbf{S}_2^T = (\mathbf{C}^T \mathbf{C})^{-1} \mathbf{C}^T \mathbf{T}_s \mathbf{P}_2^T = \mathbf{R} \mathbf{P}_2^T \quad \text{Equation 5.9}$$

Where  $\mathbf{R} = (\mathbf{C}^T \mathbf{C})^{-1} \mathbf{C}^T \mathbf{T}_s$  is a full rank square matrix and the superscript ‘-1’ represents the matrix inverse. If the spectrum of a test sample ( $\mathbf{x}_{\text{test}}$ ) is measured on the secondary instrument, the concentration vector ( $\mathbf{c}_{\text{test}}$ ) of the component in that sample can be estimated by  $\hat{\mathbf{c}} = \mathbf{x}_{\text{test}} (\mathbf{S}_2^T)^+$ , where the superscript ‘+’ symbolises the Moore-Penrose generalised inverse. The difference between  $\mathbf{x}_{\text{test}}$  and its related spectrum ( $\mathbf{x}_{\text{trans}}$ ), as if it were measured on the primary instrument, can be expressed as  $\mathbf{x}_{\text{test}} - \mathbf{x}_{\text{trans}} = \hat{\mathbf{c}} (\mathbf{S}_2^T - \mathbf{S}_1^T)$ . Therefore,  $\mathbf{x}_{\text{trans}}$  can be calculated using Equation 5.10.

$$\mathbf{x}_{\text{trans}} = \mathbf{c}_{\text{test}} \mathbf{S}_1^T + \mathbf{x}_{\text{test}} - \mathbf{c}_{\text{test}} \mathbf{S}_2^T = \mathbf{x}_{\text{test}} (\mathbf{S}_2^T)^+ \mathbf{S}_1^T + \mathbf{x}_{\text{test}} - \mathbf{x}_{\text{test}} (\mathbf{S}_2^T)^+ \mathbf{S}_2^T \quad \text{Equation 5.10}$$

Through the substitution of Equation 5.9 into Equation 5.10, Equation 5.11 will form.

$$\mathbf{x}_{\text{trans}} = \mathbf{x}_{\text{test}} (\mathbf{P}_2^T)^+ \mathbf{P}_1^T + \mathbf{x}_{\text{test}} - \mathbf{x}_{\text{test}} (\mathbf{P}_2^T)^+ \mathbf{P}_2^T \quad \text{Equation 5.11}$$

To complete the transfer, the multivariate calibration built using the initial spectra acquired on the primary instrument is used to predict the components in the test spectra from the transform spectra created in the SST procedure.

## 5.3 Results

Various combinations of the three Fibre Photonics ATR probes and three MIR spectrometer systems were used to analyse the 10 calibration samples and 6 test samples. Detailed in Table 5.3 are the seven different combinations of spectrometer and probe that were investigated.

**Table 5.3: Combinations of spectrometer system and ATR probe used to analyse the calibration and test samples of acetone, ethanol and ethyl acetate.**

Combination number	Spectrometer	Probe*
1	MB155	Probe 1
2	MB155	Probe 2
3	MB3000	Probe 2
4	MB3000	Probe 3
5	MB3000	Probe 1
6	FTLA2000	Probe 1
7	FTLA2000	Probe 2

\* Probes 1 and 2: 12 mm outer diameter, Probe 3: 2.7 mm outer diameter.

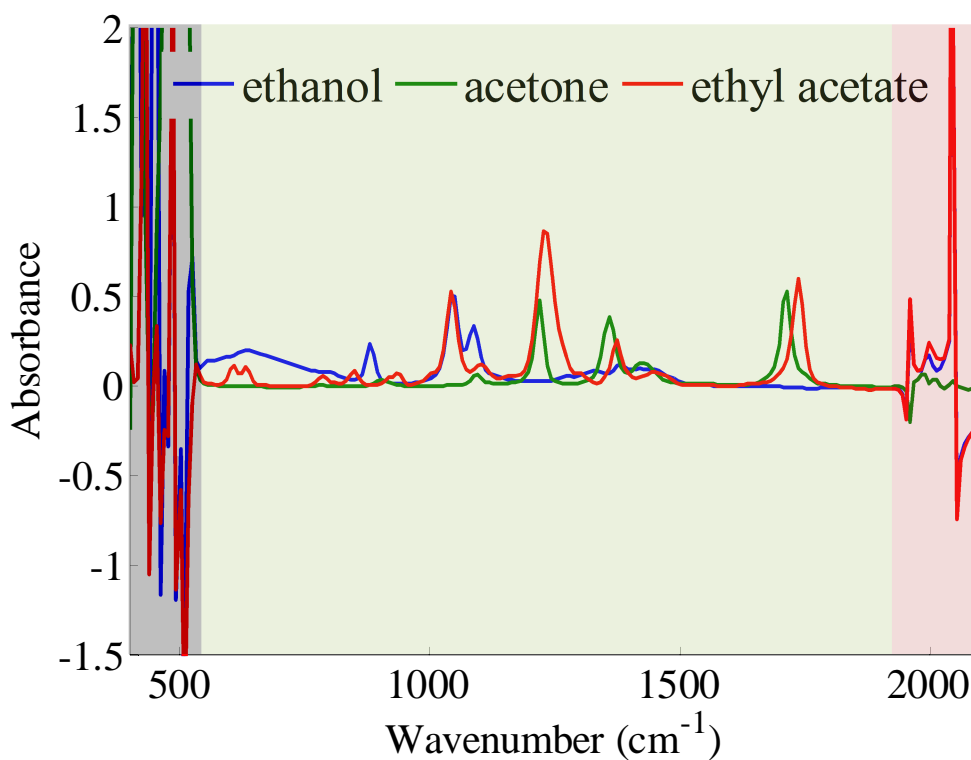
PCA and optimised PLS calibration models were prepared using the spectral data acquired with the different combinations of instrument arrangements. The multivariate calibration models were transferred and used to predict the concentrations for the test spectra acquired using different instrumental arrangements. The effect on the error of prediction was assessed when transferring these calibration models and implementing calibration transfer algorithms to aid the transfer.

### 5.3.1 Analysis of solvent mixtures

#### 5.3.1.1 Determination of trends in data

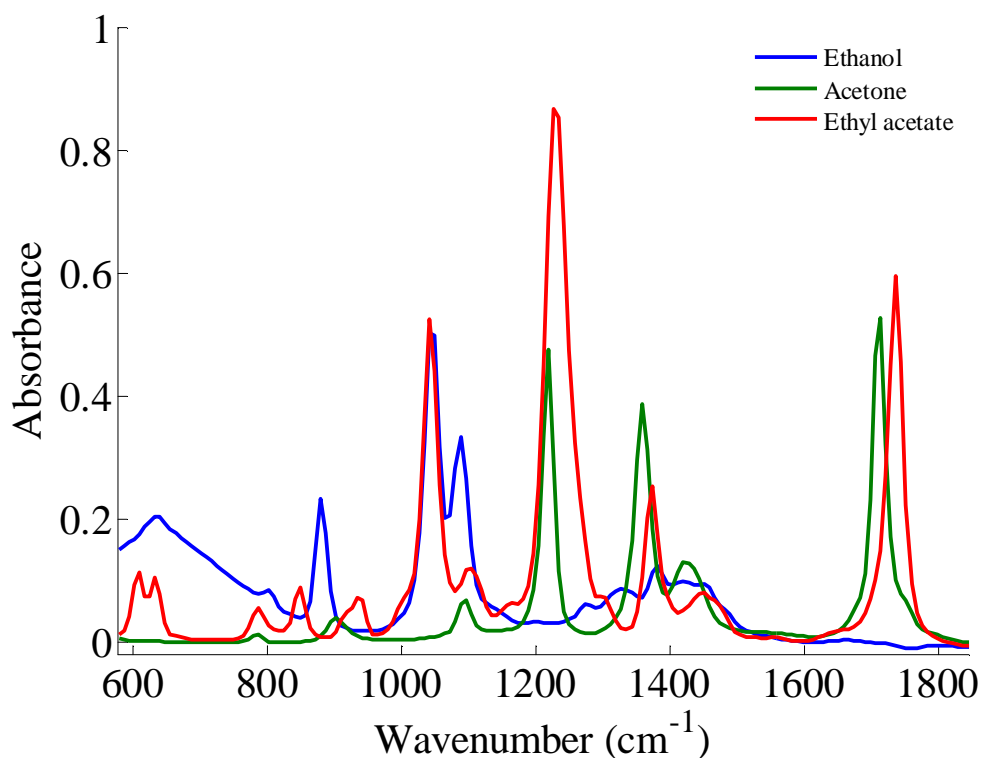
Spectra were plotted and analysed to identify regions in the data that would provide information about the samples and remove the regions that only contribute noise to the measurements. The region 579 to 1844  $\text{cm}^{-1}$  was identified as being most useful for the analysis of the sample mixtures; Figure 5.2 indicates the areas where only

noise or non-transmitting regions of the spectra appear. Also highlighted in Figure 5.2 is the area of specific interest for this work based on previous work by Holden.<sup>81</sup>



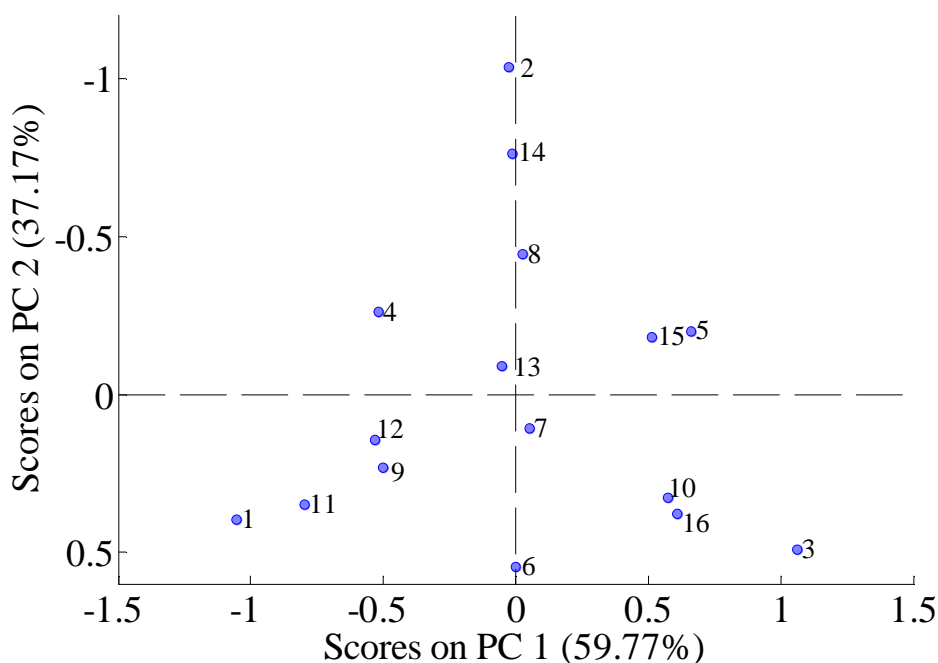
**Figure 5.2:** Overlaid MIR absorbance spectra of acetone, ethanol and ethyl acetate showing the regions of specific interest  as well as ‘noise’  and non-transmitting  areas of the spectra.

Figure 5.3 shows the overlaid absorbance spectra for each of the three pure components for the selected region, 579 – 1844 cm<sup>-1</sup>.



**Figure 5.3:** ATR MIR absorbance spectra of acetone, ethanol and ethyl acetate in the range 579 – 1844  $\text{cm}^{-1}$ ; obtained using instrument combination 5 (See Table 5.3).

Principal component analysis (PCA) was used to find the combination of variables that described any major trends in the data. The PCA scores plot was used to assess if the spectral data produced results similar to the mixture design (Figure 5.1). Initially PCA was carried out on each spectral data set collected from the different combination of instrumental systems. Scores on PC1 were plotted against scores on PC2 for each data set and compared to the mixture design; see Figure 5.4 for the scores plot determined from the data collected using the MB3000 spectrometer and probe 1 (combination 5). The overall structure is fairly similar with most of the points arising in the same spectral space. However, there are some differences, namely points 8 and 12 - 16 that are shifted in comparison to their position in the mixture design plot owing to experimental fluctuations in the spectra. A similar evaluation can be made of the PCA scores for the other six data sets.



**Figure 5.4: Scores on PC1 vs. scores on PC2 for spectral data collected on MB3000 spectrometer with the probe 1 (combination 5; see also Figure 5.3).**

The spectral data for all seven data sets obtained with the various probe – spectrometer systems were combined into one matrix and subjected to PCA to determine if there were any trends between the data sets. Plots of scores on PC1 vs. scores on PC2 for the samples, probes and spectrometers were analysed for similarities and differences (Figure 5.5, Figure 5.6, and Figure 5.7, respectively). Figure 5.5 displays the changes in the scores for all the samples analysed, indicating the variation seen for each sample when the probe – spectrometer combinations are changed. Some samples appear to have a larger variation than others, for example calibration sample 3 and 10 and test sample 6 (all circled in red) in comparison to calibration sample 1 and 2 and test sample 4 (all circled in blue). Only the samples from the 12 mm probe – spectrometer combinations have been circled. Figure 5.6 displays the variation seen for the different probes; the points for probe 3 appear closest together in scores space, whereas, the points for probe 2 have the greatest variation with the points more spread out. Figure 5.7 indicates the similarity of the three spectrometers, where the major variation observed is the cluster of green points for the MB3000 spectrometer; this is due to the effect from the 2.7 mm probe rather than a difference in the spectrometer system.

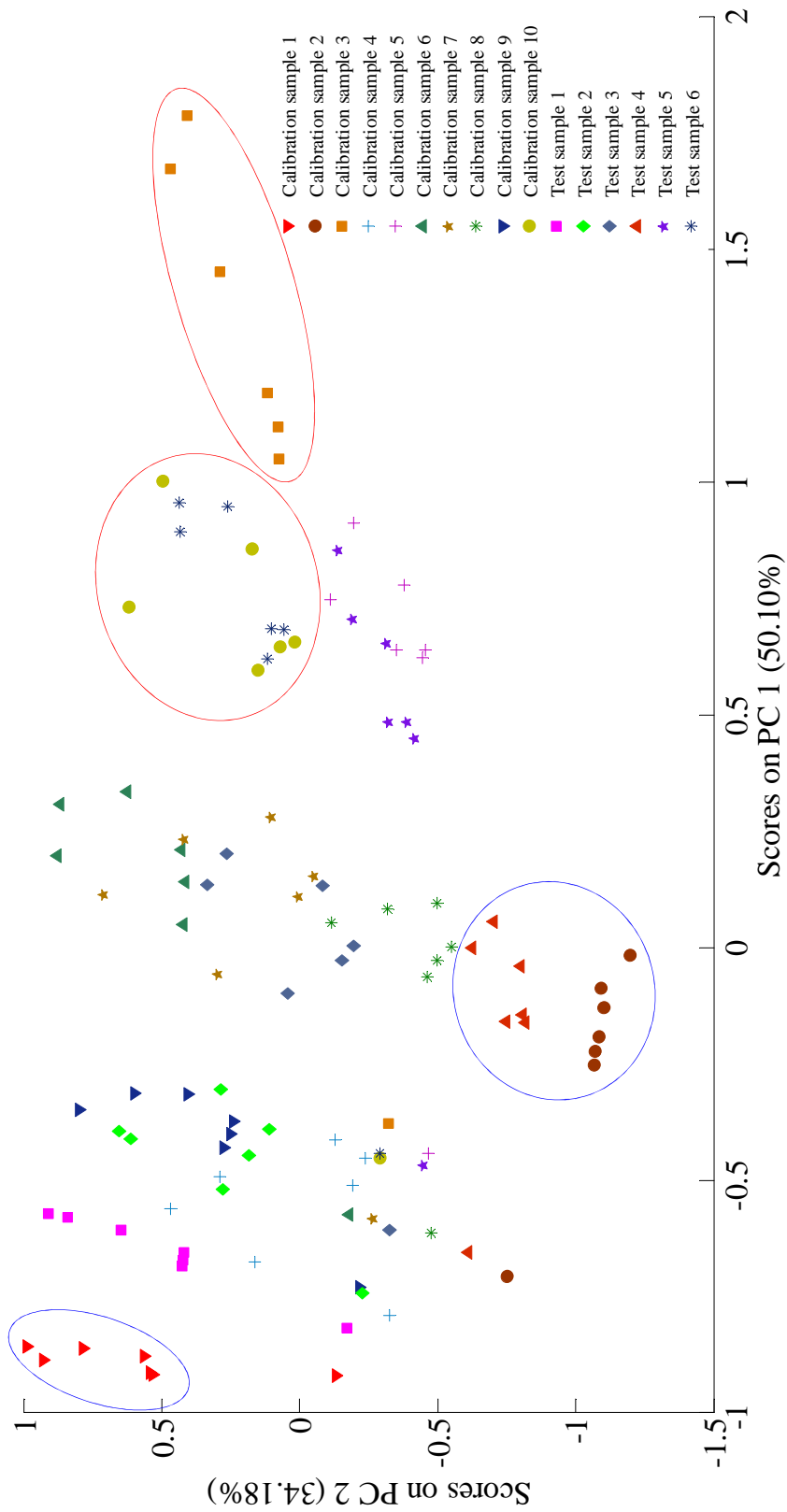


Figure 5.5: Scores on PC1 vs. scores on PC2 for the ten calibration samples and six test samples of the seven combinations described in Table 5.3.

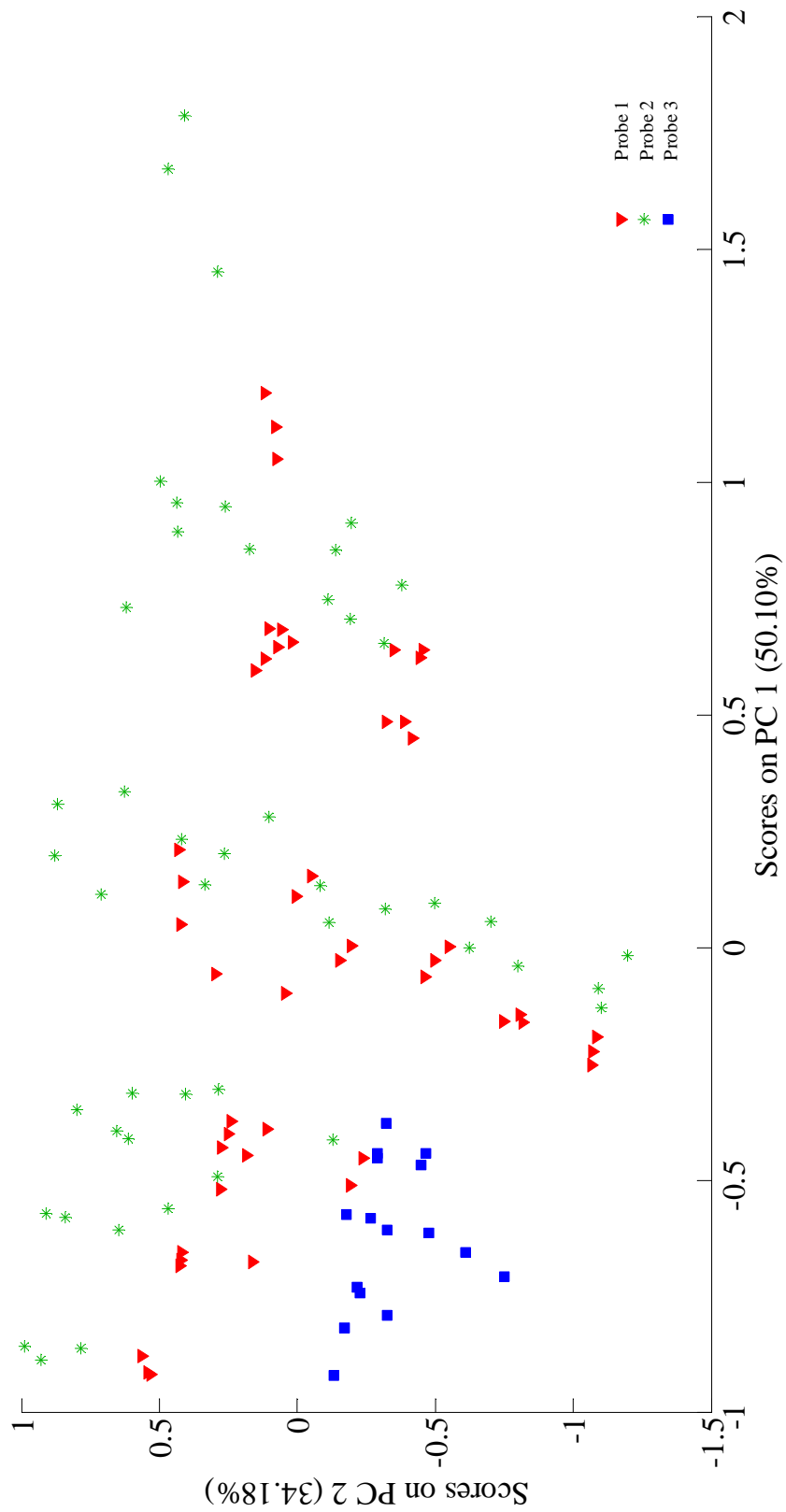


Figure 5.6: Scores on PC1 vs. scores on PC2 for the three different probes of the seven combinations described in Table 5.3.

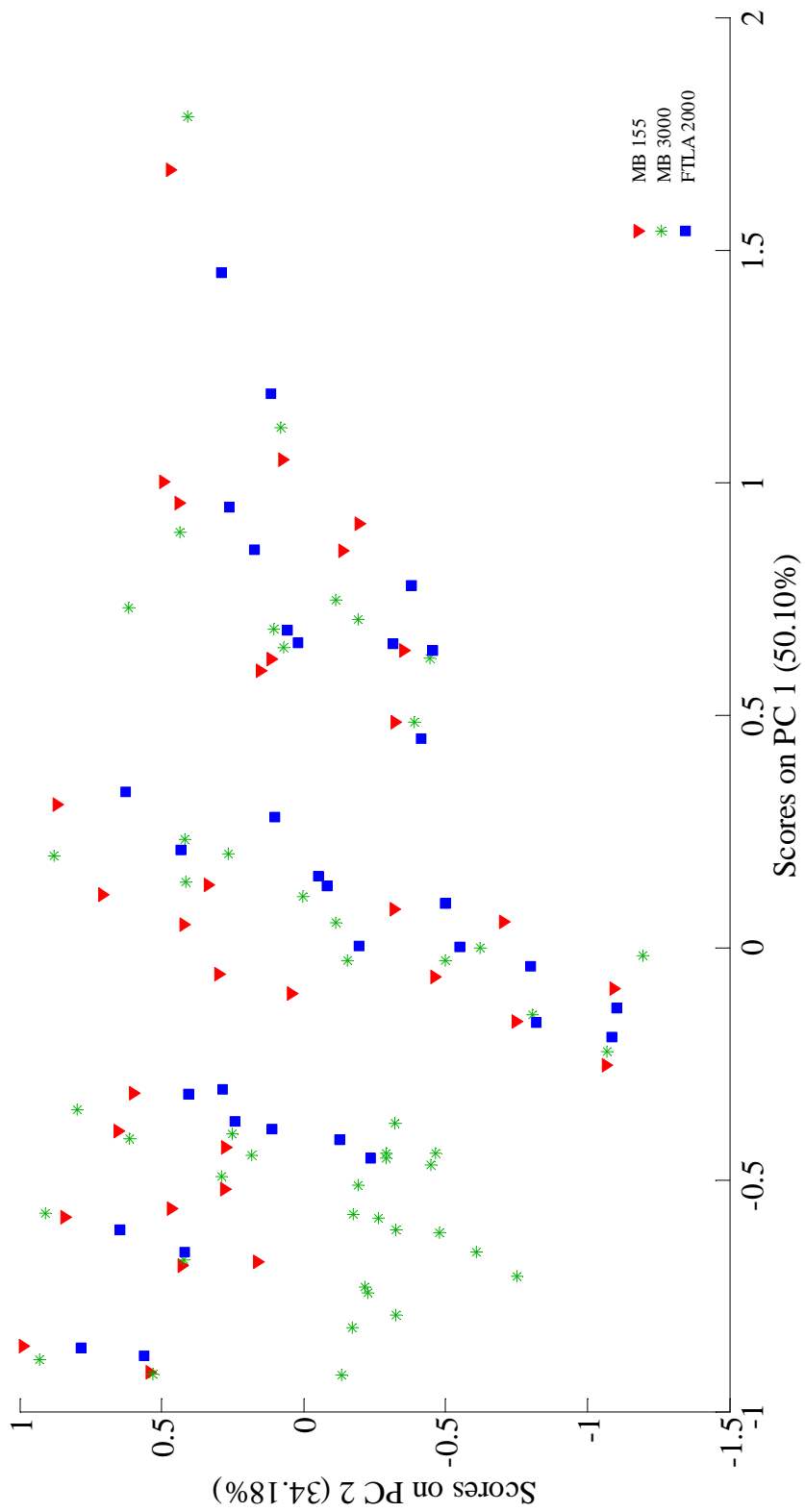


Figure 5.7: Scores on PC1 vs. scores on PC2 for the three different spectrometers of the seven combinations described in Table 5.3.

On assessing the PCA scores plots for the samples, probes and spectrometers several conclusions can be made:

- There is a greater variation between the two 12 mm probes shown for the pure ethyl acetate sample in comparison with the ethanol and acetone samples (calibration samples 1, 2 and 3 represent ethanol, acetone and ethyl acetate), see Figure 5.5 and Figure 5.6. A similar conclusion can be derived from the spectra, however, it is more difficult to observe.
- All three probes convey similar structures in space with the largest variation seen for the 12 mm probe 2, see Figure 5.6.
- The data for three spectrometers all display similar structures in space with little differences noted (see Figure 5.7).
- There is a greater variation shown between the probes than between the spectrometers, see Figure 5.6 and Figure 5.7.

In industry it can be common to require more than one probe for the analysis of a process, e.g. multiplexing multiple probes to a spectrometer or scaling up a process requiring a smaller probe for the small scale analysis and a larger probe as the process is scaled up. The results here show that changing between probes or using multiple probes will cause variations in the analysis, which can be problematic when monitoring a process for which calibration models have been established, but the probe needs to be altered. For this reason research has increased in the area of robust calibration model building and the use of calibration model transfer to allow the same model to be used even when probes or spectrometers are changed.

### **5.3.1.2 Calibration model optimisation using DoEman software**

In the analysis of spectral data, good calibration models are essential in order to achieve accurate predictive results. CPACT design of experiment software, DoEman, was used to select the pre-processing conditions for the spectra that would give the best predictive and robust calibration models. The different factors that can influence the model that were reviewed are listed in Table 5.4.

**Table 5.4: Table of the factors assessed in DoEman that can influence the model for the MIR data.**

Factors	Regression method	Derivatives	Mean centring	Principal components
Levels	PLS	No derivatisation	No mean centring	1 - 10
	PCR	1 <sup>st</sup> derivative 2 <sup>nd</sup> derivative	Mean centring	

Using the DoEman graphical user interface through Matlab software, the spectral data were loaded and the factors and their levels were input for analysis. Design of experiment software analyses each independent factor (e.g. derivatives) as well as the interaction of pairs of factors (derivatives vs. mean centring) to produce root mean square error of calibration (RMSEC) and root mean square error of prediction (RMSEP) plots for interpretation. The level that minimises the RMSEC and RMSEP values will contribute to the best predictive and robust model. Shown in Figure 5.8 and Figure 5.9 are the RMSEC and RMSEP plots, respectively, for the spectral data collected with the MB3000 spectrometer and probe 1 (combination 5), analysed using the DoEman graphical user interface.

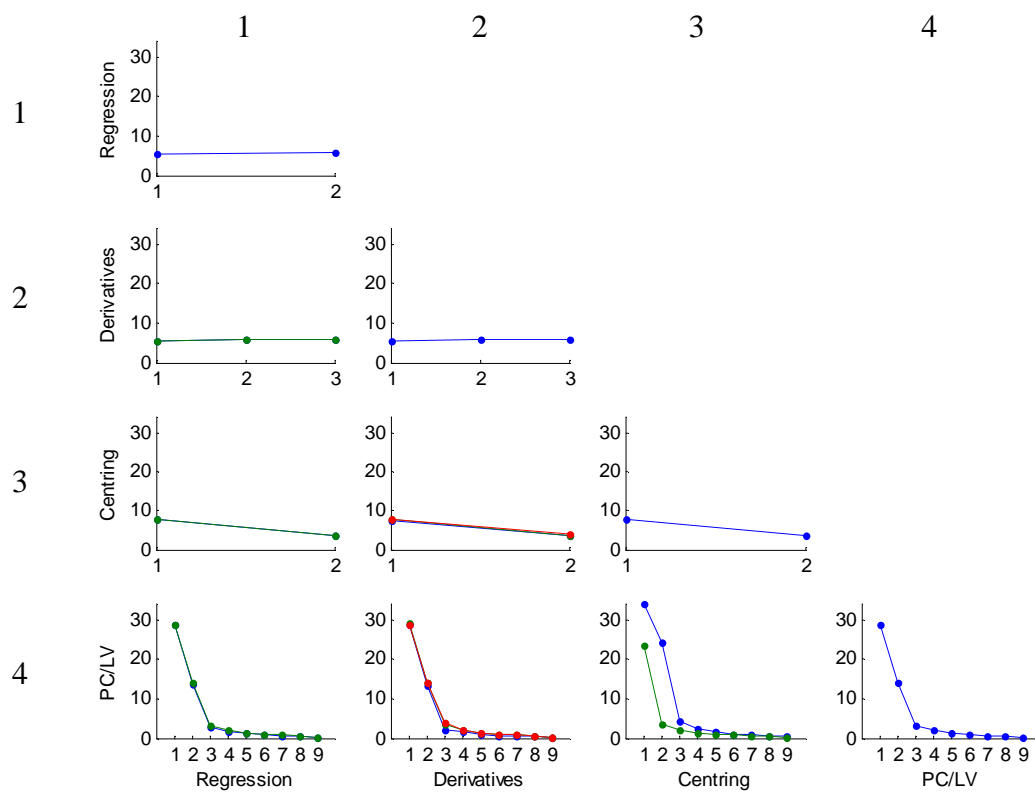


**Figure 5.8: The effects of the different factors on the RMSEC values for the spectral data acquired with the MB3000 spectrometer and 12 mm probe 1. [The plots along the main diagonal of the plot matrix show the main effect, and the other plots show interaction effects between pairs of factors. The levels indicated by the column labels correspond to the different lines in the plots (blue, green and red relate to levels 1, 2 and 3, respectively), while the levels for the row labels are found along the x-axis in the plots.]**

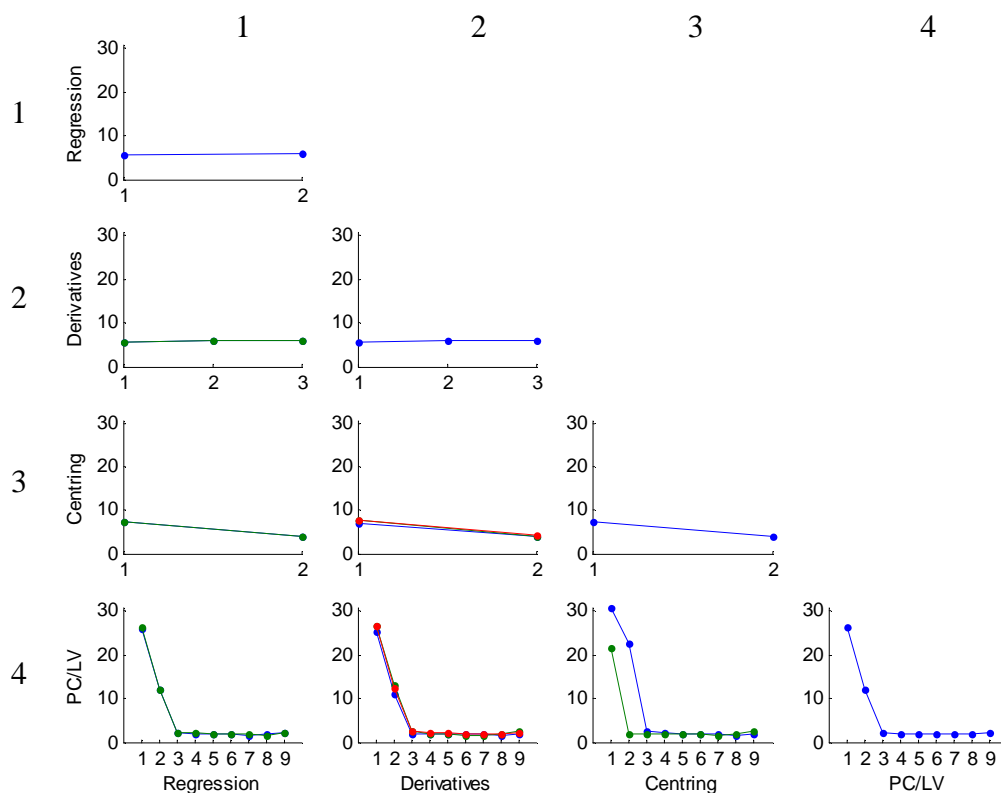


**Figure 5.9:** The effects of the different factors on the RMSEP values for the spectral data acquired on MB3000 spectrometer with 12 mm probe 1. [The plots along the main diagonal of the plot matrix show the main effect, and the other plots show interaction effects between pairs of factors. The levels indicated by the column labels correspond to the different lines in the plots (blue, green and red relate to levels 1, 2 and 3, respectively), while the levels for the row labels are found along the x-axis in the plots.]

In Figure 5.8 and Figure 5.9, the notation (q, r), where q gives the row number and r gives the column number, is used. The number on the x axis relates to each level of the variable for the row; e.g. in plot (1, 1) of Figure 5.8 refers to the regression methods, where point 1 relates to PLS and 2 relates to PCR. In addition, the different coloured lines relate to the levels of the factor for the column; e.g. in plot (3, 2) of Figure 5.9, points 1 and 2 on the x axis relate to no mean centring and mean centring, respectively, and the blue, green and red lines relate to no derivation, 1<sup>st</sup> derivative and 2<sup>nd</sup> derivative, respectively.

On interpretation of both the RMSEC and RMSEP plots, the optimal conditions for the spectral data collected with the MB3000 spectrometer and 12 mm probe 1 were:

PLS regression, with mean centring and no derivation of the spectra. The output conditions from the DoEman analysis are transferred with the spectral data into PLS Toolbox for PLS calibration to be completed. From the DoEman plot (4, 3) of Figure 5.9, the green line referring to the use of mean centring suggests that including two principal components/latent variables will give the best predictive model, however, this interpretation was only used as a guideline. The principle behind DoEman assumes that there is an independent test set, however this is not always the case, therefore, the actual number of latent variables required was re-evaluated in the PLS Toolbox from the model that produced the minimum value of the root mean square error of cross-validation (RMSECV) obtained using leave-one-out cross validation.

RMSEC and RMSEP plots were produced for each set of spectral data collected from the MIR analysis, using the DoEman graphical user interface to determine the optimal conditions. The conditions were found to be the same for each spectral data set analysed by MIR spectroscopy: PLS regression, with mean centring and no derivation of the spectra. To investigate how well the DoEman software can help to determine the best conditions that led to the best predictive and most robust models, two non-optimal conditions were also tested where the levels for pre-processing factors were altered (Table 5.5).

**Table 5.5: Table of two non-optimum sets of conditions tested for the MIR spectral data.**

	Non-optimum 1	Non-optimum 2
Regression method	PLS	PLS
Derivative	1st derivative	No derivative
Mean centring	Mean centred	No centring

The spectra and each set of pre-processing conditions were transferred to PLS Toolbox in Matlab and used to build multivariate PLS calibration models. The models were then used to predict the concentrations of each separate component present in the test samples. The accuracy of the concentration predictions of each component obtained with each set of conditions were then compared to indicate any

advantages of using design of experiments for multivariate calibration model building in this example. The expected and predicted concentrations of the three analytes were tabulated and the RMSEP values were calculated to determine numerically the level of error associated with each of the predictions. This approach was used to obtain concentration predictions for the samples from the spectra measured with all the spectrometer – probe combinations (Table 5.6 to Table 5.12) and several conclusions can be made:

- Whilst some predictions are good, in each data set there are poorer predictions, even for the optimal pre-processing conditions.
- Overall, there is no clear advantage of the optimal set versus the other 2 sets of pre-processing conditions which suggests that for this example the selection of the parameters is not critical.
- The best RMSEP values are shown for ethyl acetate and the worst are for ethanol. The main reason is due to the overlapping of the component spectra; the bands of ethanol overlap with most of the ethyl acetate and acetone bands. Therefore, when low concentrations of ethanol are present in high concentrations of the other components, a lot of the ethanol information is obscured. Although the ethyl acetate bands also overlap with the other bands, there are more ethyl acetate bands across the range of the spectrum and these are well represented in the regression coefficient for the ethyl acetate models and so easier to model.
- The FTLA2000 spectrometer results give the best RMSEP values.
- Probe 1 RMSEP values are better than probe 2 results when used for analysis with the MB3000 spectrometer and MB155 spectrometer. However, probe 2 provides better RMSEP values than probe 1 when used for analysis with the FTLA2000 spectrometer; reviewing the spectra and regression coefficients it is unclear why this is the case.
- Overall the best set of predictions resulted from the use of a FTLA2000 spectrometer with probe 2.

**Table 5.6: Expected and predicted concentrations for acetone, ethanol and ethyl acetate from models built with optimal and non-optimal conditions MB155 spectrometer with 12 mm probe 1 (concentrations in % w/w).**

MB155 12 mm probe 1											
Acetone				Ethanol				Ethyl Acetate			
Expected Concentration	Optimal prediction	Non-optimal 1	Non-optimal 2	Expected Concentration	Optimal prediction	Non-optimal 1	Non-optimal 2	Expected Concentration	Optimal prediction	Non-optimal 1	Non-optimal 2
6.0	12.4	11.6	11.0	85.0	75.0	76.1	72.7	9.0	8.6	9.3	9.2
26.0	25.8	25.4	26.1	61.0	62.8	62.8	62.4	13.0	12.3	12.1	11.9
42.0	40.0	39.7	40.6	33.0	38.2	38.7	39.4	25.0	27.9	26.6	26.9
83.0	85.7	86.2	85.9	10.1	8.1	8.3	4.2	7.0	6.9	6.3	6.5
47.0	49.9	49.9	49.9	7.0	2.6	3.4	2.6	46.0	50.9	50.9	50.5
11.0	18.4	18.5	17.4	18.0	15.7	16.7	17.2	71.0	69.1	69.0	69.1
<b>RMSEP</b>	4.4	4.3	<b>3.8</b>	<b>RMSEP</b>	5.1	<b>4.7</b>	6.4	<b>RMSEP</b>	2.5	2.3	<b>2.2</b>

**Table 5.7: Expected and predicted concentrations for acetone, ethanol and ethyl acetate from models built with optimal and non-optimal conditions with MB155 spectrometer with 12 mm probe 2 (concentrations in % w/w).**

MB155 12 mm probe 2											
Acetone				Ethanol				Ethyl Acetate			
Expected Concentration	Optimal prediction	Non-optimal 1	Non-optimal 2	Expected Concentration	Optimal prediction	Non-optimal 1	Non-optimal 2	Expected Concentration	Optimal prediction	Non-optimal 1	Non-optimal 2
6.0	6.6	13.2	12.3	85.0	74.9	76.5	72.6	9.0	9.5	9.9	10.1
26.0	27.3	24.6	25.9	61.0	62.9	62.8	63.0	13.0	12.7	12.4	12.5
42.0	42.9	36.1	40.4	33.0	36.7	36.9	39.0	25.0	28.5	27.0	27.5
83.0	90.9	87.4	89.1	10.1	5.6	4.8	5.7	7.0	8.7	8.1	8.1
47.0	52.3	48.9	52.3	7.0	0.6	0.6	2.3	46.0	51.2	50.9	50.5
11.0	18.3	17.7	18.9	18.0	16.4	17.4	17.3	71.0	65.8	65.0	65.6
<b>RMSEP</b>	<b>4.9</b>	5.1	5.3	<b>RMSEP</b>	5.5	<b>5.2</b>	6.3	<b>RMSEP</b>	3.4	3.3	<b>3.1</b>

**Table 5.9: Expected and predicted concentrations for acetone, ethanol and ethyl acetate from models built with optimal and non-optimal conditions for the MB3000 spectrometer with 12 mm probe 2 (concentrations in % w/w).**

<b>MB3000 12 mm probe 2</b>											
<b>Acetone</b>				<b>Ethanol</b>				<b>Ethyl Acetate</b>			
Expected Concentration	Optimal prediction	Non-optimal 1	Non-optimal 2	Expected Concentration	Optimal prediction	Non-optimal 1	Non-optimal 2	Expected Concentration	Optimal prediction	Non-optimal 1	Non-optimal 2
6.0	6.3	8.7	8.7	85.0	79.9	81.8	75.2	9.0	12.7	9.8	11.5
26.0	19.8	22.4	22.1	61.0	63.8	63.8	60.5	13.0	13.9	14.3	13.9
42.0	38.1	36.2	40.0	33.0	31.7	30.9	33.3	25.0	31.2	31.5	30.2
83.0	75.8	79.3	78.3	10.1	11.5	12.0	7.8	7.0	8.6	9.7	9.7
47.0	48.2	48.4	49.2	7.0	3.0	2.5	0.9	46.0	46.2	48.4	47.2
11.0	13.8	16.2	17.5	18.0	15.8	15.6	16.3	71.0	65.4	67.9	67.1
<b>RMSEP</b>	4.4	<b>4.0</b>	<b>4.0</b>	<b>RMSEP</b>	3.1	<b>3.0</b>	4.9	<b>RMSEP</b>	3.8	3.4	<b>3.1</b>

**Table 5.8: Expected and predicted concentrations for acetone, ethanol and ethyl acetate from models built with optimal and non-optimal conditions for the MB3000 spectrometer with 2.7 mm probe (concentrations in % w/w).**

<b>MB3000 2.7 mm probe</b>											
<b>Acetone</b>				<b>Ethanol</b>				<b>Ethyl Acetate</b>			
Expected Concentration	Optimal prediction	Non-optimal 1	Non-optimal 2	Expected Concentration	Optimal prediction	Non-optimal 1	Non-optimal 2	Expected Concentration	Optimal prediction	Non-optimal 1	Non-optimal 2
6.0	10.4	8.5	9.9	85.0	81.8	81.4	77.7	9.0	7.4	7.5	8.6
26.0	25.0	24.1	24.5	61.0	63.2	63.6	63.6	13.0	11.6	11.7	12.4
42.0	42.0	42.0	41.2	33.0	33.6	35.0	35.8	25.0	25.3	25.3	25.3
83.0	86.4	84.9	84.5	10.1	7.0	8.9	4.1	7.0	6.9	6.9	7.1
47.0	52.8	50.6	50.9	7.0	2.5	2.2	2.0	46.0	44.4	44.7	47.7
11.0	15.0	15.9	14.7	18.0	15.0	16.9	18.0	71.0	70.7	70.5	68.5
<b>RMSEP</b>	3.7	<b>2.9</b>	<b>2.9</b>	<b>RMSEP</b>	3.0	<b>2.9</b>	4.6	<b>RMSEP</b>	1.1	<b>1.0</b>	1.3

**Table 5.11: Expected and predicted concentrations for acetone, ethanol and ethyl acetate from models built with optimal and non-optimal conditions for the MB3000 spectrometer with 12 mm probe 1 (concentrations in % w/w).**

MB3000 12 mm probe 1											
Acetone				Ethanol				Ethyl Acetate			
Expected Concentration	Optimal prediction	Non-optimal 1	Non-optimal 2	Expected Concentration	Optimal prediction	Non-optimal 1	Non-optimal 2	Expected Concentration	Optimal prediction	Non-optimal 1	Non-optimal 2
6.0	6.8	6.3	6.1	85.0	83.6	83.4	82.1	9.0	8.7	8.8	8.7
26.0	23.6	24.2	24.7	61.0	64.3	63.5	64.9	13.0	11.8	11.9	12.2
42.0	42.7	43.0	42.9	33.0	33.7	33.9	34.4	25.0	23.8	24.0	25.3
83.0	84.6	84.6	83.5	10.1	9.5	9.4	5.1	7.0	6.3	7.0	5.9
47.0	49.9	49.3	49.1	7.0	3.7	4.2	3.6	46.0	44.1	44.6	47.7
11.0	13.4	13.5	11.6	18.0	17.8	18.3	19.4	71.0	70.3	71.1	70.6
<b>RMSEP</b>	2.0	1.7	<b>1.1</b>	<b>RMSEP</b>	2.0	<b>1.7</b>	3.3	<b>RMSEP</b>	1.1	<b>0.8</b>	0.9

**Table 5.10: Expected and predicted concentrations for acetone, ethanol and ethyl acetate from models built with optimal and non-optimal conditions with FTLA2000 spectrometer with 12 mm probe 1 (concentrations in % w/w).**

FTLA2000 12 mm probe 1											
Acetone				Ethanol				Ethyl Acetate			
Expected Concentration	Optimal prediction	Non-optimal 1	Non-optimal 2	Expected Concentration	Optimal prediction	Non-optimal 1	Non-optimal 2	Expected Concentration	Optimal prediction	Non-optimal 1	Non-optimal 2
6.0	7.5	7.4	4.8	85.0	84.7	83.8	82.3	9.0	7.8	8.7	8.3
26.0	26.4	26.4	25.6	61.0	61.3	60.4	60.2	13.0	12.3	12.8	12.4
42.0	42.4	42.3	41.5	33.0	33.1	33.7	32.2	25.0	24.6	24.5	24.7
83.0	81.6	80.6	76.4	10.1	12.5	12.7	4.4	7.0	6.0	8.1	7.0
47.0	48.7	47.4	44.6	7.0	6.5	7.3	3.3	46.0	44.8	44.3	45.5
11.0	14.2	13.6	9.7	18.0	18.0	18.5	17.0	71.0	68.0	70.4	68.8
<b>RMSEP</b>	1.7	<b>1.5</b>	3.0	<b>RMSEP</b>	<b>1.0</b>	1.2	3.0	<b>RMSEP</b>	1.5	<b>0.9</b>	1.0

**Table 5.12: Expected and predicted concentrations for acetone, ethanol and ethyl acetate from models built with optimal and non-optimal conditions with FTLA2000 spectrometer with 12 mm probe 2 (concentrations in % w/w).**

<b>FTLA2000 12 mm probe 2</b>											
<b>Acetone</b>				<b>Ethanol</b>				<b>Ethyl Acetate</b>			
Expected Concentration	Optimal prediction	Non-optimal 1	Non-optimal 2	Expected Concentration	Optimal prediction	Non-optimal 1	Non-optimal 2	Expected Concentration	Optimal prediction	Non-optimal 1	Non-optimal 2
6.0	6.2	6.4	5.4	85.0	85.3	84.3	84.3	9.0	8.7	8.4	8.5
26.0	25.6	26.0	27.4	61.0	61.1	60.5	62.6	13.0	12.6	12.7	12.9
42.0	43.0	44.2	45.2	33.0	31.7	32.2	34.0	25.0	24.3	23.9	24.8
83.0	82.5	82.2	81.0	10.1	10.3	10.9	9.1	7.0	7.5	7.3	7.4
47.0	48.5	47.7	48.4	7.0	4.8	5.8	5.2	46.0	46.1	46.0	46.6
11.0	12.4	12.6	12.3	18.0	16.7	17.5	17.2	71.0	71.2	71.6	71.0
<b>RMSEP</b>	<b>1.0</b>	<b>1.2</b>	<b>1.8</b>	<b>RMSEP</b>	<b>1.2</b>	<b>0.8</b>	<b>1.2</b>	<b>RMSEP</b>	<b>0.4</b>	<b>0.6</b>	<b>0.4</b>

Referring back to the RMSEP plot from the DoEman study (Figure 5.9) it is not surprising that there was not a big effect when the pre-processing conditions such as derivatives and mean centring were changed, as there are no big differences shown in the plots. Although the optimal model was not always determined as having the lowest RMSEP value, this study has shown some merits in the use of DoEman as a tool for future model building. Using the DoEman software can save time in model building, as for more complex spectral data, the analyst would be required to analyse several options independently to determine the best model. DoEman software saves this time by indicating to the analyst a good choice of pre-processing conditions to use for the calibration model building. It must also be noted that using the DoEman software does not give a conclusive result, it produces plots of RMSEC and RMSEP that can then be interpreted by the analyst and, therefore, there is a margin for error in the interpretation of the plots.

### **5.3.2 Comparison of calibration transfer algorithms**

The optimisation of multivariate calibration models is extremely important in determining reliable quantitative results for a given process. Equally important are the maintenance and durability of the optimised model. Multivariate models require a lot of time and effort to instill the robustness that is required of them and usually they are intended for use over a long period of time. However, small instrumental changes can cause multivariate models to become invalid, often requiring full model recalibration. Different methods have been employed to aid the lifetime and validity of these calibration models if instrumental changes occur. Two well used spectral response standardisation approaches (DS and PDS) as well as a newer procedure (SST) have been investigated for the transfer of the calibration model for the solvents analysis.

#### **5.3.2.1 Multiplexing of two probes – transfer of calibration model**

The multiplexing of two probes to the same instrument has been investigated as a potential industrial example. This example was chosen to show the impact of using two similar probes to simultaneously analyse the same system in different vessels with the probes multiplexed to the same instrument when the calibration is based on

only one of the probes. The use of calibration standardisation algorithms can be of great benefit in industry for this type of example as only one full calibration would be required and the algorithms can be used to transfer the reference calibration to other set-ups. In this example, two 12 mm probes, probe 1 and 2, were used to acquire spectra of calibration and test samples when coupled with the FTLA2000 spectrometer. The two probes used in this example have the same outside diameter; however the manufacturing process used to build each probe was subtly different. Therefore, there is the possibility of slight differences in the spectra, which as Figure 5.10 illustrates involved differences in the intensity of the peaks.

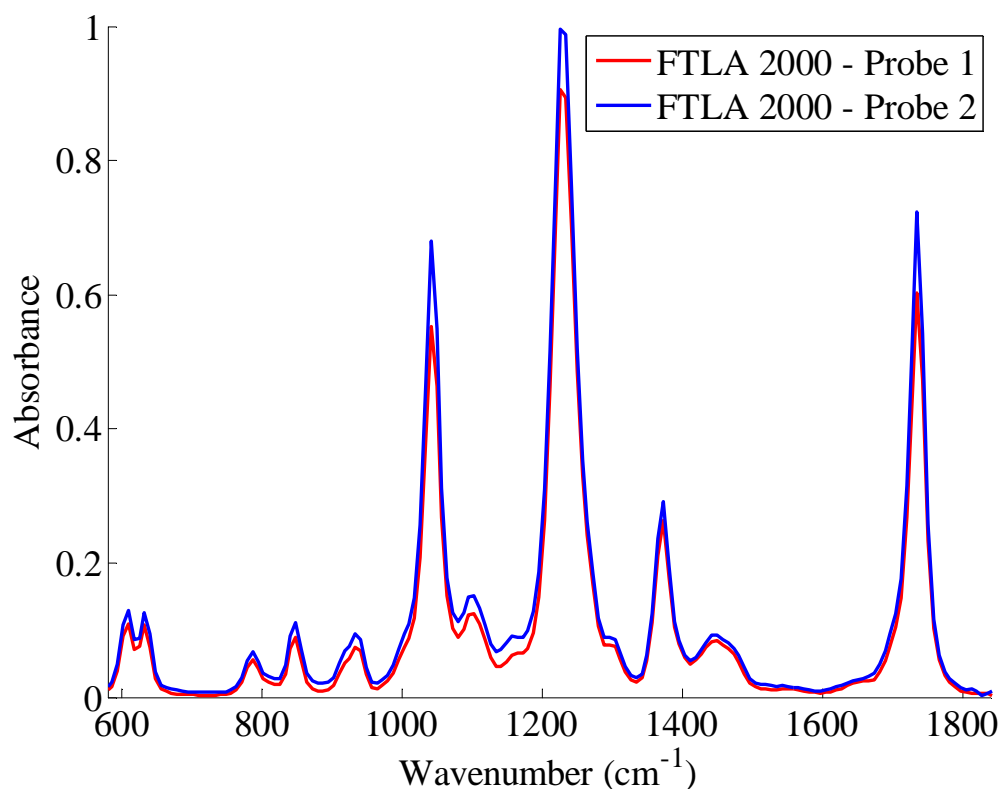


**Figure 5.10: Overlaid calibration spectra (calibration 3) acquired on the FTLA2000 spectrometer with two 12 mm probes.**

This means it would be difficult to build a reference calibration based on FTLA2000 - 12 mm probe 2 and get adequate results when used to predict spectra acquired with FTLA2000 - 12 mm probe 1. The spectral data was transferred to Matlab where the pre-processing conditions selected in section 5.3.1.2 were completed and the calibration model built. Table 5.13 shows the RMSEP values

when the calibration model was transferred, where the secondary test spectra were acquired with the probe 1 - FTLA2000 combination.

**Table 5.13: Comparison of RMSEP values for acetone, ethanol and ethyl acetate when the test spectra are acquired with a different probe than that used when the reference calibration was built. (Spectrometer FTLA2000, Reference – probe 2 and Secondary – probe 1)**

Reference model: FTLA 2000 - 12 mm probe 2			
	Acetone	Ethanol	Ethyl acetate
Reference calibration/ Reference test	1.0	1.2	0.4
Reference calibration/ Secondary test	7.3	3.5	4.4

The effect of transferring the reference calibration to use with test spectra collected with an alternative probe is a marked increase in the RMSEP value; this is especially the case for acetone and ethyl acetate. If standardisation algorithms such as DS, PDS and SST are used where all of the calibration standards are involved in the standardisation, improvements can be seen. Table 5.14 shows the RMSEP values for this transfer when DS, PDS and SST have been employed. For the PDS algorithm the window size had to be optimised to determine the best RMSEP values. SST required the optimisation of the number of singular values; this is a simple and relatively efficient process in comparison to the optimisation of the window size of PDS.

**Table 5.14: Comparison of RMSEP values for acetone, ethanol and ethyl acetate when the test spectra are acquired with a different probe than that used when the reference calibration was built and DS, PDS and SST are applied. (Spectrometer FTLA2000, Reference – probe 2 and Secondary – probe 1)**

	Reference model: FTLA 2000 - 12 mm probe 2		
	Acetone	Ethanol	Ethyl acetate
Reference calibration/ Reference test	1.0	1.2	0.4
Reference calibration/ Secondary test	7.3	3.5	4.4
Reference calibration/ Secondary test – DS used	1.4	0.9	0.7
Reference calibration/ Secondary test – PDS used (window size....)	1.9 (9)	1.1 (11)	1.2 (9)
Reference calibration/ Secondary test – SST used	1.6	1.0	1.0

All three algorithms have been used successfully to improve the RMSEP when the transfer of the reference model was completed. The RMSEP values for all three analytes have been significantly reduced when compared to a direct transfer with no algorithms implemented, see Table 5.14. The test spectra that are to be quantified are corrected and made to look like they had been acquired on the system used for the original model building process. The transformation of the test spectra acquired with probe 1 corrected to look like they have been acquired on probe 2 can be seen in Figure 5.11, Figure 5.12 and Figure 5.13, where the algorithms DS, PDS and SST have been used, respectively. The corrected spectra, originally acquired on probe 1, should now look more like probe 2 than the original probe 1 spectra.

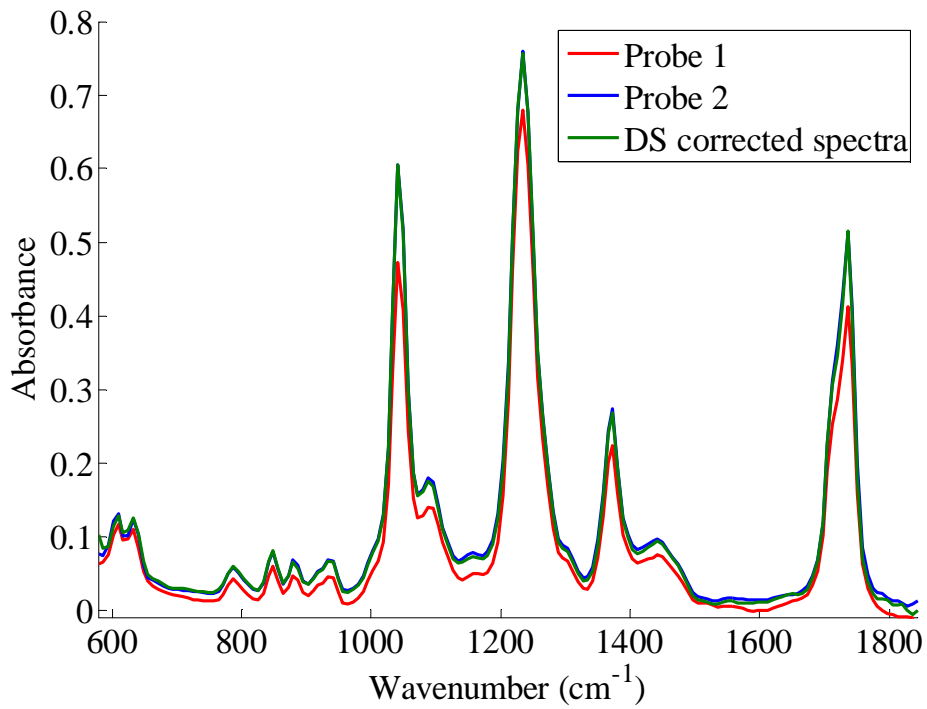


**Figure 5.11:** Test spectra (test 6) acquired on the FTLA2000 spectrometer with two 12 mm probes 1 and 2 overlaid with transformed corrected test spectra determined using DS.

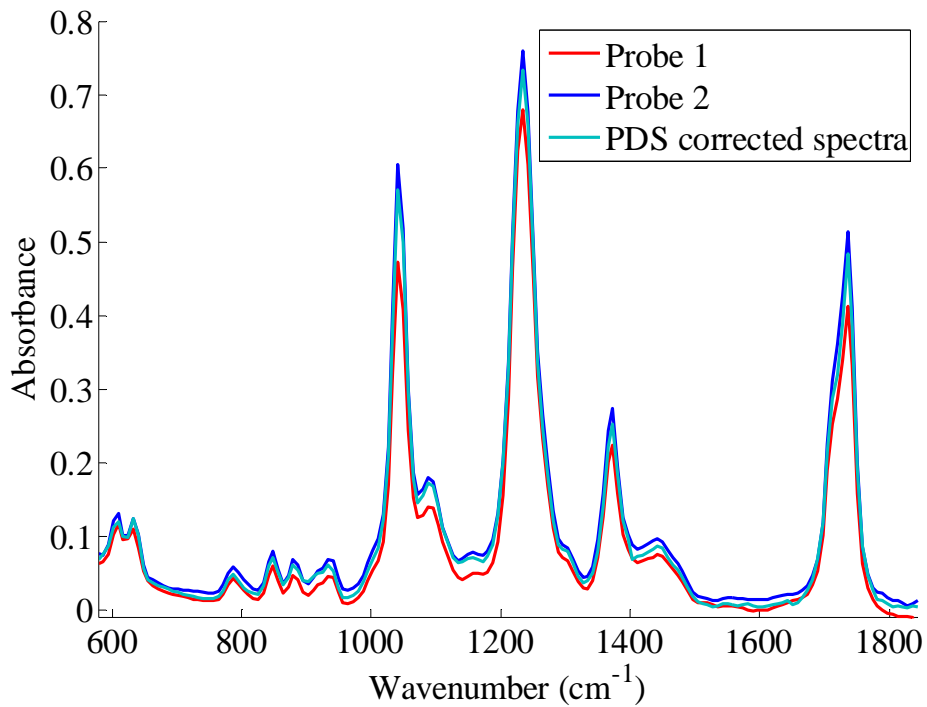


**Figure 5.12:** Test spectra (test 6) acquired on the FTLA2000 spectrometer with two 12 mm probes 1 and 2 overlaid with transformed corrected test spectra determined using PDS (window size 9).

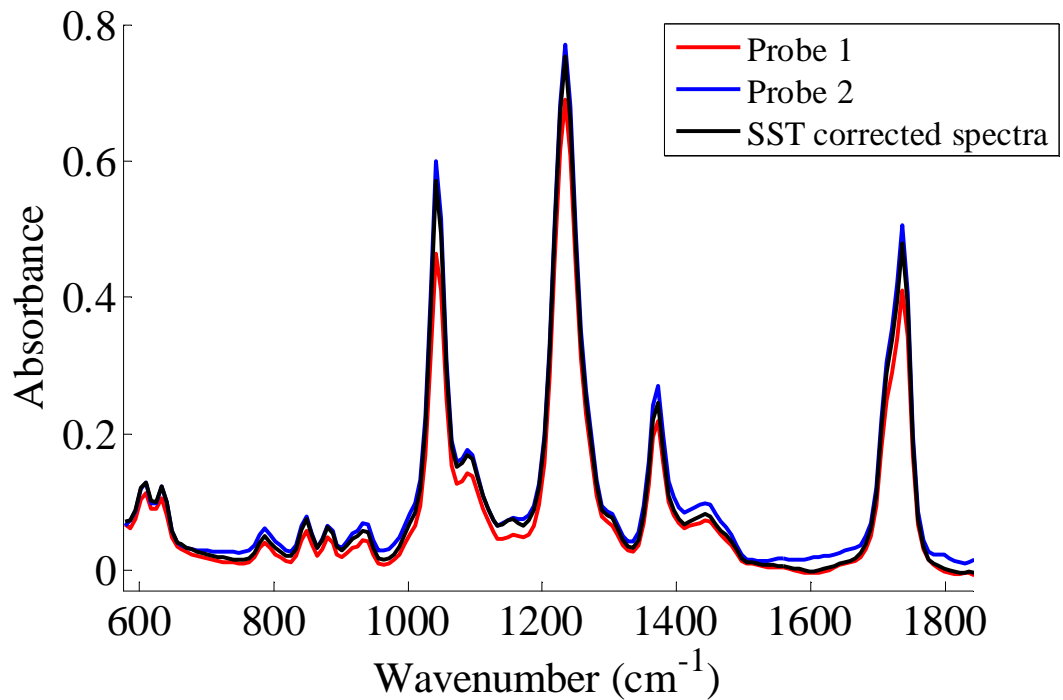


**Figure 5.13: Test spectra (test 6) acquired on the FTLA2000 spectrometer with two 12 mm probes 1 and 2 overlaid with transformed corrected test spectra determined using SST.**

The corrected spectra where DS and PDS were used, compare relatively well with those obtained with probe 2. The corrected spectrum where SST was used still has significant areas of the spectrum that resemble probe 1; however, there are some areas that compare well with probe 2. The spectra corrected using the DS algorithm provided a better spectral comparison to probe 1 than the PDS and SST corrected spectra and hence lower RMSEP values were found for this transformation, see Table 5.14.

### **5.3.2.2 Transfer of all multivariate calibration models with all calibration samples**

The multiplexing of two probes to one spectrometer can occur in industry and the above example indicates the benefits of using multivariate calibration transfer algorithms as an aid to transferring one model between two probes. However, there are many reasons for implementing these transfer algorithms in practice. Therefore the spectral data that was collected using the seven combinations of MIR instrument

and probe, (Table 5.15) have been used to assess the problems that arise when transferring calibration models between these sets of conditions.

**Table 5.15: List of different combinations of spectrometers and probes (replicate of Table 5.3, for convenience).**

Combination number	Spectrometer	Probe*
1	MB155	Probe 1
2	MB155	Probe 2
3	MB3000	Probe 2
4	MB3000	Probe 3
5	MB3000	Probe 1
6	FTLA2000	Probe 1
7	FTLA2000	Probe 2

\* Probes 1 and 2: 12 mm outer diameter, Probe 3: 2.7 mm outer diameter.

The spectral data were transferred to Matlab, pre-processing was carried out and models were built using the optimal conditions determined from DoEman. Each calibration model was transferred and used to predict the concentrations of the three components acetone, ethanol and ethyl acetate present in the six test mixtures analysed by a different instrumental set up; Table 5.16 details the transfers that were assessed. For example, a reference calibration model that was built using spectral data obtained from analysing calibration samples on the MB3000 spectrometer fitted with the 12 mm ATR probe 1 was transferred and used to predict the concentrations of the components in the six test samples that had been analysed using a secondary instrument – probe combination, e.g. FTLA2000 spectrometer fitted with 12 mm ATR probe 2. Using a column and row notation (x, y) where x are the columns and y are the rows then the aforementioned example would be (5, 7) in Table 5.16. The blue boxes represent predictions where no transfer had taken place, i.e. the calibration model was built with spectra collected on the same instrument as the test samples were analysed and predicted.

**Table 5.16: Matrix table representing the model transfers.**

		Reference model						
		1	2	3	4	5	6	7
Secondary instrument	1	1,1	2,1	3,1	4,1	5,1	6,1	7,1
	2	1,2	2,2	3,2	4,2	5,2	6,2	7,2
	3	1,3	2,3	3,3	4,3	5,3	6,3	7,3
	4	1,4	2,4	3,4	4,4	5,4	6,4	7,4
	5	1,5	2,5	3,5	4,5	5,5	6,5	7,5
	6	1,6	2,6	3,6	4,6	5,6	6,6	7,6
	7	1,7	2,7	3,7	4,7	5,7	6,7	7,7

For each model transfer combination, RMSEP values were calculated and the results were compared with the RMSEP values that had been previously obtained when no model transfer had taken place (see Table 5.6 – Table 5.12). The comparison was used to determine if the RMSEP value increased and if so by how much. Similarly, to assess the calibration transfer algorithms, direct standardisation (DS), piecewise direct standardisation (PDS) and the newer procedure spectral space transformation (SST) were carried out in Matlab. The results were compared to the RMSEP values previously calculated to determine where DS, PDS and SST algorithms could aid calibration model transfers.

PDS differs from DS methods in the use of the spectrum, DS requires the use of the entire spectrum, whereas PDS uses small channel windows around the channel of interest and therefore a window size is required. This window size can be optimised and in the case of this research a set of standardisation transforms were calculated using various window sizes for all of the spectral data sets to determine a suitable window size. The RMSEP values that were calculated for all the spectral data were reviewed to determine the optimal window size for the PDS transfer. A stipulation for the selection of the window size for PDS is that it can only be an odd number. Comparing the RMSEP values for the entire set of window sizes (1, 3, 5...165) for all of the transfers, there does not appear to be any sizable changes in the RMSEP values as the window sizes were changed. As there is no sizable change in the RMSEP values when a large window size is chosen compared to a small window size, the RMSEP values for the first ten window sizes (1, 3, 5... 19) were inspected

further to determine which window size from this selection was most suitable. The mean of the RMSEP values was taken for the results of each of the secondary instrument configurations and then plotted to show what the optimal window size was. This was completed for each of the three analytes and can be viewed in Appendix 5.2. The window sizes determined were 9, 11 and 9 for acetone, ethanol and ethyl acetate, respectively. Another parameter which requires optimisation in PDS is also required by SST, namely the number of principal components (PCs). In PDS the principal components are involved in the calculation of the transform matrix; for this study this was not optimised manually, however, the default setting in Matlab was used. In SST the principal components represent the spectral information which is retained after the singular value decomposition step. Du *et al.*<sup>58</sup> observed that using a large number of principal components made no significant impact on the predictive accuracy. It was suggested that this parameter could be set to a value equal to or slightly larger than the number of significant singular values. Therefore, DS and SST have advantages of easy implementation over the PDS algorithm. After the necessary optimisation and implementation of the three algorithms the model transfers were completed and the RMSEP statistic calculated. The numerical results for the RMSEP calculation for the model transfers, with and without the aid of calibration model transfer algorithms, can be viewed in the following tables.

Table 5.17, Table 5.18, Table 5.19 and Table 5.20 provide the results of acetone for the model transfers without the use of algorithms and with the use of DS, PDS and SST, respectively.

**Table 5.17: Acetone RMSEP values for all calibration model transfers completed by MIR analysis.**

Acetone		Reference model						
		1	2	3	4	5	6	7
Secondary instrument	1	4.4	20.3	10.4	65.3	6.1	7.1	6.9
	2	10.3	4.9	5.1	91.1	15.8	17.7	10.4
	3	11.5	11.5	4.4	92.3	13.7	15.7	8.5
	4	19.1	61.6	24.4	3.7	19.1	20.0	22.9
	5	7.6	17.0	7.8	78.4	2.0	1.9	6.4
	6	7.8	18.3	8.5	77.7	2.2	1.7	7.3
	7	7.9	8.1	5.0	87.2	6.0	6.4	1.0

**Table 5.18: Acetone RMSEP values for all calibration model transfers completed by MIR analysis with DS algorithms applied.**

Acetone		Reference model						
		1	2	3	4	5	6	7
Secondary instrument	1	4.4	1.9	4.1	2.4	4.4	4.8	4.3
	2	5.3	4.9	9.7	8.5	7.4	6.7	6.8
	3	6.4	4.9	4.4	3.2	4.8	6.3	5.5
	4	4.1	2.9	4.4	3.7	3.5	3.8	3.7
	5	4.9	3.1	2.2	2.5	2.0	2.7	2.5
	6	8.4	3.2	9.4	10.1	2.4	1.7	1.4
	7	9.9	5.6	2.3	5.3	0.7	2.0	1.0

**Table 5.19: Acetone RMSEP values for all calibration model transfers completed by MIR analysis with PDS algorithms applied.**

Acetone		Reference model						
		1	2	3	4	5	6	7
Secondary instrument	1	4.4	2.2	4.5	5.2	4.9	5.1	5.1
	2	5.5	4.9	5.6	5.5	5.4	5.5	5.4
	3	4.9	3.4	4.4	4.6	4.4	4.5	4.5
	4	4.7	5.2	4.5	3.7	3.6	3.7	3.7
	5	2.6	1.9	2.2	2.0	2.0	1.7	1.7
	6	3.6	2.9	2.6	2.1	2.0	1.7	1.9
	7	2.9	2.9	2.6	1.3	1.5	1.0	1.0

**Table 5.20: Acetone RMSEP values for all calibration model transfers completed by MIR analysis with SST algorithms applied.**

Acetone		Reference model						
		1	2	3	4	5	6	7
Secondary instrument	1	4.4	2.0	4.4	7.1	4.9	5.1	5.2
	2	6.0	4.9	5.5	8.1	5.9	5.8	5.8
	3	6.5	3.6	4.4	16.5	5.4	5.0	4.8
	4	4.6	2.2	4.1	3.7	4.8	5.0	5.1
	5	2.5	1.9	1.7	5.7	2.0	1.9	1.9
	6	3.0	4.4	2.0	5.4	1.9	1.7	1.6
	7	3.1	3.6	2.3	4.4	1.7	1.1	1.0

Table 5.21, Table 5.22, Table 5.23 and Table 5.24 provide the results of ethanol for the model transfers without the use of algorithms, and with the use of DS, PDS and SST, respectively.

**Table 5.21: Ethanol RMSEP values for all calibration model transfers completed by MIR analysis.**

Ethanol		Reference model						
		1	2	3	4	5	6	7
Secondary instrument	1	5.1	8.5	10.2	93.4	6.6	8.1	7.2
	2	8.1	5.5	4.3	117.7	12.9	12.9	9.3
	3	5.8	3.9	3.1	111.2	10.4	11.8	8.3
	4	20.9	21.8	35.4	3.0	23.8	25.1	24.6
	5	6.6	9.9	7.4	103.0	2.0	2.8	3.2
	6	8.1	11.2	8.2	106.1	2.1	1.0	3.5
	7	8.1	9.5	3.4	124.8	4.8	4.0	1.2

**Table 5.22: Ethanol RMSEP values for all calibration model transfers completed by MIR analysis with DS algorithms applied.**

Ethanol		Reference model						
		1	2	3	4	5	6	7
Secondary instrument	1	5.1	5.9	3.1	3.1	4.8	5.7	5.4
	2	5.6	5.5	6.1	9.2	8.8	9.4	9.1
	3	9.2	9.7	3.1	2.9	3.9	4.8	4.7
	4	5.2	5.1	3.0	3.0	3.1	2.8	2.7
	5	5.4	6.5	3.4	2.0	2.0	2.0	1.8
	6	10.3	11.3	2.1	6.7	1.8	1.0	0.9
	7	12.4	13.1	3.0	3.9	1.4	1.7	1.2

**Table 5.23: Ethanol RMSEP values for all calibration model transfers completed by MIR analysis with PDS algorithms applied.**

Ethanol		Reference model						
		1	2	3	4	5	6	7
Secondary instrument	1	5.1	5.0	4.4	5.5	5.0	5.0	4.9
	2	5.5	5.5	5.7	5.9	5.4	5.4	5.4
	3	4.6	4.1	3.1	5.3	3.8	4.0	3.8
	4	3.7	4.1	5.6	3.0	3.9	4.1	4.1
	5	2.1	2.0	2.5	1.9	2.0	2.0	2.0
	6	2.5	2.3	2.4	2.1	1.1	1.0	1.1
	7	1.9	1.7	2.6	1.6	1.0	1.0	1.2

**Table 5.24: Ethanol RMSEP values for all calibration model transfers completed by MIR analysis with SST algorithms applied.**

Ethanol		Reference model						
		1	2	3	4	5	6	7
Secondary instrument	1	5.1	5.1	4.3	5.8	5.1	5.0	5.1
	2	5.5	5.5	5.7	7.4	5.8	5.8	5.8
	3	4.1	4.0	3.1	7.8	3.8	3.8	3.8
	4	3.5	3.5	3.5	3.0	3.6	3.6	3.6
	5	2.0	2.0	2.5	2.5	2.0	2.0	2.0
	6	1.6	1.4	2.5	2.5	1.0	1.0	1.0
	7	1.2	1.1	3.0	2.8	1.1	1.2	1.2

Table 5.25, Table 5.26, Table 5.27 and Table 5.28 provide the results of ethyl acetate for the model transfers without the use of algorithms, and with the use of DS, PDS and SST, respectively.

**Table 5.25: Ethyl acetate RMSEP values for all calibration model transfers completed by MIR analysis.**

Ethyl acetate		Reference model						
		1	2	3	4	5	6	7
Secondary instrument	1	2.5	9.2	7.7	45.9	1.6	3.1	5.4
	2	13.0	3.4	4.2	56.9	6.0	7.7	2.7
	3	10.0	3.9	3.8	48.5	4.2	4.9	1.9
	4	30.1	32.8	31.0	1.1	23.2	29.0	25.1
	5	1.6	8.5	7.0	45.5	1.1	2.0	4.6
	6	1.7	8.5	7.2	48.0	1.2	1.5	4.4
	7	8.9	2.8	2.2	62.1	5.2	5.4	0.4

**Table 5.26: Ethyl acetate RMSEP values for all calibration model transfers completed by MIR analysis with DS algorithms applied.**

Ethyl acetate		Reference model						
		1	2	3	4	5	6	7
Secondary instrument	1	2.5	0.9	5.5	1.8	2.0	2.6	2.5
	2	4.5	3.4	4.5	2.8	3.2	4.7	3.9
	3	2.2	1.5	3.8	1.7	1.9	2.2	2.1
	4	2.8	1.0	2.4	1.1	1.4	1.4	1.6
	5	2.5	0.9	3.5	0.8	1.1	1.9	1.7
	6	2.9	1.1	4.1	2.7	1.2	1.5	0.7
	7	2.5	1.1	3.4	1.4	0.7	0.7	0.4

**Table 5.27: Ethyl acetate RMSEP values for all calibration model transfers completed by MIR analysis with PDS algorithm applied.**

Ethyl Acetate		Reference model						
		1	2	3	4	5	6	7
Secondary instrument	1	2.5	2.6	2.1	1.9	1.6	2.0	1.9
	2	3.4	3.4	3.2	2.9	2.6	3.0	2.7
	3	4.3	4.1	3.8	4.4	3.5	3.8	3.4
	4	4.5	4.2	3.8	1.1	2.1	2.9	2.5
	5	1.2	1.4	0.9	1.7	1.1	0.9	0.9
	6	1.7	1.7	1.7	1.7	1.3	1.5	1.2
	7	1.1	1.2	0.7	1.3	0.3	0.3	0.4

**Table 5.28: Ethyl acetate RMSEP values for all calibration model transfers completed by MIR analysis with SST algorithm applied.**

Ethyl Acetate		Reference model						
		1	2	3	4	5	6	7
Secondary instrument	1	2.5	2.5	2.3	6.4	1.2	1.9	1.7
	2	3.6	3.4	3.1	6.2	2.5	3.3	2.7
	3	4.2	3.9	3.8	10.0	3.7	4.0	3.4
	4	5.1	5.0	4.9	1.1	3.9	4.5	4.2
	5	1.2	1.3	1.2	6.7	1.1	0.9	0.8
	6	1.5	1.4	1.4	5.8	1.8	1.5	1.0
	7	1.3	1.2	0.9	5.9	1.2	0.3	0.4

On assessing the results for the transfer of calibration models with and without the use of calibration model transfer algorithms several conclusions can be made:

- Transfer of calibration models when the spectrometer, probe or both are changed causes an increase in the RMSEP values when compared with the original models.
- Changing the probe appears to have a greater effect on the predictive ability of a model than when the spectrometer is changed; this is not surprising when the results of section 5.3.1.1 are considered. Larger errors were shown when transferring models that were developed with a different probe diameter to that of the data acquired on the secondary instrument, e.g. column 4 in Table 5.18, Table 5.22 and Table 5.26 where no algorithms were used to aid the

transfer; the reference model was acquired with a 2.7 mm probe, however, the secondary instruments included 12 mm probes.

- The RMSEP values increased considerably when no algorithm was used to aid the transfer, especially in the case of ethanol, see Table 5.21. The use of DS, PDS or SST algorithms successfully decreased the RMSEP values in comparison with the transfer of calibration models without the use of the algorithms. In the case of ethanol, there was a large decrease in the RMSEP value when DS, PDS or SST was used.
- Some of the results when the algorithms were used for the transfer give better RMSEP values than the results when no transfer has taken place. It is possible that the difference between the results is within the variation of these models if spectra collected at multiple time points were used. For example, if spectra were acquired on the reference instrument several times throughout the day and the RMSEP calculated when no transfer has taken place for each time point, the variation between the errors may be the same as observed here; it would be useful to test this theory out in the future.
- Some DS transfers resulted in an increase in RMSEP values in comparison to the transfer of calibration models without the use of algorithms, for example the DS results in 1,6 and 1,7 in Table 5.18 have larger errors than the equivalent 1,6 and 1,7 in Table 5.17 where no algorithms were used. This is due to poor transform spectra being produced by applying the DS algorithm for these examples, resulting in poorer predictions and larger RMSEP values, The number of occurrences was reduced when PDS or SST was applied, as the transform spectra looked more like the spectra that were acquired with the original system that the calibration model was built upon.
- The use of SST algorithm resulted in similar results to those obtained when using DS and PDS; an exception occurred when the original model was built using the MB3000 and 2.7 mm probe (column 4 in the tables). For example the SST results for ethyl acetate in Table 5.28 are similar to the DS and PDS results for ethyl acetate given in Table 5.26 and Table 5.27, with the exception of column 4.

- The results produced with the MB155 spectrometer are generally poorer, suggesting that the spectrometer performance is having a major impact on the quality of the results obtained. For example, compare the results in 5,1 with 5,5 and 5,6 in Table 5.21; the RMSEP for the original model with no transfer (5,5) is similar to the results from a transfer to the FTLA2000 series spectrometer (5,6), however the results for the transfer to the MB155 spectrometer (5,1) have larger errors.

### **5.3.3 Investigation using a subset of calibration samples**

Previously in section 5.3.2.2, transfers between different spectrometers and probes were investigated when all calibration samples were involved in the transfer. The results showed that SST provided comparable results to DS and PDS with the exception of when the reference model was originally built from data collected on the MB3000 spectrometer with the smaller 2.7 mm probe. This issue was investigated to determine if the SST algorithm could be improved to provide better results for this transfer.

The transfer of a reference model for a 2.7 mm probe to predict analyte concentrations for spectra acquired with a 12 mm probe is potentially quite an important example for industry, as it may arise when scaling up a process. So, the results obtained for this example were considered further. In particular, different numbers of calibration samples involved in the calibration transfer process were investigated and the RMSEP values compared for the three algorithms discussed.

#### **5.3.3.1 Improvement to SST algorithm**

The absorbance values collected by the 12 mm probe are far larger than those acquired by the 2.7 mm probe, see Figure 5.14. The reason for the absorbance difference is due to changes in the manufacturing design; probe 1 is the standard 12 mm dual fibre probe design in comparison to probe 3 which is a mono fibre design which incorporates a smaller diamond cone. These changes will influence the pathlength and hence the absorbance of the probes, and are described in more detail in chapter 4.

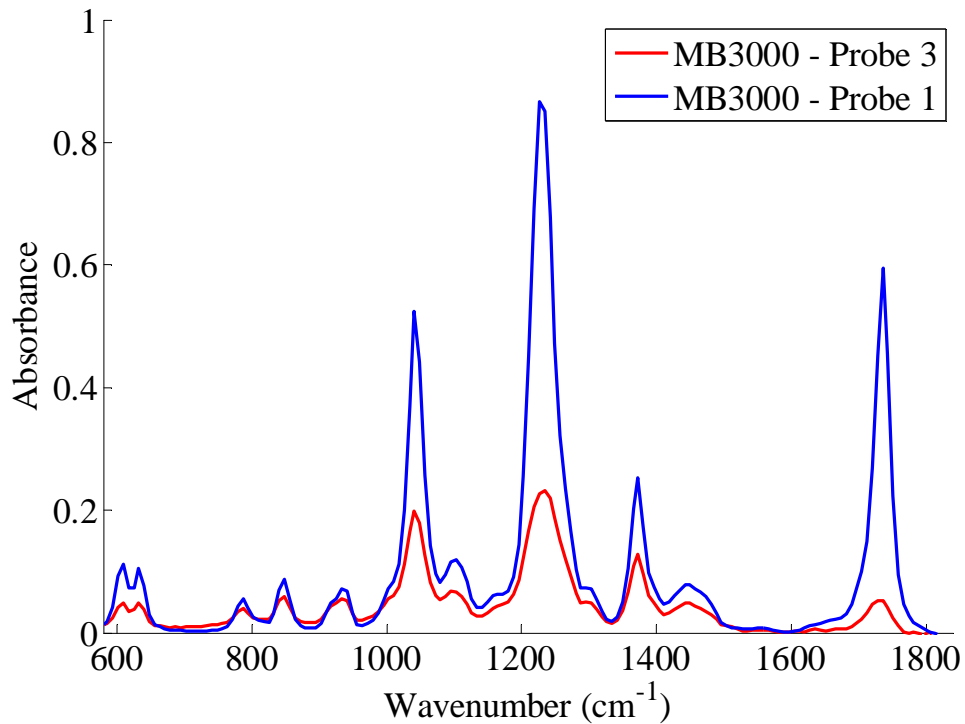


**Figure 5.14: Overlaid spectra acquired on the MB3000 spectrometer with 12 mm probe 1 and a 2.7 mm probe.**

The singular value decomposition of the combined spectra part of the SST algorithm will tend to explain the variations of the minor factors of the larger 12 mm probe rather than describing the major factors in the smaller 2.7 mm probe. This then leads to inaccuracies when completing the transfer and so the RMSEP values are not reduced as much as with DS or PDS for this particular transfer. For example, consider the situation when calibration transfer was completed when the reference is probe 3 and the secondary set-up is probe 1 ((4, 5) in Table 5.17 - Table 5.28); the results have been extracted and are re-presented in Table 5.29.

**Table 5.29: Comparison of RMSEP values for acetone, ethanol and ethyl acetate when the test spectra are acquired with a different probe than that used when the reference calibration was built and DS, PDS and SST are applied. (Spectrometer MB3000 Reference – probe 3 and Secondary –probe 1)**

	Reference model : MB3000 probe 3		
	Acetone	Ethanol	Ethyl acetate
Reference calibration/ Secondary test	78.4	103.0	45.5
Reference calibration/ Secondary test – DS used	2.5	2.0	0.8
Reference calibration/ Secondary test – PDS used (Window size...)	2.0 (9)	1.9 (11)	1.7 (9)
Reference calibration/ Secondary test – SST used	4.2	2.2	3.5

To overcome the issue with SST, an improvement was made whereby the spectral data sets to be standardised were scaled. This scaling eliminated the major differences in absorbance observed between the spectra obtained with the 12 mm probe and the 2.7 mm probe. The spectral data that are to be standardised are scaled by a factor of  $\text{Var } 1 / \text{Var } 2$ , where Var 1 and Var 2 are the standard variation of the bigger diameter probe and the smaller diameter probe, respectively. The calibration transfer described in Table 5.29 was completed using the SST algorithm incorporating scaling and the results are compared with the previous RMSEP values obtained, see Table 5.30.

**Table 5.30: Comparison of RMSEP values for acetone, ethanol and ethyl acetate when the test spectra are acquired with a different probe than that used when the reference calibration was built and DS, PDS and SST are applied. (Spectrometer MB3000 Reference – probe 2.7 mm probe and Secondary – 12 mm probe 1)**

	Reference model : MB3000 probe 3		
	Acetone	Ethanol	Ethyl acetate
Reference calibration/ Reference test	3.7	3.0	1.1
Reference calibration/ Secondary test	78.4	103.0	45.5
Reference calibration/ Secondary test – DS used	2.5	2.0	0.8
Reference calibration/ Secondary test – PDS used (Window size...)	2.0 (9)	1.9 (11)	1.7 (9)
Reference calibration/ Secondary test – SST used	4.2	2.2	3.5
Reference calibration/ Secondary test –SST incorporating scaling	1.6	1.5	0.9

The improvement to the SST algorithm was shown to be successful, with the RMSEP values reduced for all three analytes when compared with the original SST algorithm. The improved SST algorithm is now comparable to or better than the DS and PDS algorithms for this transfer. Employing the same scaling method to the data for the DS and PDS algorithm has no effect on the final transformed spectra and so will not have an influence on the RMSEP values. This is due to the way the transform is created, as detailed in section 5.2.4. The use of the scaling method was also investigated for the other transfers when SST was employed, as these spectra do not vary greatly in intensity, scaling has little effect; therefore, no improvement can be gained if scaling was to be used for transfers other than those where there is a large difference in intensity.

### 5.3.3.2 Leverage – sample selection

The purpose of using calibration standardisation algorithms for transfer of models is to limit the need for a full recalibration if the model becomes invalid. The three standardisation algorithms investigated in this work require samples to be analysed on both the reference and the secondary system. This can still be quite time consuming if there are a large number of calibration samples in the reference calibration and so ideally a smaller subset would be used when applying these standardisation algorithms. Using a smaller selected subset of calibration samples will reduce the time involved in the transfer. To determine the selection of samples that were to be used in the standardisation, leverage analysis was completed. Leverage is a measure of the influence of a given sample on the regression. The samples were selected in order of furthest away from the multivariate mean of the calibration samples. The sample selection order was 3, 2, 1, 4, 5, 8, 10, 6, 7 and 9.

With the sub-set of samples selected, calculations using DS, PDS and SST were completed for the simulated process scale-up example. The number of calibration samples included in the sub-set was altered from 6 up to 10 and the RMSEP values were reviewed. The PDS algorithm required the window size to be optimised each time the sub-set of calibration samples was altered and this was completed for each analyte. RMSEP values for window sizes 1, 3, 5...21 were investigated and the optimum window size for each analyte and transfer set was selected. For the SST algorithm, the number of singular values was selected to obtain the optimum result, as suggested by Du *et al.*<sup>58</sup>

### 5.3.3.3 Process scale-up – calibration transfer example

The DS, PDS and improved SST algorithms were investigated when the number of calibration samples involved in the transfer was altered from 6 – 10. The samples were selected using the leverage method and the optimised algorithms were implemented. Plots of RMSEP vs. Number of samples included in the transform were analysed to determine the effect that changing the number of samples has on the final RMSEP value. Figure 5.15, Figure 5.16 and Figure 5.17 provide the results for the transfers for acetone, ethanol and ethyl acetate, respectively.

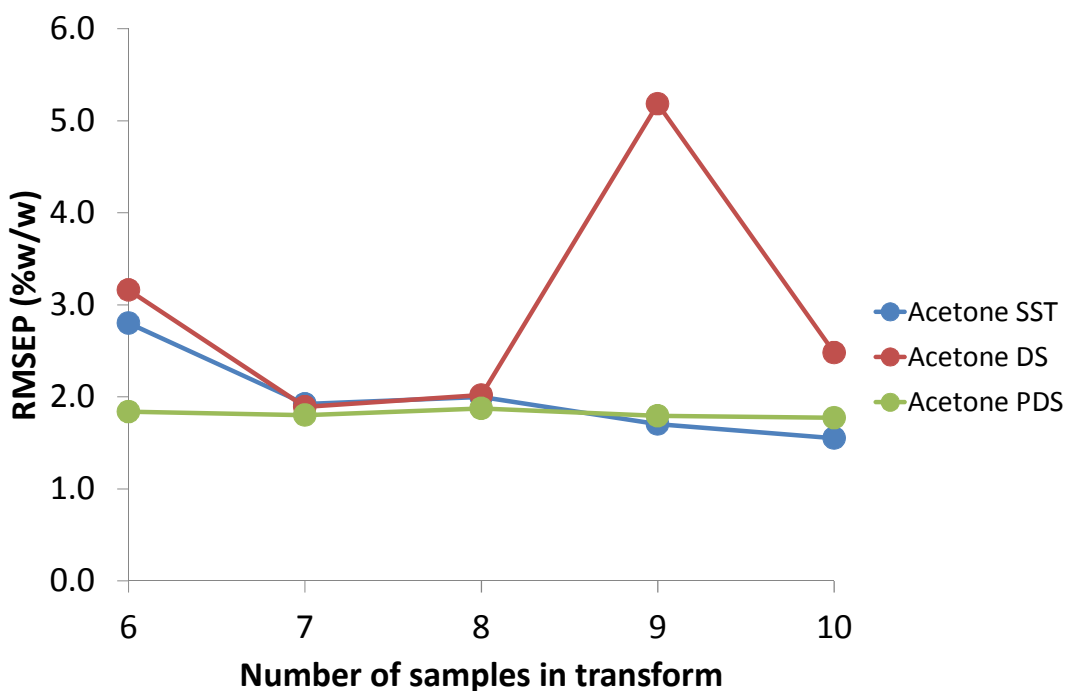


Figure 5.15: Comparison of RMSEP values for DS, PDS and improved SST when number of samples involved in the transform are altered for acetone (sample order 3, 2, 1, 4, 5, 8, 10, 6, 7 and 9).

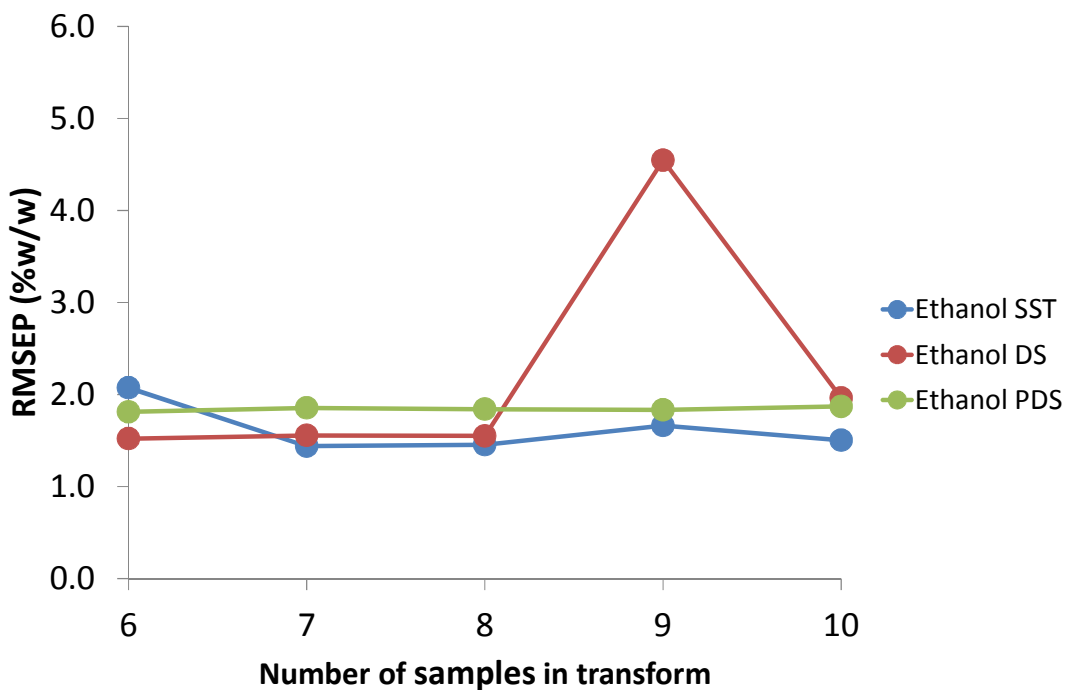
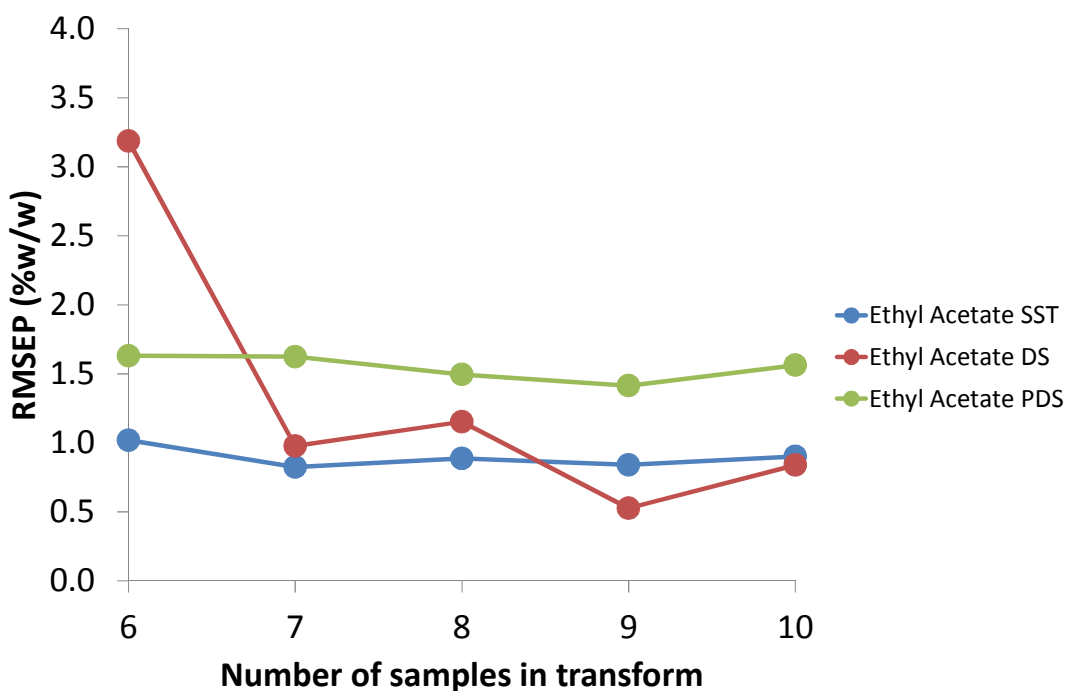


Figure 5.16: Comparison of RMSEP values for DS, PDS and improved SST when number of samples involved in the transform are altered for ethanol (sample order 3, 2, 1, 4, 5, 8, 10, 6, 7 and 9).



**Figure 5.17: Comparison of RMSEP values for DS, PDS and improved SST when number of samples involved in the transform are altered for ethyl acetate (sample order 3, 2, 1, 4, 5, 8, 10, 6, 7 and 9).**

The RMSEP results for the DS algorithm show an increase when 9 samples are involved in the transform for acetone and ethanol. The sample selection order was 3, 2, 1, 4, 5, 8, 10, 6, 7 and 9, indicating that the addition of sample 7 in the transform means the spectra are not transformed as well with the DS algorithm; both PDS and SST appear unaffected. The RMSEP values lower again after the addition of the tenth sample, calibration sample 9, suggesting that this sample contains information that allows better transformed spectra and hence DS can perform better. The overlaid transformed spectra from DS, SST and PDS when 8, 9 or 10 samples are involved in the transform are given in Figure 5.18, Figure 5.19 and Figure 5.20. Reviewing the spectra in Figure 5.19 there are regions,  $600 - 800 \text{ cm}^{-1}$ ,  $1200 - 1300 \text{ cm}^{-1}$  and  $1600 - 1800 \text{ cm}^{-1}$ , where there are differences in the DS transformed spectra when compared to PDS and SST. Referring to the overlaid pure component spectra of the three analytes in Figure 5.3, two of the regions where DS performs poorly include areas where there are no bands present for acetone ( $600 - 800 \text{ cm}^{-1}$ ) or ethanol ( $1600 - 1800 \text{ cm}^{-1}$ ). It could be that when sample 7, which is a 1:1:1 mixture of the three components, is included in the transform it is more difficult to ascertain the bands

from the acetone and ethanol in the regions discussed and so the final predictions for acetone and ethanol are worse than for ethyl acetate when 9 samples are included in the transform. With the addition of the tenth sample (Figure 5.20), the transform improves and hence the RMSEP results are better.

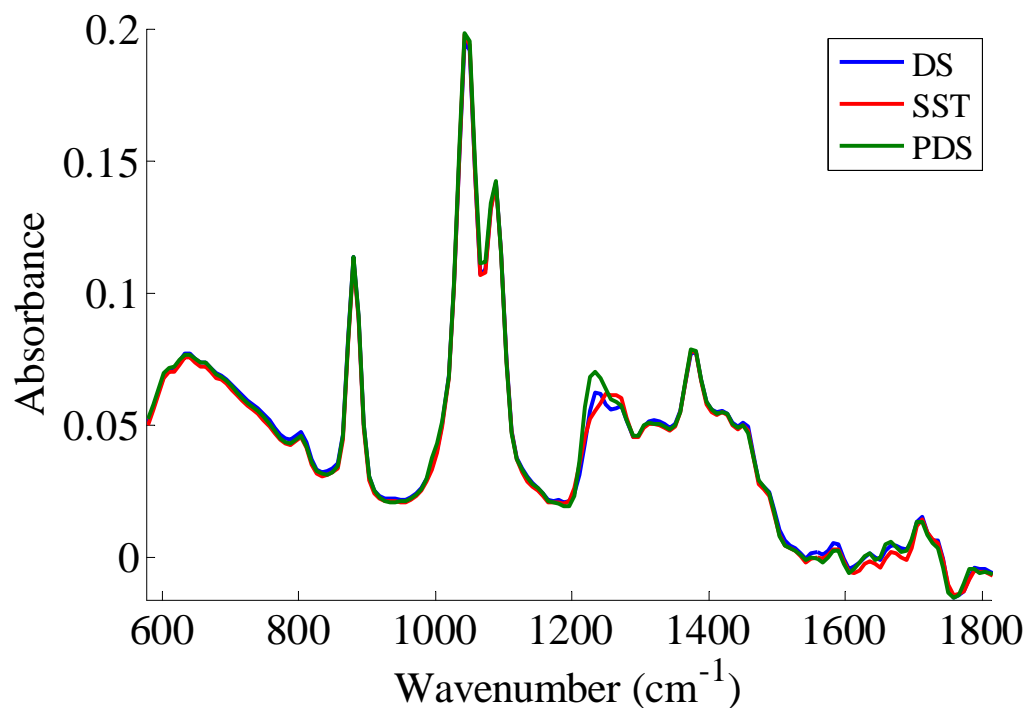


**Figure 5.18: Overlay of transformed test spectra (test 1) from DS, SST and PDS (window size 15) when eight calibration samples were included in the transfer.**

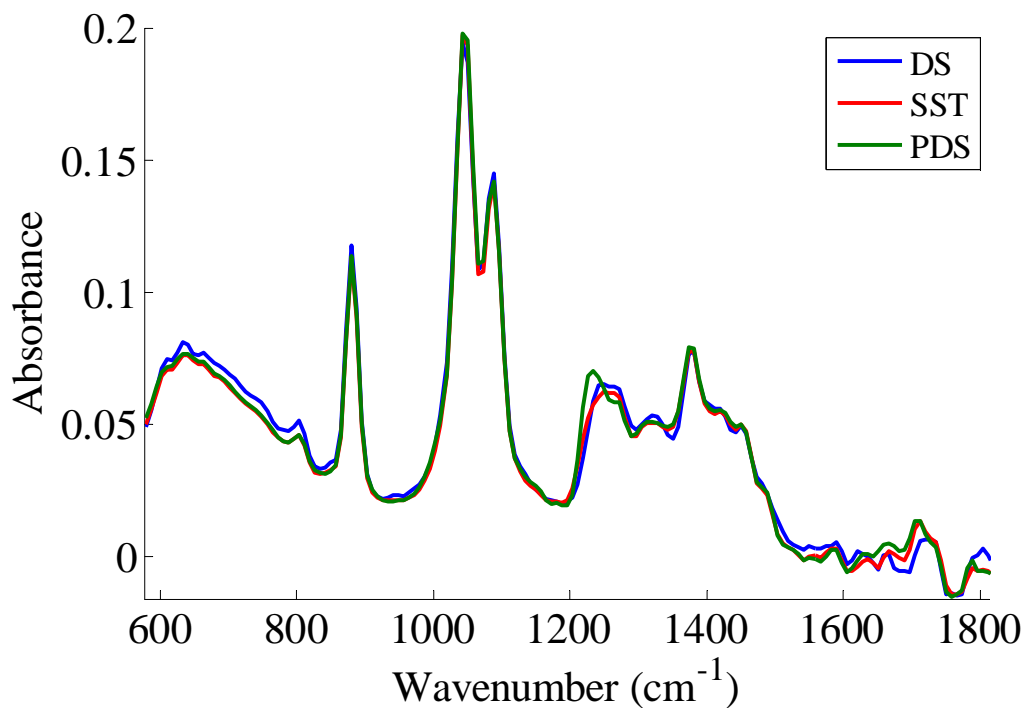


Figure 5.19: Overlay of transformed test spectra (test 1) from DS, SST and PDS (window size 15) when nine calibration samples were included in the transfer.

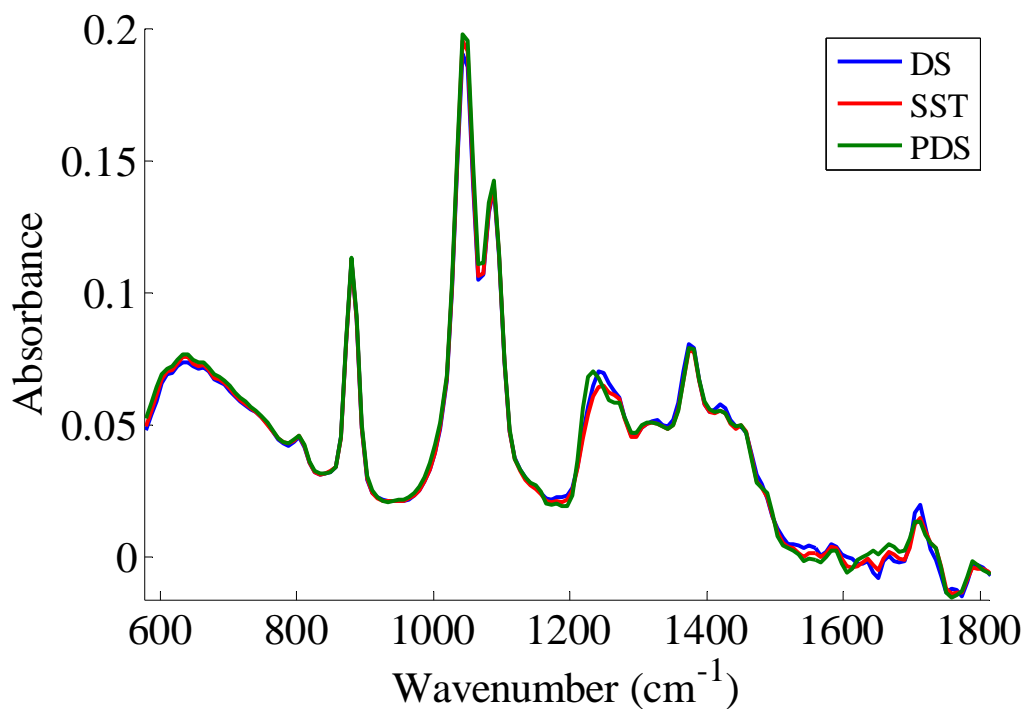


Figure 5.20: Overlay of transformed test spectra (test 1) from DS, SST and PDS (window size 15) when ten calibration samples were included in the transfer.

If the final order of the ninth and tenth samples were reversed so that sample 7 was added last (3, 2, 1, 4, 5, 8, 10, 6, 9 and 7), the RMSEP results improve when 9 samples are included in the transform. Figure 5.21, Figure 5.22 and Figure 5.23 provide the results for the transfers for acetone, ethanol and ethyl acetate when the order of the last two samples is changed.

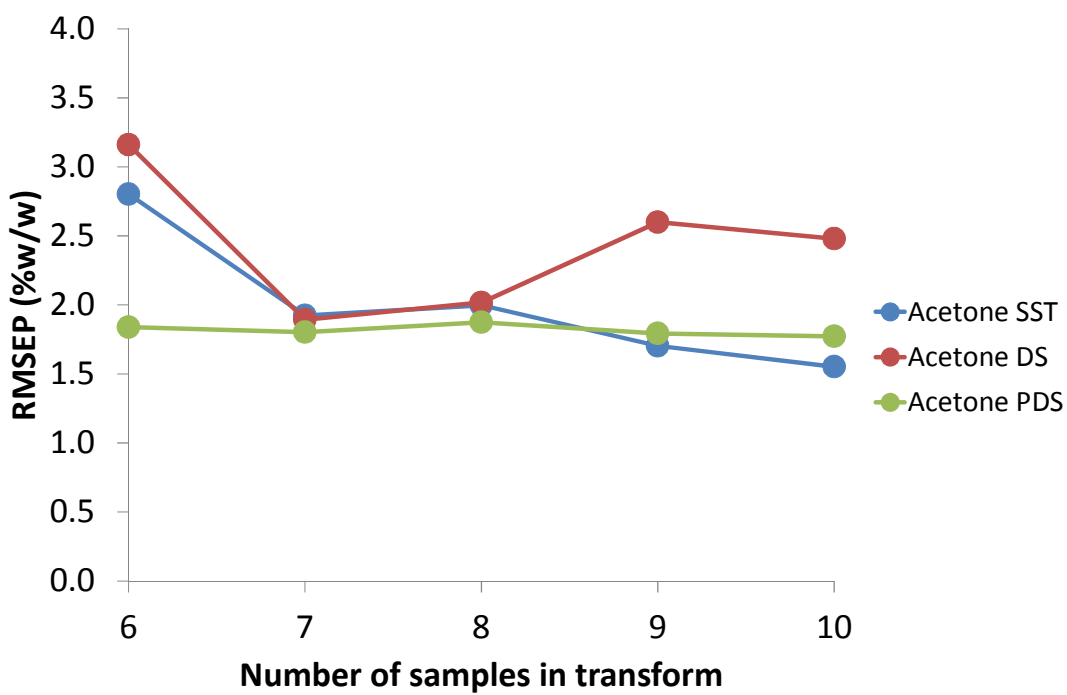


Figure 5.21: Comparison of RMSEP values for DS, PDS and improved SST when number of samples involved in the transform are altered for acetone (sample order 3, 2, 1, 4, 5, 8, 10, 6, 9 and 7).

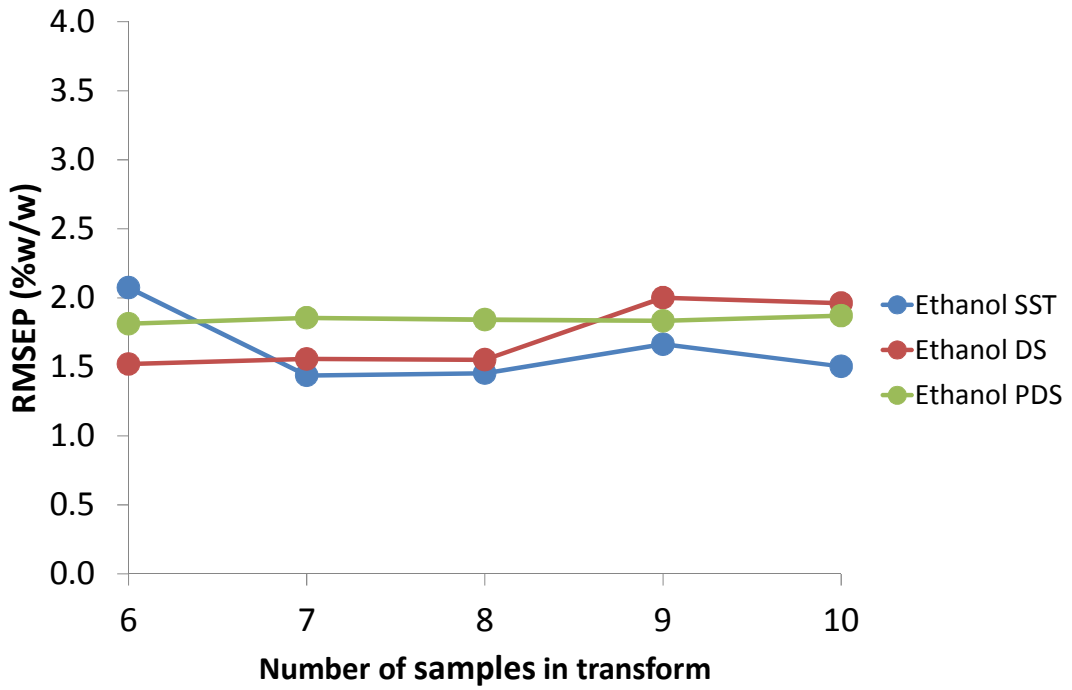


Figure 5.22: Comparison of RMSEP values for DS, PDS and improved SST when number of samples involved in the transform are altered for ethanol (sample order 3, 2, 1, 4, 5, 8, 10, 6, 9 and 7).

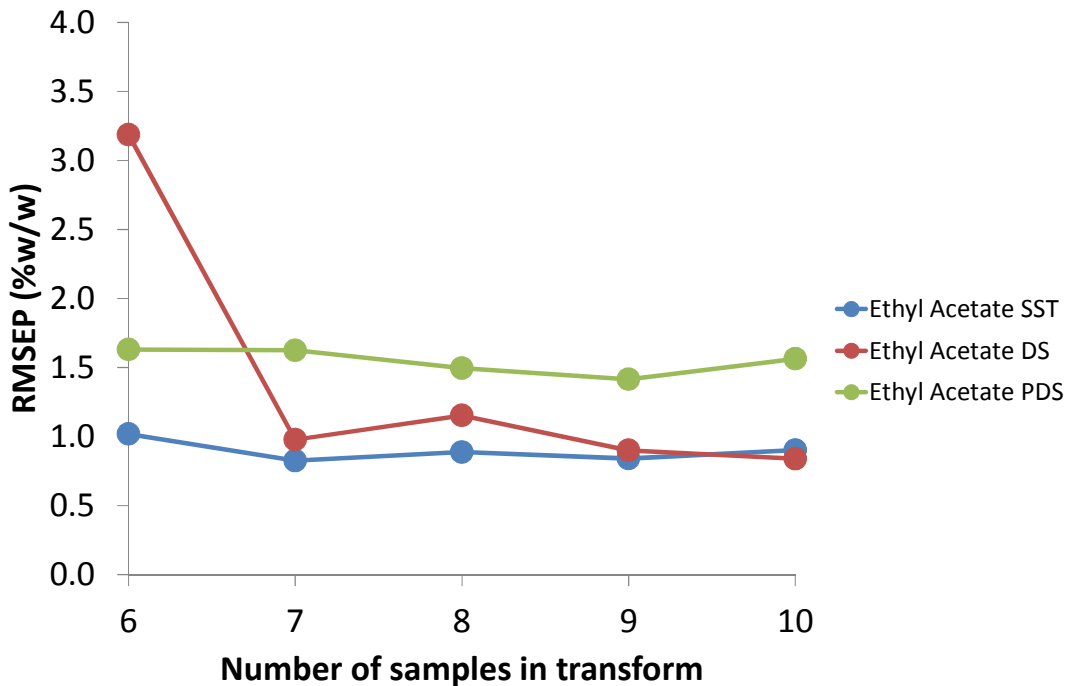


Figure 5.23: Comparison of RMSEP values for DS, PDS and improved SST when number of samples involved in the transform are altered for ethyl acetate (sample order 3, 2, 1, 4, 5, 8, 10, 6, 9 and 7).

On assessing the results for the transfer of the calibration model when the number of calibration samples involved in the transfer is altered, some conclusions can be made:

- DS shows the greatest sensitivity, with fluctuations in RMSEP values when the number of calibration samples used in the transfer is altered, however this difference is small.
- Both PDS and improved SST provide similar and consistent results when the number of samples used for the transfer is altered, however SST has the advantage of simpler implementation over PDS. SST requires the optimisation of one parameter in comparison with PDS which requires the optimisation of multiple parameters including the window size which must be optimised each time a change is made, which can be time consuming.
- As the number of samples included in the transfer is increased the RMSEP values are similar for all three transfers if the order of the last two samples is changed.
- If SST with no scaling incorporated is used, then the RMSEP values are much greater and DS and PDS provide better results when fewer samples are included in the transfer. Again the results are similar for all three transfers when larger numbers of samples are involved in the transfer.

## 5.4 Conclusions

The Fibre Photonics ATR probes were able to analyse the solvent mixtures and provide good quality spectra for use in calibration model building. It was observed in this research that the use of good spectrometers is required to gain the best results from these probes; for example, if a spectrometer has a poorer detector or a detector that is not optimised specifically for the MIR range then the results will be worse than those from a spectrometer that contains optimised components. The straight transfer of calibration models resulted in large RMSEP values being observed; changing the probe had a greater effect on the error of prediction than changing the spectrometer. When the algorithms DS, PDS and SST were applied to the transfer of the calibration models, the RMSEP values were seen to decrease by at least a factor of 2 in the majority of cases and in some instances by a factor of greater than 10. SST was shown to have issues in transferring a reference model for a 2.7 mm probe to predict concentrations for spectra acquired with a 12 mm probe; although the algorithm could be used to reduce the errors in comparison to the straight transfer, the errors in some instances were double that obtained by DS and PDS for this transfer example. By incorporating a scaling factor into the SST algorithm better results were obtained for the transfer between a 2.7 mm and a 12 mm probe, with the results being comparable to or better than those obtained from DS and PDS. Implementing a scaling factor will only improve the results for SST when there are large intensity differences; scaling factors will not influence the results if there are only small intensity differences for SST or for the use of DS and PDS.

Overall DS showed a greater sensitivity to change when the number of samples involved in the transfer was altered; PDS and SST incorporating scaling provided similar and consistent results when the number of calibration samples was altered for the example discussed. An advantage of SST is that it only requires the optimisation of one parameter, making this algorithm easy to implement and achieve good results with lower numbers of calibration samples included in the transfer. PDS has multiple parameters which can be optimised, but only the window size was optimised in this study; however, this is a very time consuming process. SST can get comparable or better results more efficiently than PDS.

## 5.5 References

1. O. E. de Noord, *Chemom. Intell. Lab. Syst.*, 1994, **25**, 85-97.
2. B. M. Wise, N. B. Gallagher, R. Bro, J. M. Shaver, W. Windig and R. S. Koch, Eigenvector Research Inc., USA, 2006.
3. R. N. Feudale, N. A. Woody, H. W. Tan, A. J. Myles, S. D. Brown and J. Ferre, *Chemom. Intell. Lab. Syst.*, 2002, **64**, 181-192.
4. F. van den Berg and Å. Rinnan, in *Infrared Spectroscopy for Food Quality Analysis and Control*, Academic Press, San Diego, 2009, pp. 105-118.
5. I. S. Adhietty, J. A. McGuire, B. Wangmaneerat, T. M. Niemczyk and D. M. Haaland, *Anal. Chem.*, 1991, **63**, 2329-2338.
6. D. Ozdemir, M. Mosley and R. Williams, *Appl. Spectrosc.*, 1998, **52**, 1203-1209.
7. F. Despaigne, D. L. Massart and P. Chabot, *Anal. Chem.*, 2000, **72**, 1657-1665.
8. H. Swierenga, W. G. Haanstra, A. P. D. Weijer and L. M. C. Buydens, *Appl. Spectrosc.*, 1998, **52**, 7-16.
9. J. K. Holland, E. K. Kemsley and R. H. Wilson, *J. Sci. Food Agric.*, 1997, **75**, 391-400.
10. H. Swierenga, P. J. de Groot, A. P. de Weijer, M. W. J. Derksen and L. M. C. Buydens, *Chemom. Intell. Lab. Syst.*, 1998, **41**, 237-248.
11. Koehler, G. W. Small, R. J. Combs, R. B. Knapp and R. T. Kroutil, *Anal. Chem.*, 2000, **72**, 1690-1698.
12. W. Ni, S. D. Brown and R. Man, *J. Chemom.*, 2011, **25**, 130-137.
13. B. Igne, J.-M. Roger, S. Roussel, V. Bellon-Maurel and C. R. Hurburgh, *Chemom. Intell. Lab. Syst.*, 2009, **99**, 57-65.
14. B. Igne and C. R. Hurburgh, *J. Chemom.*, 2010, **24**, 75-86.
15. J.-M. Roger, F. Chauchard and V. Bellon-Maurel, *Chemom. Intell. Lab. Syst.*, 2003, **66**, 191-204.
16. D. Ozdemir, M. Mosley and R. Williams, *Appl. Spectrosc.*, 1998, **52**, 599-603.
17. C. V. Greensill, P. J. Wolfs, C. H. Spiegelman and K. B. Walsh, *Appl. Spectrosc.*, 2001, **55**, 647-653.
18. S. K. Setarehdan, J. J. Soraghan, D. Littlejohn and D. A. Sadler, *Anal. Chim. Acta*, 2002, **452**, 35-45.
19. C. L. Stork and B. R. Kowalski, *Chemom. Intell. Lab. Syst.*, 1999, **48**, 151-166.
20. A. J. Myles, T. A. Zimmerman and S. D. Brown, *Appl. Spectrosc.*, 2006, **60**, 1198-1203.
21. K. E. Kramer and G. W. Small, *Appl. Spectrosc.*, 2007, **61**, 497-506.
22. J. H. Kalivas, G. G. Siano, E. Andries and H. C. Goicoechea, *Appl. Spectrosc.*, 2009, **63**, 800-809.
23. M. R. Kunz, J. Ottaway, J. H. Kalivas and E. Andries, *J. Chemom.*, 2010, **24**, 218-229.
24. M. R. Kunz, J. H. Kalivas and E. Andries, *Anal. Chem.*, 2010, **82**, 3642-3649.

25. Y. Wang, D. J. Veltkamp and B. R. Kowalski, *Anal. Chem.*, 1991, **63**, 2750-2756.
26. M. Forina, G. Drava, C. Armanino, R. Boggia, S. Lanteri, R. Leardi, P. Corti, P. Conti, R. Giangiaco, C. Galliena, R. Bigoni, I. Quartari, C. Serra, D. Ferri, O. Leoni and L. Lazzeri, *Chemom. Intell. Lab. Syst.*, 1995, **27**, 189-203.
27. D. M. Haaland and D. K. Melgaard, *Vib. Spectrosc.*, 2002, **29**, 171-175.
28. J. S. Shenk and M. O. Westerhaus, *Crop Sci.*, 1991, **31**, 1694-1696.
29. E. Bouveresse, C. Hartmann, D. L. Massart, I. R. Last and K. A. Prebble, *Anal. Chem.*, 1996, **68**, 982-990.
30. E. Bouveresse, D. L. Massart and P. Dardenne, *Anal. Chim. Acta*, 1994, **297**, 405-416.
31. E. Bouveresse, D. L. Massart and P. Dardenne, *Anal. Chem.*, 1995, **67**, 1381-1389.
32. J. Fontaine, J. Hörr and B. Schirmer, *J. Agric. Food. Chem.*, 2004, **52**, 701-708.
33. E. Fernandez-Ahumada, A. Garrido-Varo, J. E. Guerrero, D. Perez-Marin and T. Fearn, *J. Agric. Food. Chem.*, 2008, **56**, 10135-10141.
34. Y. Wang and B. R. Kowalski, *Anal. Chem.*, 1993, **65**, 1301-1303.
35. Y. Wang and B. R. Kowalski, *Appl. Spectrosc.*, 1992, **46**, 764-771.
36. Y. Wang, M. J. Lysaght and B. R. Kowalski, *Anal. Chem.*, 1992, **64**, 562-564.
37. Z. Wang, T. Dean and B. R. Kowalski, *Anal. Chem.*, 1995, **67**, 2379-2385.
38. E. Bouveresse and D. L. Massart, *Chemom. Intell. Lab. Syst.*, 1996, **32**, 201-213.
39. E. Bouveresse and D. L. Massart, *Vib. Spectrosc.*, 1996, **11**, 3-15.
40. P. J. Gemperline, J. H. Cho, P. K. Aldridge and S. S. Sekulic, *Anal. Chem.*, 1996, **68**, 2913-2915.
41. F. Despagne, D. L. Massart, M. Jansen and H. van Daalen, *Anal. Chim. Acta*, 2000, **406**, 233-245.
42. K.-S. Park, Y.-H. Ko, H. Lee, C.-H. Jun, H. Chung and M.-S. Ku, *Chemom. Intell. Lab. Syst.*, 2001, **55**, 53-65.
43. C. M. Wehlburg, D. M. Haaland and D. K. Melgaard, *Appl. Spectrosc.*, 2002, **56**, 877-886.
44. F. Barboza and R. Poppi, *Anal. Bioanal. Chem.*, 2003, **377**, 695-701.
45. N. S. Sahni, T. Isaksson and T. Næs, *Appl. Spectrosc.*, 2005, **59**, 487-495.
46. M. Watari and Y. Ozaki, *Appl. Spectrosc.*, 2006, **60**, 529-538.
47. E.-L. Bergman, H. Brage, M. Josefson, O. Svensson and A. Sparén, *J. Pharmaceut. Biomed.*, 2006, **41**, 89-98.
48. G. G. Siano and H. C. Goicoechea, *Chemom. Intell. Lab. Syst.*, 2007, **88**, 204-212.
49. M. Sohn, F. E. Barton and D. S. Himmelsbach, *Appl. Spectrosc.*, 2007, **61**, 414-418.
50. Y. Sulub, R. LoBrutto, R. Vivilecchia and B. Wabuyele, *Vib. Spectrosc.*, 2008, **46**, 128-134.
51. Y. Sulub, R. LoBrutto, R. Vivilecchia and B. W. Wabuyele, *Anal. Chim. Acta*, 2008, **611**, 143-150.
52. C. F. Pereira, M. F. Pimentel, R. K. H. Galvao, F. A. Honorato, L. Stragevitch and M. N. Martins, *Anal. Chim. Acta*, 2008, **611**, 41-47.

53. W. Ni, S. D. Brown and R. Man, *Anal. Chim. Acta*, 2010, **661**, 133-142.
54. M. Boiret, L. Meunier and Y. M. Ginot, *J. Pharmaceut. Biomed.*, 2011, **54**, 510-516.
55. Y. Ge, C. L. S. Morgan, S. Grunwald, D. J. Brown and D. V. Sarkhot, *Geoderma*, 2011, **161**, 202-211.
56. Z.-P. Chen, J. Morris and E. Martin, *Anal. Chem.*, 2005, **77**, 1376-1384.
57. Z.-P. Chen and J. Morris, *Analyst*, 2008, **133**, 914-922.
58. W. Du, Z.-P. Chen, L.-J. Zhong, S.-X. Wang, R.-Q. Yu, A. Nordon, D. Littlejohn and M. Holden, *Anal. Chim. Acta*, 2011, **690**, 64-70.
59. Z.-P. Chen, L.-M. Li, R.-Q. Yu, D. Littlejohn, A. Nordon, J. Morris, A. S. Dann, P. A. Jeffkins, M. D. Richardson and S. L. Stimpson, *Analyst*, 2011, **136**, 98-106.
60. Z.-P. Chen, J. Morris, A. Borissova, S. Khan, T. Mahmud, R. Penchev and K. J. Roberts, *Chemom. Intell. Lab. Syst.*, 2009, **96**, 49-58.
61. E. Bouveresse, C. Casolino and C. de la Pezuela, *J. Pharmaceut. Biomed.*, 1998, **18**, 35-42.
62. B. Walczak, E. Bouveresse and D. L. Massart, *Chemom. Intell. Lab. Syst.*, 1997, **36**, 41-51.
63. Y. Xie and P. K. Hopke, *Anal. Chim. Acta*, 1999, **384**, 193-205.
64. T. Isaksson and T. Næs, *Appl. Spectrosc.*, 1988, **42**, 1273-1284.
65. T. B. Blank, S. T. Sum, S. D. Brown and S. L. Monfre, *Anal. Chem.*, 1996, **68**, 2987-2995.
66. F. Despagne, B. Walczak and D.-L. Massart, *Appl. Spectrosc.*, 1998, **52**, 732-745.
67. Q. Fei, M. Li, B. Wang, Y. Huan, G. Feng and Y. Ren, *Chemom. Intell. Lab. Syst.*, 2009, **97**, 127-131.
68. S. D. B. Hu-Wei Tan, *J. Chemom.*, 2001, **15**, 647-663.
69. J. Yoon, B. Lee and C. Han, *Chemom. Intell. Lab. Syst.*, 2002, **64**, 1-14.
70. Y. Liu and S. D. Brown, *Anal. Bioanal. Chem.*, 2004, **380**, 445-452.
71. W. I. Friesen, *Appl. Spectrosc.*, 1996, **50**, 1535-1540.
72. V. O. Santos, F. C. C. Oliveira, D. G. Lima, A. C. Petry, E. Garcia, P. A. Z. Suarez and J. C. Rubim, *Anal. Chim. Acta*, 2005, **547**, 188-196.
73. L. Duponchel, C. Ruckebusch, J. P. Huvenne and P. Legrand, *J. Mol. Struct.*, 1999, **480-481**, 551-556.
74. T. Chen, J. Morris and E. Martin, *Chemom. Intell. Lab. Syst.*, 2007, **87**, 59-67.
75. P. J. Brown, *Chemom. Intell. Lab. Syst.*, 2007, **87**, 68-69.
76. T. Chen, J. Morris and E. Martin, *Chemom. Intell. Lab. Syst.*, 2007, **87**, 69-71.
77. N. Sha, *Chemom. Intell. Lab. Syst.*, 2007, **87**, 67-68.
78. J. Sjöblom, O. Svensson, M. Josefson, H. Kullberg and S. Wold, *Chemom. Intell. Lab. Syst.*, 1998, **44**, 229-244.
79. N. A. Woody, R. N. Feudale, A. J. Myles and S. D. Brown, *Anal. Chem.*, 2004, **76**, 2595-2600.
80. W. Fan, Y. Z. Liang, D. L. Yuan and J. J. Wang, *Anal. Chim. Acta*, 2008, **623**, 22-29.
81. *Personal communication*, M. Holden, University of Strathclyde, Glasgow, 2008.

82. G. R. Flåten and A. D. Walmsley, *Analyst*, 2003, **128**, 935-943.
83. A. Owen, PhD thesis, University of Strathclyde., 2006.

## 6 Whisky analysis

### 6.1 Introduction

#### 6.1.1 Scotch whisky

Whisky is the name given to the distilled product from the fermentation of cereals that has been matured in oak casks. A whisky that is matured in Scotland is termed a Scotch whisky. However, for a whisky to be considered as a genuine Scotch whisky it must adhere to the guidelines set out in the Scotch Whisky Regulations 2009 (SWR).<sup>1</sup> The legislation covers the ingredients used: the water source (which must be in Scotland), the process of production, the distillation and the maturation processes. Scotch whisky must be distilled at a distillery in Scotland from water and malted barley (to which only whole grains of other cereals may be added). In this research, samples referred to as malt indicate the use of only malted barley in the production of whisky, whereas, samples referred to as grain indicate the use of malted barley, and other malted and un-malted cereals in the production of whisky.

The classifications of Scotch whisky defined in law and set out in the SWR are as follows:

- “Single Malt Scotch Whisky”: is a Scotch whisky that is distilled in batches at a single distillery from water and malted barley in pot stills. There cannot be addition of any other cereals.
- “Single Grain Scotch Whisky”: is a Scotch whisky that is distilled at a single distillery from water and malted barley. It can have the addition of other malted or un-malted cereals but does not comply with the definition of Single Malt Scotch Whisky or Blended Scotch Whisky.
- “Blended Malt Scotch Whisky”: is a blend of two or more Single Malt Scotch Whiskies, which have been distilled at more than one distillery.
- “Blended Grain Scotch Whisky”: is a blend of two or more Single Grain Scotch Whiskies, which have been distilled at more than one distillery.
- “Blended Scotch Whisky”: is a blend of one or more Single Malt Scotch Whiskies with one or more Single Grain Scotch Whiskies.

The only ingredient that can be added other than cereal/grain, yeast and water is a specified grade of plain spirited caramel colorant.

### **6.1.2 Manufacturing of Scotch whisky**

There are five main stages in the manufacture of Scotch whisky: malting (germination), mashing (extraction), fermentation, distillation and maturation.

#### Malting

The malting stage converts the plain barley grain into malted barley. The process involves the immersion of the barley grain in water and leaving for two to three days, a process called ‘steeping’. During this process the water will activate the growth mechanism of the barley. The barley is laid out to germinate on malting floors for seven to fourteen days and turned regularly to allow even germination and prevent a build-up of heat. The temperature of the germination must be controlled to avoid the barley killing itself. More modern techniques involve drum maltings, where the barley is slowly turned in large drums cooled by air. During the malting process the enzymes which are activated convert the starches in the barley grain into sugars.<sup>2,3</sup>

The malt is then transferred to kilns for drying; the temperature inside the kilns must be increased gradually and must not exceed 70°C to avoid the destruction of the malt enzymes. Traditionally in the Highlands and Islands most drying was over peat fires, however, over the years the majority of the peat was gradually replaced by alternatives, such as coal. Although, some small amounts of peat were still added at the start and end of the drying to create the recognisable smoky flavours in the whisky. Whiskies produced from malt dried in a peat kiln have a smokier flavour to whiskies produced from malt dried in coal kilns. In the Lowlands where coal production was common and peat was not available, coal kilns were used; this gave the whisky a lighter un-smoked flavour. After drying in the kiln, the malt is ready for the next stage in the manufacture of whisky.<sup>2-4</sup>

### Mashing

In the mashing stage, the malt is ground into coarse flour, known as malt grist, and mixed with hot water in different stages. The water and malt grist mixture, commonly known as mash, is transferred into a mash tun and stirred to allow the enzymes in the malt to release the starches still remaining in the malt into sugars. After the mashing process, the liquid, called the wort is released from the mash tun into a vessel called the underback. The process is repeated, adding hot water, stirring and draining the liquid several times. The solid mash of spent grain left at the end of this process is called draff; this by-product is sold on for cattle feed. The wort is cooled and used in the fermentation stage.<sup>2, 5</sup>

### Fermentation

The wort is transferred from the underback through a cooler, reducing the temperature from around 63 - 68°C to around 22 - 24°C. It is then transferred into the fermenting vessels, termed wash backs, where yeast can be added and the fermentation started. The yeast converts the sugars present in the wort to ethanol (alcohol) and small quantities of other components. These other components are known as congeners and they include a range of compounds including esters, aldehydes, acids, phenols, hydrocarbons and other high order alcohols. Whiskies can contain multiple congeners that are important as they add to their unique flavour and character. Acetaldehyde is produced from the oxidation of ethanol and makes up 90% of the total aldehyde content in whisky. The aldehydes can give a strong odour and contribute to the distinctive taste of a whisky, even in small quantities. The fermentation stage converts the sugars into an alcohol with approximately 8 – 10% v/v ethanol content. This low alcohol liquid is termed the wash and is used in the distillation stage of the manufacture of whisky.<sup>2, 6-9</sup>

### Distillation

Traditionally in pot-still distilleries a double batch distillation process is used, although there a couple of distilleries that practice triple distillation to ensure a lighter spirit with a higher natural strength. The triple distillation process is similar to the distillation processes used in Ireland and is generally found in lowland

distilleries, although it is less common than the double batch distillation approach. The wash from the fermentation is charged into the first pot still, termed wash still, to separate the alcohol from the water and waste in the wash. This still is heated and maintained just below the boiling point of water, allowing the alcohol and other compounds which are more volatile to pass over the still neck and condense in the condenser known as the worm. The distillate from the wash still which is termed low wines is collected in the low wines charger. After all the alcohol vapours are distilled through the wash stills the process is stopped and the waste and water are discharged. The low wines are then transferred into the low wines or spirit still where a further distillation process is completed in a similar manner to the wash still, however, at a more controlled level. The most volatile components which are distilled first are directed back to the low wines charger for further distillation. At the point where the distillate is at the desired strength and quality the distillate is collected, known as the centre cut. This new spirit which is normally around 60% v/v is directed to the spirit vessel. When the process is near completion the remaining volatile components are directed back to the low wines charger for further distillation with a new batch of low wines. The copper pot stills vary in both size and shape from one distillery to another and can have an impact on the characteristics of the whisky. The copper pot-still double batch distillation approach can be expensive, therefore, continuous distillation was developed by Stein and Coffey.<sup>10</sup> However, it was realised with development of continuous distillation that lower levels of flavour congeners were produced irrespective of the quality of malt that was used. Therefore, it was unnecessary to use expensive malt to produce the inevitable milder flavour produced from continuously distilled spirit, as a mash that has mostly un-malted cereal would provide an acceptable product. So grain whiskies and blended whiskies are mostly derived from continuous distillation.<sup>2, 10, 11</sup>

### Maturation

After the distillation process, the colourless whisky can be transferred to oak casks for maturation. The oak cask is acknowledged as one of the most important factors to influence the final quality of the whisky. In the time the whisky spends inside the cask, changes to the chemical composition occur, and the powerful aromas of the

distillate will convert into the mellow characteristics found in the whisky product. The colour also changes in this process, from the colourless distillate to a golden brown whisky. The casks used for maturation can either be new or have been previously used for Scotch whisky, Sherry or Bourbon maturation. The cask can vary in size, but cannot exceed 700 L in volume, in accordance with the SWR. Also, the maturation must proceed for a minimum of three years for a whisky to be classified as a Scotch whisky.<sup>2, 12</sup>

Heat treatment of the casks can have an important role for maturing the distillate. There are two methods of heating; first is toasting the wood, this is a milder form of heat treatment and is a prolonged process; the second is charring of the wood, this is a faster process which involves heating the inside of the cask until it catches fire and becomes carbonised, leaving a layer of carbon on the inner surface. There are two main goals from heat treatment;<sup>12</sup>

- The degradation of the polymers in the wood to produce flavour compounds which will be extracted into the product during maturation.
- The destruction of the unpleasant aroma compounds present in the wood to prevent these being transferred to the product.

During maturation, several reactions occur and generally fall into two classifications; additive and subtractive. Additive reactions will introduce or produce new aroma compounds in the product, whilst subtractive reactions will remove or modify components of the spirit. An important example of an additive action is the extraction of congeners from the cask, for example, the thermal degradation of wood polymers during the heat treatment process. Interactions between the wood and the components of the distillate can form new aroma compounds. Congener addition can occur through the reaction of ethanol with lignin in the wood to produce ethanol-lignin which can subsequently produce lignin degradation products. Lactones are volatile components that are extracted from oak, known as oak or whisky lactone and their concentration is thought to increase during the maturation process.<sup>8, 12-14</sup> Subtractive reactions usually include evaporation of low boiling compounds or the degradation of components by the carbonised surface of the wood.<sup>12</sup>

As briefly mentioned above, maturation can take place in casks which have been previously used for maturation. The repeated use of casks in this way will decrease the quantity of wood compounds affecting the maturation and hence will change the mature character of the whisky. If a cask becomes exhausted, e.g. no real benefit will come of maturing a whisky in the cask, and then it can be regenerated by removing the old carbon layer and completing the heat treatment process again. This process will not completely regenerate a cask but give higher levels of extractive compounds compared to casks of other sources.<sup>12</sup>

Other important variables that are involved in the maturation stages include; maturation time and fill strength. A longer maturation time can potentially allow a greater change in chemical composition and produce mature whisky products. The spirit strength can have an effect on the extraction and formation of flavour congeners in the cask. However, it is difficult to know exactly which reactions occur, when they occur, and for how long during the maturation. There are limitations for modelling the reactions in the laboratory due to the timescales involved.<sup>2, 12</sup>

The whisky product is ready after the maturation stage and can proceed to the bottling stage if the product is a Single Malt Scotch Whisky or a Single Grain Scotch Whisky; or a number of products can be blended together and then bottled to produce a Blended Malt Scotch Whisky, Blended Grain Scotch Whisky or a Blended Scotch Whisky. Due to some of the processes discussed so far, whisky batches can vary in colour, therefore, to provide consistency in colour, plain spirit caramel – E150a is legally allowed to be added to whisky product as set out in the SWR.

### **6.1.3 Counterfeiting of Scotch whisky**

Authentic Scotch whisky must follow the strict guidelines set out in the SWR. There are, however, places around the world where products are produced, bottled and sold as Scotch whisky with a disregard for these guidelines. These illegal products are termed counterfeits and can have detrimental effects to the reputation of Scotch whisky.

The Scotch whisky industry has annual exports in excess of £3 billion and is one of the UK's leading exporters.<sup>15</sup> Therefore, authenticating and being able to detect counterfeit whiskies is highly important for financial reasons and for the protection of brand reputation. Counterfeit whiskies can have a dramatic impact on the sales and profits of the Scotch whisky industry. It is estimated by the Scotch Whisky Association (SWA)<sup>16</sup> that over a two year period 150 million counterfeit bottles claiming to be Scotch whisky were sold worldwide. The estimated impact on sales was £100 million per annum and the lost profit was in the range £10-30 million.<sup>16</sup> These figures are speculative as the exact impact of counterfeiting is hard to estimate as many cases will go undetected.

There are different forms of counterfeiting Scotch whisky including brand imitation, where a cheaper product is sold as a higher quality whisky.<sup>17</sup> Another form of counterfeiting is generic imitation, where the whisky being sold as Scotch is produced outside Scotland and does not conform to the legal requirements in the SWR. Generic imitation can also include the adulteration of an authentic Scotch whisky by adding ethanol so that a cheaper whisky may be sold as a higher value product. In some instances, colorant is added to another alcoholic product which is sold illegally as a genuine Scotch whisky.

#### **6.1.4 Identification of counterfeit whisky**

Different techniques have been used by the Scotch whisky industry since the early 1900s for authentication and detection of counterfeit samples, ranging from bench reagent chemistry to the use of advanced analytical instrumentation.<sup>17-20</sup> In general, a whisky can be characterised by three properties: the ethanol content (a Scotch whisky must adhere to a minimum alcohol content of 40% v/v); the congener profile (the whisky contains a range of congeners formed during the fermentation and maturation processes); the colour consistency (whisky can only be altered with the use of plain spirited caramel of a specified grade).<sup>1</sup>

#### 6.1.4.1 Ethanol determination

Determination of ethanol content has the potential to provide a fast and efficient way to assess if a sample is within the specification for a particular product. A number of techniques can be employed for the determination of ethanol including density measurements, spectroscopic techniques and chromatographic techniques. Gas chromatography (GC) can provide information on both the ethanol content and higher alcohol profiles in whisky, differentiate between different alcoholic beverages, and distinguish between malt and grain whiskies based on differences in the congener profile.<sup>17</sup> However, GC analysis times can be more than 10 minutes. Density measurements are commonly used to determine the ethanol content of whisky and produce accurate results although the sample must be distilled before analysis.<sup>8, 21</sup> Spectroscopic techniques can be used to determine ethanol content through fast simple analysis methods. Procedures based on NIR spectrometry have been reported for determination of ethanol in alcoholic beverages;<sup>22-27</sup> ethanol fuels;<sup>27, 28</sup> and fermentation processes.<sup>29, 30</sup> Generally, multivariate calibration algorithms are required with NIR spectrometry, which adds to the complexity of method development. Liebmann *et al.*<sup>28</sup> used a transreflectance NIR probe to determine the ethanol concentration in bioethanol productions. To obtain optimal and robust calibration models, the use of genetic algorithms and large data sets were required. Mendes *et al.*<sup>27</sup> reported an NIR spectrometric method for the determination of ethanol in fuel ethanol and beverage samples. For the analysis of beverage samples the NIR results were better than those from GC. Gallignani *et al.* described a procedure for the determination of ethanol in alcoholic beverages by NIR spectrometry<sup>23</sup> and MIR spectrometry.<sup>31</sup> Off-line analysis by NIR spectrometry was successful in determining the ethanol content in beer, wine, whisky, gin and rum samples. In the MIR study, the ethanol content of beer, vodka, gin, rum and whisky samples was determined using a micro flow transmission cell. In both the NIR and MIR studies, 1<sup>st</sup> derivative spectra were analysed to avoid the effects of baseline drift. Other MIR spectrometry applications have been reported for determination of ethanol in bioprocess monitoring<sup>32</sup> and in a range of alcoholic beverages.<sup>31, 33-36</sup> Sivakesava *et al.*<sup>32</sup> described methods for monitoring a bioprocess using MIR and Raman spectrometries. In this study, an ATR accessory was attached to a FTIR

spectrometer to determine the concentration of ethanol without the need for any sample preparation. Raman spectrometry was used to observe the ethanol functional groups as the reaction progressed, however the quantitative results were not as accurate as those of MIR spectrometry. Nordon *et al.*<sup>37</sup> compared non-invasive NIR and Raman spectrometries for the determination of ethanol content in spirits, highlighting the potential advantages and limitations of both techniques. All of these procedures involve lab-based analysis, which is not ideal if a rapid indication of authenticity of a sample is required.

#### **6.1.4.2 Congener determination**

Some research has surrounded the maturation process of whisky production; a range of congeners are formed during the maturation process through leaching and extraction from the oak casks. The range and concentrations of the congeners can be unique to a brand of whisky. The major congeners can be readily determined by GC using a polar stationary phase and are useful in the differentiation of categories of spirits as well as between malt and grain whiskies.<sup>17</sup> Aylott *et al.*<sup>17</sup> produced a paper reviewing different analytical strategies detailing studies into capillary column GC for determination of volatile trace congeners and volatile phenols, if the sample was first chemically derivatised.

High performance liquid chromatography (HPLC) has also proved useful for the analysis of non-volatile cask-extracted congeners.<sup>38</sup> These congeners are a result of the degradation of oak lignin caused by toasting or charring prior to use or the hydrolysis by ethanol and water during maturation.<sup>13</sup>

#### **6.1.4.3 Colorant analysis**

Colour consistency of Scotch whisky is highly important and therefore is monitored throughout the production process. Most commonly measurements are taken at the blending and bottling stage and involve analysis by visible spectrometry. Mackenzie and Aylott<sup>19</sup> described a hand held instrument based on UV-visible spectrometry that can be used to confirm the authenticity of Scotch whisky samples on location, without the need to send specimens to a laboratory. Samples were analysed by

introducing the liquid into the flow cell of the handheld spectrometer and collecting the absorbance spectra. Reference data for genuine Scotch whiskies were uploaded to the device using its electronic interface; here the internal software was used to determine if the suspect sample was within the acceptable limits of the genuine brand. Establishing an acceptable range for a selection of authentic brands was difficult to achieve as these can vary from brand to brand. Therefore, acceptance limits have to be defined for each brand of whisky prior to use. If a sample was deemed as a suspect counterfeit it could be sent for further testing by GC for confirmation. The method has analysis times of less than 1 minute and allowed the rapid screening of suspect samples enabling only those samples which failed the acceptance criteria to be sent for confirmatory testing saving time and analysis costs. There is a growing need for methods like this that can provide simple and fast identification of counterfeit Scotch whisky samples.

There is also potential for analytical methods to detect counterfeits based on caramel composition. According to the SWR<sup>1</sup> only the addition of plain spirited caramel, E150a, is allowed. There are four grades of spirited caramel, E150a, E150b, E150c and E150d, their production is regulated by the European Union (E.U.) Directive 95/45.<sup>39</sup> The four grades of caramel are produced by “the controlled heat treatment of carbohydrates (commercially available food grade nutritive sweeteners which are the monomers glucose and fructose and/or polymers thereof, e.g. glucose syrups, sucrose, and/or invert syrups, and dextrose)”.<sup>39</sup> Although, additional reactants other than glucose and fructose can be used in the production of the caramels, these differ between each grade of caramel, see Table 6.1. If counterfeit samples were to contain other grades of caramel other than the legally allowed E150a, then distinguishing between different caramel colorants could provide a way to detect counterfeit samples.

**Table 6.1: Regulations for the preparation of different types of caramel, information taken from E.U. Directive 95/45.<sup>39</sup>**

Caramel grade and description	Regulations
E150a: Plain caramel	Ammonium compounds and sulfites prohibited
E150b: Caustic sulfite caramel	Caramel is prepared in the presence of sulfite compounds but ammonium compounds are prohibited.
E150c: Ammonia caramel	Caramel is prepared in the presence of ammonium compounds but sulfite compounds are prohibited.
E150d: Sulfite ammonia caramel	Caramel is prepared in the presence of ammonium and sulfite compounds.

#### **6.1.4.4 Miscellaneous methods of counterfeit identification**

Adam *et al.*<sup>40</sup> tested if copper and other metals in whisky could be used as an indicator of authenticity. The principle of this analysis was derived from the basis of whisky production; by law malt whiskies are required to be produced in copper stills, blended whiskies and other distilled spirits are not. Therefore, malt whisky samples should have a higher copper content. This method was successful at differentiation of malt whiskies from blended whiskies and other distilled spirits. However, it cannot confirm if a whisky was produced authentically in Scotland.

Harrison *et al.*<sup>4</sup> described a method for the differentiation of peats used in the preparation of malt for Scotch whisky production. In this study FTIR reflectance spectra were acquired but differences between the spectra collected were difficult to see. However, with the use of cluster analysis the peats were classified according to their geographical origin.

### 6.1.5 Basis of this study

Analysing and being able to detect counterfeit samples is very important to the Scotch whisky industry. The above review indicates different techniques and methods that have previously been used to detect counterfeits. ATR MIR spectrometry has been used in this study primarily to distinguish between authentic whisky samples and counterfeit whisky products. Whisky is a very complex matrix and therefore many different factors can be analysed to determine information about a given whisky sample. Therefore, a secondary objective is to investigate MIR spectrometry as a tool to understand how the manufacturing and maturation variables can influence the colour of whisky.

Picque *et al.*<sup>20</sup> detailed the analysis and discrimination of cognacs and other distilled drinks using MIR spectrometry. Direct analysis of the samples was achieved using an ATR cell with a zinc selenide crystal to determine ethanol content. Aliquots of the samples were also dried onto membranes and analysed by transmission MIR spectrometry. These methods showed potential for the discrimination of cognacs and other distilled drinks when used with multivariate data analysis.

A similar approach has been adopted in this study, where a combination of methods based on MIR spectrometry has been used to categorise whisky samples as either authentic or counterfeit products. The methodology described is an advance on the work of Picque *et al.* as it uses a combination of novel silver halide optical fibres and diamond ATR probes to determine the ethanol concentration in whisky samples and investigate the colorant added. The use of *in situ* measurements by MIR spectrometry allows development of simpler and faster methods of analysis than the procedures described by Picque *et al.* One of the primary aims of the study was to assess the feasibility of developing MIR spectrometric methods that could potentially be used outside the laboratory during field investigations of whisky counterfeiting. The methods used by Picque *et al.* relied on laboratory based equipment and procedures, and so, are less useful for such investigations.

Whiskies can be matured in new oak casks or more commonly in casks which have already been used for the maturation of Scotch whisky, sherry or bourbon. Depending on the type of cask used and the cask history, differences in whisky colour arise. Knowledge of how manufacturing and maturation variables influence whisky colour could provide a greater understanding of the maturation process. The ability to identify colour or differences between natural and artificial maturation could also be used in counterfeit detection. Therefore, an additional part of this study involved the initial investigation of a number of cask samples with differing maturation variables, using ATR MIR spectrometry.

## **6.2 Experimental**

### **6.2.1 Samples**

#### **6.2.1.1 Blend authenticity**

Seventeen authentic and counterfeit samples of one brand of blended whisky were analysed in a blind study using the methods outlined below. Multiple batches of four grades of caramel (five batches of caramel A, one batch of caramel B, four batches of caramel C and four batches of caramel D) were also analysed to aid determination of the colorant used in the whisky samples.

After conducting the blind trial, the company that supplied the whisky samples provided the ethanol content of each sample and an indication of the authenticity of the samples. The method that was used by the company to obtain the ethanol concentrations was based on NIR analysis. The instrument used was a Foss NIR spectrometer (model 5000) with a beverage module, which had a 3 mm pathlength. An average of 32 scans from 1100-2500 nm was used to obtain the spectrum from which the alcohol strength was derived. A multivariate PLS model was built using the region between 1550 and 1700 nm. The typical overall accuracy of the analysis was reported to be  $\pm 0.05\%$  (v/v) (based on one standard deviation).

#### **6.2.1.2 Cask investigation**

Thirty one cask samples with different maturation variables were analysed using the colorant determination method outlined below; a description of the samples and the changing factors are given in Table 6.2. Pure samples of different components that can be found in whisky were also analysed to aid determination of the spectra obtained from the cask samples, details are in Table 6.3. When counterfeiting whisky, attempts are sometimes made to extract components from wood to simulate features of whisky that occur by natural maturation. In this study, three solutions were used to extract components from toasted American wood prior to evaporating the solvent and dissolving the residue in 40% ethanol. These samples are referred to

as simulated maturation samples (Table 6.4). The spectra of dried residues of these samples were compared to those of the cask samples and counterfeit whisky samples.

**Table 6.2: List of cask whisky samples with details of the different factors.**

Cask whisky samples						
Sample No.	Distillery Number	Malt/Grain/Blend	Cask Type	Fill	Years	Peated
1	4	Grain	Bourbon	Refill	3	No
2	4	Grain	Sherry	Refill	8	No
3	4	Grain	Bourbon	Refill	12	No
4	4	Grain	Bourbon	Refill	7	No
5	4	Grain	Sherry	Refill	3	No
6	4	Grain	Bourbon	Refill	12	No
7	4	Grain	Bourbon	Refill	9	No
8	4	Grain	Sherry	Refill	11	No
9	6	Grain	Bourbon	First	8	No
10	1	Malt	Bourbon	First	12	Yes
11	1	Malt	Sherry	First	11	Yes
12	1	Malt	Bourbon	First	8	Yes
13	1	Malt	Sherry	First	7	Yes
14	2	Malt	Sherry	Refill	6	No
15	2	Malt	Sherry	First	7	No
16	2	Malt	Sherry	Refill	5	No
17	3	Malt	Bourbon	Refill	9	No
18	3	Malt	Bourbon	First	9	No
19	3	Malt	Sherry	Refill	7	No
20	3	Malt	Sherry	First	6	No
21	3	Malt	Bourbon	First	5	No
22	6	Grain	Sherry	Refill	11	No
23	6	Grain	Bourbon	First	11	No
24	6	Grain	Bourbon	First	4	No
25	4	Grain	Unspecified	Unspecified	3	No
26	1	Malt	Bourbon	Refill	4	Yes
27	1	Malt	Sherry	First	4	Yes
28	1	Malt	Bourbon	First	3	Yes
29	3	Malt	Sherry	First	3	No
30	NA*	Blend	-	-	-	No
31	5	Malt	Bourbon	Unspecified	4	No

\*Not available (NA)

**Table 6.3: List of eleven pure component samples commonly found in whisky and the concentrations analysed in this study.**

Pure component samples	
Sample name	Sample concentration* ( $\mu\text{g ml}^{-1}$ )
Coniferaldehyde	589.3
Ellagic acid	95.9
Gallic acid	606.6
Hydroxymethylfurfural (HMF)	609.7
Lactones	0.5
Scopoletin	599.5
Sinapaldehyde	600.7
Syringaldehyde	601.8
Syringic acid	599.2
Vanillic acid	601.6
Vanillin	601.8

\*Supplied concentrations; amounts in whisky are normally  $< 20 \mu\text{g ml}^{-1}$

**Table 6.4: Description of three simulated maturation samples.**

Simulated maturation samples		
Sample number	Wood type	Extraction solvent
1	Toasted American wood	Solvent extract ethyl acetate
2	Toasted American wood	Solvent extract ethanol
3	Toasted American wood	Solvent extract water

### 6.2.2 Mid-infrared spectrometry

MIR spectra were acquired with a resolution of  $16 \text{ cm}^{-1}$  in the  $400\text{--}4000 \text{ cm}^{-1}$  region using an ABB MB3000 FTIR spectrometer (Clairet Scientific, Northampton, UK) coupled with polycrystalline silver halide fibres to a hastelloy bodied ATR Fibre Photonics probe with a diamond cone (Fibre Photonics Ltd, Livingston, UK). Two probes were used to complete the work, the differences are outlined in Table 6.5; probe A was used for the blend authenticity work and probe B was used for the cask

investigation study. Spectra were acquired using Horizon MB™ FTIR software version 3.0.13.1 (ABB, Canada) and GRAMS (Graphic Relational Array Management System) /AI software version 7.00 (Galactic Industries Corporation, Salem, USA). The spectra were exported as text files from Horizon software and SPC files from GRAMS software then imported into Matlab data analysis software.

**Table 6.5: Details of Fibre Photonics ATR probes used.**

Probe	Outer diameter of probe shaft (mm)	Silver halide fibre length (m)*	Diamond crystal size (mm)
Probe A	12	1.5	3
Probe B	12	0.7	2.4

\*This is the length of the fibre when measured from diamond tip to sma connectors; the actual length of polycrystalline fibre within the probe and connected cable will be double, see chapter 4.

### 6.2.3 Methods of analysis

#### 6.2.3.1 Ethanol content determination

A specimen of each whisky sample was transferred to a glass vial into which the probe was inserted and sealed with sealing film before analysis; when not in use, the samples were sealed to prevent any evaporation of the volatile components in whisky. The probe was washed and cleaned with water and acetone and allowed to dry prior to each analysis. The spectra of the whisky samples or calibration solutions were acquired with an air background. Calibration solutions in the range 35-45% v/v ethanol were prepared by diluting an appropriate amount of ethanol (absolute puriss. p.a., Sigma-Aldrich®, UK) with distilled water. 15 scans were accumulated for each measurement (about 15 s) with three and six repeat measurements made for each calibration and sample solution, respectively. When the first derivative spectrum of a typical whisky sample was measured six times without removing the probe, the repeatability (%RSD) for intensity measurements at 1026 cm<sup>-1</sup> (ethanol peak) was 0.17%. When the probe was removed, cleaned and then reinserted six times, the measurement precision (%RSD) was only slightly increased to 0.21%.

### 6.2.3.2 Colorant determination

The probe was inverted, an air background spectrum obtained and a small aliquot (10  $\mu\text{L}$ ) of sample was injected onto the diamond crystal; a heat lamp was used to evaporate the droplet for 4 min and leave a thin film over the crystal for analysis. The probe was allowed to cool to ambient temperature and the procedure was repeated a further five times so that the dried residue from 60  $\mu\text{L}$  of sample was analysed. The cask samples analysed as part of this study ranged in colour intensity, therefore, samples with a weaker colour required the addition of 90 or 120  $\mu\text{L}$  of sample. For the analysis of the caramel samples, solutions were prepared in 40% v/v ethanol to give a colour similar to that of the whiskies. These solutions were injected onto the diamond crystal for analysis similar to the whisky samples. 51 scans were accumulated for each measurement (about 51 s). Normalised first derivative spectra were produced for analysis. When three replicate spectra were recorded for the deposit obtained from 60  $\mu\text{L}$  of a solution of batch 3 of caramel A, the average %RSD of the intensity at the eight most intense peaks in the range 1150-1700  $\text{cm}^{-1}$  was 1.0%. When spectra were obtained from three separate depositions of 60  $\mu\text{L}$  of this solution of caramel A, the %RSD was 4.5%. The results presented for analysis of dried deposits of the samples are based on the spectra obtained for three separate depositions. The results presented as part of the cask investigation are based on the spectra obtained for the six replicates of three separate depositions.

### 6.2.4 Data analysis

All data were imported into Matlab versions 7.5.0.342 (R2007b) and 7.11.0.584 (R2010b) (Mathworks Inc., Natick, MA, USA) and PLS\_Toolbox version 4.1 (Eigenvector Research Inc., WA, USA). MIR data were processed using a Savitsky-Golay first derivative filter, which employed a width of 7 data points and a second order polynomial. Spectra were analysed to identify regions in the data that would provide information about the samples and remove the regions that only contribute noise to the measurements.

#### **6.2.4.1 Blend authenticity**

The concentrations and spectra of the ethanol calibration solutions were used to produce univariate and multivariate PLS calibration models. The MIR spectra collected from the whisky samples were analysed using these models to predict the concentration of ethanol for comparison with values supplied at the end of the study. Univariate calibration models were produced from the ethanol signal at  $1026\text{ cm}^{-1}$  in the 1<sup>st</sup> derivative spectra, using Microsoft Excel (Microsoft, USA). PLS calibration models were constructed using different spectral regions; there was relatively little difference in the errors associated with each model. Therefore, all models discussed herein were constructed using the spectral region  $694\text{-}1782\text{ cm}^{-1}$ . Data were mean centred prior to analysis. The number of latent variables required (4) was determined from the model that produced the minimum value of the root mean square error of cross validation (RMSECV) obtained using leave-one-out cross validation.

To investigate the colorant in whisky samples, principal component analysis (PCA) was carried out on 155 variables in the  $625\text{-}1813\text{ cm}^{-1}$  region of the triplicate first derivative spectra of the dried residues obtained for the seventeen whisky samples and fourteen caramel samples (caramel A  $\times$  5 batches, caramel B  $\times$  1 batch, caramel C  $\times$  4 batches and caramel D  $\times$  4 batches). Data were normalised to the largest peak (in the range  $950\text{-}1050\text{ cm}^{-1}$ ) and mean centred before PCA was performed. The first two principal components described 74.7% of the variation in the data.

#### **6.2.4.2 Cask investigation**

To investigate the similarities and differences between the cask whisky samples, the colorant caramel A, simulated maturation samples and the counterfeit samples, principal component analysis was completed. Numerous PCA models were used to explore different relationships. PCA was carried out on 155 variables in the  $625\text{-}1813\text{ cm}^{-1}$  region of the first derivative spectra of the dried residues obtained for the samples. Data were normalised to the largest peak and mean centred before PCA was performed.

As part of this study, design of experiment (DoE) analysis was completed using Design-Expert (DX7) version 7.1.6 (Stat-Ease Inc., MN, USA) to determine which of the six variables (distillery number, malt/grain whisky, cask type, cask history, maturation age and the use of peat) have an impact on the spectra of the dried residue of the cask whisky samples. To complete this analysis DoE models were built to assess the variables and their levels of variance. A description of the six variables and their levels are given in Table 6.6. PCA scores of the MIR spectra of the twenty eight selected cask samples were used as the response for each sample.

**Table 6.6: Details of the variables and associated levels of variance for investigation in DoE analysis.**

Variables	Distillery number	Malt/grain whisky	Cask type	Cask history	Maturation age	Peat
Levels	1	Grain	Bourbon	First fill	3 - 5 years	Yes
	2	Malt	Sherry	Refill	6 - 9 years	No
	3				10 - 12 years	
	4					
	6					

## 6.3 Results

### 6.3.1 Blend authenticity

#### 6.3.1.1 Determination of ethanol concentration

A typical MIR absorbance spectrum of a whisky sample (sample 13) is given in Figure 6.1a. When the spectra of all the samples were compared small differences were identified in the regions 1150-1400  $\text{cm}^{-1}$  and 1500-1850  $\text{cm}^{-1}$ . Strong absorption signals at 630  $\text{cm}^{-1}$  and 1640  $\text{cm}^{-1}$  arise from the O-H bending modes. The stretching mode of C-O is evident at around 1000-1100  $\text{cm}^{-1}$ . The region 1950-2250  $\text{cm}^{-1}$  is obscured because of the diamond tip in the ATR probe and no differences between spectra could be seen in the region beyond 2250  $\text{cm}^{-1}$ . The first derivative spectrum of whisky sample 13 is shown in Figure 6.1b.

A linear response curve was obtained over the range 35-45% (v/v) ethanol when using univariate calibration ( $r^2 = 0.9966$ ;  $y = 0.0009x - 0.0010$ , where  $y$  is the first derivative of absorbance at 1026  $\text{cm}^{-1}$  and  $x$  is the ethanol concentration (% (v/v))). When the univariate model was used to analyse the whisky samples, the ethanol concentrations given in Table 6.7 were obtained. The ethanol concentrations obtained with the multivariate PLS calibration model are also given in Table 6.7. The regression coefficients for the multivariate calibration model are given in Figure 6.1c.

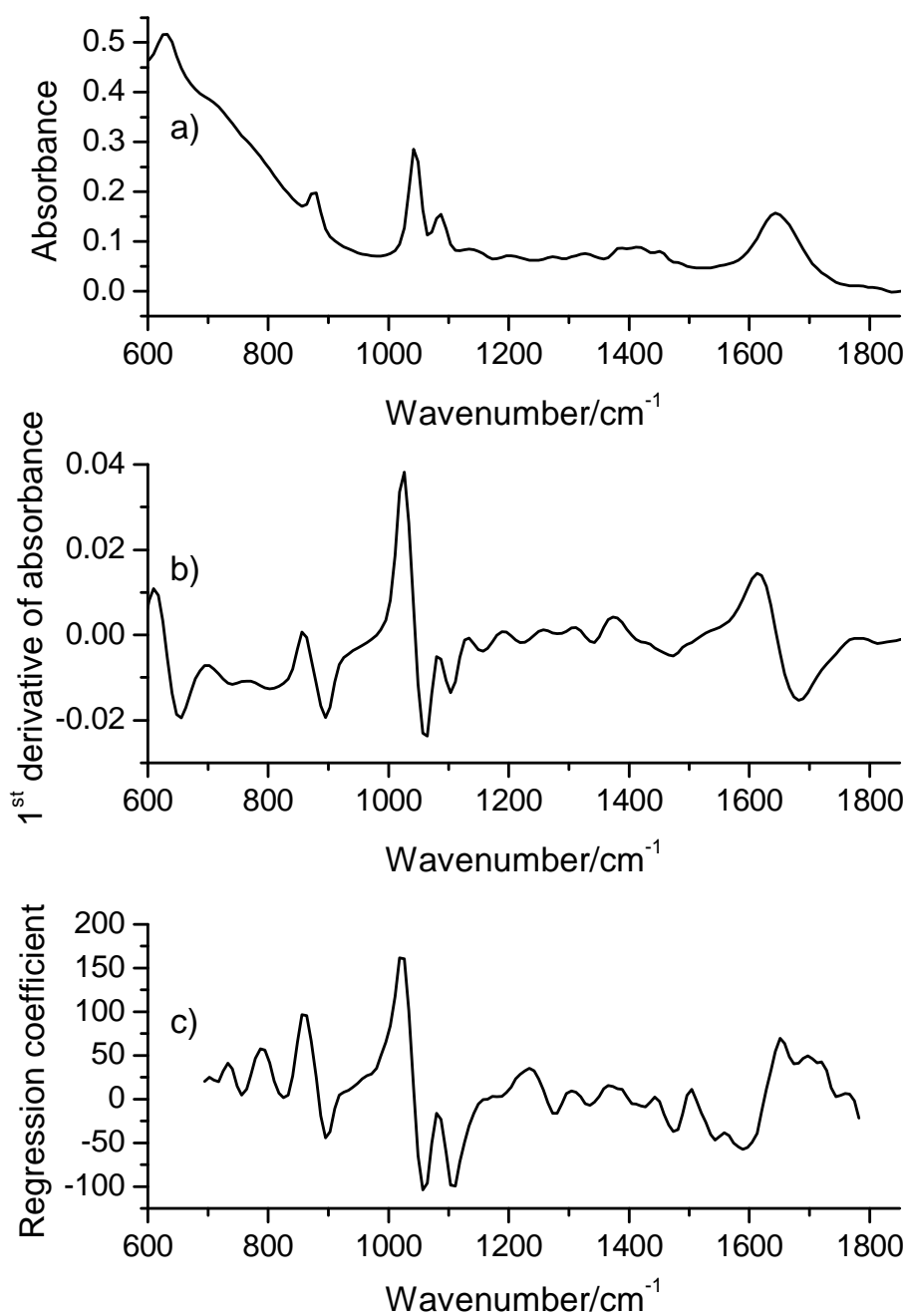


**Figure 6.1:** Typical MIR spectrum of a whisky sample (sample 13) in the region 600-1850 cm<sup>-1</sup>, (a) absorbance and (b) first derivative of absorbance, and (c) the regression coefficients for the multivariate PLS calibration model.

**Table 6.7: Mean concentrations of ethanol determined by *in situ* ATR MIR spectrometry using univariate and multivariate PLS calibration models compared with supplied concentrations.**

Whisky sample no.	Supplied concentrations <sup>b</sup>	<i>In situ</i> MIR spectrometry	
		Univariate (% (v/v)) <sup>a</sup>	PLS (% (v/v)) <sup>a</sup>
1	37.3	37.8 ± 0.22	37.8 ± 0.11
2	31.6	32.1 ± 0.11	31.8 ± 0.03
3	34.0	34.8 ± 0.20	34.6 ± 0.09
4	42.4	42.2 ± 0.15	42.2 ± 0.09
5	31.0	31.6 ± 0.08	31.5 ± 0.09
6	42.5	41.6 ± 0.07	42.5 ± 0.09
7	34.6	34.8 ± 0.09	34.8 ± 0.07
8	34.6	35.3 ± 0.13	35.1 ± 0.08
9	34.2	35.0 ± 0.09	34.9 ± 0.08
10	40.0	40.5 ± 0.08	40.5 ± 0.08
11	42.1	40.8 ± 0.09	41.9 ± 0.05
12	40.9	40.8 ± 0.13	40.9 ± 0.08
13	42.7	42.7 ± 0.15	42.8 ± 0.06
14	42.7	42.8 ± 0.12	42.7 ± 0.03
15	40.0	40.0 ± 0.11	39.9 ± 0.11
16	43.1	42.9 ± 0.17	43.2 ± 0.10
17	40.1	39.7 ± 0.22	39.8 ± 0.17

<sup>a</sup> Mean ± 99% confidence interval (n = 6).

<sup>b</sup> Provided after MIR analysis was completed; obtained by NIR analysis.

It was shown using a paired *t*-test<sup>41</sup> that there was no statistical difference (at the 99% confidence limit) between the supplied and predicted (univariate or multivariate PLS) ethanol concentrations. The relative error, defined as the difference between the predicted and supplied ethanol concentration expressed as a percentage of the supplied concentration, was calculated for each of the seventeen samples. It was possible to predict the concentration of ethanol in the whisky samples using

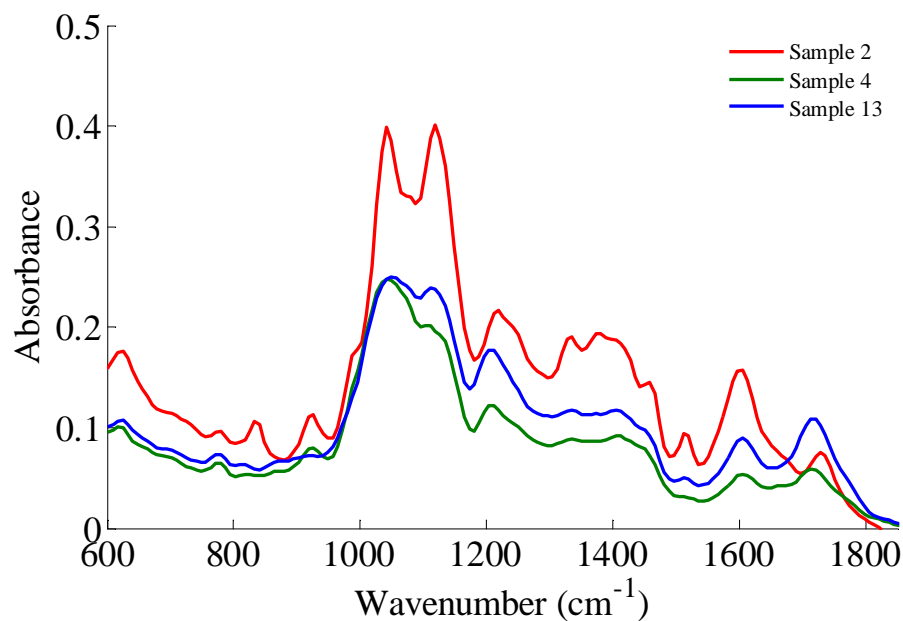
univariate and multivariate calibration with an average relative error of 1.2% and 0.8%, respectively.

The average relative errors obtained with either calibration method are lower than those reported by Tipparat *et al.*<sup>25</sup> for the determination of ethanol in liquor by flow injection NIR spectrometry (approx. 8%) and by Nordon *et al.*<sup>37</sup> for non-invasive analysis of whisky, vodka and sugary alcoholic drinks in bottles by NIR spectrometry (2.1%) and Raman spectrometry (2.9%). Further, the MIR method described gives comparable average errors to the methods of Gallignani *et al.*,<sup>23, 31, 33</sup> but does not require sample dilution.

Analysis of whisky samples by MIR spectrometry using an *in situ* ATR probe appears to offer some advantages over alternative techniques for rapid estimation of the concentration of ethanol, with an accuracy that would be suitable for initial authenticity screening. Statistical analysis of the predicted concentrations using *t*-tests (assuming equal variances)<sup>41</sup> suggested that the concentrations obtained using univariate and multivariate PLS models are the same for ten of the seventeen samples at the 99% confidence limit. Even though the results obtained for seven of the samples are statistically different, when the average relative error is used to compare the two regression methods for the entire dataset there is reasonable agreement between the two methods. Consequently, univariate calibration, which avoids the complexity and costs associated with multivariate calibration, is adequate for the purpose of initial authenticity screening.

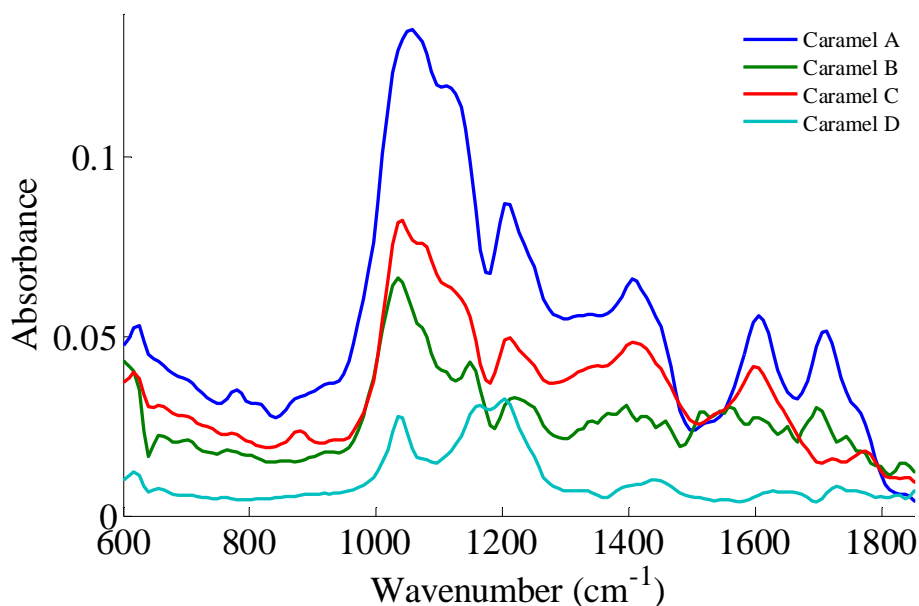
### **6.3.1.2 Analysis of dried residues**

As previously mentioned, only plain (spirit) caramel can legally be added to Scotch whisky; this colorant is covered by the E.U. Directive 95/45 and, therefore, it must adhere to purity criteria.<sup>39</sup> It is likely that the spectra of the dried residues of whisky will be dominated by the colorant, which arises from the cask and/or the addition of plain (spirit) caramel. The MIR absorbance spectra of dried residues for three of the whisky samples are given in Figure 6.2, which indicates differences between the samples.



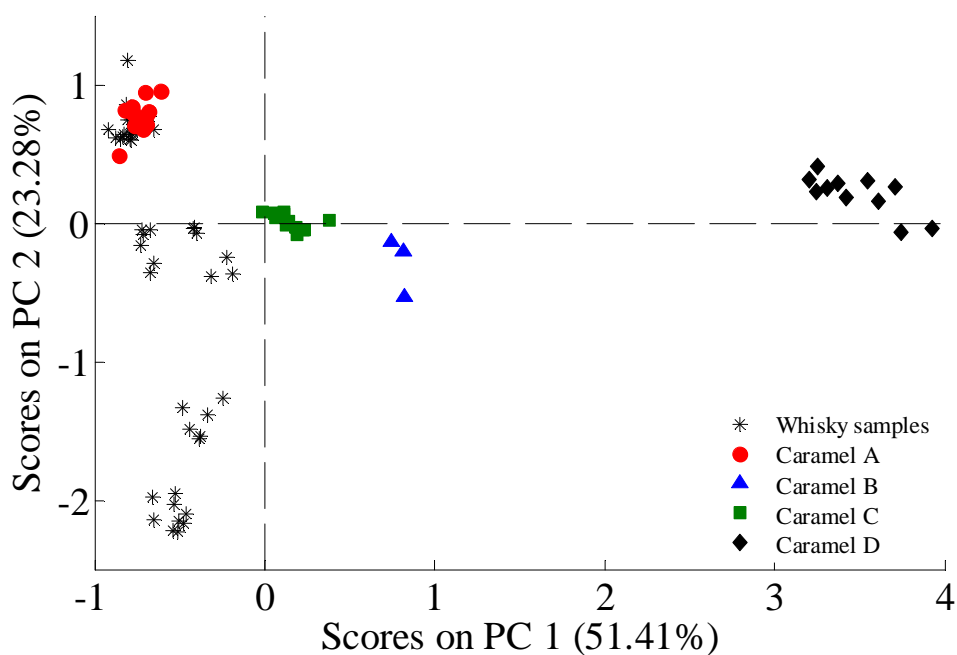
**Figure 6.2: ATR MIR absorbance spectra of the dried residues of three whisky samples detailed in Table 6.7.**

Dried residues of solutions of different caramel samples were also analysed to aid interpretation of the spectra obtained from the whiskies. The MIR spectra of four different types of caramel are given in Figure 6.3 and some similarities are apparent with the spectra shown in Figure 6.2.



**Figure 6.3: ATR MIR absorbance spectra of the dried residues of four caramel colorants.**

PCA was carried out on the 625-1813  $\text{cm}^{-1}$  region of the first derivative spectra of the dried residues obtained for the seventeen whisky samples and fourteen caramel samples (caramel A  $\times$  5 batches, caramel B  $\times$  1 batch, caramel C  $\times$  4 batches and caramel D  $\times$  4 batches). The scores plot for principal component 1 (PC1) and principal component 2 (PC2) in Figure 6.4 indicates that the within-batch and between-batch variability was much less than the spectral differences between the caramels.



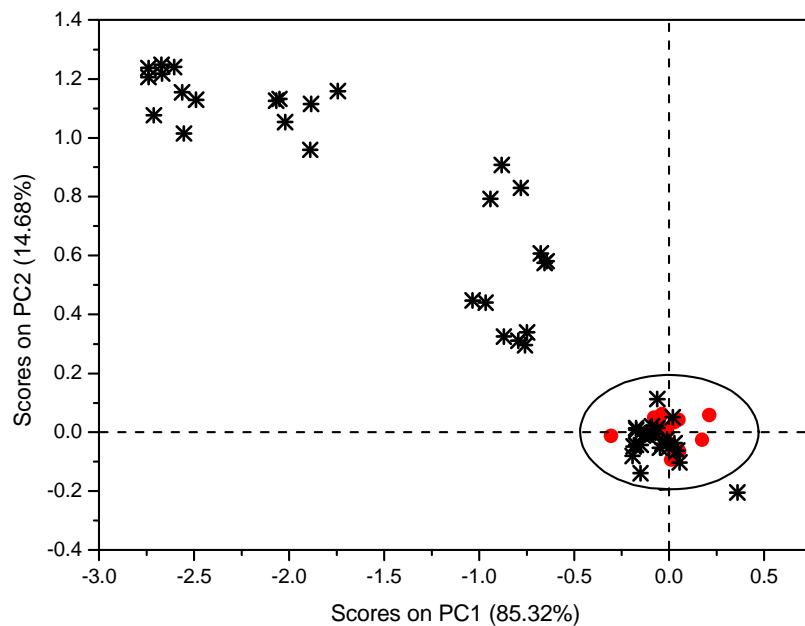
**Figure 6.4: PC1 vs. PC2 scores plot from PCA of triplicate MIR spectra of seventeen whisky samples and fourteen caramel colorants.**

Figure 6.4 indicates that there is a clear differentiation between the four types of caramel along the PC1 axis. Also, there is a distinguishing split in the whisky samples along the PC2 axis. A cluster of points for replicate measurements of some whisky samples occupy the same space as those of caramel A; there are also points for a number of whisky samples that are located well away from all the caramels in the scores plot, suggesting that other colorants may have been added to these samples.

### 6.3.1.3 Identification of counterfeit whisky

The derived ethanol concentrations were compared with the legal minimum ethanol content of whisky of 40% (v/v). Through use of a one sided  $t$ -test<sup>41</sup> at the 99% confidence limit, it was shown that seven samples had ethanol concentrations below the legal minimum of 40% (v/v) and so were potentially counterfeit (samples 1-3, 5, 7-9 and 18). Samples 4, 6 and 10-16 had ethanol concentrations above the legal minimum and so could be authentic whisky. Sample 17 just failed the  $t$ -test, but if the average relative error (1.2%) of the univariate MIR method is taken into account, this sample could have an ethanol concentration above the legal minimum and so was tentatively assigned as authentic. Further analysis of this sample is required to confirm the accuracy of this assignment. However, as shown below, the ethanol concentration alone is not a sufficient indicator of authenticity.

Caramel A is the plain (spirit) caramel that is legally allowed to be used in the production of Scotch whisky. With respect to Figure 6.4, the following procedure,<sup>42</sup> completed by Dr. Alison Nordon, was used to assess which whisky samples were in the PC1 vs. PC2 scores space for caramel A. The first two principal components of the PCA model in Figure 6.4 were retained. The dataset, comprising the PC1 and PC2 scores for the caramel and whisky samples, were then split into calibration (caramel A) and test (whisky) sets; the data for caramels B, C and D were discarded. A second PCA model was then built on the PC1 and PC2 scores values (after mean centring) for caramel A and two PCs were retained. To classify the whisky samples on the basis of their caramel content, the PC1 and PC2 score values for the whisky samples (calculated in the first PCA model) were projected into the subspace defined by the caramel A model. The 99% confidence limits for the caramel A model were calculated and any whisky samples that were out with these limits were assigned as counterfeit (see Figure 6.5).



**Figure 6.5: Projection of the PC1 and PC2 scores values, from Figure 6.4, for the whisky samples into the PC1 vs. PC2 subspace defined by the caramel A model. The model was constructed from PCA of the PC1 and PC2 scores, from Figure 6.4, for caramel A and the ellipse indicates the 99% confidence limits for the caramel A model.**

On the basis of this assessment, samples 7 and 11-17 were considered authentic while samples 1-6 and 8-10 are likely to be counterfeit. It can be seen from Figure 6.5 that the PC1 and/or PC2 score can be used to classify whisky samples as authentic or counterfeit based on caramel A content.

Although each MIR method indicates potential counterfeit samples, examining the combined set of results can elucidate more reliable information. A plot of the PC1 scores from Figure 6.5 vs. the predicted ethanol concentration from the univariate model is given in Figure 6.6 and shows clearly those samples which have been identified as authentic based on both their ethanol concentration and caramel colorant.

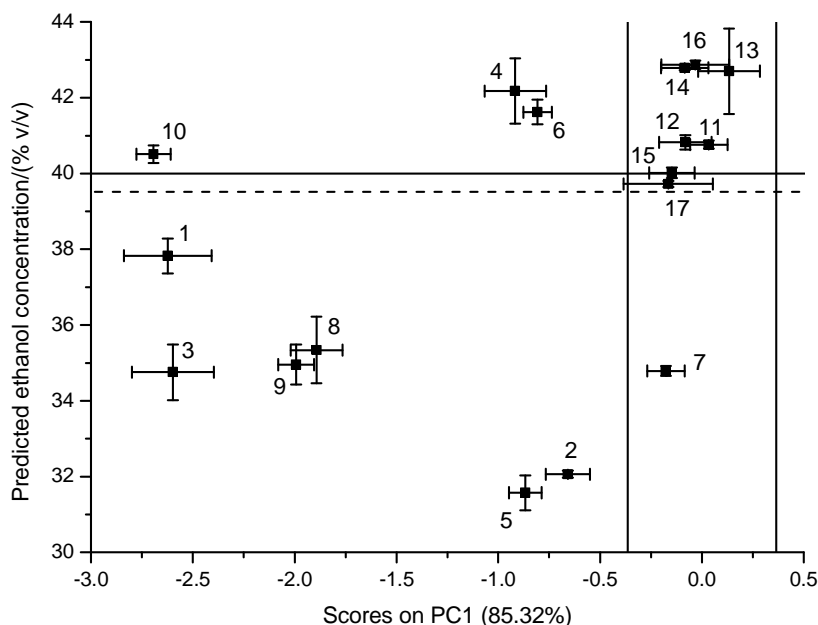


**Figure 6.6: PC1 scores, from Figure 6.5, vs. predicted ethanol concentration (%(v/v)) using the univariate model for samples 1-17. Error bars represent the mean value  $\pm$ 99% confidence interval ( $n = 6$  for predicted ethanol concentration and  $n = 3$  for PC1 scores) for each variable. The solid horizontal line indicates the minimum allowed concentration of ethanol in Scotch whisky; the dashed horizontal line indicates the lowest predicted ethanol concentration that could still be acceptable given the average relative error (1.2%) of the univariate method. The solid vertical lines are the 99% confidence limits of the PC1 score values for the caramel A model shown in Figure 6.5.**

Samples in the upper right quadrant of Figure 6.6 can be identified as authentic (samples 11-16). The upper left quadrant indicates samples that have an allowable ethanol concentration but not the legally permitted caramel colorant (samples 4, 6 and 10); if only the ethanol concentration was determined these samples would be mistakenly identified as authentic. The lower right quadrant indicates samples that have the permitted colorant, but not an allowable ethanol concentration (sample 7), which would be consistent with a counterfeit produced by diluting an authentic product. Sample 17 is also located in this quadrant, but as discussed earlier, given the average relative error (1.2%) of the univariate MIR method this sample may have an ethanol concentration above the legal minimum and so was tentatively assigned as authentic. The lower left quadrant indicates samples that have neither an allowed

ethanol concentration nor permitted colorant. So, in the blind study using the combined methods, samples 1 – 10 were identified as counterfeit whisky and samples 11 – 17 as authentic whisky. These conclusions were confirmed by the whisky company that supplied the samples. In their analysis, using a combination of spectroscopic and chromatographic techniques, it was established that the counterfeit samples were either locally produced spirit, genuine product with either added ethanol or water, or a mixture of a whisky type product and ethanol.

### 6.3.2 Cask analysis investigation

The work carried out for the blend authentication shows that the dried residues of the whisky samples are dominated by the colorant present. The whisky samples were shown to have spectra similar to that produced from caramel A colorant. However, caramel A is not always added, therefore, it is also important to understand the features in the cask samples where no additive colorant has been used. The MIR absorbance spectra of dried residues for four bourbon-cask samples and three sherry-cask samples are given in Figure 6.7 and Figure 6.8, respectively, which indicates the differences between the cask samples.

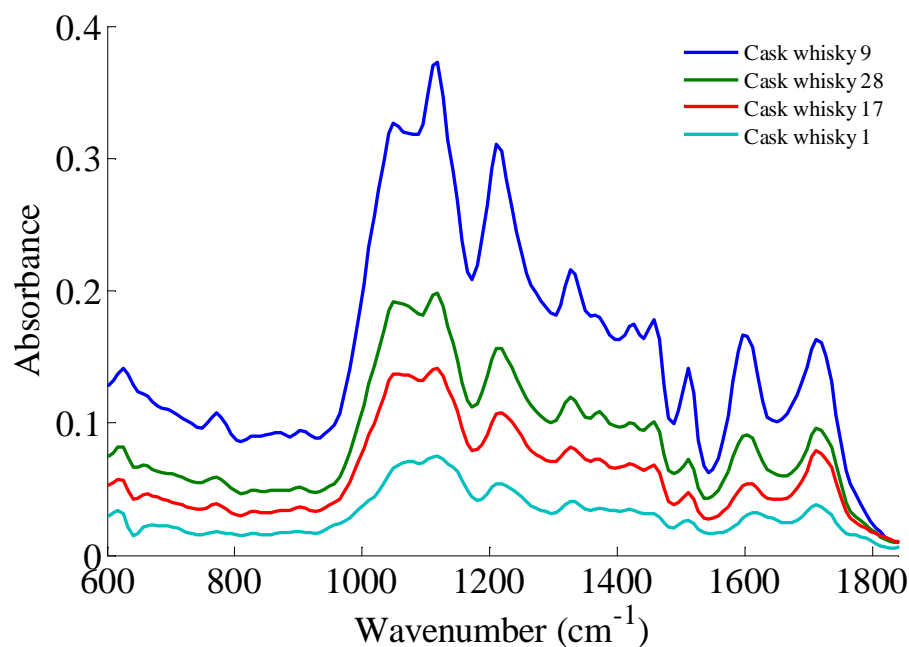
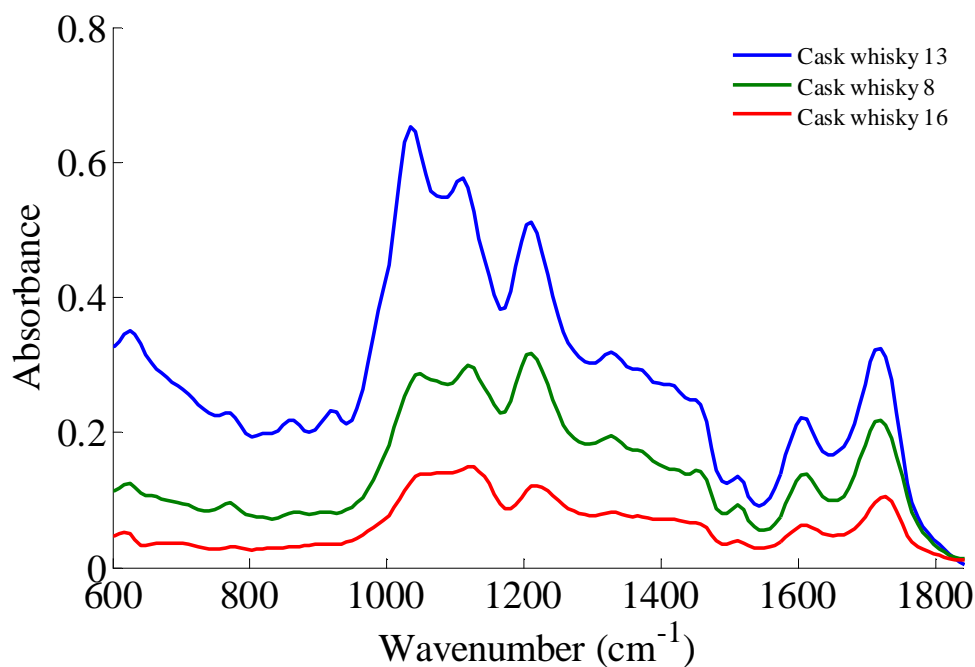
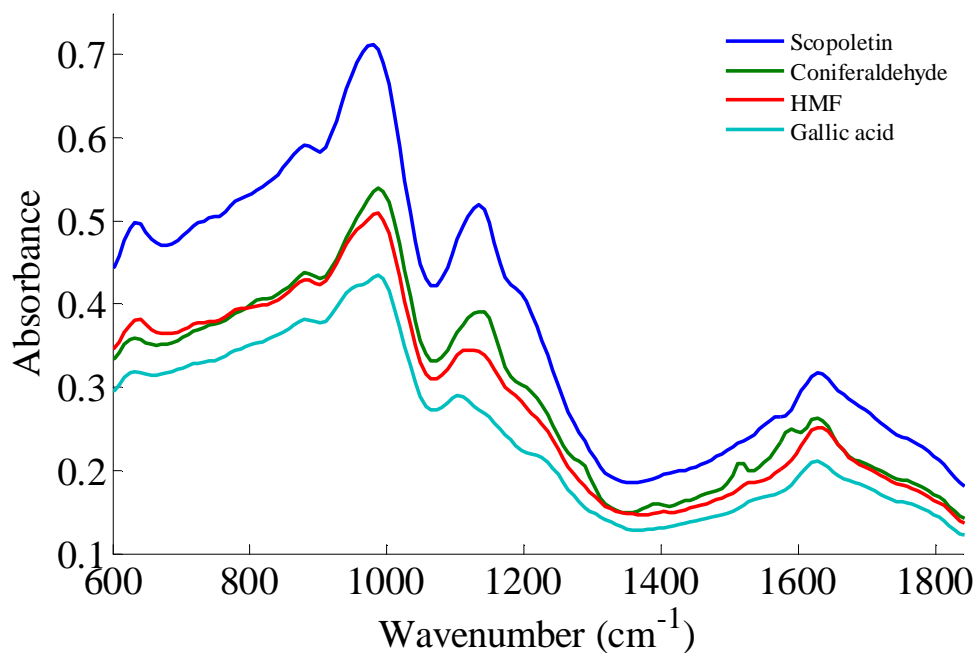


Figure 6.7: The average (n=18) ATR MIR absorbance spectra of the dried residues of four bourbon-cask whisky samples.



**Figure 6.8:** The average (n=18) ATR MIR absorbance spectra of the dried residues of three sherry-cask whisky samples.

As congeners are formed during the fermentation stage of whisky production, it is possible some of these compounds may be seen in the ATR MIR spectra. Dried residues of solutions of eleven pure component congeners that are commonly found in authentic whisky were also analysed to aid the interpretation of the spectra obtained from the cask whisky samples. Due to the high concentration of nine of the samples (around  $600 \mu\text{g ml}^{-1}$ ), only  $10 \mu\text{L}$  of each sample was analysed, the remaining two samples had low concentrations ( $95.9 \mu\text{g ml}^{-1}$  for ellagic acid and  $0.5 \mu\text{g ml}^{-1}$  for lactones) and so  $120 \mu\text{L}$  of each sample was analysed. The MIR spectra of the eleven samples are given in Figure 6.9, Figure 6.10 and Figure 6.11, respectively.



**Figure 6.9:** The average (n=18) ATR MIR absorbance spectra of the dried residues of four pure component samples.

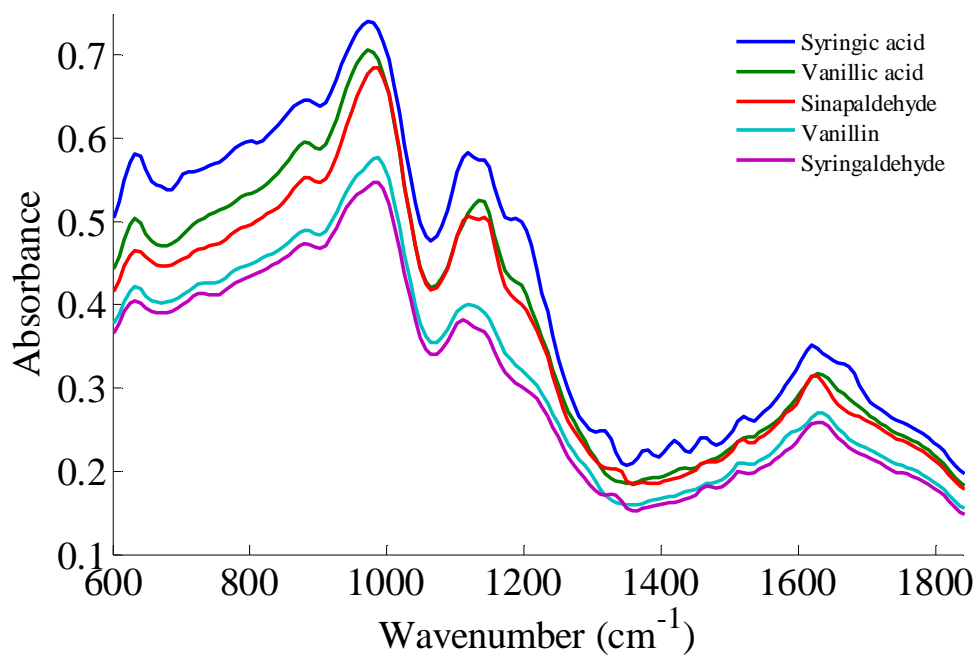


**Figure 6.10:** The average (n=18) ATR MIR absorbance spectra of the dried residues of five pure component samples.

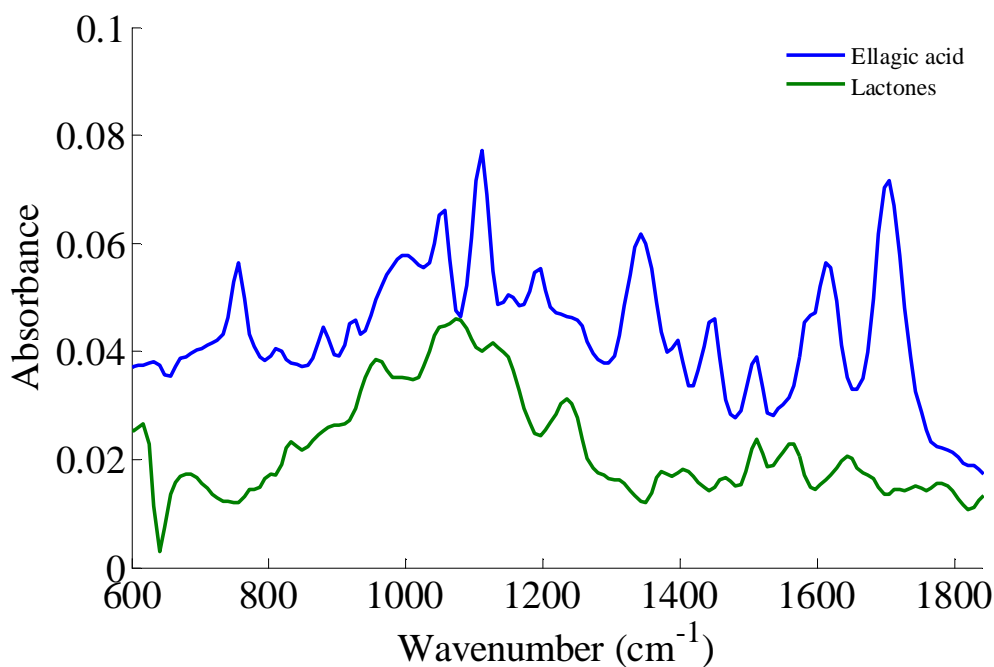


**Figure 6.11: The average (n=18) ATR MIR absorbance spectra of the dried residues of two pure component samples.**

Figure 6.9 and Figure 6.10 show only small variations in the spectra between the nine concentrated pure components. The greatest difference can be observed between ellagic acid and the lactones sample (Figure 6.11); however obtaining reproducible results for these two samples proved difficult due to the low concentrations. Each of the individual components analysed here will vary depending on the cask used, the heat treatment carried out and how many times the cask has been used before. Typically the concentrations will range from 0-10  $\mu\text{g ml}^{-1}$  for most of the components; however, some components such as ellagic acid and syringaldehyde may occur in higher amounts, e.g. up to 20  $\mu\text{g ml}^{-1}$ . Given the relative difficulty in analysing and detecting a 95.5  $\mu\text{g ml}^{-1}$  sample of ellagic acid, it is only reasonable to assume that these components are going to be very difficult to analyse by ATR MIR spectrometry. Therefore, it is believed in the analysis of the cask whisky samples the spectra will be dominated by the colorant which arises from the cask during manufacture and information regarding the components in Table 6.3 will have no or little effect on the spectra.

As part of this initial study, discussions with the Scottish Whisky Research Institute were held to determine what the desired outcomes would be. A list of questions regarding how ATR MIR spectrometry could aid in gaining a greater understanding of cask whisky samples was posed. This section will look into the feasibility of ATR MIR spectrometry for cask analysis and if it can be used to answer any of the following questions:

Q1 Can ATR MIR spectrometry determine differences in whisky manufacture variables? such as:

- cask type, e.g. bourbon and sherry
- cask history, e.g. first fill casks and refilled casks
- maturation age
- malt and grain whisky
- the use of peat

Q2 Is ATR MIR spectrometry able to differentiate between authentic maturation spectra and simulated maturation spectra?

Q3 Analysing some of the known counterfeits from the blend authenticity study, do their spectra relate to either of the authentic maturation or simulated maturation spectra?

Q4 Is there a difference between the spectra of dried residues of natural maturation samples and caramel colorant A?

Q5 If colorant was added to a cask sample, does it mask all of the spectral information of the spectra of the dried residue of natural maturation?

#### 1. Determination of whisky manufacture variables

To establish if ATR MIR spectrometry can be used to distinguish between different manufacturing variables, PCA was carried out on the  $625\text{-}1813\text{ cm}^{-1}$  region of the first derivative spectra of the dried residues obtained for the cask whisky samples. As three of the thirty one cask samples have missing information regarding the manufacturing variables, they have been discounted from this part of the study and only twenty eight of the cask whisky samples have been assessed. The MIR absorbance spectra for the three depositions of each cask sample were analysed in a

random order on different days to minimise any occurrence of systematic errors. Figure 6.12 displays the PCA scores plot of PC1 vs. PC2 that describes 64% of the variance; the cask samples have been classified according to their cask type, bourbon or sherry. With the exception of two sherry-cask samples (numbers 5 and 22) and a single deposition of a bourbon-cask sample 17 (classed as an outlier as the points for the other two depositions of sample 17 appear in the same space as the other bourbon-cask samples) there appears to be a divide along the PC1 axis between the bourbon-cask and sherry-cask samples (depicted with the ovals in Figure 6.12), which suggests that there is the potential to differentiate whisky samples by their cask type. To try and ascertain why the sherry-cask samples 5 and 22 were located in the same scores space as the bourbon-cask whiskies, all of the factors of these samples were compared with samples located in similar space in the scores plot to determine if there were any similarities. Sherry-cask sample 5 lay close in scores space to bourbon-cask sample 1, when compared all the factors were the same with the exception of the cask type. The spectra of sample 5 had more similarity to sample 1 than other grain sherry-cask samples. Sherry-cask sample 22 was harder to compare as it lay close to many of the bourbon-cask samples in the PCA scores space; as there seems to be a divide in the three depositions of this sample, those samples that lay closest to the two depositions that were most similar were compared to determine if any similarities could be found. Two bourbon-cask samples that lay close in scores space to sherry-cask samples 22 are bourbon-cask whisky samples 6 and 23, they are all grain whisky samples that are non-peated and have similar maturation ages as cask whisky sample 22; cask whisky sample 23 also has the same distillery in common. The loadings plot for PC1 (not shown), indicates that this principal component describes variation in the ranges  $1000 - 1300 \text{ cm}^{-1}$  and  $1600 - 1800 \text{ cm}^{-1}$ , where differences could be observed between bourbon- and sherry-cask samples in Figure 6.7 and Figure 6.8, respectively. However, the PCA scores plot suggests that the divide in the cask samples in PC1 is not solely attributable to a difference in cask type. Further investigations and a larger sample set including multiple batches of the same type of samples would be required to determine the variance described by PC1.

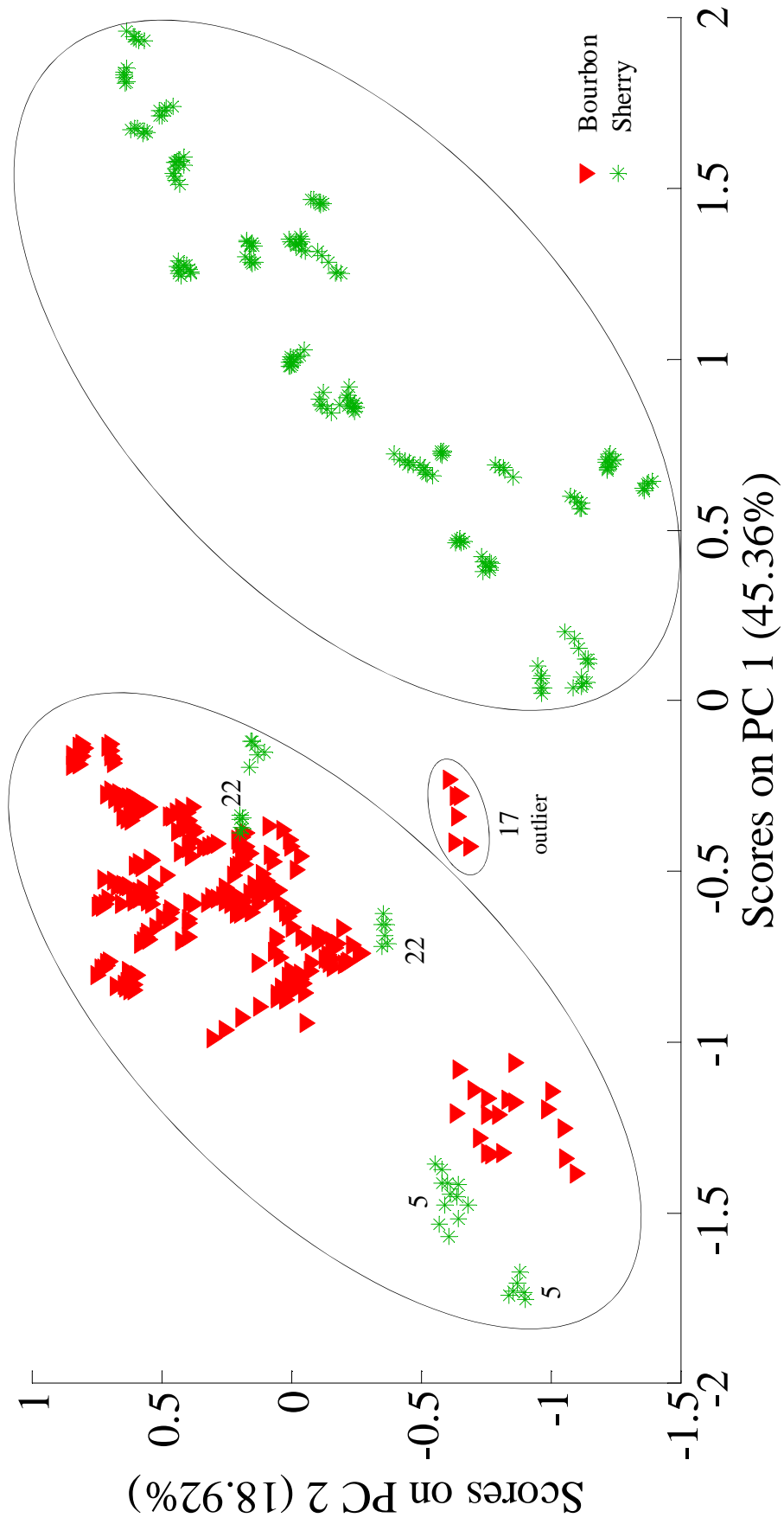


Figure 6.12: PC1 vs. PC2 scores plot from PCA of MIR spectra of twenty eight cask whisky samples.

As there was a defined divide between the bourbon-cask and sherry-cask samples when PCA was completed (with the exception of the two samples mentioned) new PCA models were built including the sherry-cask samples (thirteen samples) in one model and the bourbon-cask samples (fifteen samples) in the other model before further classification was carried out. This was to allow the major variation that was found in the first PCA model to be removed, allowing further potential determinations to be made.

The MIR absorbance spectra of the dried residues for two bourbon-cask whiskies are given in Figure 6.13 (same distillery, age, etc. with only difference in first fill or refill). It is apparent from the spectra of the first fill and refill whisky samples presented in Figure 6.13 that there are no differences in the spectra. Figure 6.14 displays the PCA scores plots of PC1 vs. PC2 that describe the variance in all the bourbon-cask samples (differences in distillery, age etc. are present between the bourbon-cask samples). The samples have been classified with respect to their cask history; if the cask was used for whisky manufacture for the first time, it has been classed as first fill, however, if it has been used for manufacture of whisky previously, it is termed refill. With the exception of sample 1 and one deposition of sample 17, the points representing the cask samples that are first fill appear in similar scores space as those points representing refill cask samples, emphasising that there is little difference in the spectra between a first fill cask whisky and a refill cask whisky. The PCA scores plot in Figure 6.14 has one deposition of sample 17 in a separate scores space to the other depositions similar to the PCA scores for all of the cask samples, suggesting that this deposition is an outlier and that this sample should be repeated again in any future studies to be sure that the spectra for this sample are representative. In addition, sample 1 has again been located in a scores space away from the other bourbon-cask samples as in the previous PCA scores plot (Figure 6.12), suggesting there is something different about this sample. Reviewing the information given about the manufacturing factors there is nothing to suggest a reason for this sample being located in different scores space.

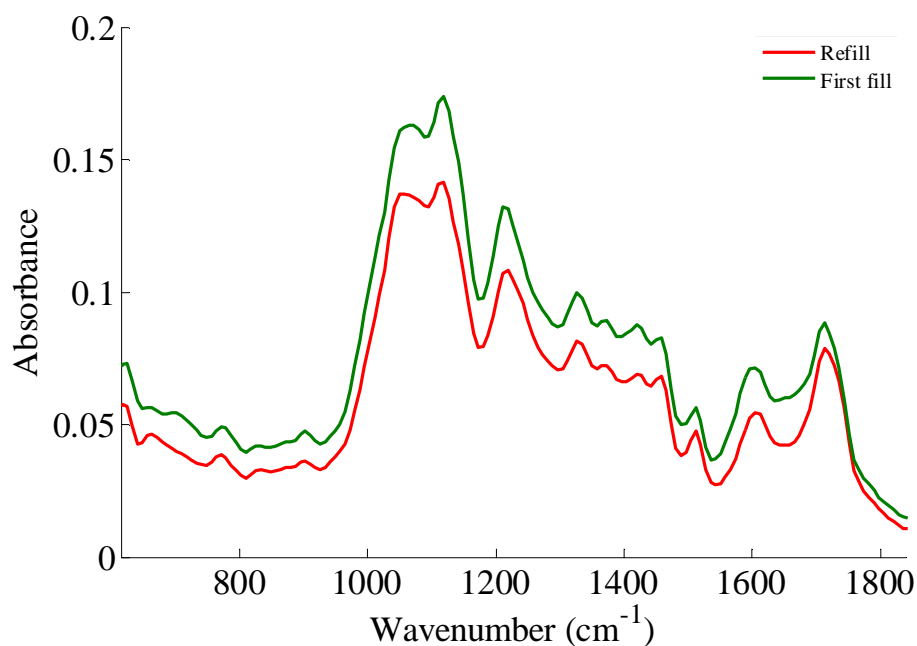


Figure 6.13: The average (n=18) ATR MIR absorbance spectra of the dried residues of a refill bourbon-cask whisky sample (number 17) and a first fill bourbon-cask whisky sample (number 18).

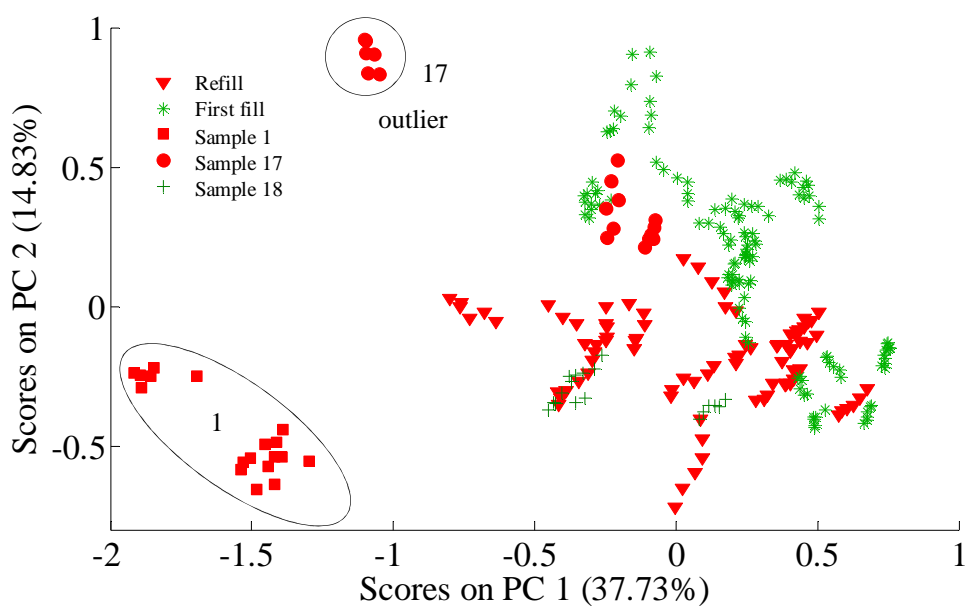


Figure 6.14: PC1 vs. PC2 scores plot from PCA of MIR spectra of fifteen bourbon-cask whisky samples, classified by cask history (first fill or refill).

The MIR absorbance spectra of the dried residues for two sherry-cask whiskies of similar origin are given in Figure 6.15. The spectrum of the first fill sherry-cask

whisky is similar to that of the refill sherry-cask whisky, with the exception of the region 1000 – 1150  $\text{cm}^{-1}$  where some small differences can be observed.

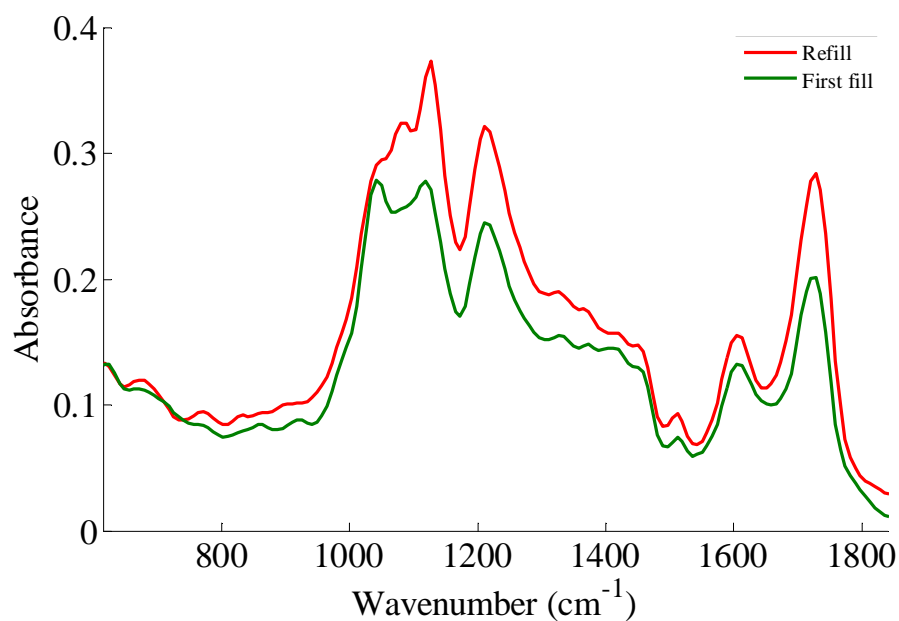


Figure 6.15: The average (n=18) ATR MIR absorbance spectra of the dried residues of a refill sherry-cask whisky sample (number 19) and a first fill sherry-cask whisky sample (number 20).

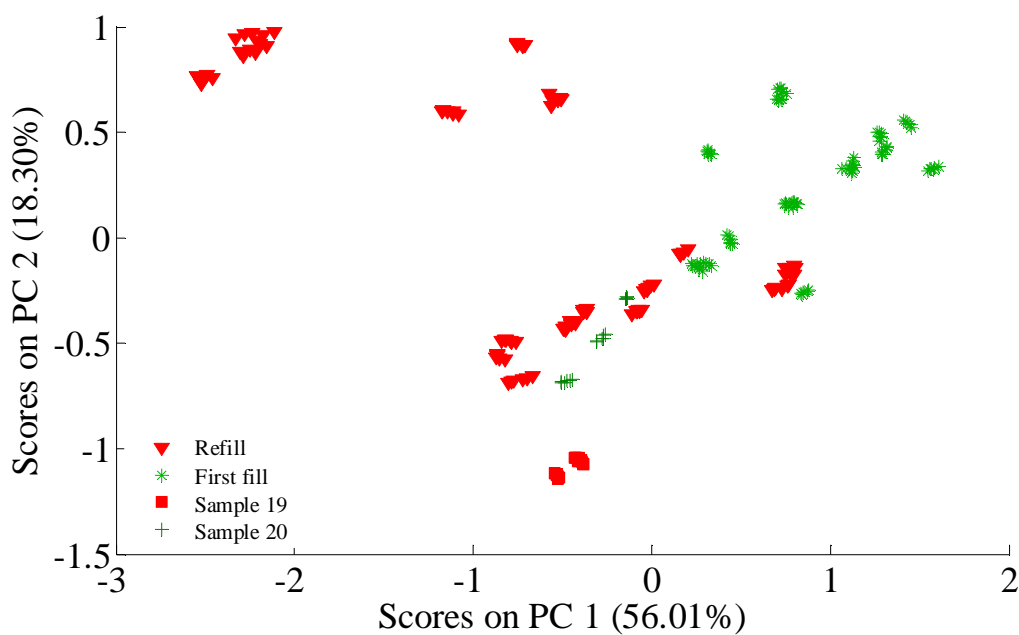


Figure 6.16: PC1 vs. PC2 scores plot from PCA of MIR spectra of thirteen sherry-cask whisky samples.

Figure 6.16 displays the PCA scores plots of PC1 vs. PC2 that describe the variance in the thirteen sherry-cask whisky samples. The cask samples have been classified as first fill or refill. Some of the points for the first fill and refill whiskies overlap, but others are in different scores space: the upper left quadrant in Figure 6.16 is populated by refill points and the upper right quadrant by first fill points.

From the results it appears that there are minimal differences in the spectra of bourbon-cask samples if they have been matured in first fill or refilled casks, however, there is the possibility that there are some differences between the spectra of sherry-cask samples. Although, the differences observed in the PCA scores plot (Figure 6.16) are likely to be a result of more than one maturation variable.

Another variable that was investigated to determine if it could impact on the spectra of dried residues of cask samples was the use of malt or grain in the manufacture of the whisky. The spectra of two similarly manufactured cask whisky samples, where there is a difference in the use of malt or grain, are given in Figure 6.17; the spectra are almost identical. Figure 6.18 displays the PCA scores plots of PC1 vs. PC2 of the bourbon-cask samples; here the samples have been classified based on the use of malt or grain. The PCA results reinforce the observations in Figure 6.17 as there is little distinction between grain and malt cask whisky samples. Equivalent information for sherry-cask samples are given in Figure 6.19 and Figure 6.20. In this case, there is greater separation of the malt and grain points in the PCA scores plot, although the points for grain samples 2 and 8 overlap the space occupied by the malt samples. Comparing the information known about the samples no similarities could be found that link grain samples 2 and 8 with the malt samples which they are close to in scores space.

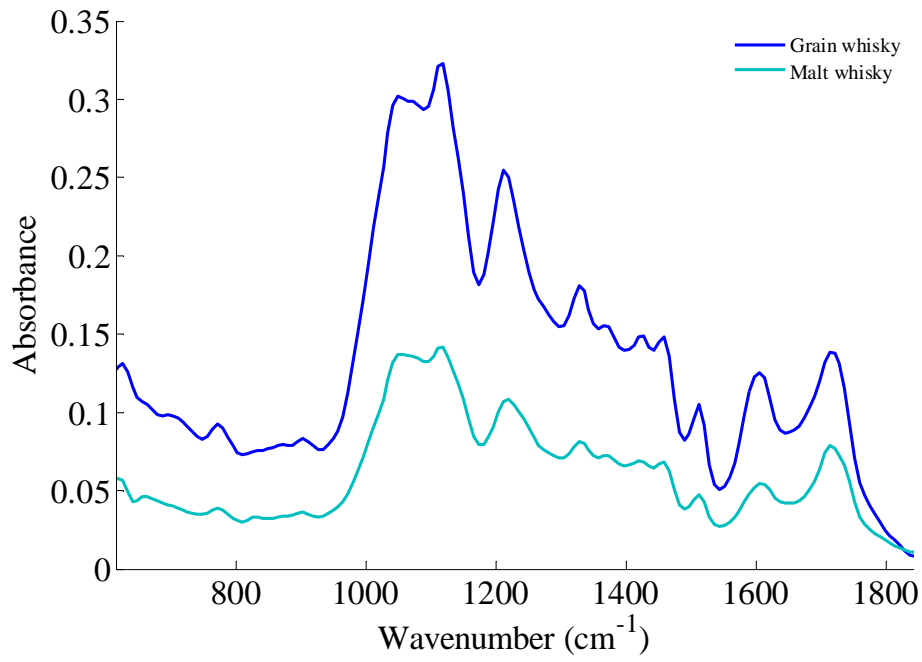


Figure 6.17: The average (n=18) ATR MIR absorbance spectra of the dried residues of a grain bourbon-cask whisky sample (number 7) and a malt bourbon-cask whisky sample (number 17).

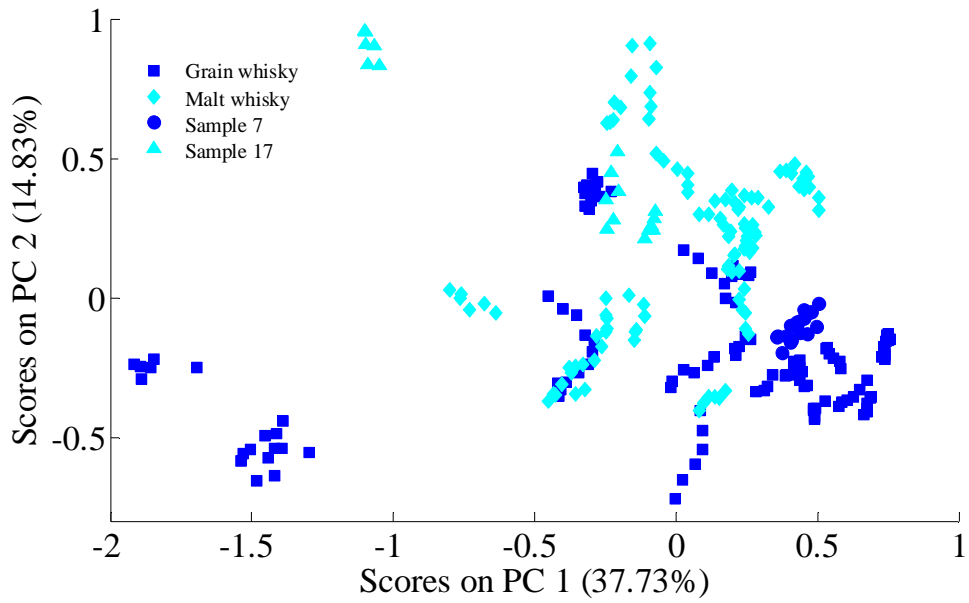


Figure 6.18: PC1 vs. PC2 scores plot from PCA of MIR spectra of fifteen bourbon-cask whisky samples, classified by malt or grain whisky.

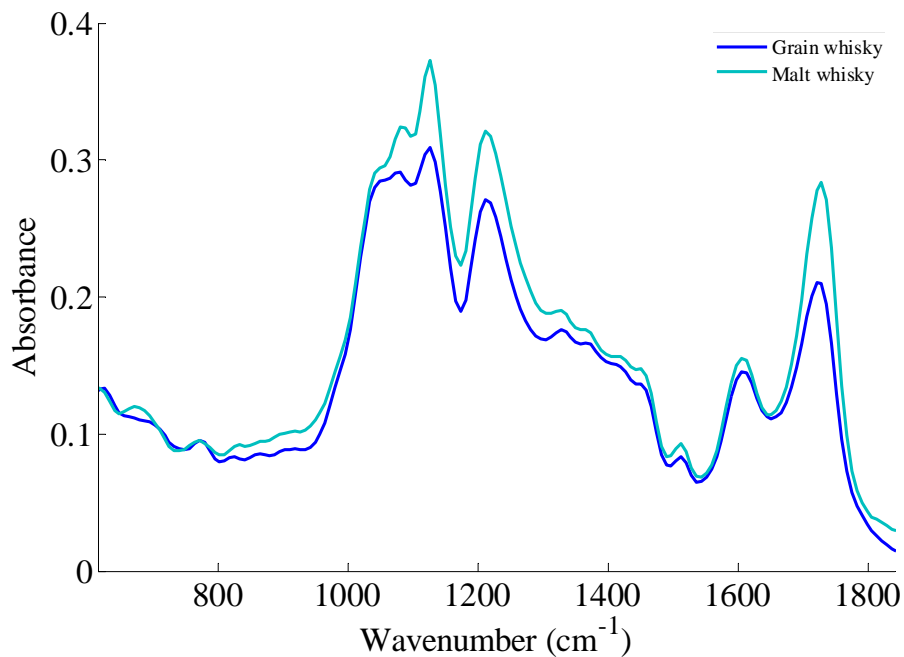


Figure 6.19: The average (n=18) ATR MIR absorbance spectra of the dried residues of a grain sherry-cask whisky sample (number 2) and a malt sherry-cask whisky sample (number 19).

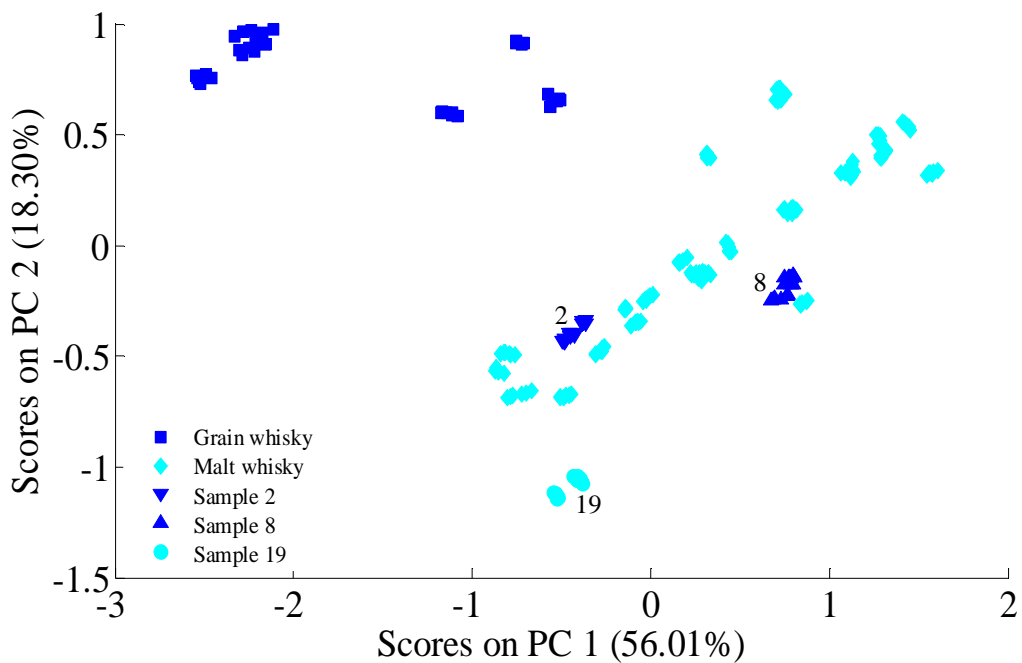


Figure 6.20: PC1 vs. PC2 scores plot from PCA of MIR spectra of thirteen sherry-cask whisky samples, classified by malt or grain whisky.

To investigate if peat has an influence on the spectra of the dried residues of cask whisky samples, the spectra of peated and non-peated samples have been compared for both bourbon-cask and sherry-cask samples; see Figure 6.21 and Figure 6.23 respectively. The corresponding PCA scores plot for the bourbon-cask and sherry-cask samples are given in Figure 6.22 and Figure 6.24, respectively. The spectra of the peated and non-peated samples seem to be comparable for both the bourbon-casks and the sherry-casks. Figure 6.22 shows that there is greater variation in the distribution of the non-peated than peated bourbon-cask samples, but they essentially occupy the same scores space. If sample 1 and the outlier for sample 17 are discounted here, the distribution of the non-peated samples does not appear so large, indicating that there is little difference between peat and non-peated bourbon-cask samples. A similar observation can be made for the sherry-cask samples, although nearly all the peated samples are in the upper right quadrant. It is unclear why the non-peated samples are more widely distributed than peated samples, although some of the spread in the sherry-cask samples can be explained. The samples that occupy the scores space in the upper left quadrant are sherry-cask whisky samples 5 and 22, these samples occupied the same scores space as bourbon-cask whisky samples rather than with the other sherry-cask whisky samples in Figure 6.12. This suggests that perhaps the reason for the distribution in Figure 6.24 for these samples is due to factors other than just being non-peated.

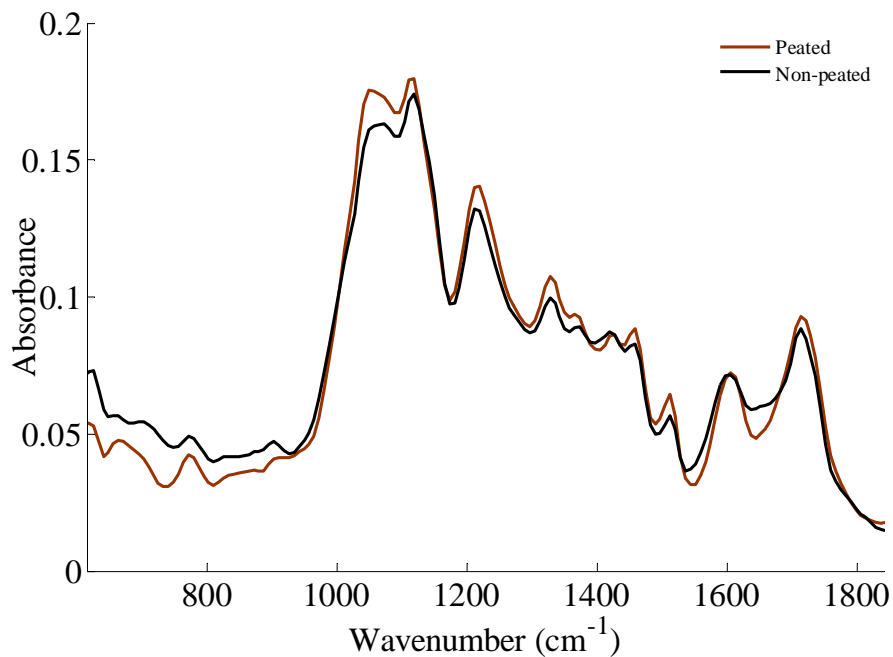


Figure 6.21: The average (n=18) ATR MIR absorbance spectra of the dried residues of a peated bourbon-cask whisky sample (number 12) and a non-peated bourbon-cask whisky sample (number 18).

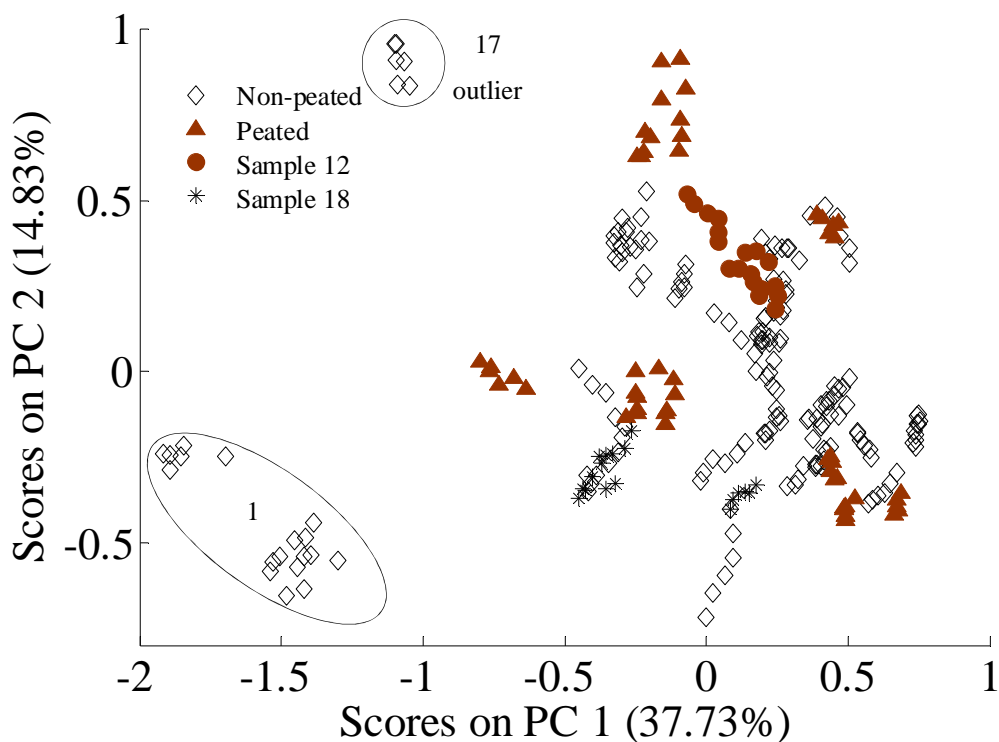


Figure 6.22: PC1 vs. PC2 scores plot from PCA of MIR spectra of fifteen bourbon-cask whisky samples, classified by the use of peat in manufacture.

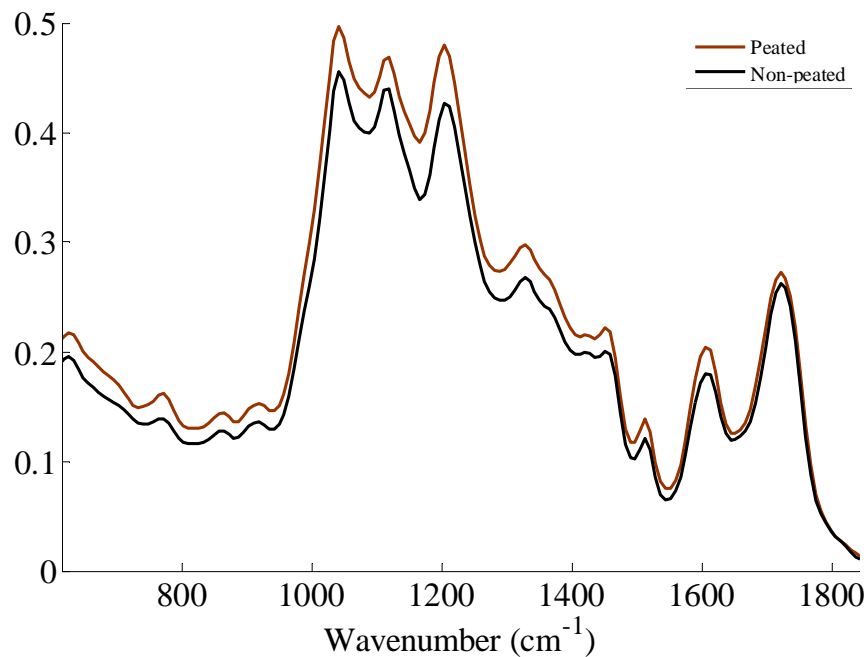


Figure 6.23: The average ATR MIR absorbance spectra of the dried residues of a peated sherry-cask whisky sample (number 27) and a non-peated sherry-cask whisky sample (number 29).

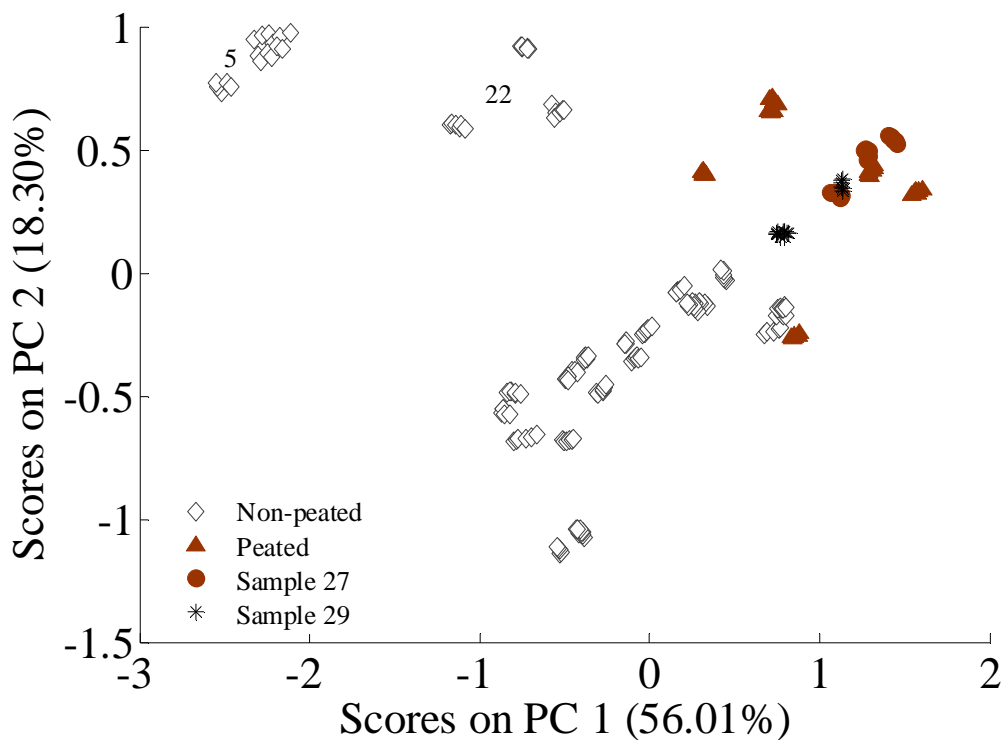


Figure 6.24: PC1 vs. PC2 scores plot from PCA of MIR spectra of thirteen sherry-cask whisky samples, classified by the use of peat in manufacture.

One maturation variable that would be useful to assess is the maturation age of a cask whisky. It is illegal to sell a whisky as Scotch whisky if it has been matured for less than 3 years and also it is illegal if a whisky is sold at the wrong maturation age. Spectra of bourbon-cask and sherry-cask whisky samples of different maturation ages have been compared and PCA has been completed to determine if differences can be observed. MIR absorbance spectra of three bourbon-cask whisky samples that span the three age ranges considered in this study are given in Figure 6.25; there is no significant observable difference in the spectra of the three whiskies. These results suggest that there are no spectral differences introduced due to the different maturation ages; this is supported by the classification of the age groups in the PCA scores plot of PC1 vs. PC2, Figure 6.26. The points representing the three age groups lie in the same scores space, the points that do occur in space away from the others are most likely a result of the influence of another variable or the combined influence of multiple variables.

The equivalent spectra and PCA plot for the sherry-cask samples are given in Figure 6.27 and Figure 6.28, respectively. The spectra are similar, with the main difference occurring in the region  $1000 - 1250 \text{ cm}^{-1}$ , where the relative intensities of the three major peaks differ between the three samples. The PCA scores plot in Figure 6.28 shows that there is more of a separation of the points for the different ages for the sherry-cask samples than for the bourbon-cask samples, however, there is not a unique space for any of the age ranges, suggesting that the differences observed are due to the combined influences of multiple maturation variables.

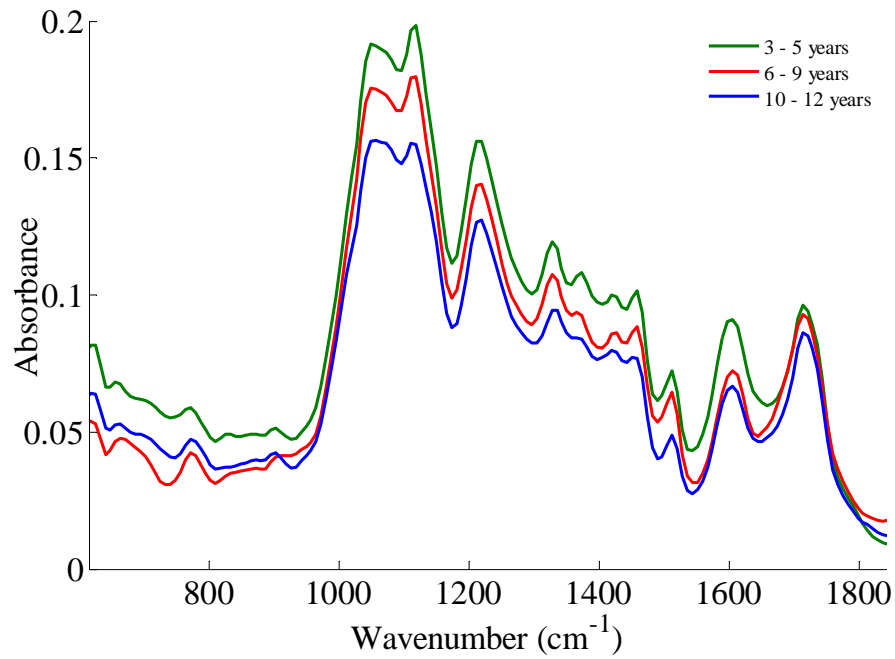


Figure 6.25: The average (n=18) ATR MIR absorbance spectra of the dried residues of bourbon-cask whisky samples of different maturation ages; ages 3 – 5 years (number 28), ages 6 – 9 years (number 12) and ages 10 – 12 years (number 10).

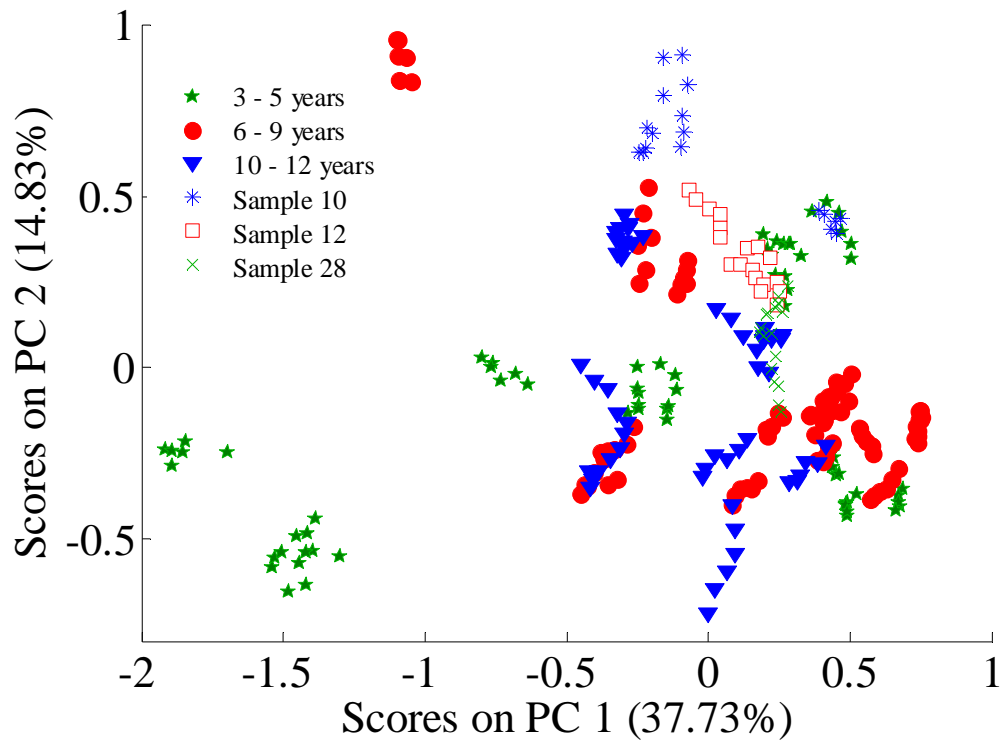


Figure 6.26: PC1 vs. PC2 scores plot from PCA of MIR spectra of fifteen bourbon-cask whisky samples, classified by their maturation ages.

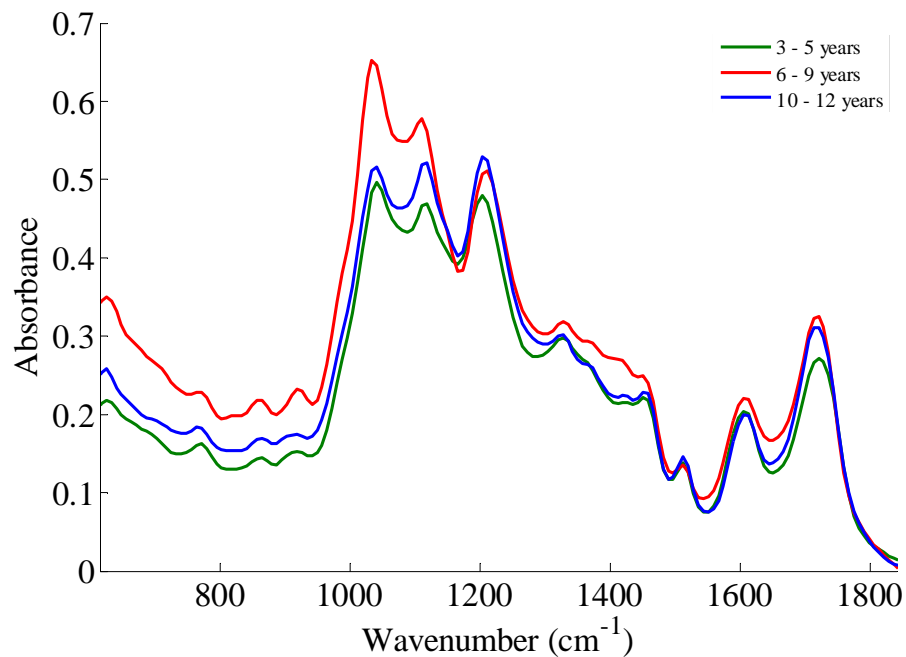


Figure 6.27: The average (n=18) ATR MIR absorbance spectra of the dried residues of sherry-cask whisky samples of different maturation ages; ages 3 – 5 years (number 27), ages 6 – 9 years (number 13) and ages 10 – 12 years (number 11).

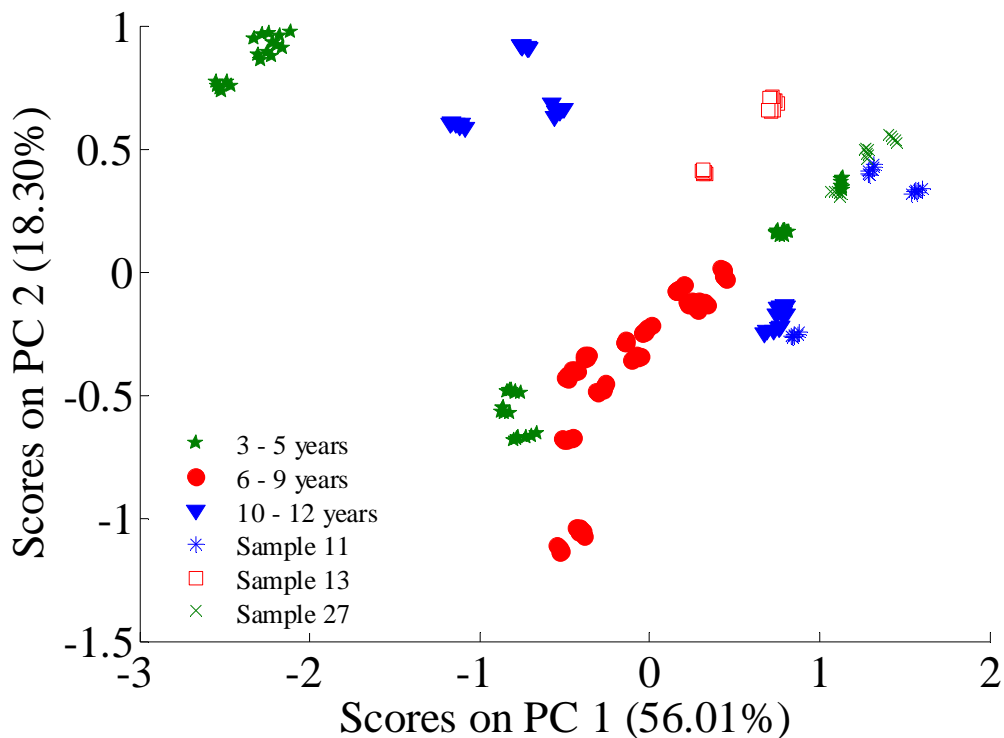


Figure 6.28: PC1 vs. PC2 scores plot from PCA of MIR spectra of thirteen sherry-cask whisky samples, classified by their maturation ages.

Evaluating the results of the PCA and spectral analysis of a range of samples where there are different manufacturing variables, a number of conclusions can be made:

- ATR MIR spectrometry could potentially be used to differentiate between bourbon-cask and sherry-cask samples.
- Differences are apparent in the PCA scores plots for both the bourbon-cask and the sherry-cask models; however, it appears as if they may result from the effects of a number of manufacturing variables.

The samples analysed as part of this study had many variables and as a result the analysis is relatively difficult. To determine which variables have an impact on the spectra of the dried residue of the cask whisky samples, design of experiment (DoE) analysis was completed using DX7 software. Different DoE models were built to include the manufacturing variables that change between the cask samples and used to determine which variables impact on the PC scores and of those, which have the greatest influence. Five models were assessed; the details are given in Table 6.8, indicating the number of factors that were included in each model. Multiple levels were used in the models and the levels associated with each factor were described previously in Table 6.6.

**Table 6.8: Details of five DoE models assessed in this study.**

Model number	Number of factors included	Name of Factors
1	6	Distillery number, Malt / Grain, Cask type, Cask history, Maturation age and Peat
2	5	Distillery number, Malt / Grain, Cask type, Cask history, Maturation age
3	4	Malt / Grain, Cask type, Cask history, Maturation age
4	4	Distillery number, Cask type, Cask history, Maturation age
5	3	Cask type, Cask history, Maturation age

When models 1 – 4 were built in DX7, problems arose: either the model’s results could not be assessed due to the number of terms that were aliased with one another, or terms had to be added into the model to allow it to be hierarchical; the results were

either misleading or the software could not provide any results. The main reason for this problem was the limited data set: many combinations of factors were not present and, therefore, could not be modelled. As a result, only model 5 could produce a hierarchical DoE model with no aliasing present and so, only this model will be discussed further. A limitation of model 5 is that only information regarding three manufacturing variables can be evaluated; cask type, cask history and the maturation age. The multi-level factorial design is illustrated in Figure 6.29 for model 5.

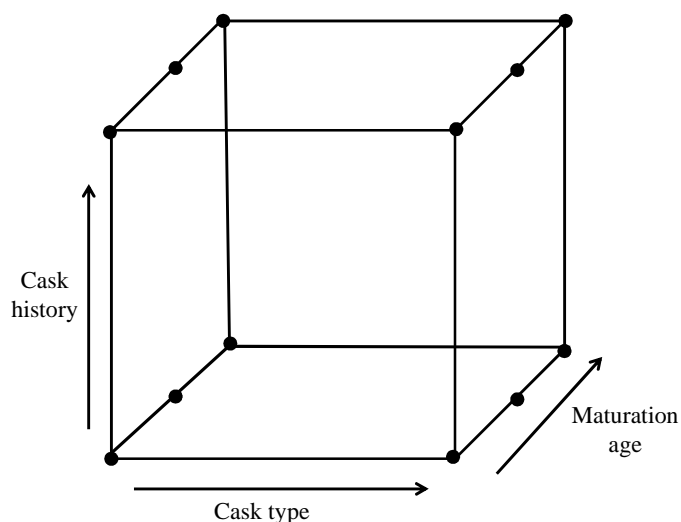


**Figure 6.29: Schematic of multi-level factorial design for model 5 assessed in DX7.**

PCA was completed for the twenty eight cask whisky samples that contained information about cask history, cask type and maturation age. The principal component scores were input as the response in DX7 and the effect of the factors and levels were assessed. Reviewing the results when PC1 scores were used as the response in the DoE analysis, all the model terms were deemed significant, suggesting that all three variables and their interactions have a significant impact on the resultant PC1 scores response. Main effects and interaction plots are produced in DX7 and these can be analysed to determine the effects on the PC1 response; as the main effects were all involved in interactions, the effect on the response could be best interpreted from the interaction plots, for this reason only the interaction plots have been discussed further. Details on the interaction AB (between cask type and cask history (fill)) for the three age groups, 3 – 5, 6 – 9, and 10 – 12 years are given in Figure 6.30, Figure 6.31 and Figure 6.32. For all three age groups it appears there is a greater difference between a first fill and refill sherry-cask than for bourbon-

casks, especially for the 3 – 5 year age group, this supports the findings found in the spectral analysis and PCA, where some changes between the spectra of whisky from first fill and refill sherry-casks could be observed. The differences observed for the sherry-cask are less for the 6 – 9 year age group in comparison to the other two age groups which have greater differences between first fill and refill. This is also true for the bourbon-cask samples, although the differences noticed here are minimal in comparison to those observed for the sherry-casks.

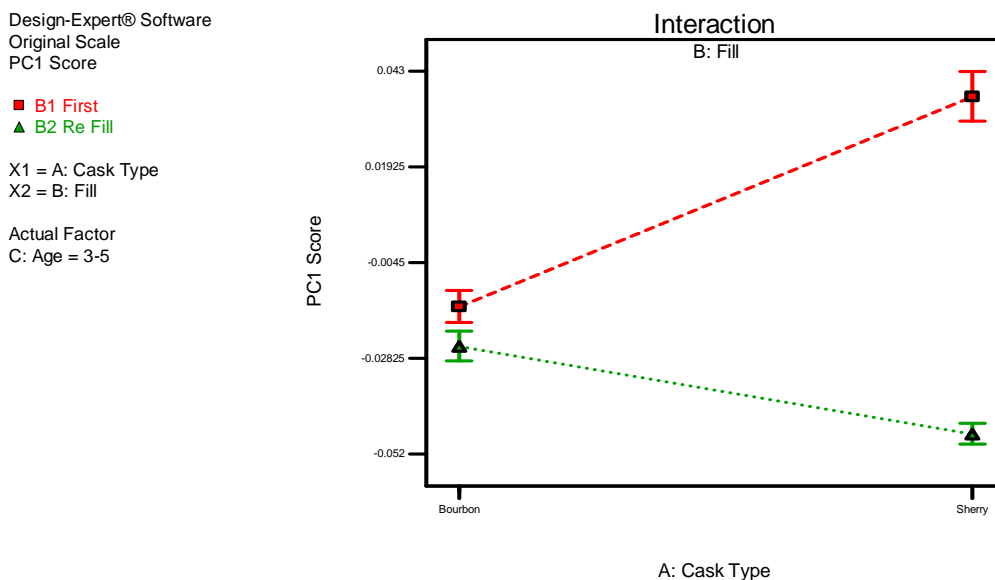


**Figure 6.30: Interaction between cask type and cask history for the age group 3 – 5 years for the response PC1 scores.**

Design-Expert® Software  
Original Scale  
PC1 Score

■ B1 First  
▲ B2 Re Fill

X1 = A: Cask Type  
X2 = B: Fill

Actual Factor  
C: Age = 6-9

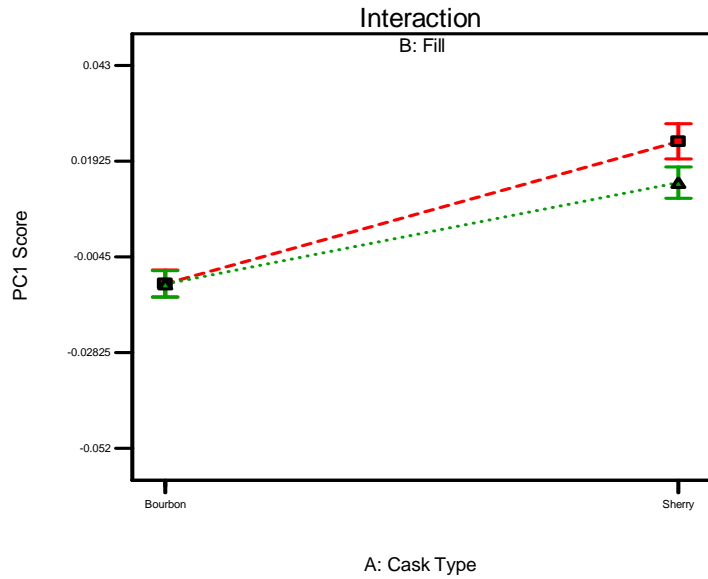


**Figure 6.31: Interaction between cask type and cask history for the age group 6 – 9 years for the response PC1 scores.**

Design-Expert® Software  
Original Scale  
PC1 Score

■ B1 First  
▲ B2 Re Fill

X1 = A: Cask Type  
X2 = B: Fill

Actual Factor  
C: Age = 10-12

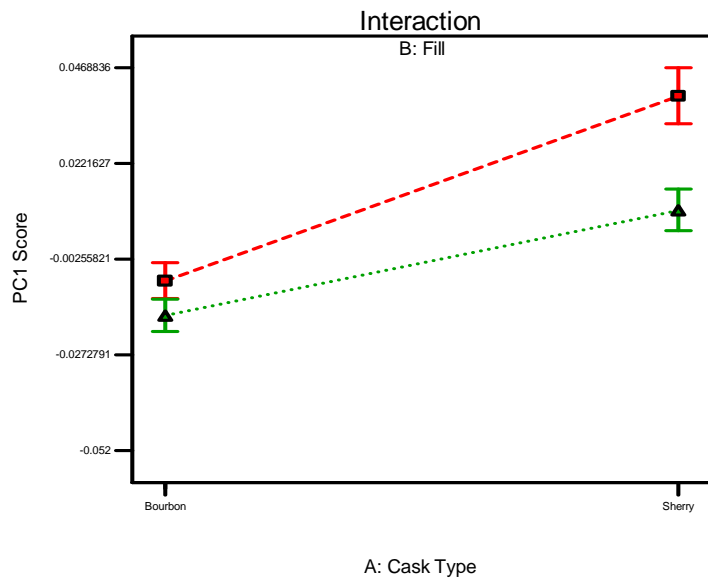


**Figure 6.32: Interaction between cask type and cask history for the age group 10 – 12 years for the response PC1 scores.**

The interaction AC represents the interaction between the cask type and age, and the interaction AC for first and refill casks is given in Figure 6.33 and Figure 6.34, respectively. The ‘I beam’ bars represent the 95% confidence limits of the least significant difference calculations carried out within DX7; if the plotted points come

outside the 'I beam' bars, the differences are unlikely to be caused by error alone and so, the differences can be attributed to factor effects. If the 'I beams' overlap then there is not a significant difference between those points. Therefore, there appears to be no interaction between the cask type and maturation age for first fill cask samples. However, there is an interaction between cask type and maturation age for refill sherry-casks where there is a change in response for the 3-5 year age range and the upper two age ranges producing higher and similar PC1 scores.

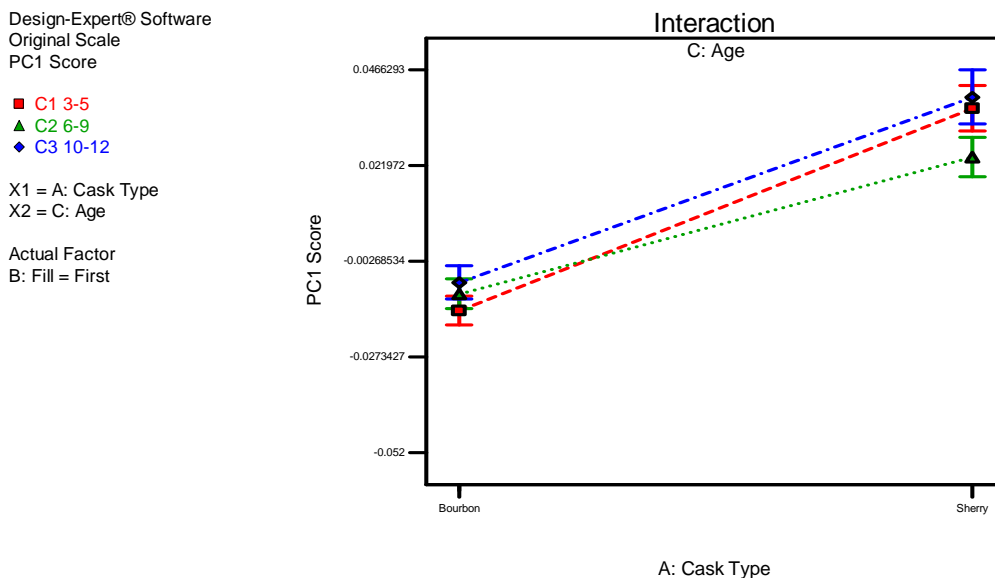


**Figure 6.33: Interaction between cask type and maturation age for first fill casks for the response PC1 scores.**

Design-Expert® Software  
Original Scale  
PC1 Score

■ C1 3-5  
▲ C2 6-9  
◆ C3 10-12

X1 = A: Cask Type  
X2 = C: Age

Actual Factor  
B: Fill = Re Fill

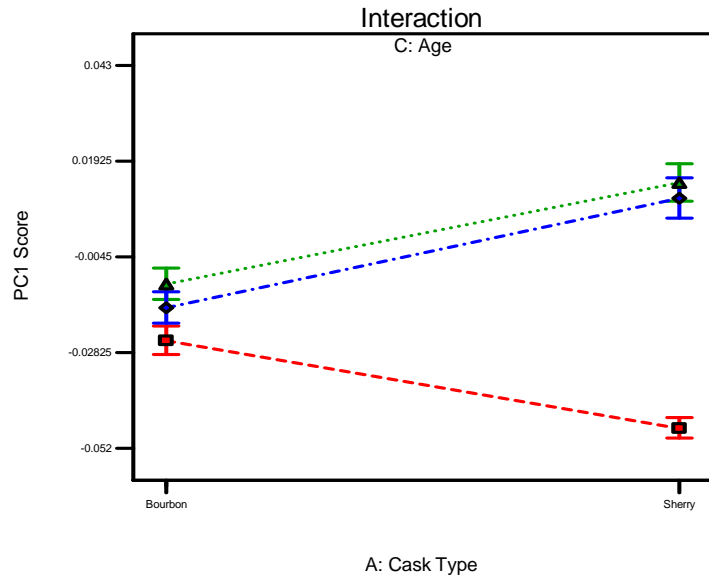


**Figure 6.34: Interaction between cask type and maturation age for refill casks for the response PC1 scores.**

The interaction BC, between cask history and maturation age for the bourbon-cask and sherry-casks are given in Figure 6.35 and Figure 6.36, respectively. The results from this interaction support those from the first two interactions, with a greater difference occurring for sherry-casks than for bourbon-casks and there is a lower PC1 score for the 3-5 year age range for the refill sherry-casks (Figure 6.36). Overall, the cask type appears to affect the PC1 scores response, however little to no effect was observed from first fill casks for all maturation ages. Whereas, for refill sherry-casks there appears to be an interaction with maturation age which affects the PC1 scores response, but only for the 3 – 5 year age group.

Design-Expert® Software  
Original Scale  
PC1 Score

- C1 3-5
- ▲ C2 6-9
- ◆ C3 10-12

X1 = B: Fill  
X2 = C: Age

Actual Factor  
A: Cask Type = Bourbon

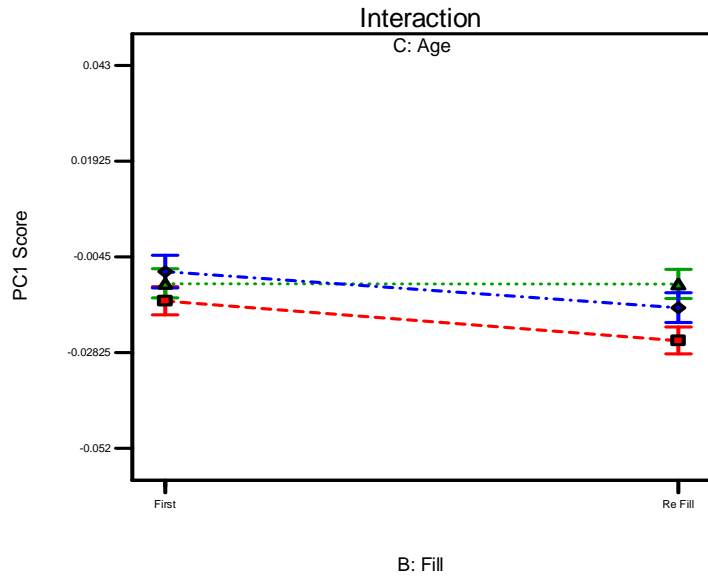


**Figure 6.35: Interaction between cask history and maturation age for bourbon-casks for the response PC1 scores.**

Design-Expert® Software  
Original Scale  
PC1 Score

- C1 3-5
- ▲ C2 6-9
- ◆ C3 10-12

X1 = B: Fill  
X2 = C: Age

Actual Factor  
A: Cask Type = Sherry

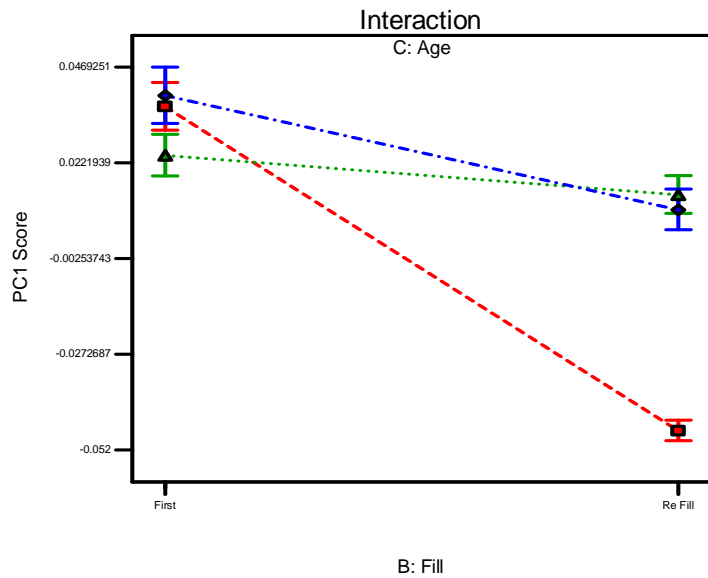


**Figure 6.36: Interaction between cask type and maturation age for sherry-casks for the response PC1 scores.**

Reviewing the results for the PC2 scores response in the DoE analysis, the model terms A, B and AC were deemed significant, these relate to cask type, cask history and the interaction between cask type and maturation age. Similar to the DX7 results

for PC1 response, the main effects were involved in interactions and, therefore, only the interaction plots have been discussed further. The interaction plots of AC for the first fill and refill samples are given in Figure 6.37 and Figure 6.38, respectively. The overlap of the ‘I beams’ for the bourbon-cask types suggests that differences in the response for PC2 scores for first fill and refill bourbon-casks is not significant for different age groups. There does appear to be an effect for sherry-casks in the age group 6 – 9 years for both the first and refill cask samples, with a higher PC2 score being observed for this age range. For the first fill sherry-casks, the age range 6 – 9 years differs from the other two providing a higher PC2 score, however from the DoE analysis this age range will produce a lower PC1 score in comparison to the other age groups. The refill sherry-cask results indicate that the age ranges 3 – 5 year and 10 – 12 year will produce similar PC2 scores, however they will be lower than the 6-9 year age range.

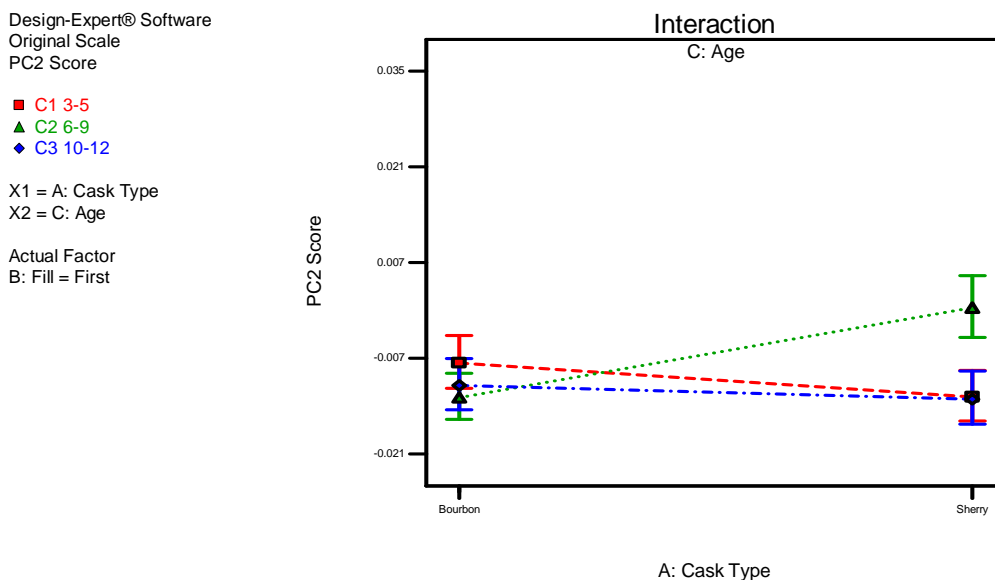


**Figure 6.37: Interaction between cask type and maturation age for first fill casks for the response PC2 scores.**

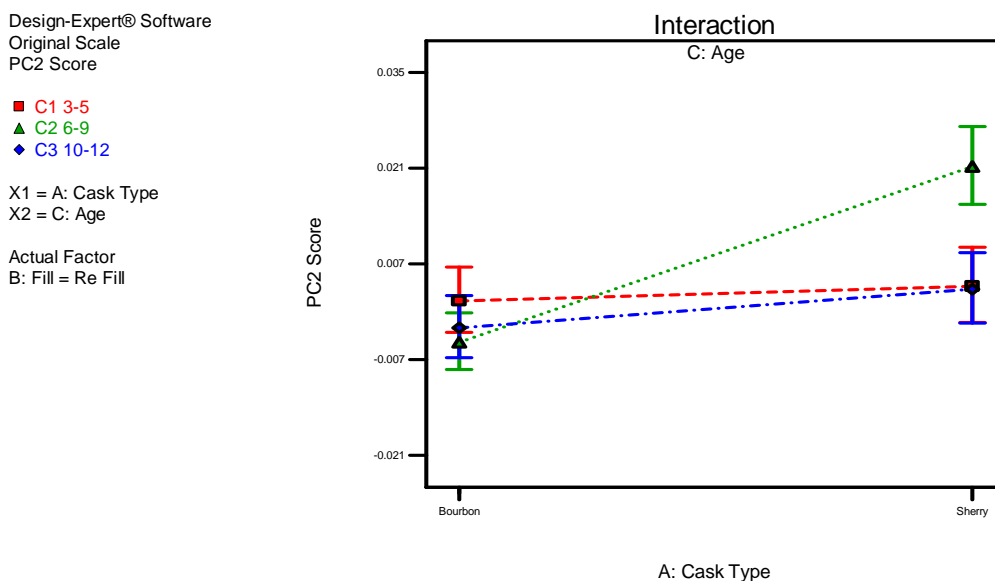


**Figure 6.38: Interaction between cask type and maturation age for refill casks for the response PC2 scores.**

Overall, the DoE analysis has shown that there is a smaller variation to the PC1 and PC2 scores for bourbon-cask samples than for sherry-cask samples, this is consistent with the results of the spectral study and PCA, where little changes could be determined; the majority of samples appeared in one cluster in the PC scores plot. A greater variation was observed for the sherry-cask samples for both PC1 and PC2 scores. The DoE analysis indicated that there was a large difference between first fill and refill sherry-casks, especially for the age ranges 3 – 5 years for PC1 and 6 – 9 years for PC2. The differences between first fill and refill sherry-casks could be observed when comparing spectra or completing PCA as were differences due to age. However, the DoE analysis could be used to determine the interaction between the cask history and maturation age, a task that was difficult using spectral analysis or even PCA.

## 2. Authentic maturation vs. simulated maturation

To determine if ATR MIR spectrometry can differentiate between authentic and simulated maturation spectra, three samples were produced by SWRI using a method to simulate the features of whisky that occur by natural maturation. To make the samples, three solvents (ethyl acetate, ethanol and water) were used individually to

extract components from the shavings of toasted American oak. In each case the extraction involved use of the solvent close to its boiling point for a large proportion of the eight hour extraction time. The coloured solutions were then evaporated to dryness to remove the extraction solvent, and then re-dissolved in 40% v/v ethanol / 60% v/v water before analysis. The three solvents used for the procedure, produced different results in terms of colour. The ethyl acetate extraction produced a very weakly straw coloured solution; ethanol extraction produced a stronger more golden colour, and water extraction produced a dark orange-brown colour. The three samples were analysed using the dried residue analysis method and the spectra were compared to those of authentically matured cask samples. The spectra of the three simulated maturation samples are compared with those of the two cask samples in Figure 6.39 and the differences between the spectra of the authentic samples and simulated maturation samples can be observed.

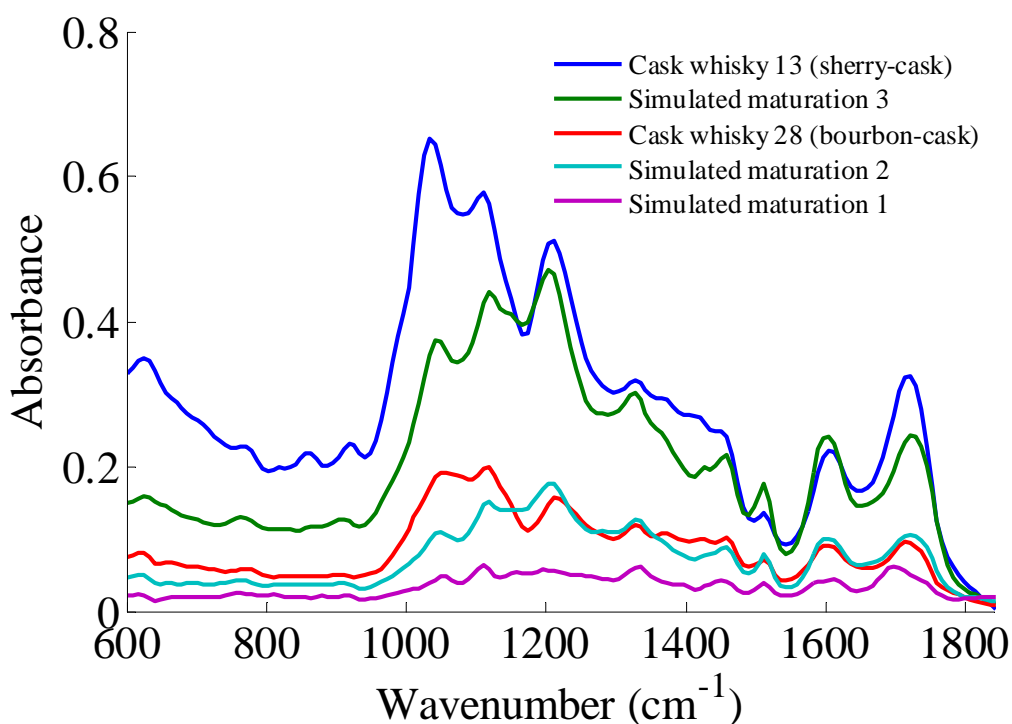


**Figure 6.39: The average ATR MIR absorbance spectra of the dried residues of three cask whisky samples and three simulated maturation samples.**

PCA was carried out on the 625-1813  $\text{cm}^{-1}$  region of the first derivative spectra of the dried residues obtained for the thirty one cask whisky samples and the three simulated maturation samples to demonstrate the differences between the samples.

Data were normalised to the largest peak and mean centred before PCA was performed. The scores plot of PC1 vs. PC2 (describing a total of 59% of the variance) is given in Figure 6.40.

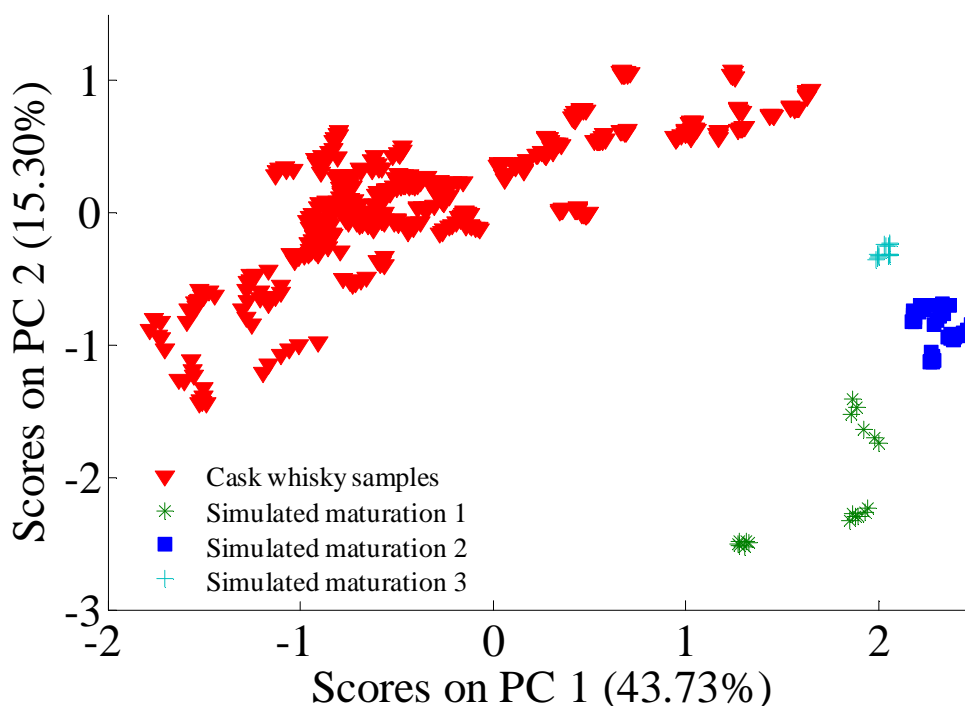


**Figure 6.40: PC1 vs. PC2 scores plot from PCA of MIR spectra of thirty one cask whisky samples and three simulated maturation samples.**

The difference between the authentically matured cask samples and the simulated maturation samples can be clearly seen. Looking at the absorbance spectra of the samples and the PCA scores plot it is possible to differentiate between the authentically matured cask samples and the simulated maturation samples. In the future, if samples suspected of not being authentically matured were to be investigated, comparison of ATR MIR spectra of dried residues should give an indication as to authenticity. However, to accommodate a range of authentic cask samples, a more robust process is required. Therefore, a PCA model was built using only the authentic cask samples; the simulated maturation samples were then analysed using this PCA model to determine if the differences between the samples could be ascertained. The scores plot of PC1 vs. PC2 describing 62% of the variance for the cask samples, with the analysis of the simulated maturation samples, is given in Figure 6.41.

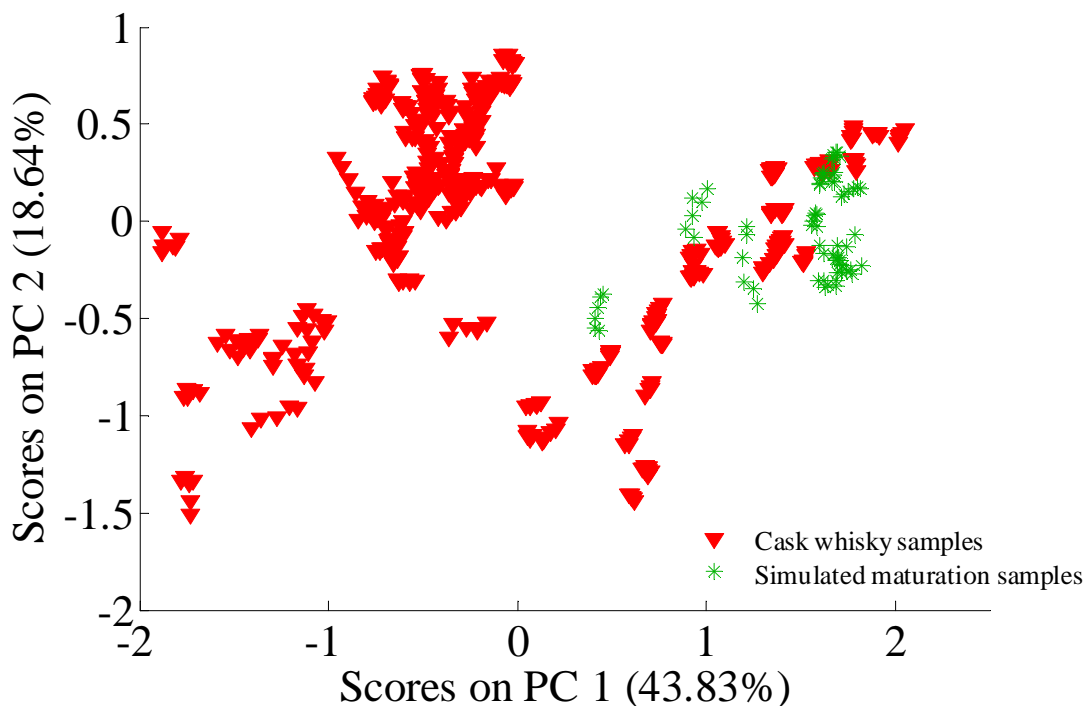


**Figure 6.41: PC1 vs. PC2 scores plot from PCA of MIR spectra of thirty one cask whisky samples with the analysis of three simulated maturation samples.**

Reviewing the results of the PCA given in Figure 6.41, the simulated maturation samples appear in the same space as some of the cask samples. This is not surprising; although some differences could be found in the spectra in Figure 6.39, all the samples shared the majority of the same peaks; it was in the relative intensities of the peaks that varied. The loading for PC1 describes the variation in the ranges  $1000 - 1300 \text{ cm}^{-1}$  and  $1600 - 1800 \text{ cm}^{-1}$ , where a lot of the variation is minimised due to the normalisation processing step. The loading for PC2 describes similar regions to PC1 but also includes the  $925 - 1000 \text{ cm}^{-1}$  range and the region around  $1400 \text{ cm}^{-1}$ . Although PC1 and PC2 can be used to differentiate the cask samples, no differences could be found to distinguish the simulated maturation samples from some of the cask samples, suggesting that the spectra are quite similar. The loading for PC3 mainly describes variation in the range  $1600 - 1800 \text{ cm}^{-1}$ ; reviewing the spectra in Figure 6.39 there is very little differences observed in this range and so the results of PC1 vs. PC3 in Figure 6.42 are not unexpected. The loading for PC4 describes some variation across the range of the spectra, but appears to describe the variation in the range  $625 - 900 \text{ cm}^{-1}$  more than the other PCs. Therefore, differences between the

cask samples and the simulated maturation samples can still be determined if the scores of PC1 vs. PC4 are considered (Figure 6.43).

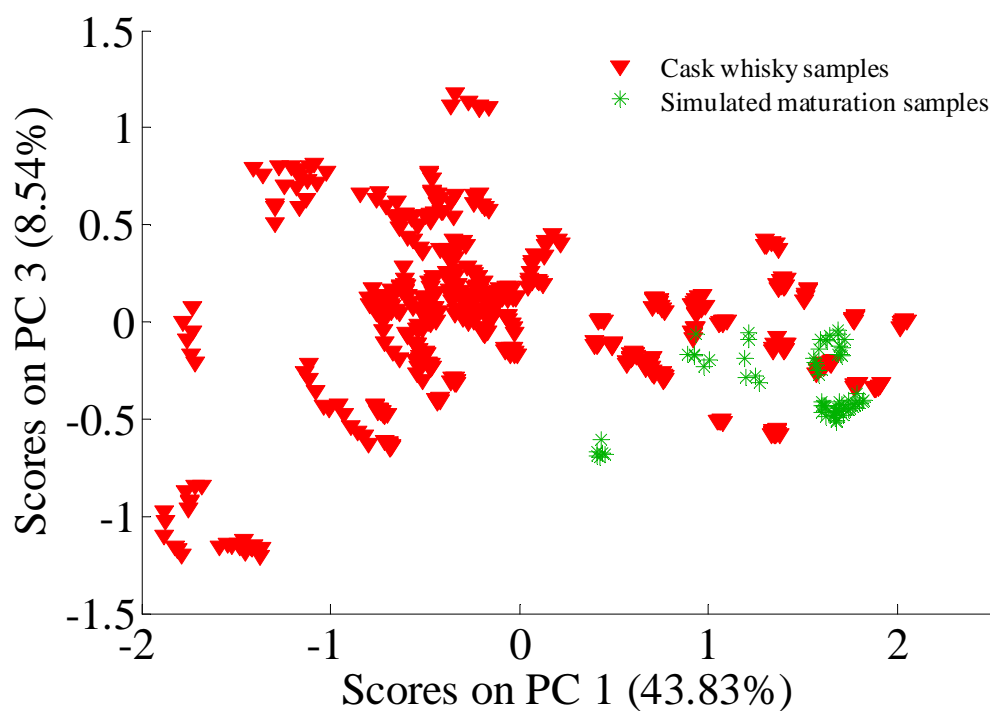


**Figure 6.42: PC1 vs. PC3 scores plot from PCA of MIR spectra of thirty one cask whisky samples with the analysis of three simulated maturation samples.**

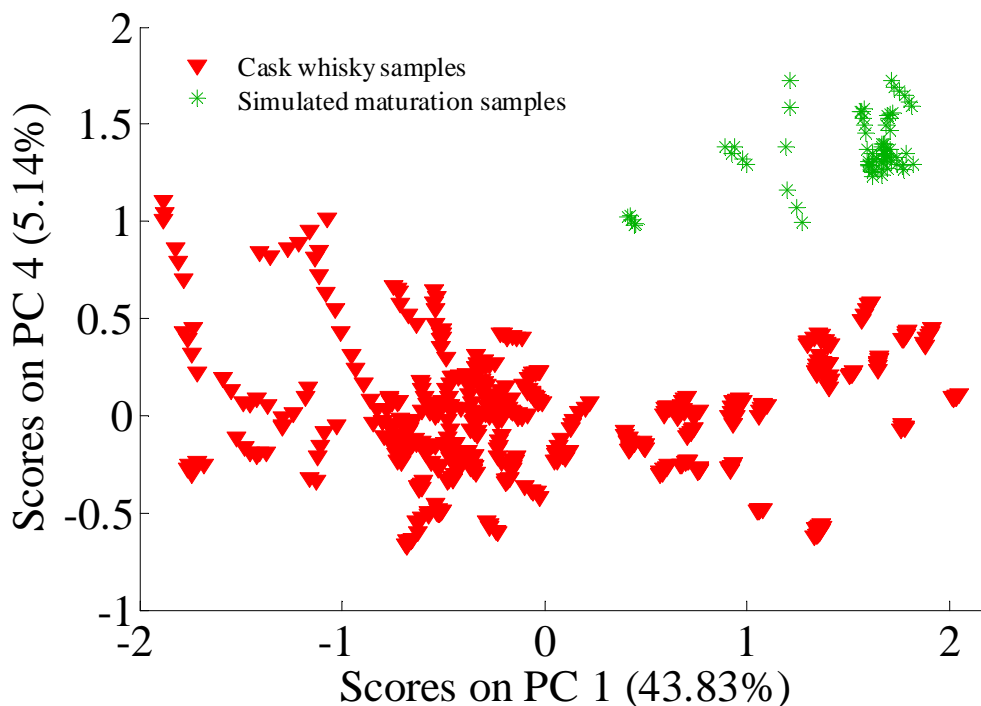


**Figure 6.43: PC1 vs. PC4 scores plot from PCA of MIR spectra of thirty one cask whisky samples with the analysis of three simulated maturation samples.**

MIR spectrometry has the ability to differentiate between the authentic cask whisky and simulated maturation samples analysed as part of this study. Analysing the simulated maturation samples with a PCA model previously built on only authentic cask whisky samples, it was still possible to establish the differences between the sample sets, indicating the potential for future determination of counterfeit samples based on differences in the maturation of the suspect samples.

### 3. Counterfeit sample spectra vs. maturation spectra

Five samples that were categorised as counterfeit from the blend authenticity work were selected and analysed to determine if their spectra were similar to either the authentic maturation cask whisky samples or the simulated maturation samples. Comparing the spectra of the counterfeit samples to the spectra of the cask samples and the simulated maturation sample, differences were apparent. PCA was completed on the  $625\text{-}1813\text{ cm}^{-1}$  region of the normalised first derivative spectra of the dried residues obtained for the thirty one cask whisky samples, the three simulated

maturation samples and the five counterfeit whisky samples. The scores plot of PC1 vs. PC2 describing 62% of the variance is given in Figure 6.44.

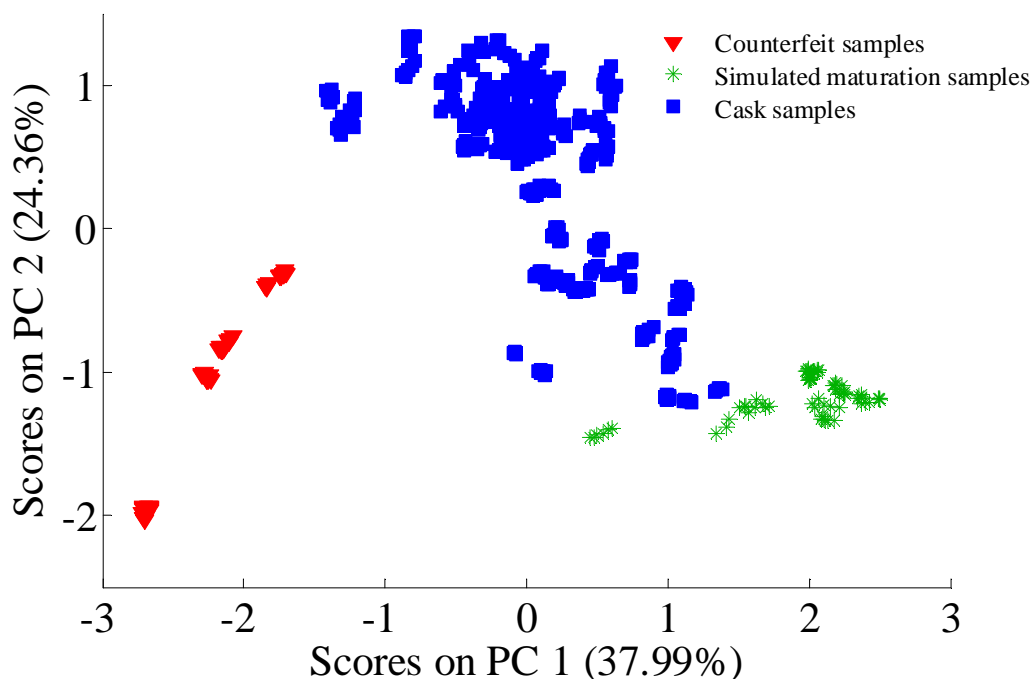


**Figure 6.44: PC1 vs. PC2 scores plot from PCA of MIR spectra of thirty one cask whisky samples, three simulated maturation samples and five counterfeit whisky samples.**

Reviewing the results of the scores plot of PC1 vs. PC2, the counterfeit samples all appear in scores space away from either the cask samples or the simulated maturation samples, suggesting that differences can be seen when comparing the spectra of these samples. In the case of the five counterfeit samples analysed as part of this study, the spectra do not appear to relate to either the authentic maturation of the cask samples or the simulated maturation samples, suggesting that the methods used to produce these counterfeit samples did not successfully mimic the features of whisky that normally occur by natural maturation.

#### 4. Caramel colorant spectra vs. maturation spectra

The MIR absorbance spectra obtained from the dried residues for one batch of caramel A colorant and four cask whisky samples are given in Figure 6.45, where the differences can be observed. The cask whisky samples were chosen to compare the spectral features of different cask whisky samples to determine if the caramel A colorant had similarities to any of those cask whisky samples. Cask whisky samples

1 and 8 are examples of grain bourbon-cask and sherry-cask whiskies, respectively, and the cask whisky samples 13 and 28 represent malt sherry-cask and bourbon-cask whiskies, respectively.

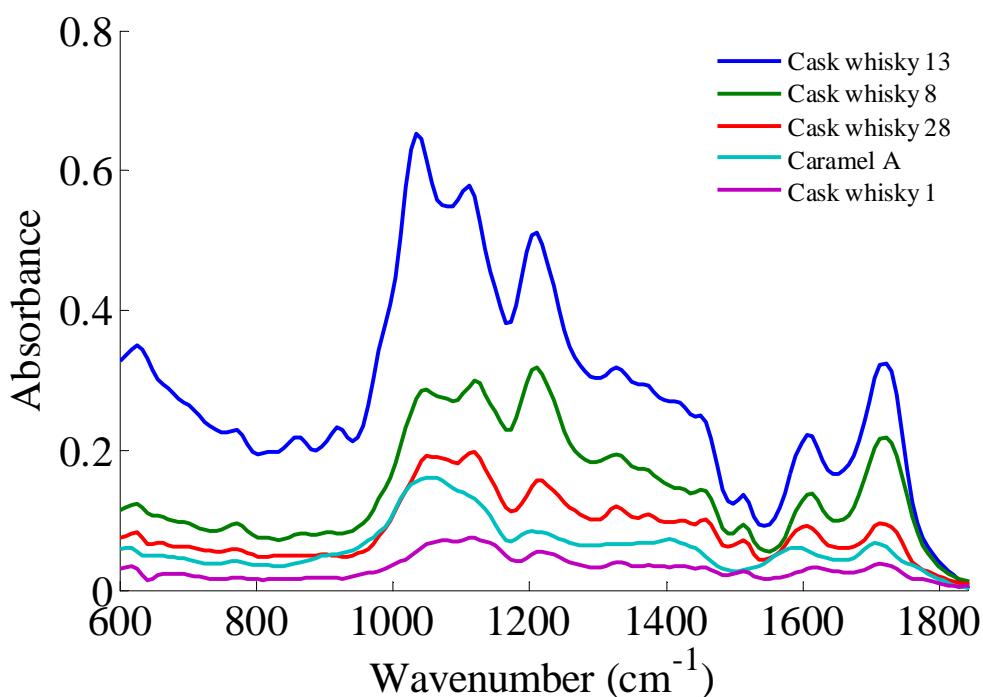


**Figure 6.45:** The average ATR MIR absorbance spectra of the dried residues of caramel colorant A and cask whisky samples 1, 8, 13 and 27. Cask whisky samples 1 and 8 are examples of grain bourbon-cask and sherry-cask whiskies, respectively, and the cask whisky samples 13 and 28 represent malt sherry-cask and bourbon-cask whiskies, respectively.

PCA was performed on the dried residues of the caramel A sample and the thirty one cask whisky samples to determine any similarities or differences between the natural maturation spectra of the cask samples and the spectra of the caramel colorant. The scores plot of PC1 vs. PC2 describing 60% of the data is given in Figure 6.46. The loadings plots for PCs 1 and 2 are given in Figure 6.47 and Figure 6.48, respectively. The loadings plot for PC1 (Figure 6.47) appears to describe the region 1000 – 1300  $\text{cm}^{-1}$  well, in addition it describes some of the variation up to 700  $\text{cm}^{-1}$  and after 1650  $\text{cm}^{-1}$ . The loadings for PC2 (Figure 6.48) seems to describe the variation over a wider range with the 900-1100  $\text{cm}^{-1}$  range having a larger weighting. The points in the scores plot representing caramel A appear in a single cluster, though they appear close to some of the cask samples. It is possible that the spectra have

some similarities in the regions of the spectra described by the loadings in Figure 6.47 and Figure 6.48.

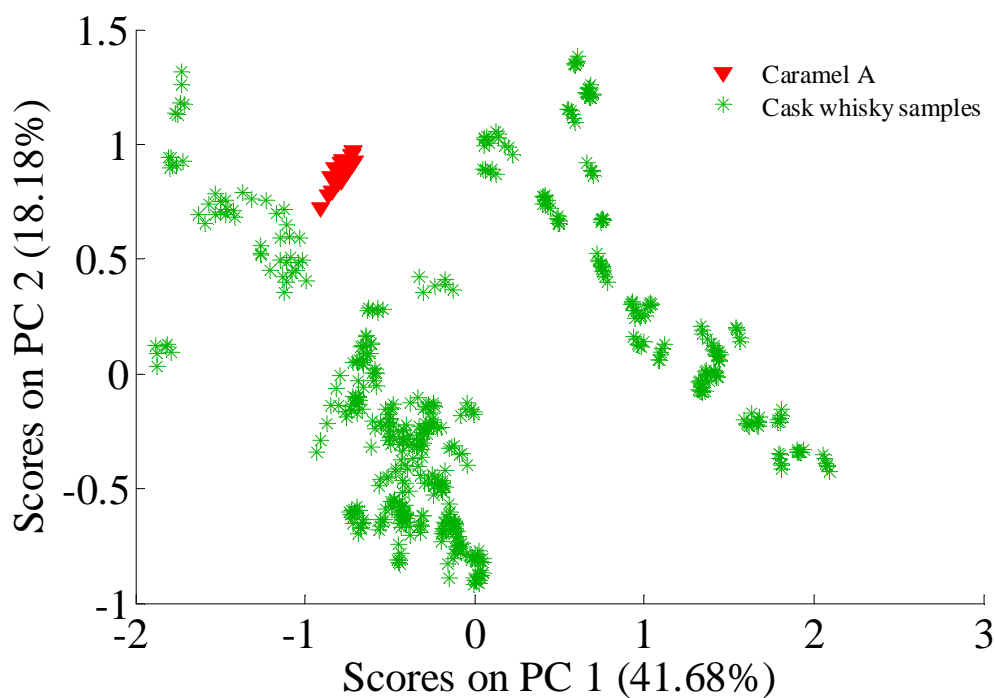


Figure 6.46: PC1 vs. PC2 scores plot from PCA of MIR spectra of thirty one cask whisky samples, and one batch of caramel A colorant.

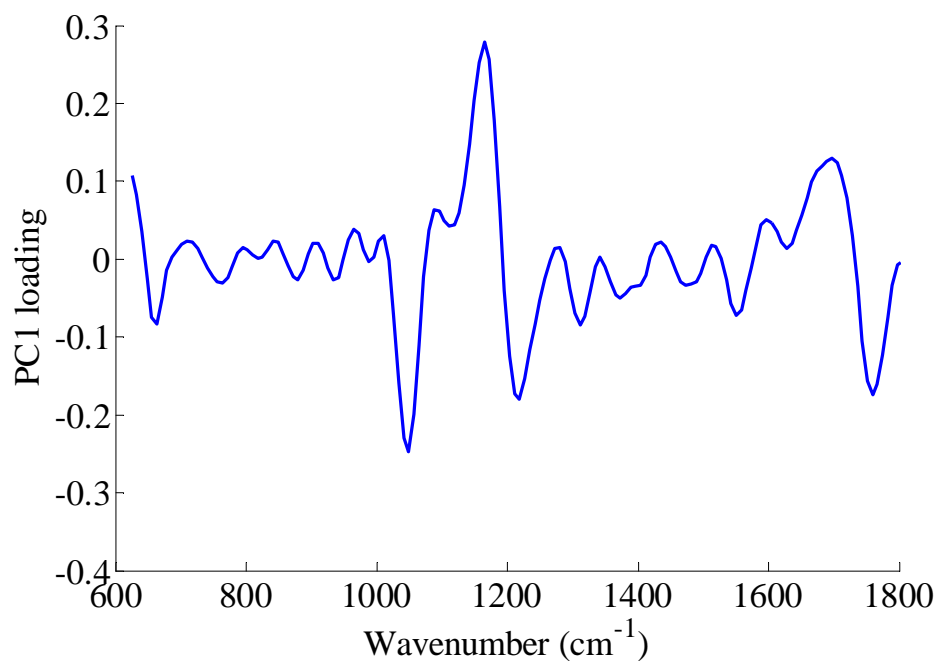
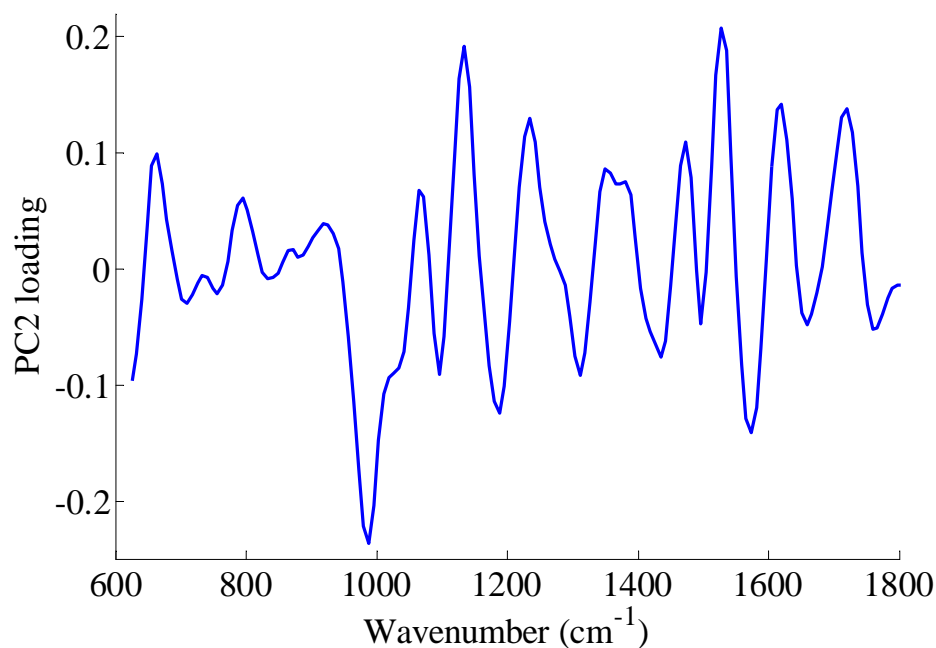
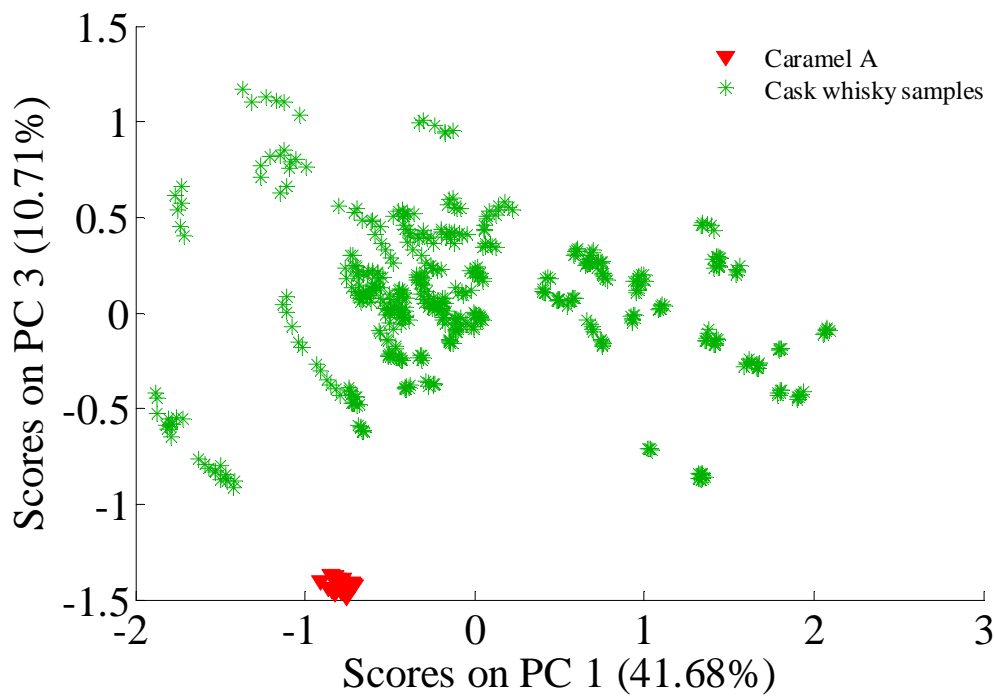


Figure 6.47: Loadings plot for PC1 from PCA of MIR spectra of thirty one cask samples and caramel colorant A.



**Figure 6.48: Loadings plot for PC2 from PCA of MIR spectra of thirty one cask samples and caramel colorant A.**

The scores plot of PC1 vs. PC3 was also generated to compare the samples; this plot describes 52% of the data, Figure 6.49. The points representing caramel A in Figure 6.49 occur in a single cluster, separated away from all of the points representing the cask samples, indicating differences between the colorant and the cask samples. The points representing caramel A are split along the PC3 axis suggesting that this principal component describes the variance between the cask samples and the colorant well. The loadings plot for PC 3 is given in Figure 6.50; the variation described is over a wide range, however the range 1400 – 1800  $\text{cm}^{-1}$  has a larger weighting in the loadings plot of PC3 than for PC1 and PC2, suggesting that this region contains differences between the spectra that can separate the samples. Examining the spectra in Figure 6.45, the cask whiskies have many spectral features; around 1550  $\text{cm}^{-1}$  the cask samples have a peak that the caramel A sample does not exhibit.



**Figure 6.49: PC1 vs. PC3 scores plot from PCA of MIR spectra of thirty one cask whisky samples, and one batch of caramel A colorant.**

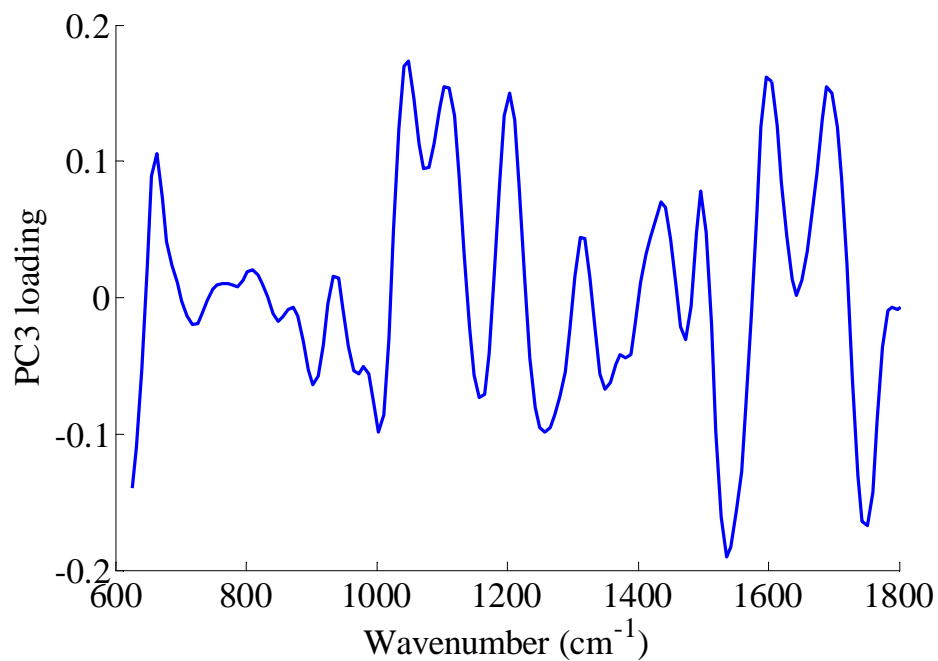


**Figure 6.50: Loadings plot for PC3 from PCA of MIR spectra of thirty one cask samples and caramel colorant A.**

The results shown indicate that there is a difference in the spectra between caramel colorant A and cask whisky samples of natural maturation. Some differences can be observed in the absorbance spectra; though the differences can also be determined by PCA. The caramel A points do appear in their own cluster when PC1 vs. PC2 scores plot is analysed, however, a clearer separation of the points representing caramel A can be determined in the scores plot of PC1 vs. PC3, as this reflects better spectral differences in the region around  $1550\text{ cm}^{-1}$ .

#### 5. Effect of addition of caramel colorant to a cask sample

Previously, it has been discussed that the spectrum of the dried residue of a whisky sample will be dominated by the colorant components of the sample, e.g. the addition of caramel colorant or from natural colour from the maturation stages. However, it is unknown if through the addition of caramel to a sample, the spectral features found from the maturation are obscured due to the dominant caramel spectra. To investigate the addition of caramel colorant, a sub-sample of a cask whisky sample (number 7) had a small amount of caramel A colorant added to slightly darken the colour of the whisky. The dried residue of this prepared sample was analysed by ATR MIR spectrometry and the spectra acquired were compared to the ATR MIR spectra of the individual samples of caramel A and original cask sample 7. The overlaid MIR absorbance spectra of the three samples are given in Figure 6.51.

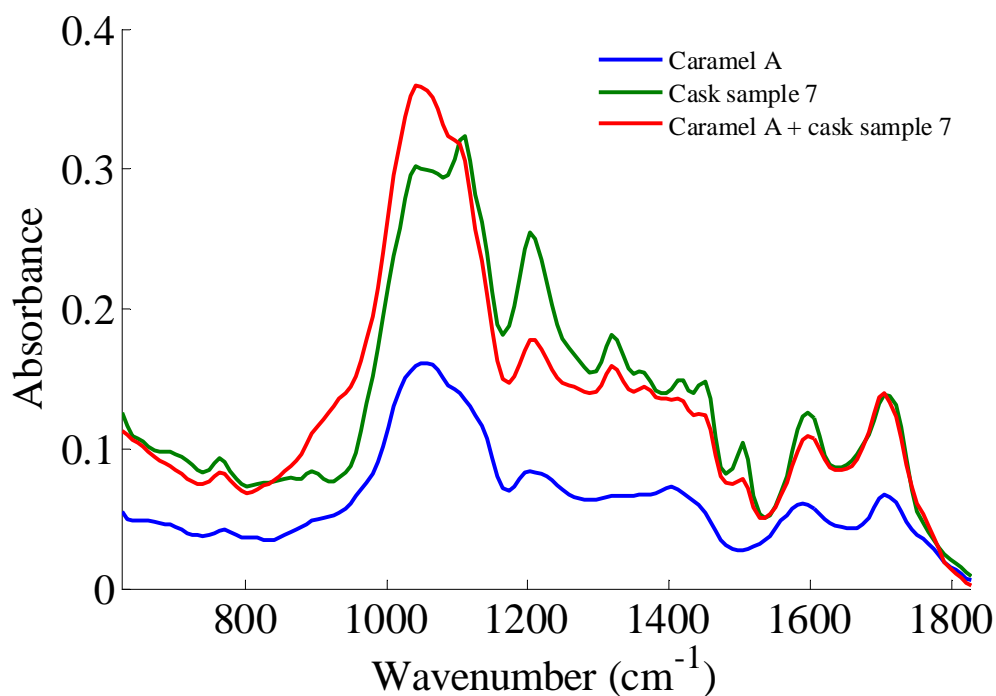


**Figure 6.51: The average ATR MIR absorbance spectra of the dried residues of caramel colorant A, cask sample 7 and cask sample 7 with caramel A colorant added.**

The spectrum of the sample of whisky and caramel colorant is similar to the caramel A spectrum in the regions  $600\text{-}1150\text{ cm}^{-1}$  and  $1550\text{-}1825\text{ cm}^{-1}$ . The region  $1150\text{-}1550\text{ cm}^{-1}$  displays a greater resemblance to the spectrum of original cask sample 7 than that of the caramel colorant. As a result of adding colorant to a sample of authentically matured whisky it is still possible to see some spectral features that relate to the components present in the whisky from maturation. In this case PCA was not used to analyse the data; to determine any differences by PCA, a greater number of samples would need to be analysed to allow the analysis to be representative.

## 6.4 Conclusions

MIR spectrometry with a diamond ATR immersion probe and polycrystalline silver halide fibres has been used for the direct and simple determination of the ethanol concentration in whisky and the identification of counterfeit samples. The predicted concentrations of ethanol were comparable to the supplied concentrations, confirming the accuracy of the method. Univariate and multivariate calibration models were compared with no significant differences demonstrated from the results of both procedures. By analysing dried residues of whisky and caramel samples on the ATR probe it was possible, using PCA, to distinguish between different caramel colorants and different whisky samples.

A combination of the results of both MIR methods allows rapid and simple assessment of suspect samples and provides advantages over alternative techniques for identification of counterfeit whisky, especially for the rapid and simple assessment of suspect samples through random spot checks out of the laboratory. For example, Aylott *et al.*<sup>17</sup> described procedures based on direct-injection GC and chemical derivatisation GC-MS that could be used to confirm the authenticity of Scotch whisky. These procedures require lab based instrumentation which is expensive and involve longer analysis times than the MIR methods described here. However, GC and GC-MS can provide more detailed information about a sample, such as higher alcohol profile and trace congeners present. NIR methods<sup>23, 37</sup> have comparable analysis times to MIR spectrometry, but often the analysis is more complex requiring the use of multivariate calibration procedures for ethanol determination. The MIR methods described here offer simple analysis procedures and also provide more spectral information than comparable NIR methods. Density measurements<sup>8, 21</sup> are used to determine the alcohol strength of whisky and can produce accurate results, although, the ethanol must be removed from the sample before a measurement can be taken. Even though this technique can be applied on-line in distilleries it provides limited information about the sample, e.g. no information on colorant used is provided for authenticity testing.

The methodology has the potential to be developed into a portable instrument similar to the device for UV-visible spectrometry described by Mackenzie and Aylott.<sup>19</sup> Although the MIR methods require a longer total analysis time, they have the advantage of providing more comprehensive spectral information than UV-visible spectrometry. Development of the MIR methodology into a portable instrument would permit screening of suspect samples in the field, with any samples identified as potentially counterfeit being brought back to the laboratory for more extensive investigation based on, e.g., congener analysis.

An initial investigation of a number of cask samples with different maturation variables was completed to assess the feasibility of ATR MIR spectrometry to answer a number of questions:

Q1 Can ATR MIR spectrometry determine differences in whisky manufacture variables?

It is possible to determine differences in the ATR MIR spectra of cask whisky samples that have originated from different cask types, e.g. bourbon or sherry. There are smaller variations in the PCA for bourbon-cask whisky samples than for sherry-cask whisky samples; therefore, being able to differentiate between bourbon-cask whisky samples is difficult. Greater variations were seen for the sherry-cask whisky samples where differences in cask history, the use of malt or grain, maturation age and use of peat occurred. However, it has been determined that colour of the whisky samples and hence the scores in PCA are influenced by multiple factors. The work completed in this research suggests that the manufacturing variables, cask type, cask history and maturation age all affect the scores. DoE analysis supported the findings from the spectral analysis and PCA, where minimal variations could be determined for bourbon-cask samples. Spectral analysis and PCA were successfully used to determine variations in sherry-cask samples; however, DoE analysis could be used to aid in determination of the interaction between manufacturing variables. It is unlikely that discrimination of bourbon-cask samples would be possible using this method.

Q2 Is ATR MIR spectrometry able to differentiate between authentic maturation spectra and simulated maturation spectra?

This research has demonstrated the ability of ATR MIR spectrometry to differentiate between the authentic cask whisky samples and the simulated maturation samples. It was possible to build a robust PCA model on the authentic cask whisky samples and use this model to analyse and establish the differences between the simulated maturation samples and the authentic maturation samples. These results indicate the potential for future determination of counterfeit samples based on differences in the maturation of the suspect samples.

Q3 Analysing some of the known counterfeits from the blend authenticity study, do their spectra relate to either of the authentic maturation or simulated maturation spectra?

The spectra of the counterfeit samples analysed as part of this study do not appear to relate to either the authentic maturation of the cask whisky samples or the simulated maturation samples, indicating that the features of the counterfeit samples differ from the features in whisky that occur by natural maturation or the features in the simulated maturation samples.

Q4 Is there a difference between the spectra of dried residues of natural maturation samples and caramel colorant A?

ATR MIR spectrometry was successfully used to analyse the spectra of dried residues of cask samples and caramel colorant A. The results indicate that there is a difference in the spectra between caramel colorant A and cask whisky samples of natural maturation which can be observed in the absorbance spectra or by PCA.

Q5 If colorant was added to a cask sample, does it mask all of the spectral information of the spectra of the dried residue of natural maturation?

The addition of colorant caramel A to a cask sample does mask the spectral information in regions of the spectra; however, one region retained the spectral features from the original cask whisky sample. These results indicate that not all the

features of the spectra of the dried residue of natural maturation will be masked after the addition of caramel colorant A.

This investigation has shown that it may be possible to distinguish between sherry-cask whisky samples based on their manufacturing variables; however, a more advanced study would be required to fully understand the effect that the different variables will have on the PC scores. The methodology described could be used to distinguish between authentic whiskies containing no caramel and counterfeit samples by comparison of spectra of dried residues of suspect samples with a spectral library of authentic products.

This research has demonstrated the great potential for ATR MIR spectrometry to be used for the identification of counterfeit Scotch whiskies based on the determination of ethanol concentration and the spectra of the dried residues of the samples. The latter measurement has also been shown to have scope as a procedure to gain a greater understanding of the impact of manufacturing variables on the generation of the colour of whisky.

## 6.5 References

1. *The Scotch Whisky Regulations 2009*, <http://www.legislation.gov.uk/ukxi/2009/2890/contents/made>, 2011.
2. M. S. Moss and J. R. Hume, *The making of Scotch whisky*, James & James, Edinburgh, 1981.
3. G. N. Bathgate, in *Whisky*, eds. I. Russell, G. Stewart and C. Bamforth, Academic Press, San Diego, 2003, pp. 1-24.
4. B. Harrison, J. Ellis, D. Broadhurst, K. Reid, R. Goodacre and F. G. Priest, *J I Brewing*, 2006, **112**, 333-339.
5. T. C. S. Dolan, in *Whisky*, eds. I. Russell, G. Stewart and C. Bamforth, Academic Press, San Diego, 2003, pp. 27-73.
6. I. Campbell, in *Whisky*, eds. I. Russell, G. Stewart and C. Bamforth, Academic Press, San Diego, 2003, pp. 115-150.
7. H. B. Haag, J. K. Finnegan, P. S. Larson and R. B. Smith, *Toxicol. Appl. Pharmacol.*, 1959, **1**, 618-627.
8. R. Aylott, in *Whisky*, eds. I. Russell, G. Stewart and C. Bamforth, Academic Press, San Diego, 2003, pp. 275-306.
9. L. Nykanen and I. Nykanen, in *Volatile compounds in foods and beverages*, ed. H. Maarse, Marcel Dekker Inc., New York, 1991, pp. 547-580.
10. I. Campbell, in *Whisky*, eds. I. Russell, G. Stewart and C. Bamforth, Academic Press, San Diego, 2003, pp. 179-206.
11. D. A. Nicol, in *Whisky*, eds. I. Russell, G. Stewart and C. Bamforth, Academic Press, San Diego, 2003, pp. 153-176.
12. J. Conner, K. Reid and F. Jack, in *Whisky*, eds. I. Russell, G. Stewart and C. Bamforth, Academic Press, San Diego, 2003, pp. 209-240.
13. J. M. Conner, A. Paterson and J. R. Piggott, *J. Sci. Food Agric.*, 1992, **60**, 349-353.
14. A. H. Varnam and J. P. Sutherland, in *Beverages: Technology, Chemistry and Microbiology*, Aspen Publishers Inc., New York, 1994, pp. 400-448.
15. in Record exports as Scotch whisky defies downturn, Scotch Whisky Association, 2010, Issue 15/04/2010 <http://www.scotch-whisky.org.uk/swa/files/Exports2009.pdf>, Accessed 31/08/2011.
16. *Explanatory Memorandum to the Scotch Whisky Regulations 2009, No. 2890*, UK Government, 2009 [http://www.opsi.gov.uk/si/si2009/em/ukxiem\\_20092890\\_en.pdf](http://www.opsi.gov.uk/si/si2009/em/ukxiem_20092890_en.pdf), Accessed 31/08/2011.
17. R. I. Aylott, A. H. Clyne, A. P. Fox and D. A. Walker, *Analyst*, 1994, **119**, 1741-1746.
18. R. E. B. Duncan and J. M. Philp, *J. Sci. Food Agric.*, 1966, **17**, 208-214.
19. W. M. MacKenzie and R. I. Aylott, *Analyst*, 2004, **129**, 607-612.
20. D. Picque, P. Lieben, G. Corrieu, R. Cantagrel, O. Lablanquie and G. Snackers, *J. Agric. Food. Chem.*, 2006, **54**, 5220-5226.
21. J. González-Rodríguez, P. Pérez-Juan and M. D. Luque de Castro, *Talanta*, 2003, **59**, 691-696.
22. M. Galignani, S. Garrigues and M. de la Guardia, *Anal. Chim. Acta*, 1994, **296**, 155-161.

23. M. Gallignani, S. Garrigues and M. Delaguardia, *Analyst*, 1993, **118**, 1167-1173.
24. B. R. Buchanan, D. E. Honigs, C. J. Lee and W. Roth, *Appl. Spectrosc.*, 1988, **42**, 1106-1111.
25. P. Tipparat, S. Lapanantnoppakhun, J. Jakmunee and K. Grudpan, *Talanta*, 2001, **53**, 1199-1204.
26. S. Engelhard, H. G. Löhmansröben and F. Schael, *Appl. Spectrosc.*, 2004, **58**, 1205-1209.
27. L. S. Mendes, F. C. C. Oliveira, P. A. Z. Suarez and J. C. Rubim, *Anal. Chim. Acta*, 2003, **493**, 219-231.
28. B. Liebmann, A. Friedl and K. Varmuza, *Anal. Chim. Acta*, 2009, **642**, 171-178.
29. A. G. Cavinato, D. M. Mayes, Z. Ge and J. B. Callis, *Anal. Chem.*, 1990, **62**, 1977-1982.
30. T. Yano, T. Aimi, Y. Nakano and M. Tamai, *J. Ferment. Bioeng.*, 1997, **84**, 461-465.
31. M. Gallignani, S. Garrigues and M. Delaguardia, *Anal. Chim. Acta*, 1994, **287**, 275-283.
32. S. Sivakesava, J. Irudayaraj and A. Demirci, *J. Ind. Microbiol. Biotechnol.*, 2001, **26**, 185-190.
33. M. Gallignani, C. Ayala, M. d. R. Brunetto, J. L. Burguera and M. Burguera, *Talanta*, 2005, **68**, 470-479.
34. D. W. Lachenmeier, *Food Chem.*, 2007, **101**, 825-832.
35. D. W. Lachenmeier, R. Godelmann, M. Steiner, B. Ansay, J. Weigel and G. Krieg, *Chem Cent J*, 2010, **4**.
36. D. W. Lachenmeier, E. Richling, M. G. Lopez, W. Frank and P. Schreier, *J. Agric. Food. Chem.*, 2005, **53**, 2151-2157.
37. A. Nordon, A. Mills, R. T. Burn, F. M. Cusick and D. Littlejohn, *Anal. Chim. Acta*, 2005, **548**, 148-158.
38. M. Lehtonen, *J Assoc Off Ana Chem*, 1983, **66**, 71-78.
39. *Laying down specific purity criteria concerning colours for use in foodstuffs, COMMISSION DIRECTIVE 95/45/EC*, European commission, [http://ec.europa.eu/food/fs/sfp/addit\\_flavor/flav13\\_en.pdf](http://ec.europa.eu/food/fs/sfp/addit_flavor/flav13_en.pdf), 1995.
40. T. Adam, E. Duthie and J. Feldmann, *J I Brewing*, 2002, **108**, 459-464.
41. J. N. Miller and J. C. Miller, *Statistics and Chemometrics for Analytical Chemistry*, 5th edn., Pearson Prentice Hall, Harlow, 2005.
42. R. G. Brereton, *Chemometrics for Pattern Recognition*, John Wiley & Sons, Ltd, Chichester, 2009.

## **7 MIR and NIR spectrometry for fermentation analysis**

### **7.1 Introduction**

#### **7.1.1 Monitoring fermentation processes**

Fermentation processes are generally recognized as the use of a submerged liquid culture of selected strains of microorganisms, plant or animal cells, for the manufacture of product(s) or to gain a better insight into the physiology of the different cell types. In the modern fermentation industry, aerobic cultivations dominate and are used to produce a range of high value products. With the continued drive for fermentation processes to produce high quality, high value products, it is important that the processes can be better understood and controlled.<sup>1</sup> The implementation of monitoring and control procedures can result in increased efficiency, productivity and reproducibility, reduced costs and improved quality control. The active compound in a fermentation process is very sensitive to changes in its environmental conditions; therefore, a small uncontrolled change can cause a major variation in the process efficiency and productivity and in some instances can result in a failed product.<sup>2</sup> To be able to achieve adequate control it is necessary to make accurate and reliable measurements of the process at timely intervals. Commonly, off-line measurements are performed on samples that are taken from the bulk medium in the process and then analysed at the end of the process. Although this approach does allow for accurate measurements, the main drawback is the delay between when the sample is taken and when the results from the measurement are determined.<sup>2</sup> It is clear that this form of analysis cannot be used for process monitoring and control as in the majority of cases the process would have been completed before the results are known. Another limitation to off-line measurements surrounds the sampling; fermentation processes are highly dependent on sterility, therefore, it is critical when taking the sample for the off-line measurement there is sufficient prevention of contamination.<sup>3</sup> However, even with the limitations discussed, off-line measurements are still prevalent in the fermentation industry. In contrast, in-line techniques can be used to measure directly the process in the reactor providing real-time information; the requirement of this type of measurement is the ability to sterilize in advance with the reactor. This approach allows for early

detection of possible problems and allows immediate action to resolve the problem. In-line monitoring has the advantage of allowing process monitoring and control in real time. In practice the most common in-line control measurements that are used in fermentation processes are pH and dissolved oxygen, due to the successful implementation of insertion probes which can be sterilised with the reactor.<sup>1-3</sup>

Roychoudhury *et al.*<sup>4</sup> discussed the characteristics required for the “ideal” monitoring technology for bioprocesses including fermentation processes; some of these characteristics include: rapid, non-destructive, multi-analyte monitoring, operable in (near) real time, capable of automation and robust. There are few technologies which can meet all of these characteristics, however, vibrational spectroscopy is observed as approaching the ideal. Both NIR and MIR spectrometry can offer multi-analyte information in a few minutes or less; therefore, a vast amount of research into the use of NIR and MIR spectrometry for analysis of fermentation samples has taken place. Research in NIR and MIR spectrometry applied to fermentation processes has evolved from analyzing and monitoring less challenging systems to more complex ones. Likewise, there has also been the tendency to implement off/at-line or *ex situ* systems first and then move towards the more challenging *in situ* measurements.<sup>5</sup> Some examples of each approach are described below.

#### NIR spectrometry examples

Arnold *et al.*,<sup>6</sup> Scarff *et al.*<sup>7</sup> and Cervera *et al.*<sup>5</sup> reviewed the use of NIR spectrometry for monitoring and control of fermentation processes, highlighting some of the challenges. One main challenge with NIR spectrometry surrounds the chemical complexity of the fermentation process, as it is difficult to relate the spectral variations observed to changes in concentration levels of the individual constituents. In addition, challenges arise for *in situ* NIR spectrometry, where the probe is subject to the conditions present in the bioreactor, including vigorous agitation and aeration. Also, these probes must be able to withstand the sterilization procedures and cope with large variations in the biomass concentration and hence, scattering conditions. Off-line NIR measurements of shake flasks were used by Macaloney *et al.*<sup>8</sup> to

indicate the feasibility of NIR spectrometry for the quantitative determination of biomass and glycerol in *E. coli* fermentation processes. Even with the relative difficulty of relating spectral variations to specific constituents, this study showed the possibility for the quantification of individual constituents through the use of multivariate calibration. Yano *et al.*<sup>9</sup> described the use of off-line NIR spectrometry to quantitatively predict the concentrations of individual constituents in rice vinegar fermentation. Off-line studies implementing NIR spectrometry were completed by Arnold *et al.*<sup>10</sup> and Crowley *et al.*<sup>11</sup> in more complex fermentation processes, where large changes in the matrix or viscosity were observed. Examples of at-line NIR spectrometry for analysis of fermentation processes are also apparent.<sup>12, 13</sup> Although at-line measurements can provide quicker results and are, therefore, more suited to process monitoring and control than off-line measurements, they still have the limitation of requiring sampling from the reactor without the disruption to the process or causing contamination. González-Vara *et al.*<sup>14</sup> implemented the use of NIR spectrometry with full automation for the process optimization of L-(+)-lactic acid. In this study, an external circulation loop was successfully used allowing continuous feed back into the reactor after microfiltration and lactate extraction. The use of external circulation loops require careful set-up including the use of *in situ* sterilization to prevent contamination; even with this in place the risk of compromising the sterility of the system is quite high. Many examples of in-line analysis using *in situ* NIR transmission<sup>15, 16</sup> or transfectance<sup>17-20</sup> probes or non-invasive NIR reflectance<sup>21-23</sup> probes have been reported. Arnold *et al.*<sup>16</sup> compared the use of at-line and *in situ* NIR measurements to monitor the biomass of an industrial fed-batch *E. coli* process. The NIR transmission probes were able to be steam sterilized and successfully used to monitor the complex aerated fed-batch process. However, the at-line and in-line modes were used to different success and, therefore, the suitability of each mode must be considered when choosing between them. Differences were observed in the available wavelength regions between the two modes, the in-line NIR transmission probe was more suited to the region 400 – 2000 nm, due to the adverse signal to noise in the region 2000 – 2500 nm. The probe also suffers from gas phase effects and vibrational effects caused by the agitation and aeration, respectively; in addition, the probe can be affected by fouling. However,

even with these possible effects, *in situ* models for the monitoring of biomass were still achievable. The issues of *in situ* NIR probes are less evident for mammalian cell culture processes, as these involve lower agitation rates, gas phases create less of an impact, and they are generally clean homogenous non-viscous broths. Therefore, the problems discussed above are less of a hindrance for *in situ* analysis of mammalian cell culture processes. Roychoudhury *et al.*<sup>20</sup> used *in situ* NIR transfectance probes for single probe analysis and multiple probes in multiple reactors to monitor an industrial mammalian cell culture process. The probes used in the study were custom designed for their application and, therefore, were able to undergo sterilization with the reactor. Calibration models were developed to predict the concentration of glucose and lactate using the single probe and multiple probes; both sets of models produced low standard error of predictions. The use of reflectance probes attached to the side of the reactor vessel can monitor the process non-invasively; as the probe is placed outside of the process environment it can be put in place after sterilization. Nordon *et al.*<sup>23</sup> discussed the use of non-invasive NIR spectrometry to monitor the seed stage of a fermentation process. Although, changes observed for the biomass signal could be attributed to growth and fragmentation, which indicated changes in the metabolic activity, variations in the spectral response were observed when changes in stir rate, biomass concentration and morphology occurred. These results indicated that quantitative models for the prediction of biomass concentration will be less reliable unless information on stir rate and variations in light scattering, etc. can be incorporated into the model.

#### MIR spectrometry examples

As with NIR spectrometry, there is great interest in the use of MIR spectrometry for monitoring and control of fermentation processes. Roychoudhury *et al.*<sup>4</sup> reviewed the literature and discussed the advantages and limitations of MIR spectrometry for real-time measurements of bioprocess monitoring. One of the major challenges with implementing MIR spectrometry for monitoring and control of fermentation processes is that it is often used as the secondary technique, therefore, the accuracy can only be as good as that of the selected reference method. Yet, advantages in terms of ease of use, fast measurement times, possibility of multi-analyte analysis

and non-destructive measurements have seen this technique implemented for fermentation analysis. Similarly to *in situ* NIR spectrometry, *in situ* MIR probes are required to undergo sterilization with the reactor. Many examples of off-line<sup>24-31</sup>, at-line<sup>32, 33</sup>, on-line<sup>34-36</sup> and *in situ*<sup>37-43</sup> MIR spectrometry exist for the analysis of various fermentation processes. Crowley *et al.*<sup>24</sup> discussed the use of off-line MIR analysis with an ATR accessory to monitor a *Pichia pastoris* fed-batch process after the process was complete. PLS models were built with reference assays for two substrates, glycerol and methanol, as well as the product; these models were validated using spectral data from further fermentations. Predictions with low root mean square errors were possible and minimal to no pre-processing was required depending if it was the substrates or product models. However, all samples used in this study were filtered, hence the reason for completing off-line analysis. Fayolle *et al.*<sup>25</sup> used an off-line transmission flow-through cell for the analysis of samples from a fermentation process producing lactic acid; here the samples did not require filtration before analysis. The models produced were successfully used to determine the concentrations of substrate, major metabolites and lactic acid. Roychoudhury *et al.*<sup>32, 33</sup> described the use of at-line MIR spectrometry for monitoring antibiotic fermentation processes; at-line had clear advantages over off-line MIR measurements as information about the process could be determined during the process. In addition, the use of at-line for this process was advantageous as it allowed the samples to be filtered before analysis; a process that cannot be completed *in situ*. Examples of on-line MIR analysis to monitor and control fermentation processes have been reported by Schenk *et al.*<sup>34, 35</sup> using flow-through cells connected to the reactor and a computer system which allowed automated control of the feeding rate. With the advances in ATR probe design and optical fibres for use in MIR spectrometry, a vast amount of research using *in situ* ATR MIR spectrometry has been reported for many applications. However, one of the main challenges of *in situ* probes for fermentation analysis has been the ability to sterilise the probe along with the reactor; with the development of ATR probes such as those described by Doak and Phillips,<sup>44</sup> where the tip and shaft could be steam sterilized *in situ*, many more instances where *in situ* ATR MIR spectrometry has been used for the monitoring and control of fermentation process have been observed. Doak and Phillips<sup>44</sup> indicated in their research that their

*in situ* MIR probe set-up was unaffected by agitation or aeration rates, which has a clear advantage over the *in situ* NIR probes described by Arnold *et al.*<sup>16</sup> Kornmann *et al.*<sup>37-39</sup> evaluated the use of *in situ* ATR probes for fermentation processes; *in situ* ATR MIR spectrometry was successfully implemented to monitor and control a highly viscous *Gluconacetobacter xylinus* fed-batch culture process and offered many advantages over on-line methods, such as rapid analysis, ease of operation and no requirement for sample removal.<sup>38</sup>

### **7.1.2 Use of combined data**

As previously mentioned, there are a great number of reports into the use of spectroscopy for *in situ* monitoring of processes with many perceived advantages. This increased use of in-line analysis has led to rapidly increasing quantities of data. To capture the different sources of variation, multiple calibrations must be performed, which mean a significant amount of work to find the best calibration from each individual technique for the specific process. Occasionally NIR and MIR spectrometry can be used to provide different information about a process: as Karoui *et al.*<sup>45</sup> reported, MIR and NIR methods were used to determine different parameters in emmental cheese; NIR spectrometry was useful for the determination of the fat content and the total nitrogen content, and MIR spectrometry was useful for the quantitative determination of sodium chloride. In this instance, combining the spectral data did not provide any improvement over using the two techniques separately. However, there are instances where the combination of the spectral data from separate techniques may provide calibration models with better overall performance or allow the determination of certain properties in the system. Therefore, research has progressed into the use of data combination for these purposes. Dearing *et al.*<sup>46</sup> described a simple process of scaling and fusing the spectra from different techniques into one contiguous system. The data from Raman and MIR spectrometry as well as nuclear magnetic resonance spectrometry were fused together to produce a resultant calibration model that provided a reduction in the RMSEP in comparison to models built using the separate spectra. A similar procedure was completed by Iñón *et al.*<sup>47</sup> for the combination of MIR and NIR spectral data to produce a calibration model that improved the predictive

performance compared with that of separate models; however, it was commented that the improvements were not significant. Cuadrado *et al.*<sup>48</sup> investigated the use of combined MIR and NIR spectral data for the determination of wine parameters. Reviewing the results of each technique separately, the NIR region produced statistically better models than those from the MIR region. However, the combination of the two data sets improved the determination for glycerol and total sulfur dioxide. The improvement for the determination of these parameters proved significant in this research, as it provided a quantitative method rather than just a screening method that was available when the spectral regions were used separately. Cozzolino *et al.*<sup>49</sup> successfully used the concatenation of MIR and NIR spectral data with PLS discriminant analysis models to correctly identify the geographical origin of 93% of Australian wines in comparison to 73% and 86% by NIR or MIR analysis, respectively. Another example where the use of combined NIR and MIR spectral data has been beneficial was in the analysis of temperature dependent protein structural transitions. Navea *et al.*<sup>50</sup> incorporated combined MIR and NIR spectral data with multivariate curve resolution to aid the understanding of the temperature dependent evolution of  $\beta$ -lactoglobulin. Only the combined analysis of the NIR and MIR data allowed the detection and modeling of the three protein conformations involved in the process. These three proteins otherwise could not have been resolved if MIR or NIR spectrometry were used separately due to the similarity in the pure spectral shapes. With this success, the intermediate conformation, which cannot be isolated experimentally, was able to be fully characterised from a mechanistic and structural point of view.

### **7.1.3 Basis of this study**

The above review has shown the extensive use of NIR and MIR spectrometry for monitoring and control of fermentation processes. In addition, the benefits of the combination of NIR and MIR spectral data have been shown in different applications. The use of a combined probe which incorporates NIR and MIR capability could provide potential benefits. Most simply, a combined probe would allow the simultaneous analysis of both NIR and MIR spectra through a single point in the process. This would save space in terms of the number of probes needed to be

inserted into the process as well as allowing NIR and MIR spectral measurements to be taken from the same point in the process. This would allow some constituents to be analysed by one technique and others by the second technique. Other benefits from the use of a combined probe would most likely come from the combination of the data itself, such as the examples discussed above.

In this research, a feasibility study has been completed to investigate the use of NIR and MIR spectrometry for the prediction of three properties of a *Pichia pastoris* fermentation process. The NIR and MIR measurements of the batch phase and continuous steady state phase of the fermentation were completed off-line after the reaction was complete. Separate PLS calibration models built using the NIR and MIR spectral data from the batch phase were used to determine the predictive ability of each spectral technique for the analysis of glycerol, ammonium ions and optical density (OD). Samples from the continuous steady state phase were used to spike known concentrations of glycerol and ammonium sulfate to aid with the analysis. The results were compared to determine any possible advantages of producing a combined NIR-MIR probe for *in situ* analysis of fermentation processes.

## **7.2 Experimental**

### **7.2.1 Samples**

Fermentation broth samples were provided by Mariana Fazenda, a post-doctoral research assistant in the Strathclyde Institute of Pharmaceutical and Biomedical Sciences, who carried out the fermentation and collected the samples. The fermentation broth samples were removed from the fermenter and a small quantity of each sample was separated out into a container and frozen for analysis at the end of the process. To determine the concentration in the broth samples, reference assays were completed by Mariana and the data passed on for use in this investigation. The glycerol and ammonium ion concentrations were obtained using enzymatic reference assay kits and the optical density was measured using a spectrophotometer at 600 nm. Samples were removed from the reaction vessel and diluted before analysis. The absorbance determined for the diluted samples was then multiplied by the dilution factor to determine the optical density value for the original sample. The results from the reference measurements for the fermentation samples of the batch phase are given in Table 7.1 (samples 1 – 7). Twelve samples were selected from the continuous steady state phase, where the concentrations remained fairly constant, and used to spike in known concentrations of glycerol and ammonium sulfate, for use in the PLS model building process. The concentration of the added analytes were calculated and added to the reference measurement concentration; the total concentrations for ammonium ions and glycerol are also given in Table 7.1 (samples 8 – 19).

**Table 7.1: Reference and calculated values of optical density, glycerol and ammonium ion concentrations.**

Sample number	Description	Optical density (OD)	Glycerol (g / L)	Ammonium ion (g / L)
1	Fermentation sample	0.1	50.2	4.4
2	Fermentation sample	1.2	50.8	4.7
3	Fermentation sample	14.7	38.4	4.6
4	Fermentation sample	15.8	27.7	4.7
5	Fermentation sample	16.7	4.4	5.1
6	Fermentation sample	17.8	3.8	5.4
7	Fermentation sample	18.3	0.0	5.8
8	Spiked sample	n / a	26.0	6.0
9	Spiked sample	n / a	20.4	6.7
10	Spiked sample	n / a	51.2	7.8
11	Spiked sample	n / a	38.7	9.2
12	Spiked sample	n / a	38.0	7.8
13	Spiked sample	n / a	3.2	5.7
14	Spiked sample	n / a	26.3	8.6
15	Spiked sample	n / a	52.7	4.6
16	Spiked sample	n / a	14.3	5.6
17	Spiked sample	n / a	22.4	7.3
18	Spiked sample	n / a	13.6	4.4
19	Spiked sample	n / a	1.6	6.7

n / a = not applicable

### 7.2.2 NIR spectrometry

NIR spectra were acquired with a resolution of 2 nm in the 1100 – 2500 nm range using a Model 6500 NIR spectrometer (Foss-NIR Systems, Silver Spring, MD, USA) in transmission mode with a 0.5 mm pathlength cuvette using the sample transport module. 32 co-added scans of the samples were analysed with an air background. Samples were equilibrated to room temperature and scanned in triplicate; the spectra were exported as Excel files and imported into Matlab, where the spectra were averaged ( $n = 3$ ) before data analysis.

### 7.2.3 MIR spectrometry

MIR spectra were acquired with a resolution of  $16\text{ cm}^{-1}$  in the  $400\text{--}4000\text{ cm}^{-1}$  region using an ABB MB3000 FTIR spectrometer (Clairet Scientific, Northampton, UK) coupled with a 1 m polycrystalline silver halide fibre to a 30 cm long, 12 mm o.d. hastelloy bodied ATR probe with a diamond cone (Fibre Photonics Ltd, Livingston, UK). 51 co-added scans of the samples were analysed with an air or water background. Samples were equilibrated to room temperature before analysis; the probe was immersed into the sample and six repeat measurements were acquired. The probe was removed, cleaned and reinserted for analysis using the same procedure to complete two further measurements. Spectra were acquired using Horizon MB™ FTIR software version 3.0.13.1 (ABB, Canada); the spectra were exported as text files and then imported into Matlab data analysis software, where the spectra were averaged ( $n = 18$ ) before data analysis.

### 7.2.4 Data analysis

All spectral data were imported into Matlab version 7.11.0.584 (R2010b) (Mathworks Inc., Natick, MA, USA) and PLS\_Toolbox version 4.1 (Eigenvector Research Inc., WA, USA). MIR and NIR data were processed using a Savitsky-Golay first or second derivative filter, which employed a width of 15 data points and a second order polynomial. Spectra were plotted and analysed to identify regions in the data that would provide information about the samples and remove the regions that only contribute noise to the measurements.

The optical density and concentrations of glycerol and ammonium ions determined from the reference assays were used along with the average spectral data from the fermentation samples for each of the techniques to produce multivariate PLS calibration models. The PLS calibration models were constructed using different spectral regions discussed in section 7.3. Data were mean centred prior to analysis and the number of latent variables were determined for each model that produced the minimum value of the root mean square error of cross validation (RMSECV) obtained using leave-one-out cross validation; the number of latent variables selected for each model are also detailed in section 7.3.

### 7.3 Results

The seven samples collected from the batch phase of the fermentation show an increase in the optical density and a decrease in the glycerol concentration, see Figure 7.1. The ammonium ion concentration was kept constant and as such the concentration differences are much smaller between the samples. During the continuous steady state phase of the fermentation, concentrations of glycerol and ammonium ion were kept around the same level to allow the fermentation to proceed.

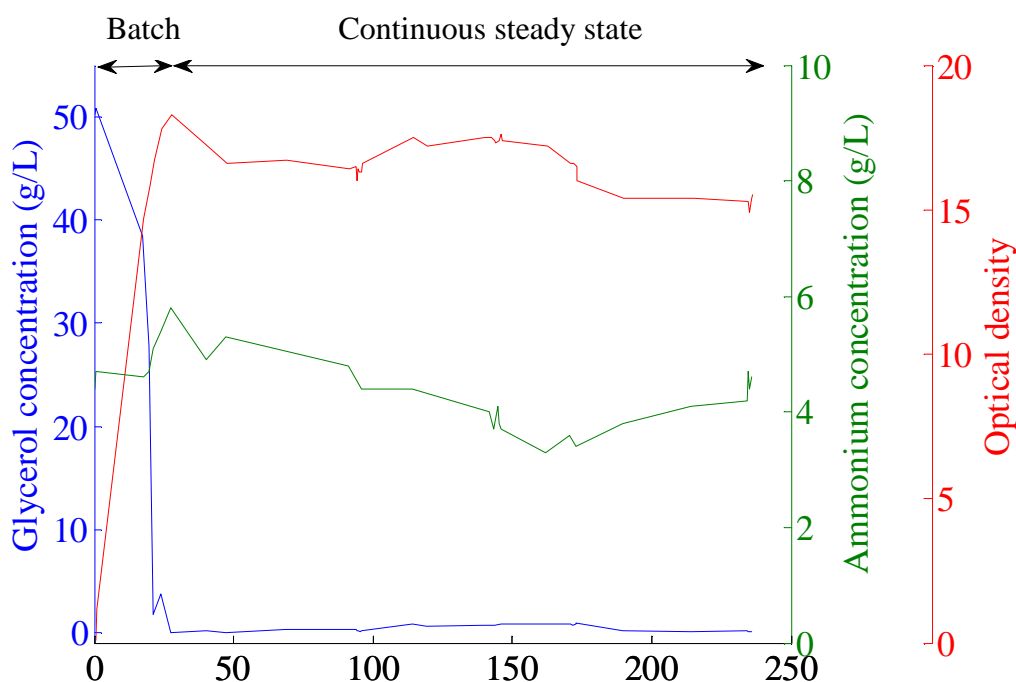


**Figure 7.1: Profile of supplied reference assay results for the fermentation reaction.**

PLS models were built to predict the optical density, glycerol and ammonium ions present in the batch phase of the fermentation reaction using the NIR and MIR spectral data (discussed further in sections 7.3.1, 7.3.2 and 7.3.3). As there were only seven samples and one reaction completed for this study, a leave one out approach was selected as the most appropriate method to obtain the predictions for the samples, whereby a model was built with all but one sample and used to predict the concentration of the sample left out. Therefore, the sample being predicted was not contained within the model building process, but all other samples were, with the exception that the samples with the lowest and highest concentrations were always

contained within the model and, therefore, these samples were not predicted. Reviewing the reference results of OD and glycerol in Table 7.1 for samples 1 – 7, there is a large change in the values between samples 2 and 3 for OD and 4 and 5 for glycerol. To generate samples with intermediate concentrations, samples were spiked with known amounts of the analyte to provide extra samples for model building that extend over the full range of concentrations. This was not possible for optical density and, therefore, only the seven fermentation broth samples were used for the model building process. As the concentrations of the samples from the continuous steady state phase were fairly similar, this allowed a selection of twelve samples to be used to spike with known concentrations of glycerol to aid PLS model building and prediction. For the glycerol predictions, the twelve spiked samples and seven batch samples were used in the model building process.

The concentrations of ammonium ion for the batch fermentation samples covered a small concentration range; this can also provide difficulties when building calibration models for prediction. To overcome this potential issue, the same samples selected for the spiking of glycerol, were also spiked with known concentrations of ammonium sulfate; this increased the total number of samples used for building the model to include the batch and spiked samples and, therefore, also widened the concentration range to improve the predictive ability of the model. Absorbance, first derivative and second derivative spectral data were used in the modelling for each analyte and compared to determine the best results.

### **7.3.1 Optical density prediction**

The overlaid NIR absorbance spectra for samples 1 – 7 are given in Figure 7.2. An increase in absorbance can be observed from sample 1 through to 7, with the largest observed increase between samples 2 and 3, consistent with the increase in optical density.

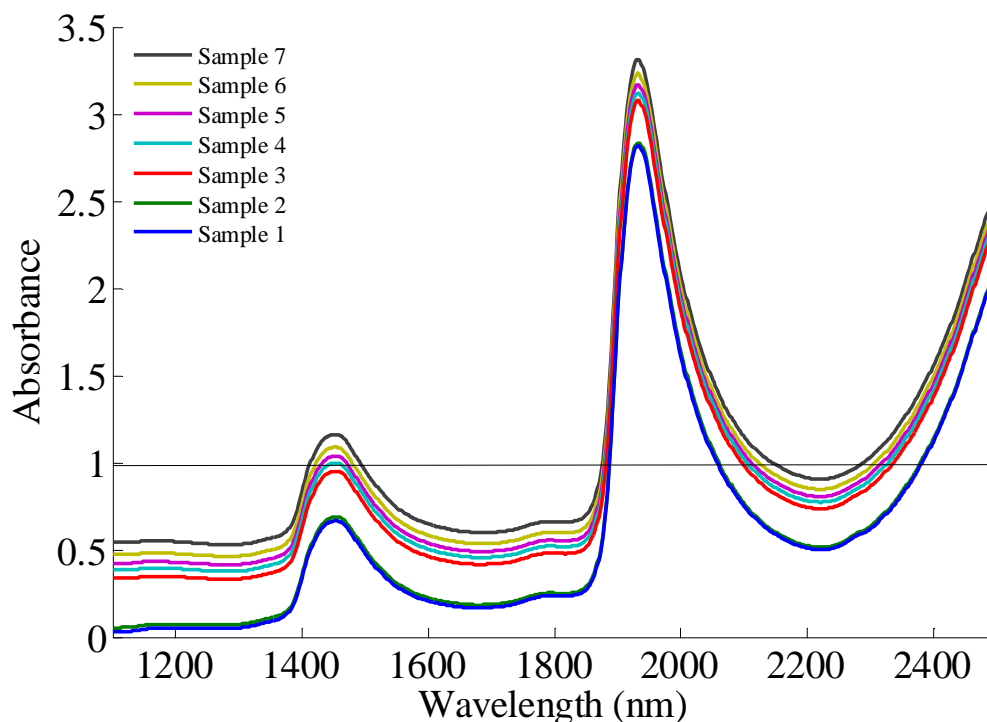


**Figure 7.2: Overlaid NIR absorbance spectra in the range 1100 – 2500 nm for samples 1 – 7 taken from fermentation reaction.**

As the change in absorbance was observed across the entire spectral region, PLS models were built to predict optical density using the largest spectral region possible. When building the PLS model, ideally the spectral areas where absorbance values are below 1.0 should be used; therefore, regions of the spectra were selected on this principle and used to build a PLS model for the prediction of optical density. The overlaid MIR absorbance spectra for samples 1 – 7 are given in Figure 7.3 and only small changes can be observed between the spectra. To build calibration models for the prediction of optical density, the same principle that was used for the NIR data was adopted for the MIR data. So, the data for the whole spectral range under an absorbance of 1.0 was included in the model, namely,  $617 - 1836 \text{ cm}^{-1}$  as shown in Figure 7.3.

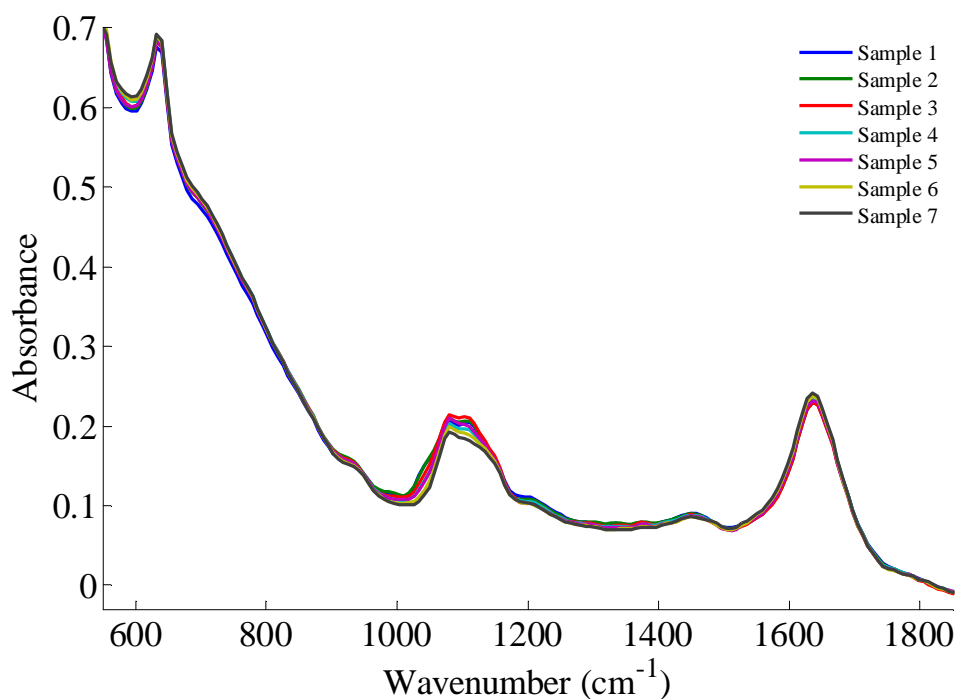


**Figure 7.3: Overlaid MIR absorbance spectra in the range 617 – 1836 cm<sup>-1</sup> for samples 1 – 7.**

Absorbance, first derivative and second derivative data were used to build models and predict the optical density of the batch samples and the results from the NIR and MIR analysis are given in Table 7.2. Using the leave one out approach, the samples with the lowest (sample 1) and highest (sample 7) values remained in the model and, therefore, were not predicted, so for optical density only samples 2 – 6 were analysed.

**Table 7.2: Results for the prediction of optical density for samples 2 – 6 for NIR and MIR spectral data.**

		NIR				MIR							
Wavelength regions used for building model (nm)		Absorbance data		1 <sup>st</sup> derivative data		2 <sup>nd</sup> derivative data		Absorbance data		1 <sup>st</sup> derivative data		2 <sup>nd</sup> derivative data	
Sample number	Measured value	Predicted value [3]*	Predicted value [3]*	Predicted value [3]*	Predicted value [3]*	Measured value	Predicted value [2]*	Predicted value [2]*	Predicted value [2]*	Predicted value [2]*	Predicted value [2]*	Predicted value [2]*	Predicted value [2]*
1	0.1	-	-	-	-	0.1	-	-	-	-	-	-	-
2	1.2	1.2	1.4	1.4	1.4	1.2	5.4	3.2	3.2	3.2	3.4	3.4	3.4
3	14.7	14.3	14.4	14.6	14.6	14.7	13.8	14.6	14.6	14.6	14.4	14.4	14.4
4	15.8	15.9	15.8	15.8	15.8	15.8	14.2	12.9	12.9	12.9	12.2	12.2	12.2
5	16.7	17	17	16.8	16.8	16.7	15.6	16.6	16.6	16.6	17.4	17.4	17.4
6	17.8	17.8	17.9	17.7	17.7	17.8	18.5	18.9	18.9	18.9	18.5	18.5	18.5
7	18.3	-	-	-	-	18.3	-	-	-	-	-	-	-
	RMSEP	0.2	0.2	0.1	0.1	RMSEP	2.1	1.6	1.6	1.6	1.9	1.9	1.9
	R <sup>2</sup> of trendline for measured vs. predicted plot	0.9989	0.999	0.9998	0.9998	R <sup>2</sup> of trendline for measured vs. predicted plot	0.9452	0.9346	0.9346	0.9346	0.9062	0.9062	0.9062

\*[Number of principal components selected for model]

The results for the prediction of optical density were good when NIR data was used, with RMSEP values of 0.2 or less and  $R^2$  values of 0.99 or greater. The predictions from the models built with the 2<sup>nd</sup> derivative data produced the best results; however, the differences between the results for each model are minimal. An example of the measured vs. predicted plot using 2<sup>nd</sup> derivative data is given in Figure 7.4 (other plots are not shown but provide similar results).

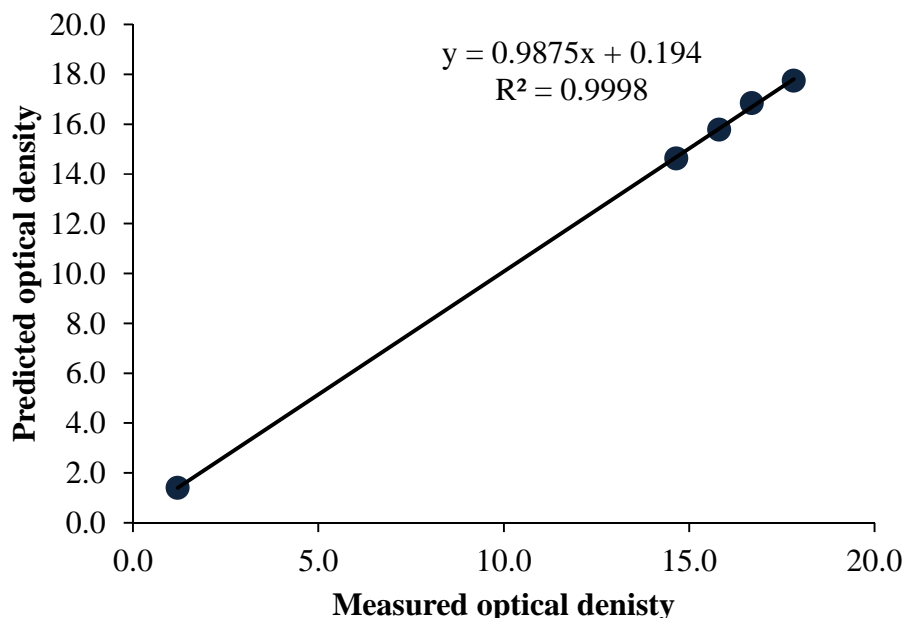


**Figure 7.4: Measured vs. predicted optical density determined using PLS model with 2<sup>nd</sup> derivative NIR data.**

The results for the prediction of optical density when MIR data was used in the model building were not as good as those obtained with the NIR data. Considering the  $R^2$  values for the MIR results in Table 7.2, absorbance and 1<sup>st</sup> derivative data provide better results for the prediction of optical density than using 2<sup>nd</sup> derivative data. The predictions for sample 2 appear to be poor for all three models for the MIR results. There are large differences in optical density between samples 2 and 3 and it is possible that the variation in the data is not well described in the model due to the small number of samples. If more samples were analysed across the range of the optical density, better results may be observed. However, unfortunately it was not possible to collect any further samples and test this theory for this data set.

### 7.3.2 Glycerol concentration prediction

For the predictions of glycerol concentration from NIR data, specific regions of the spectra were selected where changes in glycerol may be found and they are listed in Table 7.3.

**Table 7.3: Assignment of regions where bands associated with glycerol may appear in NIR.**

Region number	Functional group	Approximate wavelength region (nm)	Comments
1	CH	1175 – 1225	2 <sup>nd</sup> overtone band
2	CH	1425 – 1475	1 <sup>st</sup> overtone of combination band
3	CH	1680 – 1775	1 <sup>st</sup> overtone band
4	CH	2275 – 2445	Combination band
5	CH <sub>2</sub>	1145 – 1220	2 <sup>nd</sup> overtone band
6	CH <sub>2</sub>	1390 – 1440	1 <sup>st</sup> overtone of combination band
7	CH <sub>2</sub>	1675 – 1750	1 <sup>st</sup> overtone band
8	CH <sub>2</sub>	2250 – 2415	Combination band
9	OH	1410 – 1475	1 <sup>st</sup> overtone band
10	OH	2060 – 2090	Combination band

Region numbers 2, 6, 9 and 10 will all be masked by strong water bands, therefore, the ranges selected to build models for the prediction of glycerol included the region numbers 1, 3-5 and 7-8. Some changes in the regions selected were observed as indicated in Figure 7.5 and Figure 7.6 for first and second derivative data, respectively; noticeable changes were also noted in the range 2198 – 2398 nm for the second derivative data (not shown).

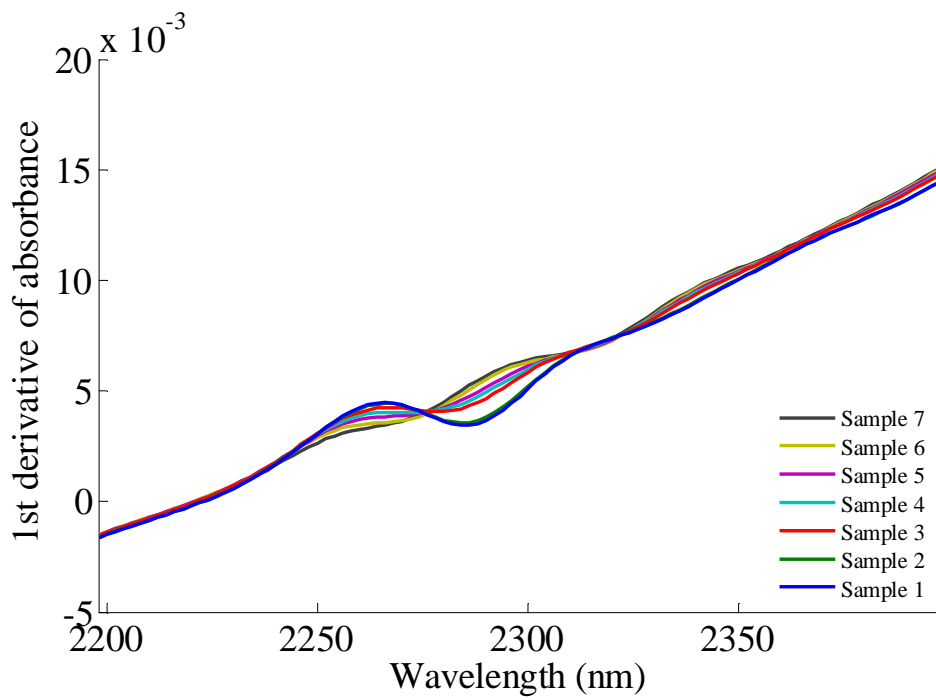


Figure 7.5: Overlaid NIR 1<sup>st</sup> derivative of absorbance spectra in the range 2198 – 2398 nm for samples 1 – 7 taken from fermentation reaction, used for prediction of glycerol concentration.

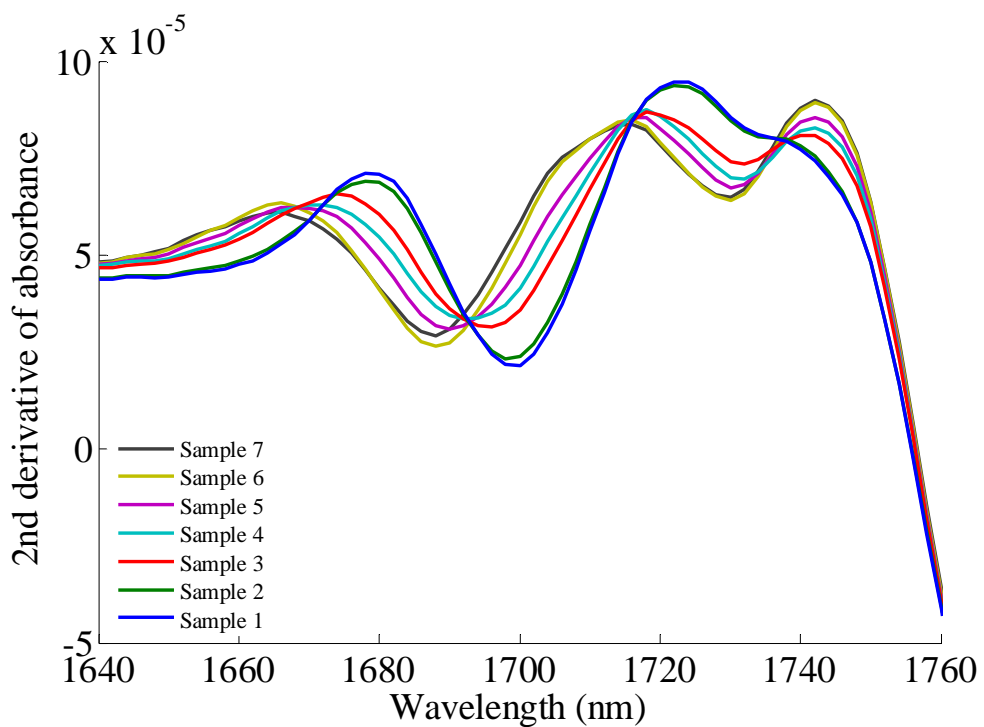
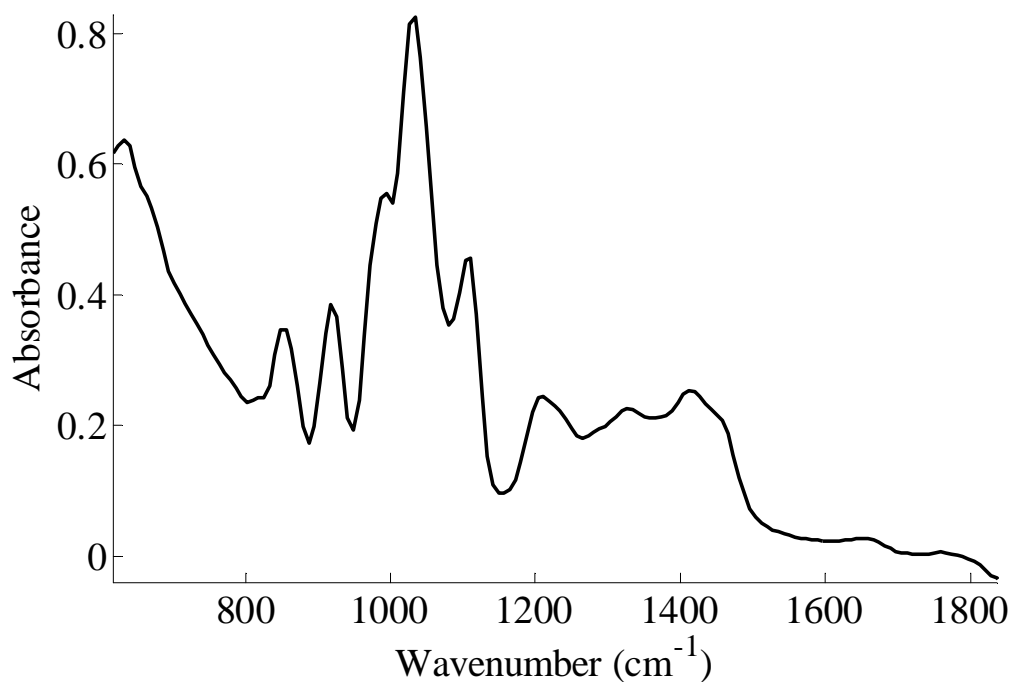


Figure 7.6: Overlaid NIR 2<sup>nd</sup> derivative of absorbance spectra in the range 1640 – 1760 nm for samples 1 – 7 taken from fermentation reaction, used for prediction of glycerol concentration.

To determine where glycerol bands occur in the MIR region, the spectra of pure glycerol was acquired, see Figure 7.7.



**Figure 7.7: ATR MIR absorbance spectra of pure glycerol in the range 617 – 1836 cm<sup>-1</sup>.**

Overlaying a spectrum of pure glycerol and sample 1, see Figure 7.8, only small regions can be associated with glycerol in the broth samples. The main reason for this is that the intensity of the glycerol bands reduce significantly when dissolved in water, also many of the bands of glycerol are masked by the broad band of sulfate from the ammonium sulfate present in the samples. Only one free glycerol band in the range 1304 – 1512 cm<sup>-1</sup>, due to the CH deformations of the CH<sub>2</sub>, could be observed and was used to build the calibration model (see Figure 7.8).

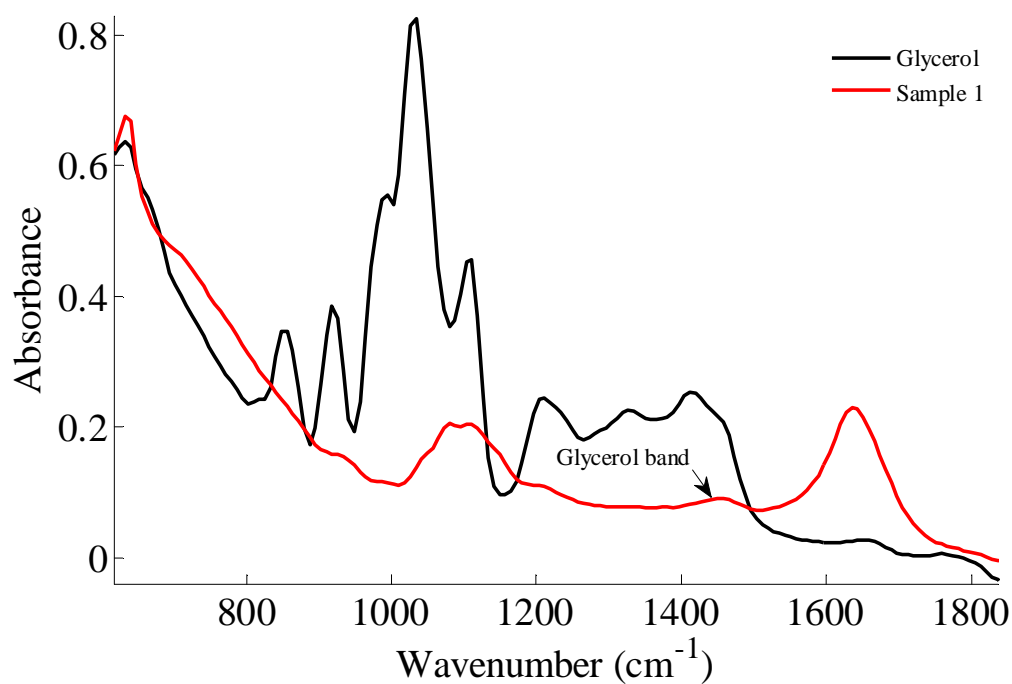


**Figure 7.8: Overlaid ATR MIR absorbance spectra in the range 617 – 1836  $\text{cm}^{-1}$  of glycerol and fermentation broth sample 1.**

A similar scenario existed for the glycerol concentration as that for the optical density: there are a few samples at lower concentrations and then a large gap where higher concentrations are observed. To compensate for the lack of a range of concentrations and aid the development of the models for prediction, twelve continuous steady state samples spiked with known concentrations of glycerol were analysed by NIR and MIR spectrometry and used in the model building process. Using the leave one out approach, one sample was left out and the other eighteen samples (batch and spiked samples) included in the model building. The samples with the lowest and highest concentration for the glycerol models were respectively, sample 7 from the batch phase and sample 15, a sample with spiked glycerol concentration. These two samples always remained in the model and so this allowed the prediction of the rest of the samples. Absorbance, first derivative and second derivative data were used to build models and predict the glycerol concentration of the batch samples (samples 1 – 6) and the results from the NIR and MIR analysis are given in Table 7.4. Predictions for the remaining spiked samples (samples 8-14 and 16-19) were also predicted during the analysis; the predicted results for these samples are not shown, however, for NIR analysis the RMSEP values were less than

3.5 g/L and the  $R^2$  values of the trendlines for the measured vs. predicted plots were 0.95 or greater; for MIR analysis the RMSEP values were less than 4.8 g/L and the  $R^2$  values of the trendlines for the measured vs. predicted plots were 0.91 or greater.

**Table 7.4: Results for the prediction of glycerol concentration for samples 1 – 6 for NIR and MIR spectral data.**

		NIR				MIR			
Wavelength regions used for building model (nm)		Absorbance data	1 <sup>st</sup> derivative data	2 <sup>nd</sup> derivative data	Wavenumber region used for building model (cm <sup>-1</sup> )	Absorbance data	1 <sup>st</sup> derivative data	2 <sup>nd</sup> derivative data	
1178 – 1226, 1640 – 1760, 2198 – 2398					1304 – 1512				
Sample number	Measured concentration (g/L)	Predicted concentration (g/L) [6]*	Predicted concentration (g/L) [4]*	Predicted concentration (g/L) [4]*	Measured concentration (g/L)	Predicted concentration (g/L) [5]*	Predicted concentration (g/L) [7]*	Predicted concentration (g/L) [7]*	Predicted concentration (g/L) [7]*
1	50.2	52.5	53.2	52.5	50.2	56	52.7	50.7	50.7
2	50.8	50	50.4	48.6	50.8	52.3	51.9	53.7	53.7
3	38.4	34.1	32.8	35.2	38.4	33.5	32.4	30	30
4	27.7	25.1	24.1	24.6	27.7	21.3	25	25	25
5	4.4	15.6	15	14.6	4.4	16.1	11.3	13	13
6	3.8	2.1	2.2	2.4	3.8	1.8	3.4	2.4	2.4
7	0	-	-	-	0	-	-	-	-
RMSEP		5.2	5.3	4.8	RMSEP	6.3	4	4	5.2
R <sup>2</sup> of trendline for measured vs. predicted plot		0.9321	0.9269	0.943	R <sup>2</sup> of trendline for measured vs. predicted plot	0.8979	0.957	0.9282	0.9282

\*[Number of principal components selected for model]

Overall the results for the prediction of glycerol are reasonable. For NIR analysis, 2<sup>nd</sup> derivative data gave the best results, whereas, it was 1<sup>st</sup> derivative data that produced the best results for MIR analysis. When reviewing the predictions for each individual batch sample it is apparent that the prediction for sample 5 is very poor for both the NIR and MIR regions. The NIR and MIR spectra for this sample do not appear different to the other samples and so at this stage it is unclear why this prediction is poorer than the rest.

If sample 5 is removed from the data set entirely and the leave one out approach completed again to build calibration models and predict the concentration of glycerol then the RMSEP values are reduced and the  $R^2$  values move closer to unity, see Table 7.5. This indicates that PLS models built on the selected spectral regions show promise for future predictions of glycerol concentrations in fermentation samples. The predictions from the models built with absorbance, 1<sup>st</sup> derivative and 2<sup>nd</sup> derivative data provided comparable results when NIR data were used, however, for the MIR spectra better results were obtained if 1<sup>st</sup> derivative data were used.

**Table 7.5: Results for the prediction of glycerol concentration for samples 1-4 and 6 for NIR and MIR spectral data.**

		NIR				MIR			
Wavelength regions used for building model (nm)		Absorbance data	1 <sup>st</sup> derivative data	2 <sup>nd</sup> derivative data	Wavenumber region used for building model (cm <sup>-1</sup> )	Absorbance data	1 <sup>st</sup> derivative data	2 <sup>nd</sup> derivative data	
1178 – 1226, 1640 – 1760, 2198 – 2398					1304 – 1512				
Sample number	Measured concentration (g/L)	Predicted concentration (g/L) [6]*	Predicted concentration (g/L) [7]*	Predicted concentration (g/L) [5]*	Measured concentration (g/L)	Predicted concentration (g/L) [5]*	Predicted concentration (g/L) [7]*	Predicted concentration (g/L) [4]*	
1	50.2	52.2	51.1	51.6	50.2	54.0	50.8	50.3	
2	50.8	49.4	49.8	49.0	50.8	53.7	52.7	55.6	
3	38.4	37.7	38.0	39.2	38.4	39.0	37.4	40.1	
4	27.7	28.7	28.6	27.6	27.7	23.5	25.2	22.7	
6	3.8	5.4	4.2	4.3	3.8	5.1	6.3	7.0	
7	0	-	-	-	0	-	-	-	
RMSEP		1.4	0.7	1.1	RMSEP	2.7	1.7	3.2	
R <sup>2</sup> of trendline for measured vs. predicted plot		0.9952	0.9984	0.9963	R <sup>2</sup> of trendline for measured vs. predicted plot	0.9816	0.9889	0.9653	

\*[Number of principal components selected for model]

### 7.3.3 Ammonium ion concentration prediction

For the predictions of the ammonium ion concentration, specific parts of the NIR spectra were selected based on regions that could be associated with the ammonium ions, as indicated in Table 7.6.

**Table 7.6: Assignment of regions where bands associated with the ammonium ions may appear in NIR.**

Region number	Functional group	Approximate wavelength region (nm)	Comments
1	NH	1480 – 1520	1 <sup>st</sup> overtone band
2	NH	2120 – 2210	Combination band

When considering the spectra, it is likely that the 1<sup>st</sup> overtone N-H band will be masked by water, therefore, PLS models were built on region 2 only; where small changes could be observed (see Figure 7.9).

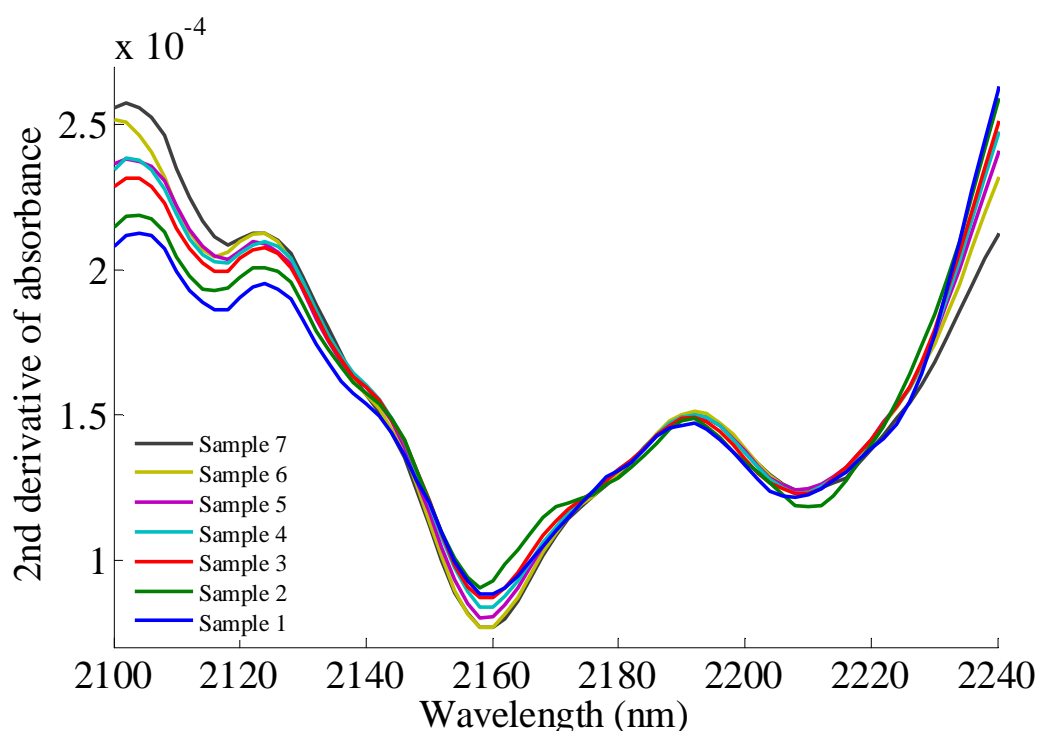


**Figure 7.9: Overlaid NIR 2<sup>nd</sup> derivative of absorbance spectra in the range 2100 – 2240 nm for samples 1 – 7 taken from fermentation reaction, used for prediction of ammonium ion concentration.**

Unfortunately in the MIR region, the N-H bands for the ammonium ions were masked by the water peaks and as such the ammonium ion concentration could not be determined when an air background was used, as was employed for all other predictions. However, reviewing the spectra of a sample spiked with a known concentration of ammonium sulfate when a water background was used, the N-H bend could be observed, see Figure 7.10.

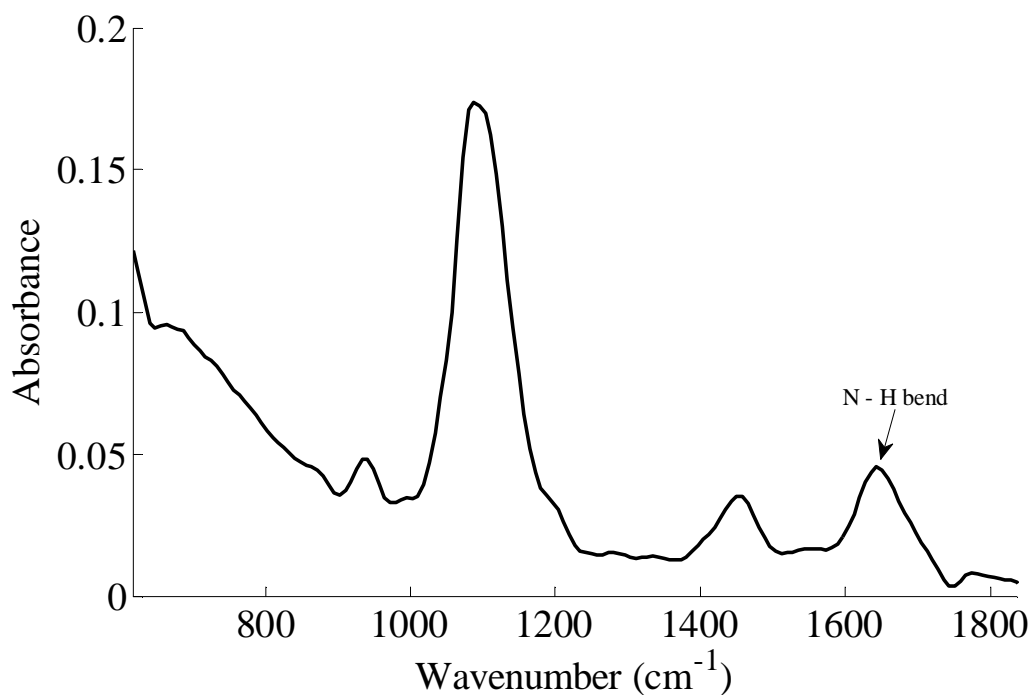


**Figure 7.10: ATR MIR absorbance spectra in the range 617 – 1836 cm<sup>-1</sup> of spiked sample 8 when a water background was used.**

Looking at the spectra of the seven batch samples in this selected region, small changes can be observed; see Figure 7.11 for the changes in the second derivative data of the batch samples.

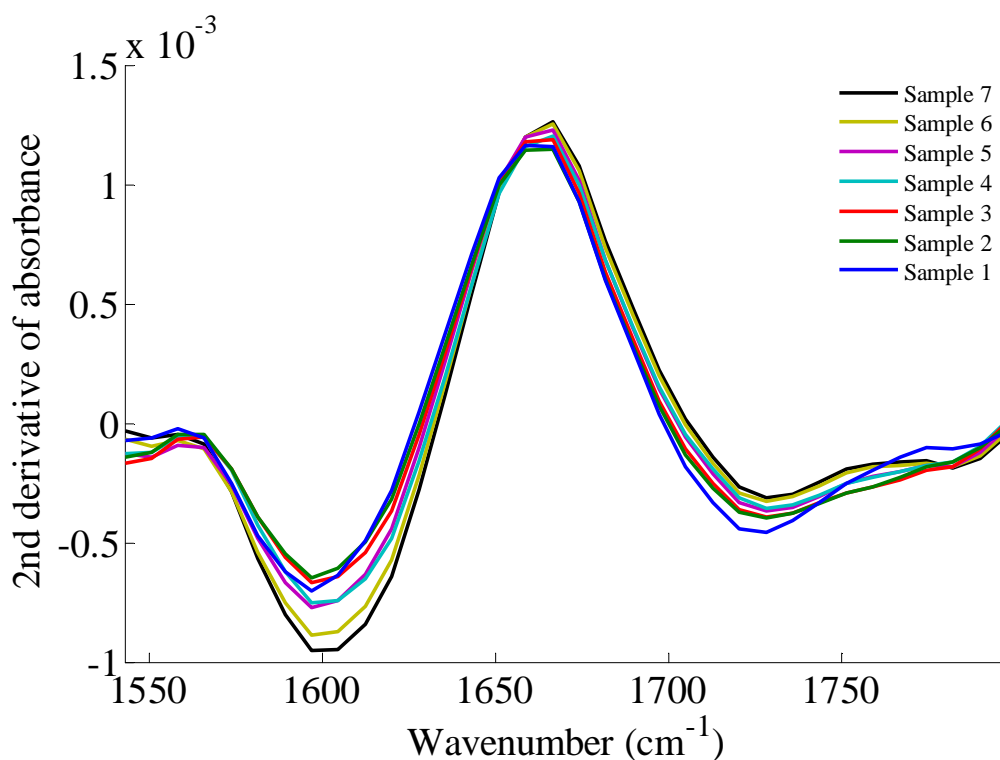


**Figure 7.11: Overlaid MIR 2<sup>nd</sup> derivative of absorbance spectra in the range 1543 – 1798 cm<sup>-1</sup> for samples 1 – 7 taken from fermentation reaction, used for prediction of ammonium ion concentration.**

As the concentration of ammonium ions changed over a small range (between 4.4 and 5.8 g/L) the twelve spiked samples used for the glycerol concentration predictions were also spiked with known amounts of ammonium sulfate to widen the concentration range (between 4.4 and 9.2 g/L). As before, a leave one out approach was used and the samples with the lowest and highest concentration of ammonium ions always remained in the model (spiked samples 18 and 11, respectively). The concentrations of ammonium ions in batch samples 1-7 and spiked samples 8-10, 12-17 and 19 were predicted using absorbance, first derivative and second derivative NIR or MIR data and the results are given in Table 7.7 for the batch samples.

**Table 7.7: Results for the prediction of ammonium for samples 1 – 7 for NIR and MIR spectral data.**

		NIR				MIR			
Sample number	Wavelength region used for building model (nm)	Absorbance data		1 <sup>st</sup> derivative data		2 <sup>nd</sup> derivative data		Wavenumber region used for building model (cm <sup>-1</sup> )	
		Measured concentration (g/L)	Predicted concentration (g/L) [5]*	Measured concentration (g/L)	Predicted concentration (g/L) [5]*	Measured concentration (g/L)	Predicted concentration (g/L) [5]*	Measured concentration (g/L)	Predicted concentration (g/L) [5]*
	2100 – 2240								
1	4.4	4.6	4.5	4.3	4.4	4.6	4.7	4.7	4.7
2	4.7	4.4	4.5	4.8	4.7	4.5	4.7	4.7	4.7
3	4.6	4.7	4.7	4.7	4.6	4.6	4.7	4.7	4.8
4	4.7	4.9	5	4.7	4.7	5	4.7	5	4.9
5	5.1	5	5.1	5.2	5.1	4.9	4.7	4.7	5.1
6	5.4	5.2	5.3	5.5	5.4	5.4	5.3	5.3	5.4
7	5.8	5.8	5.7	5.6	5.8	5.7	5.6	5.6	5.4
	RMSEP	0.2	0.1	0.1	RMSEP	0.2	0.2	0.2	0.2
	R <sup>2</sup> of trendline for measured vs. predicted plot	0.8751	0.9229	0.9399	R <sup>2</sup> of trendline for measured vs. predicted plot	0.878	0.7672	0.878	0.9421

\*[Number of principal components selected for model]

The results for the prediction of ammonium ions seem acceptable for the fed batch samples. For both the NIR and the MIR data, the RMSEP values were low for all models. Predictions from models built with 2<sup>nd</sup> derivative data produced better R<sup>2</sup> values for the trendline of the measured concentrations vs. the predicted concentrations of the batch samples. When the predicted concentrations of the batch and spiked samples were considered the RMSEP and R<sup>2</sup> values for NIR analysis improved, see Table 7.8. However, for the MIR data no improvement was obtained, and little correlation between measured and predicted concentrations could be determined.

**Table 7.8: Comparison of RMSEP and R<sup>2</sup> values for prediction of ammonium ion concentration for selected samples using NIR data.**

	Batch samples (1-7)			Batch and spiked samples (1-10, 12-17 and 19)		
	Absorbance	1 <sup>st</sup> derivative data	2 <sup>nd</sup> derivative data	Absorbance	1 <sup>st</sup> derivative data	2 <sup>nd</sup> derivative data
RMSEP	0.2	0.1	0.1	0.1	0.1	0.1
R <sup>2</sup> value	0.8751	0.9229	0.9399	0.9902	0.9943	0.9932

These results suggest that the selected region of the NIR spectra may be suitable for the prediction of ammonium ion concentration. Further work is required with larger data sets to determine if the selected region of the MIR spectra can provide accurate predictions of ammonium ion concentrations.

Overall, PLS calibration models were used to successfully predict the optical density and concentrations of glycerol and ammonium ions from NIR data and predict the concentration of glycerol using MIR data.

#### **7.3.4 Combination of MIR and NIR data for the prediction of glycerol**

Examples of data fusion to improve the predictions of analytes have been discussed in section 7.1.2. The results obtained so far for this study have shown that calibration models built from MIR or NIR data can be used for the prediction of glycerol concentrations. However, it may be possible to observe some improvements of the predictions of glycerol concentrations if the MIR and NIR data are fused together. The predictions of glycerol concentrations using each technique separately suggested using first derivative MIR data provided better results, whereas, absorbance, first derivative and second derivative NIR data provided comparable results. Therefore, as an initial investigation into the use of fused data for the prediction of glycerol concentrations, the first derivative data of MIR and NIR regions were concatenated into one data matrix. As the scales were similar to one another, the data could be fused directly with no other pre-treatment. The concatenated data matrix was then used with the glycerol reference data for the batch and spiked samples using the leave one out approach to predict the concentrations of glycerol in the samples. The lowest (sample 7) and the highest (sample 15) concentrations always remained in the model, allowing the prediction of the glycerol concentrations in the batch and spiked samples (samples 1-4, 6, 8-14 and 16-19). For reasons discussed previously in section 7.3.2, sample 5 was left out of this process. The results from the combined data are given in Table 7.9 alongside the results for the predictions of glycerol when MIR and NIR data were used individually.

**Table 7.9: Results for the prediction of glycerol for samples 1-4, 6, 8-14 and 16-19 using fused MIR (1304 – 1512 cm<sup>-1</sup>) and NIR (1178-1226, 1640-1760 and 2198-2398 nm) data.**

Sample number	Measured concentration (g/L)	MIR 1 <sup>st</sup> derivative data	NIR 1 <sup>st</sup> derivative data	Fused MIR and NIR 1 <sup>st</sup> derivative data
		Predicted concentration (g/L) [7]*	Predicted concentration (g/L) [7]*	Predicted concentration (g/L) [6]*
1	50.2	50.8	51.1	51.4
2	50.8	52.7	49.8	49.5
3	38.4	37.4	38.0	38.5
4	27.7	25.2	28.6	27.1
5	4.4	-	-	-
6	3.8	6.3	4.2	5.1
7	0.0	-	-	-
8	26.0	24.0	26.9	26.6
9	20.4	25.4	19.7	20.1
10	51.2	48.6	51.0	51.3
11	38.7	38.2	37.6	37.4
12	38.0	39.1	39.4	39.9
13	3.2	4.0	4.0	3.4
14	26.3	28.2	26.5	26.5
15	52.7	-	-	-
16	14.3	12.8	14.4	13.2
17	22.4	19.0	21.0	21.3
18	13.6	14.4	12.1	14.3
19	1.6	1.8	2.5	1.9
	RMSEP	2.1	0.9	0.9
	R <sup>2</sup> of trendline for measured vs. predicted plot	0.9826	0.9975	0.997

\*[Number of principal components selected for model]

Reviewing the prediction of the glycerol concentrations given in Table 7.9 the overall RMSEP and  $R^2$  results for the fused data are comparable to those obtained with the NIR data individually; the MIR data gave poorer results. This suggests the possibility that the model may be weighted more by the NIR data and hence the reason for the similar results. However, when the predictions for each sample are studied, some of the predictions are improved when compared to the NIR results, suggesting that the fused data does influence the predictions. To ascertain if the PLS model is dominated by the NIR data, the regression coefficients were plotted against the variable number, see Figure 7.12.

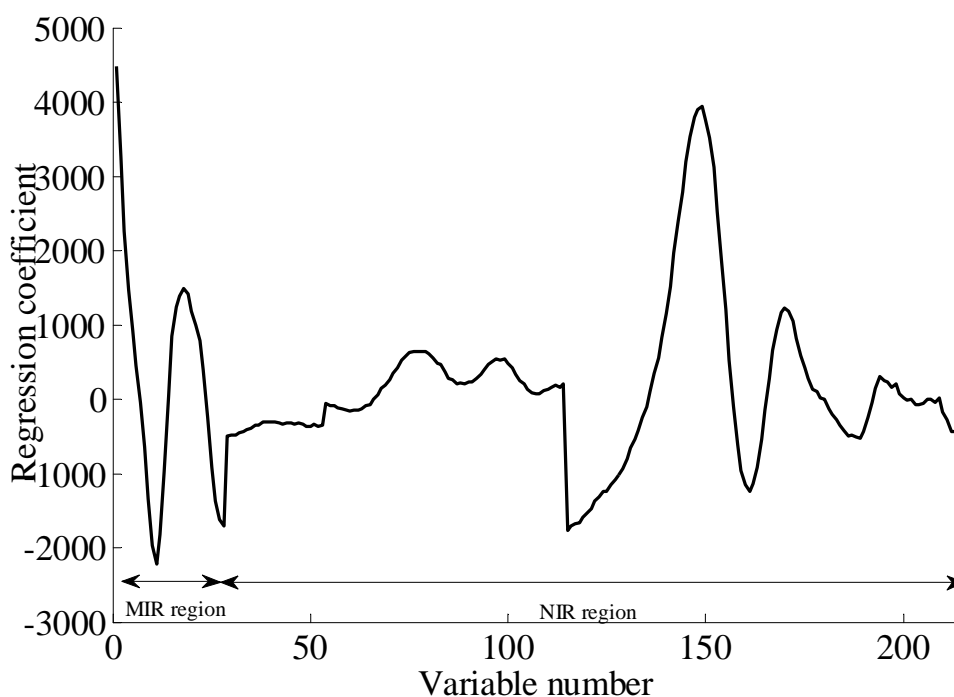


**Figure 7.12: Regression coefficients for the PLS model built with the fused MIR and NIR data.**

Reviewing the regression coefficients for the PLS model using the fused data, the MIR and NIR regions are both clearly used in the model and will contribute to the overall predictions. The regression coefficients for the combined PLS model were compared with the regression coefficients of the individual MIR and NIR PLS models, see Figure 7.13 and Figure 7.14, respectively.

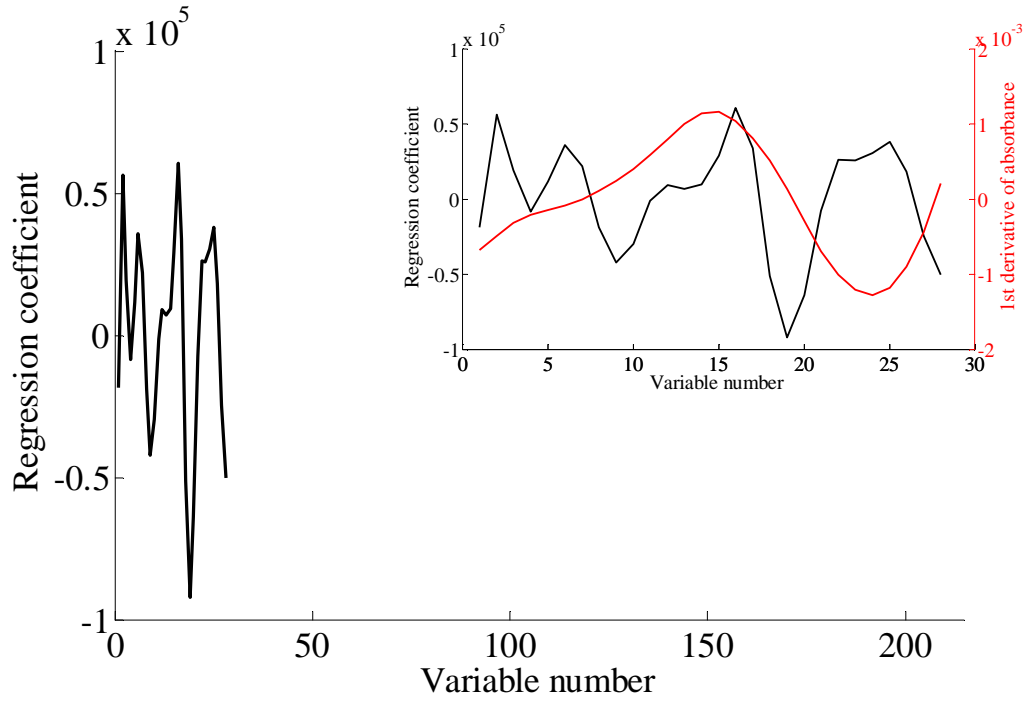


**Figure 7.13: Regression coefficients for the PLS model built with only the MIR data; subplot displays overlaid regression coefficient and 1<sup>st</sup> derivative of absorbance data for sample 1.**

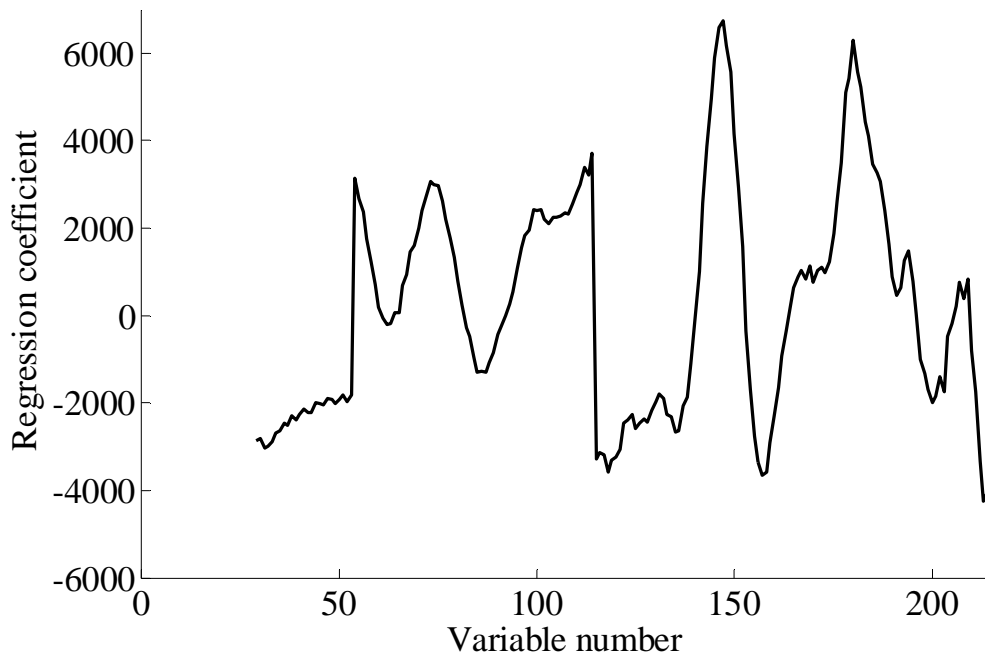


**Figure 7.14: Regression coefficients for the PLS model built with only the NIR data.**

The regression coefficients for the PLS model built with only NIR data are similar to the regression coefficients for the NIR region for the PLS model built with the fused data, suggesting that both calibration models are similar for the NIR region. The regression coefficients for the PLS model built with only MIR data, however, are different from the regression coefficients for the MIR region of the PLS model built with the fused data. If the regression coefficients from the PLS models for the MIR regions are compared with a spectrum of a fermentation sample (Figure 7.15), then the regression coefficients for the PLS model built with only MIR data (Figure 7.13) appear to describe noise, whereas, the regression coefficients for the PLS model from the fused data (subplot of Figure 7.15) are more similar to a spectrum of a fermentation sample, demonstrating an anti-correlated relationship, although it is slightly shifted.

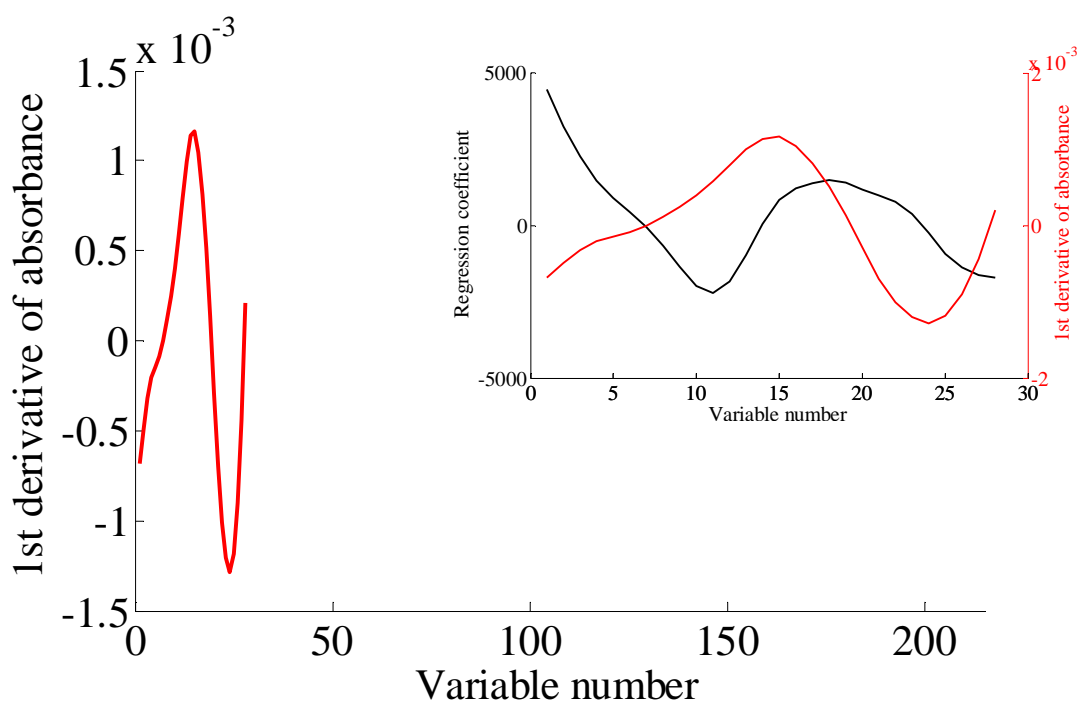


**Figure 7.15: First derivative of absorbance spectrum of a batch fermentation sample (sample 1), subplot displays overlaid regression coefficient of MIR region of fused data from Figure 7.12 and 1<sup>st</sup> derivative of absorbance data for sample 1.**

These results suggest that by fusing the data together and building a PLS model on the combined MIR and NIR data, the NIR region has helped to improve the MIR calibration in the fused data model. The MIR data, which provided slightly poorer results, did not degrade the NIR calibration. Overall, the results from the fused data were comparable with the NIR results and improved on the MIR results indicating the potential for data fusion to aid in model building. Future investigation of the benefits of fusing spectral data may best concentrate on examples where MIR and NIR data provide alternative complementary information about a process.

## 7.4 Conclusions

Both NIR and MIR spectrometry have been used to varying degrees of success to analyse and predict the optical density and the concentrations of glycerol and ammonium ions in batch fermentation samples. As there was only a small number of samples from the batch phase, samples from the continuous steady state phase were spiked with known amounts of glycerol and ammonium sulfate to aid the predictions of the concentrations of these substrates.

For the predictions of optical density, the results were better when NIR data were used in comparison to MIR data, however, it may be possible to improve the MIR predictions if more samples were available. Based on the results at this stage, indications are that NIR spectrometry may be more suitable for the prediction of optical density. There were only small differences between the predictions when absorbance, first derivative or second derivative data were used in the model, indicating the use of absorbance data in model building may provide acceptable results.

For the glycerol concentration predictions, sample 5 was poorly predicted by either NIR or MIR spectrometry. When sample 5 was removed from the calibration, the overall predictions were improved. For the MIR region, 1<sup>st</sup> derivative data provided the best results, whereas, for the NIR region, 2<sup>nd</sup> derivative data produced the best results; however, the differences between each model were minimal. This can be explained by the baseline offset of the spectra; there was a greater offset in the NIR data than the MIR data. Therefore, taking the 1<sup>st</sup> derivative of the MIR spectral data removed the majority of any baseline offset; however, NIR data required the 2<sup>nd</sup> derivative to further remove the effect of sloping baseline offsets. The predicted glycerol concentrations are comparable for MIR and NIR data; indicating the possibility of either or both techniques being used for the determination of glycerol.

The prediction of ammonium ion concentration was more difficult than for glycerol and optical density, as the water in the fermentation sample masks most of the bands associated with the ammonium ions. For NIR spectra, a small region was determined

where the N-H combination band may be found, however, only small changes were observed, even when reviewing the spectra of the samples spiked with a higher ammonium ion concentration. In spite of this, it was still possible to obtain reasonable predictions for the concentration of ammonium ions using NIR spectra, with the best results produced when second derivative data were used. In contrast, in the MIR region the N-H band is masked substantially by water, therefore, predictions cannot be obtained when using an air background. To overcome this, a water background was used, revealing the N-H band. As with NIR spectrometry, only small changes could be observed between the spectra and the results produced using MIR data were very poor if all samples (batch and spiked) were assessed; if only the batch samples are considered then the predictions appear better. Comparing the results obtained from the NIR and MIR regions, the NIR data may provide better models for the predictions of ammonium ion concentration.

Based on the results from this study, there may be some potential for the combination of the two techniques in one probe for the prediction of the concentration of the three properties discussed. Simplistically, the combination of transmission NIR and ATR MIR spectrometry into one probe would allow the spectra in each region to be acquired simultaneously at the same point in the reactor. The NIR absorbance and derivative data could be used to monitor the optical density and ammonium ion concentration, respectively, of the fermentation broth as the reaction progressed and derivative data of either NIR or MIR could be used for the prediction of glycerol concentrations. As NIR spectrometry can be used solely for the determination of the three properties it is plausible to suggest that using only an *in situ* NIR probe would provide satisfactory information. However, these results are based purely on off-line samples and the effects of agitation and aeration on the ability of NIR models to provide reasonable results have been discussed in the literature. ATR MIR spectrometry is not affected by agitation and aeration to the same extent as transmission NIR spectrometry; therefore, the combination of the two techniques could overcome any potential issues that may arise from *in situ* analysis. To be able to predict the concentrations of ammonium ions by NIR spectrometry *in situ*, the probe must contain silica fibres that allow analysis in the range between 2000 –

2500 nm. In addition, any probe used for *in situ* analysis of fermentation samples is required to be sterilised with the reactor, therefore, the combined probe design would have to incorporate this requirement. Polycrystalline silver halide fibres are produced through an extrusion process at around 180°C and, therefore, once the fibres are extruded they cannot be exposed to these temperatures or the fibres will degrade. Consequently, the fibres must be protected from prolonged exposure to high temperatures to permit sterilisation. If a combined probe were developed for *in situ* fermentation analysis benefits may be realised for some substrates through fusion of the two spectral data sets, especially if the contributions to the quantification by each technique were complementary.

## 7.5 References

1. B. McNeil and L. M. Harvey, *Practical fermentation technology*, John Wiley & Sons, Chichester, England 2008.
2. V. Vojinović, J. M. S. Cabral and L. P. Fonseca, *Sensor. Actuat. B-Chem.*, 2006, **114**, 1083-1091.
3. S. Beutel and S. Henkel, *Appl. Microbiol. Biotechnol.*, 2011, **91**, 1493-1505.
4. P. Roychoudhury, L. M. Harvey and B. McNeil, *Anal. Chim. Acta*, 2006, **571**, 159-166.
5. A. E. Cervera, N. Petersen, A. E. Lantz, A. Larsen and K. V. Gernaey, *Biotechnol. Progr.*, 2009, **25**, 1561-1581.
6. S. A. Arnold, L. M. Harvey, B. McNeil and J. W. Hall, in BioPharm International, Advanstar Communications, Inc., 2002, <http://biopharminternational.findpharma.com/biopharm/data/articlestandard/biopharm/472002/38556/article.pdf>, Accessed 04/10/2011.
7. M. Scarff, S. A. Arnold, L. M. Harvey and B. McNeil, *Crit. Rev. Biotechnol.*, 2006, **26**, 17-39.
8. G. Macaloney, J. W. Hall, M. J. Rollins, I. Draper, B. G. Thompson and B. McNeil, *Biotechnol. Tech.*, 1994, **8**, 281-286.
9. T. Yano, T. Aimi, Y. Nakano and M. Tamai, *J. Ferment. Bioeng.*, 1997, **84**, 461-465.
10. S. A. Arnold, L. Matheson, L. M. Harvey and B. McNeil, *Biotechnol. Lett.*, 2001, **23**, 143-147.
11. J. Crowley, S. A. Arnold, N. Wood, L. M. Harvey and B. McNeil, *Enzyme Microb. Technol.*, 2005, **36**, 621-628.
12. S. A. Arnold, J. Crowley, S. Vaidyanathan, L. Matheson, P. Mohan, J. W. Hall, L. M. Harvey and B. McNeil, *Enzyme Microb. Technol.*, 2000, **27**, 691-697.
13. S. Vaidyanathan, S. A. Arnold, L. Matheson, P. Mohan, B. McNeil and L. M. Harvey, *Biotechnol. Bioeng.*, 2001, **74**, 376-388.
14. A. González-Vara y R., G. Vaccari, E. Dosi, A. Trilli, M. Rossi and D. Matteuzzi, *Biotechnol. Bioeng.*, 2000, **67**, 147-156.
15. S. A. Arnold, J. Crowley, N. Woods, L. M. Harvey and B. McNeil, *Biotechnol. Bioeng.*, 2003, **84**, 13-19.
16. S. A. Arnold, R. Gaensakoo, L. M. Harvey and B. McNeil, *Biotechnol. Bioeng.*, 2002, **80**, 405-413.
17. E. Petiot, P. Bernard-Moulin, T. Magadoux, C. Gény, H. Pinton and A. Marc, *Process Biochem.*, 2010, **45**, 1832-1836.
18. T. Strother, in *Spectrosc. Eur.*, J Wiley & IM Publications, 2011, vol. 23, Issue 3 [http://www.spectroscopyeurope.com/images/stories/ArticlePDFs/NIR\\_23\\_3.pdf](http://www.spectroscopyeurope.com/images/stories/ArticlePDFs/NIR_23_3.pdf), Accessed 04/10/2011.
19. B. Liebmann, A. Friedl and K. Varmuza, *Anal. Chim. Acta*, 2009, **642**, 171-178.
20. P. Roychoudhury, R. O'Kennedy, B. McNeil and L. M. Harvey, *Anal. Chim. Acta*, 2007, **590**, 110-117.

21. N. Petersen, P. Ödman, A. E. C. Padrell, S. Stocks, A. E. Lantz and K. V. Gernaey, *Biotechnol. Progr.*, 2010, **26**, 263-271.
22. J. Reed and A. N. Davies, in Tony Davies Column, Spectroscopy Europe, J Wiley & IM Publications, 2011, vol. 23, Issue 3 [http://www.spectroscopyeurope.com/images/stories/ColumnPDFs/TD\\_23\\_3.pdf](http://www.spectroscopyeurope.com/images/stories/ColumnPDFs/TD_23_3.pdf), Accessed 04/10/2011.
23. A. Nordon, D. Littlejohn, A. S. Dann, P. A. Jeffkins, M. D. Richardson and S. L. Stimpson, *Analyst*, 2008, **133**, 660-666.
24. J. Crowley, B. McCarthy, N. S. Nunn, L. M. Harvey and B. McNeil, *Biotechnol. Lett*, 2000, **22**, 1907-1912.
25. P. Fayolle, D. Picque and G. Corrieu, *Vib. Spectrosc.*, 1997, **14**, 247-252.
26. V. G. Franco, J. C. Perín, V. E. Mantovani and H. C. Goicoechea, *Talanta*, 2006, **68**, 1005-1012.
27. A. Hashimoto, A. Yamanaka, M. Kanou, K. Nakanishi and T. Kameoka, *Bioproc. Biosyst. Eng.*, 2005, **27**, 115-123.
28. M. Cavagna, R. Dell'Anna, F. Monti, F. Rossi and S. Torriani, *J. Agric. Food. Chem.*, 2009, **58**, 39-45.
29. M. Kansiz, H. Billman-Jacobe and D. McNaughton, *Appl. Environ. Microbiol.*, 2000, **66**, 3415-3420.
30. S. Sivakesava, J. Irudayaraj and A. Demirci, *J. Ind. Microbiol. Biotechnol.*, 2001, **26**, 185-190.
31. S. Macauley-Patrick, S. A. Arnold, B. McCarthy, L. M. Harvey and B. McNeil, *Biotechnol. Lett*, 2003, **25**, 257-260.
32. P. Roychoudhury, L. M. Harvey and B. McNeil, *Anal. Chim. Acta*, 2006, **561**, 218-224.
33. P. Roychoudhury, B. McNeil and L. M. Harvey, *Anal. Chim. Acta*, 2007, **585**, 246-252.
34. J. Schenk, C. Viscasillas, I. W. Marison and U. von Stockar, *J. Biotechnol.*, 2008, **134**, 93-102.
35. J. Schenk, I. W. Marison and U. von Stockar, *J. Biotechnol.*, 2007, **128**, 344-353.
36. G. Mazarevica, J. Diewok, J. R. Baena, E. Rosenberg and B. Lendl, *Appl. Spectrosc.*, 2004, **58**, 804-810.
37. H. Kornmann, M. Rhiel, C. Cannizzaro, I. Marison and U. von Stockar, *Biotechnol. Bioeng.*, 2003, **82**, 702-709.
38. H. Kornmann, S. Valentinotti, P. Duboc, I. Marison and U. von Stockar, *J. Biotechnol.*, 2004, **113**, 231-245.
39. H. Kornmann, S. Valentinotti, I. Marison and U. von Stockar, *Biotechnol. Bioeng.*, 2004, **87**, 593-601.
40. M. H. Rhiel, M. I. Amrhein, I. W. Marison and U. von Stockar, *Anal. Chem.*, 2002, **74**, 5227-5236.
41. M. Rhiel, P. Ducommun, I. Bolzonella, I. Marison and U. von Stockar, *Biotechnol. Bioeng.*, 2002, **77**, 174-185.
42. D. P. Pollard, R. B. Buccino, N. C. Connors, T. K. Kirschner, R. O. Olewinski, K. S. Saini and P. S. Salmon, *Bioproc. Biosyst. Eng.*, 2001, **24**, 13-24.
43. J. Schenk, I. W. Marison and U. von Stockar, *Anal. Chim. Acta*, 2007, **591**, 132-140.

44. D. L. Doak and J. A. Phillips, *Biotechnol. Progr.*, 1999, **15**, 529-539.
45. R. Karoui, A. M. Mouazen, E. Dufour, R. Schoonheydt and J. De Baerdemaeker, *Eur. Food Res. Technol.*, 2006, **223**, 363-371.
46. T. I. Dearing, W. J. Thompson, C. E. Rechsteiner and B. J. Marquardt, *Appl. Spectrosc.*, 2011, **65**, 181-186.
47. F. Iñón, S. Garrigues and M. de la Guardia, *Anal Chim Acta*, 2006, **571**, 167 - 174.
48. M. Urbano Cuadrado, M. D. Luque de Castro, P. M. Pérez Juan and M. A. Gómez-Nieto, *Talanta*, 2005, **66**, 218-224.
49. D. Cozzolino, W. U. Cynkar, N. Shah and P. A. Smith, *Food Chem.*, 2011, **126**, 673-678.
50. S. Navea, A. de Juan and R. Tauler, *Anal. Chem.*, 2003, **75**, 5592-5601.

## 8 Conclusions and suggestions for future work

### 8.1 Conclusions

The aims set out at the start of this investigation, were to:

- Research the design, development and application of MIR probes for *in situ* process analysis.
- Study the use of calibration models for analyte prediction and specifically the use of calibration transfer algorithms for MIR analysis with *in situ* probes.
- Apply MIR spectrometry for the analysis of Scotch whisky including the determination of authenticity.
- Complete initial studies into the combined use of MIR and NIR *in situ* measurements for synergistic benefit in process analysis.

Many application areas are apparent for the potential use of in-line MIR or NIR spectrometry. Where some areas have already successfully implemented in-line analysis, other areas could see benefits from the implementation of in-line analysis. The literature survey indicated the potential of combined probes for in-line analysis: the combination of ATR MIR and transmission NIR spectrometry would be useful for the analysis of liquids, whereas, for solids and powder analysis a combination of MIR and NIR reflectance measurements may be beneficial. Application areas were found where currently manufactured probes, like the ATR MIR probes discussed in this thesis, could be used for *in situ* analysis to aid process monitoring and control. In addition, the potential scope for future developments of single or combined probes has been identified and could extend the product range for Fibre Photonics.

The main focus of the research discussed in this thesis was on the development and application of the ATR MIR probe for process analysis, therefore, an assessment of the performance of six ATR MIR probes was completed where design features had been altered between probes. The assessment highlighted differences in the absorbance of the spectra, the errors of prediction and the pathlength of the probes. Altering the size and geometry of the diamond crystal was established as a significant design feature, where the probe that incorporated changes in the geometry

and size of the diamond crystal (probe 3) had improved performance over the probe with original design features. Probe 3, which also incorporated the new fibre alignment and cone sealing, provided the best results when compared to the other probes tested. Another important design feature alteration was the use of modular components for the manufacture of the probes; during the study it was concluded that this change had maintained the performance of the probe, but in terms of manufacturing will provide a simpler manufacturing procedure that should provide more robust probes. The results obtained for the single fibre 2.7 mm o.d. ATR probe indicated the potential of this probe for the analysis of small sample volumes. The ATR MIR probes assessed, all produced good quality spectra and improvements were evident when comparing the results of more recently manufactured probes to those of the original design. Information regarding the development and improvement in ATR MIR probe manufacture can be used alongside potential application areas for in-line spectrometry to further develop and enhance the specifications of these probes.

Many examples of NIR calibration transfer exist in the literature; however, fewer examples of calibration transfer in MIR spectrometry are found. The research investigated the use of two well-known transfer algorithms and a newer procedure for the transfer of calibration models in MIR spectrometry. Transfers were completed where the spectrometer, probe or both had been changed and if no algorithm was used, significant errors were observed when the transfer was made. However, when implementing either of the established algorithms or the newer procedure, improvements were noticeable. Also highlighted in this study, was the potential to use calibration transfer algorithms when imitating multiplexing (between two similar probes) or imitating scale-up (between a smaller diameter probe and a larger diameter probe). In both examples all three transfer algorithms were able to transfer the calibration models successfully and reduce the errors of prediction when compared to the transfer when no algorithm was used. In the case of the newer procedure, SST, a scaling factor should be introduced when there are large differences between the spectra that are involved in the transfer. If the number of samples involved in the transfer were altered, both PDS and SST were shown to

produce good results; more variable results were observed for DS. SST provided an advantage over PDS in terms of simplicity of use. The successful use of the transfer algorithms in MIR spectrometry can aid its use for process analysis in many application areas and has indicated the benefits of using smaller diameter probes for use in scale-up.

One application area that was assessed with ATR MIR probes was the analysis of whisky; the research indicated the potential of ATR MIR spectrometry for the identification of counterfeit Scotch whiskies based on the determination of ethanol content and the spectra of dried residues of the samples. A study using the measurement of the spectra of the dried residues of cask samples has shown some scope as a procedure to gain a greater understanding of the impact of manufacturing variables on the generation of the colour of whisky. The second application area that was assessed was in the area of fermentation. The literature survey had indicated the potential use of a MIR-NIR combined probe; an initial study was completed to assess the use of NIR and MIR spectrometry for the analysis of the fermentation samples of a *Pichia pastoris* fermentation reaction. When specific regions were selected, the calibration models were able to predict the concentration of optical density, glycerol and ammonium. NIR spectrometry provided better results for the prediction of the optical density and ammonium, whereas, both NIR and MIR spectrometry produced comparable results for the prediction of glycerol. Potential benefits could arise from the combination of NIR and MIR spectrometry in the ability to analyse the three properties *in situ*, where MIR spectrometry is less susceptible to the effects from agitation than NIR spectrometry. For NIR spectrometry to monitor the ammonium concentration effectively, the *in situ* probe would be required to analyse in the region 2000 – 2500 nm. Fusing the NIR and MIR data together for the prediction of glycerol concentrations provided evidence that the NIR region helped to improve the MIR calibration in the fused model, while the MIR region did not degrade the NIR calibration. Examples where NIR and MIR spectrometry can provide alternative but complementary information about a process could provide further benefits when the two sets of data are fused together.

## 8.2 Suggestions for future work

The results of this research have indicated the potential of ATR MIR probes for a range of application areas and the potential benefits of a combined MIR-NIR probe. Further development and improvement of the ATR MIR probes to enhance the robustness and repeatability would be worthwhile. One way to achieve this would be to complete design of experiments on a wide range of the design features for the probe manufacture. This way, more design features can be investigated and a greater understanding of how each feature influences the performance of the probe can be ascertained. The results of a design of experiment approach to development should provide better and higher performance probes. A way to determine the repeatability of manufacture would be to manufacture multiple identical ATR MIR probes and compare the results. Further studies to test the robustness of Fibre Photonics probes are required if they are to be used in a range of application areas, as some areas require specific conditions. For example, for *in situ* fermentation analysis, the probe will have to undergo sterilisation which requires the probe to withstand specific temperatures and pressures. In terms of a combined MIR-NIR probe, development would be required to produce a single probe that can have both MIR and NIR optical fibres in place. From the research, for *in situ* liquid analysis ATR MIR and transmission NIR spectrometry appeared to be a suitable choice and, therefore, the probe would need to be able to incorporate an ATR crystal and transmission gap as well as two sets of optical fibres. This would require work in terms of the optical design to achieve the desired combination; if this is possible then performance testing would also be required of the developed probe.

In terms of applications, initial work has suggested that the measurement of the dried residue of cask whisky samples may be useful for the determination of the effect of manufacturing variables on the colour of the whisky. The effects determined thus far, appear to be very subtle and it is difficult to distinguish exactly how all the different factors are influencing the final colour; part of the reason was the limited sample set. Increasing the sample set to include samples with more of the factors would allow a more comprehensive design of experiments study to be carried out. In addition the determination of counterfeit samples was only carried out on blended samples that

would normally contain caramel; it would be useful to carry out an investigation with samples that do not ordinarily contain caramel and determine authenticity based on a spectral library. An on-going part of the counterfeit identification would also be to investigate a range of caramel samples from different manufacturers and establish any differences with the caramels used in this study.

MIR and NIR spectrometry have been shown in this research to predict the concentration of optical density, glycerol and ammonium for a fermentation reaction using off-line samples. The possible advantages of using a combination of MIR and NIR spectroscopy in a single probe have been discussed, however, further benefits may be realised through the combination of the data, as indicated with the initial study into the prediction of glycerol with fused MIR and NIR data. Further work is required to ascertain the accuracy of predictions of ammonium concentration using MIR data, as well as potentially investigating the use of fused MIR and NIR data for predictions of ammonium concentration. If this is successful, the next step would be to complete more fermentation reactions using *in situ* NIR and MIR probes, where models could then be built on multiple fermentations and used to predict other fermentation reactions that were not involved in the original model building. The learning from this work could be used to aid the development of a combined MIR-NIR probe.

## Publications and external presentations

### Publications

- **Detection of counterfeit Scotch whisky samples using mid-infrared spectrometry with an attenuated total reflectance probe incorporating polycrystalline silver halide fibres.**

A.C. McIntyre, M. L. Bilyk, A Nordon, G. Colquhoun and D. Littlejohn, *Analytica Chimica Acta*, 2011, 690, 228-233.

### External presentations

- **Transferability of calibration models for in-line MIR analysis with novel silver halide fibre probes.**

A. C. McIntyre, CPACT research day, University of Strathclyde, Glasgow, 2009

- **Assessing transferability of calibration models for in-line MIR analysis with novel silver halide fibre probes.**

A. C. McIntyre, CPACT research day, Newcastle University, Newcastle, 2009

- **Analysis of whisky samples using *in situ* MIR spectrometry.**

A. C. McIntyre, CPACT research day, Chemistry Innovation Centre, Runcorn, 2010

- **Improvements in MIR ATR probe technology for *in situ* process measurements.**

A. C. McIntyre, APACT 2010, Manchester, 2010

- ***In situ* monitoring of Scotch whisky using MIR spectrometry to detect counterfeit samples.**

A. C. McIntyre, RSC Younger Members Symposium, Manchester, 2010

- **Improvements in MIR ATR probe technology for *in situ* process measurements.**

A. C. McIntyre, Pitconn 2011, Atlanta, 2011

- **A comparison of calibration transfer algorithms for MIR analysis using *in situ* ATR immersion probes.**

A. C. McIntyre, EuroPACT 2011, Glasgow, 2011

- **Detection of counterfeit Scotch whisky samples using MIR spectrometry.**

A. C. McIntyre, SPIRIT meeting, St Andrews, 2011

## Appendices

**Appendix 4.1: Weights of acetone, ethanol and ethyl acetate present in each mixture.**

Mixture number	Weight of acetone (g)	Weight of ethanol (g)	Weight of ethyl acetate (g)	Total weight (g)
1 – calibration 1	0.00	19.72	0.00	19.72
2 – calibration 2	19.98	0.00	0.00	19.98
3 – calibration 3	0.00	0.00	19.23	19.23
4 – calibration 4	10.07	9.58	0.00	19.65
5 – calibration 5	9.54	0.00	9.61	19.15
6 – calibration 6	0.00	9.87	9.90	19.77
7 – calibration 7	6.46	6.41	6.05	18.92
8 – calibration 8	12.13	3.19	3.20	18.52
9 – calibration 9	3.20	11.70	2.90	17.80
10 – calibration 10	3.17	3.31	11.92	18.40
11 –test 1	1.00	13.93	1.53	16.46
12 –test 2	4.36	8.93	2.07	15.36
13 –test 3	8.64	6.56	5.15	20.35
14 –test 4	24.24	3.11	2.01	29.36
15 –test 5	13.68	2.00	13.20	28.88
16 –test 6	1.97	3.32	12.90	18.19

Example calculation of difference by weight approach used:

E.g. For mixture 1: Weight of ethanol = 19.72g

Weight of full vial + lid = 105.27g

Weight of empty vial + lid = 85.55g

→ **Weight of ethanol** = 19.72g

**Appendix 4.2: Determination of trendlines to calculate the molar absorptivity coefficient of acetone at eight selected wavenumbers**

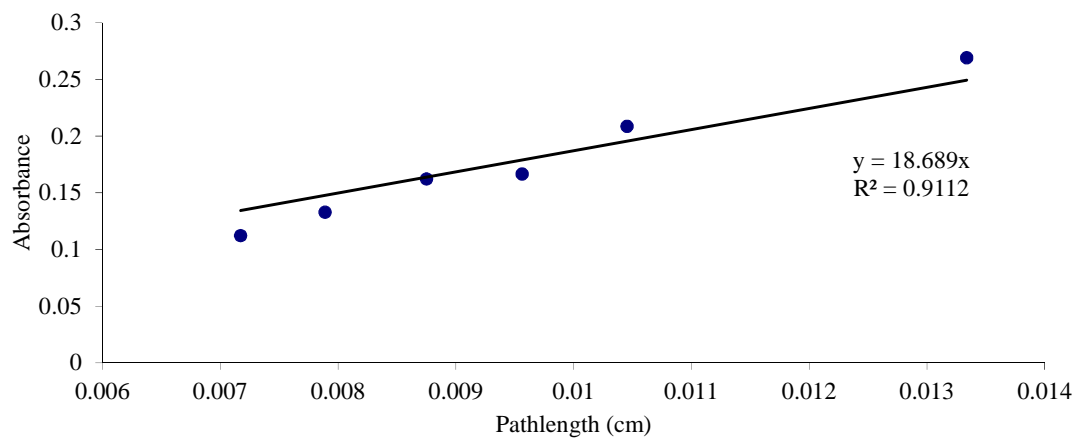


**Figure 4.22: Absorbance values for a peak at 787 cm<sup>-1</sup> acquired using the variable pathlength cell vs. the calculated pathlength of the cell. The trendline indicates the linear relationship and the equation of the line can be used to determine the molar absorptivity coefficient.**

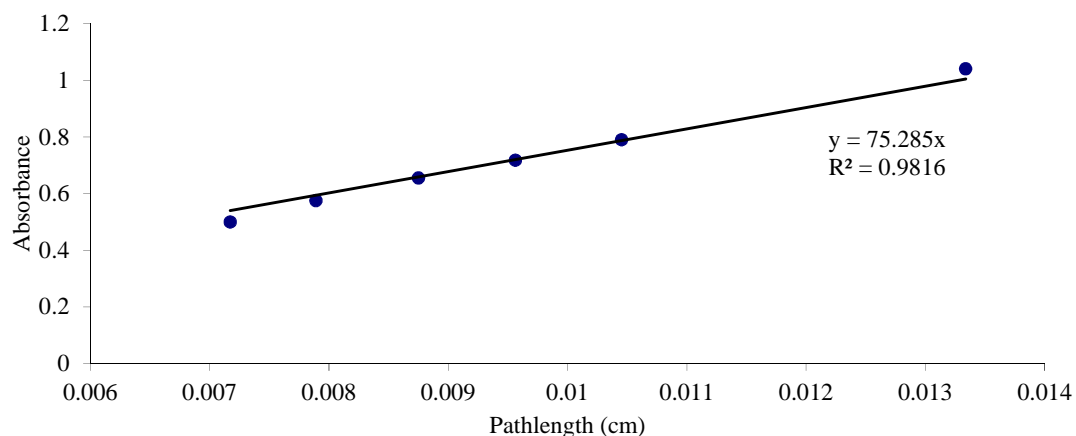


**Figure 4.23: Absorbance values for a peak at 903 cm<sup>-1</sup> acquired using the variable pathlength cell vs. the calculated pathlength of the cell. The trendline indicates the linear relationship and the equation of the line can be used to determine the molar absorptivity coefficient.**

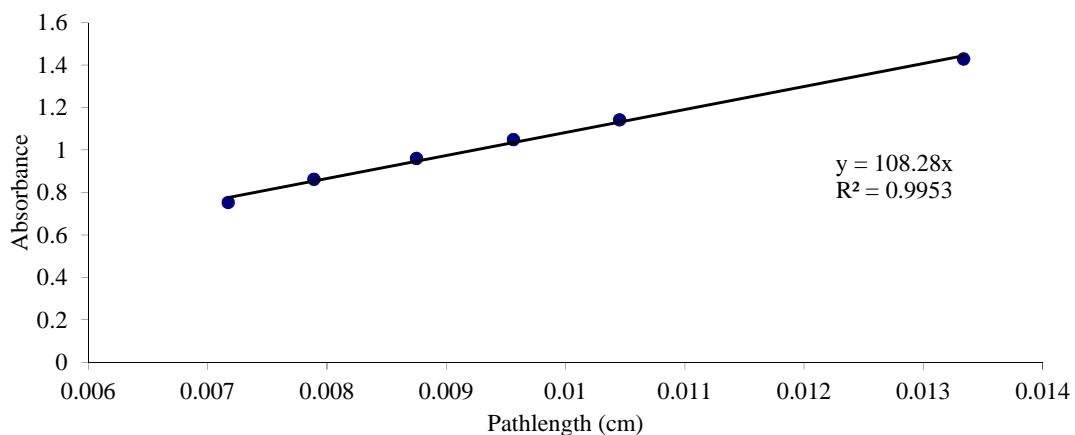


**Figure 4.24:** Absorbance values for a peak at  $1196\text{ cm}^{-1}$  acquired using the variable pathlength cell vs. the calculated pathlength of the cell. The trendline indicates the linear relationship and the equation of the line can be used to determine the molar absorptivity coefficient.

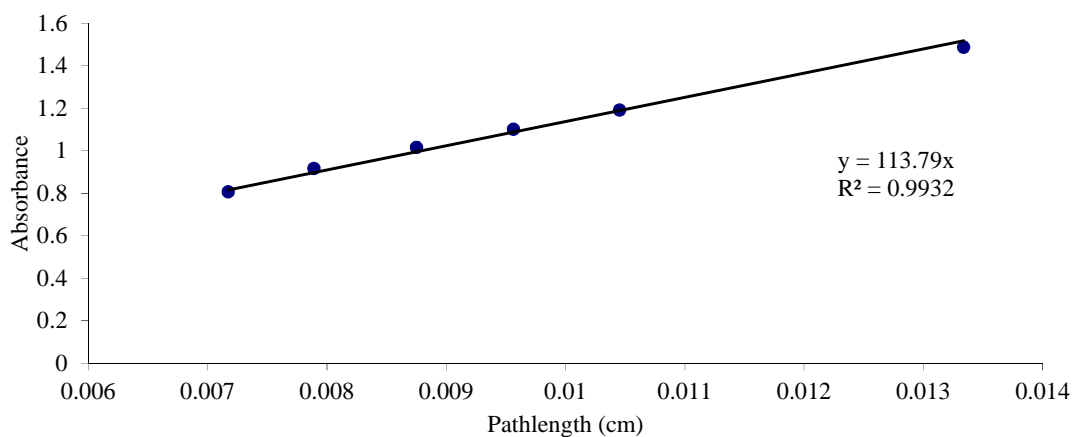


**Figure 4.25:** Absorbance values for a peak at  $1242\text{ cm}^{-1}$  acquired using the variable pathlength cell vs. the calculated pathlength of the cell. The trendline indicates the linear relationship and the equation of the line can be used to determine the molar absorptivity coefficient.

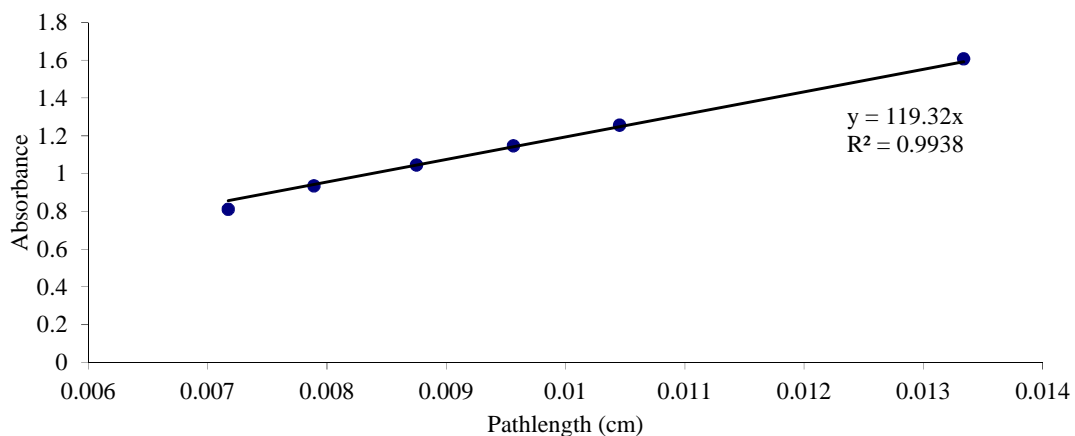


**Figure 4.26:** Absorbance values for a peak at  $1327\text{ cm}^{-1}$  acquired using the variable pathlength cell vs. the calculated pathlength of the cell. The trendline indicates the linear relationship and the equation of the line can be used to determine the molar absorptivity coefficient.

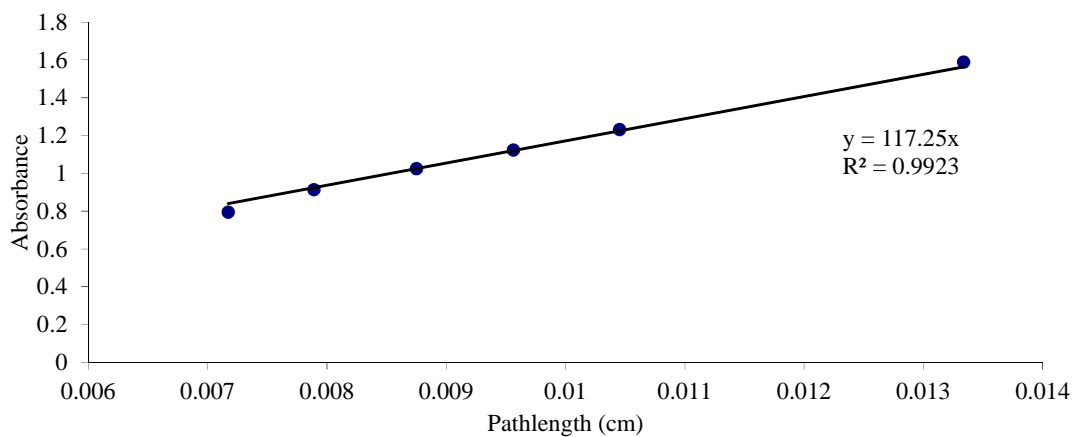


**Figure 4.27:** Absorbance values for a peak at  $1474\text{ cm}^{-1}$  acquired using the variable pathlength cell vs. the calculated pathlength of the cell. The trendline indicates the linear relationship and the equation of the line can be used to determine the molar absorptivity coefficient.

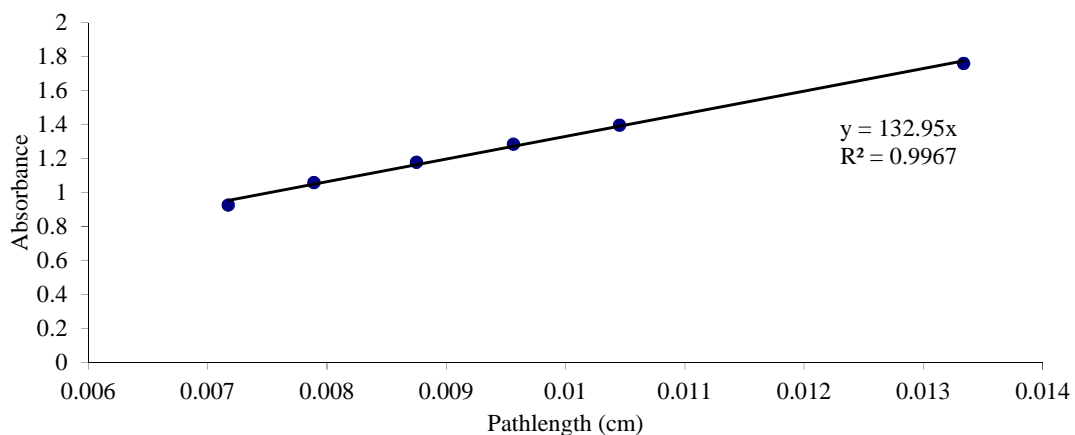


**Figure 4.28:** Absorbance values for a peak at  $1674\text{ cm}^{-1}$  acquired using the variable pathlength cell vs. the calculated pathlength of the cell. The trendline indicates the linear relationship and the equation of the line can be used to determine the molar absorptivity coefficient.

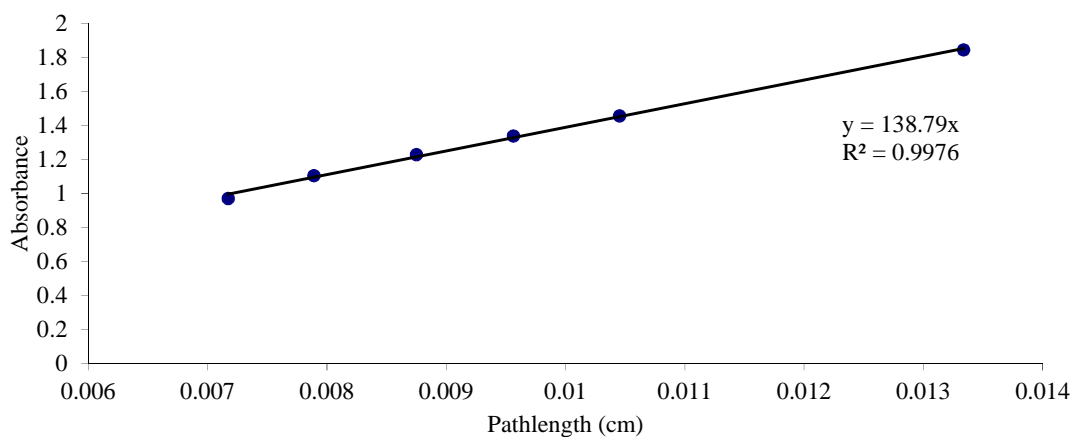


**Figure 4.29:** Absorbance values for a peak at  $1767\text{ cm}^{-1}$  acquired using the variable pathlength cell vs. the calculated pathlength of the cell. The trendline indicates the linear relationship and the equation of the line can be used to determine the molar absorptivity coefficient.

**Appendix 5.1: Weights of acetone, ethanol and ethyl acetate present in each mixture.**

Mixture number	Weight of acetone (g)	Weight of ethanol (g)	Weight of ethyl acetate (g)	Total weight (g)
1 – calibration 1	0.00	20.93	0.00	20.93
2 – calibration 2	19.24	0.00	0.00	19.24
3 – calibration 3	0.00	0.00	21.12	21.12
4 – calibration 4	8.07	8.07	0.00	16.14
5 – calibration 5	10.01	0.00	10.00	20.01
6 – calibration 6	0.00	10.00	10.06	20.06
7 – calibration 7	5.77	5.79	5.77	17.33
8 – calibration 8	11.64	3.09	3.01	17.74
9 – calibration 9	3.01	11.64	2.98	17.63
10 – calibration 10	3.00	3.01	11.64	17.65
11 –test 1	1.00	14.17	1.50	16.67
12 –test 2	4.00	9.38	2.00	15.38
13 –test 3	8.41	6.61	5.00	20.02
14 –test 4	23.71	2.87	1.99	28.57
15 –test 5	13.43	2.00	13.14	28.57
16 –test 6	2.00	3.28	12.90	18.18

Example calculation of difference by weight approach used:

$$\begin{aligned}
 \text{E.g. For mixture 1: Weight of ethanol} &= \underline{20.93\text{g}} \\
 \\ 
 \text{Weight of full vial + lid} &= 106.37\text{g} \\
 \text{Weight of empty vial + lid} &= \underline{85.44\text{g}} \\
 \rightarrow \text{Weight of ethanol} &= \underline{20.93\text{g}}
 \end{aligned}$$

Appendix 5.2: PDS window size determinations of acetone, ethanol and ethyl acetate for use in calibration transfers

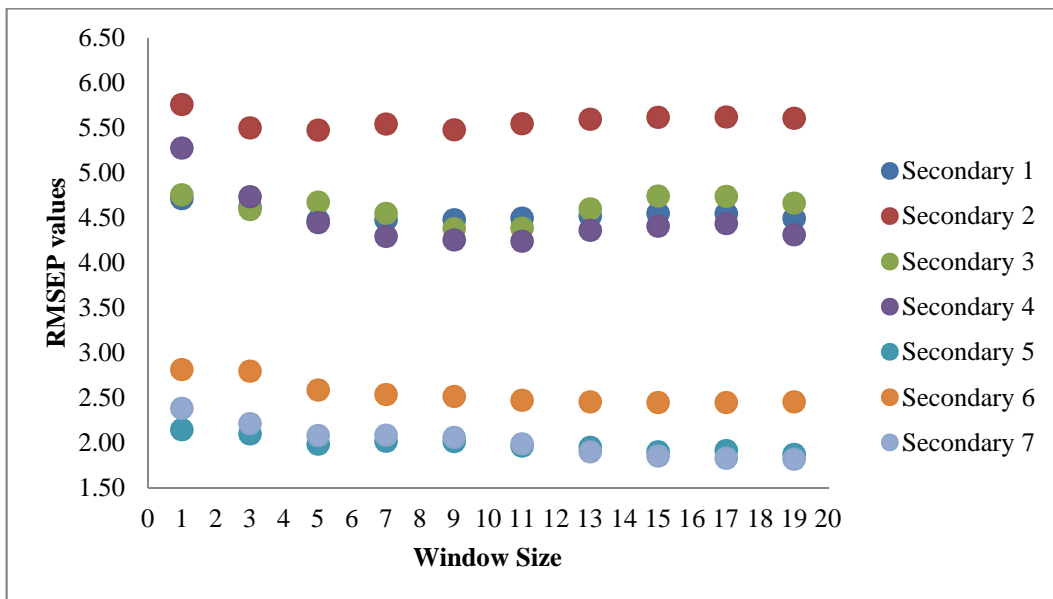


Figure 5.24: Plot of the mean RMSEP values for window sizes 1, 3, 5...19 for all models transferred to secondary instrument configurations for acetone.

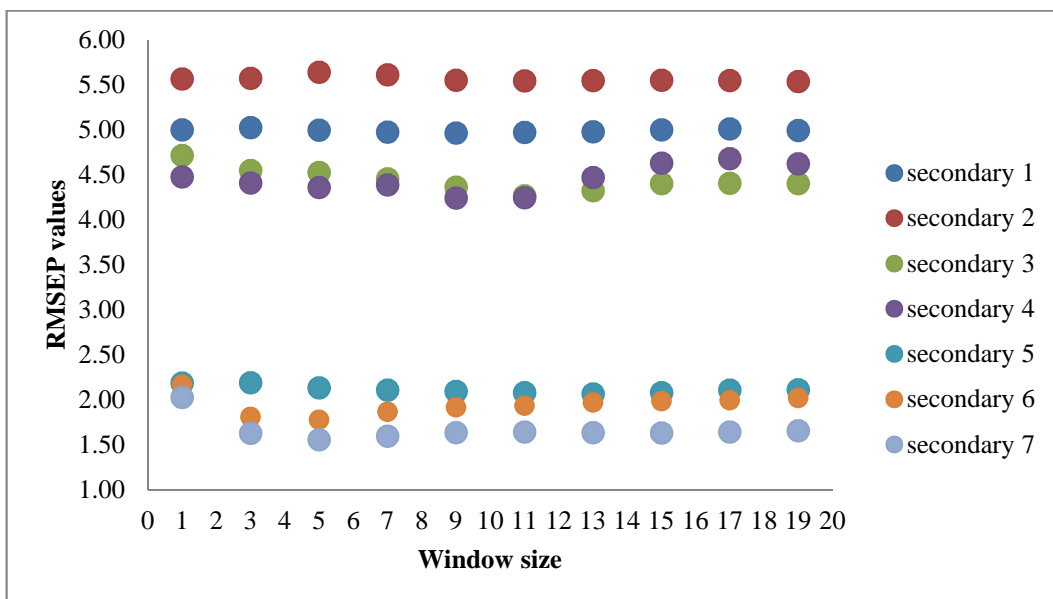


Figure 5.25: Plot of the mean RMSEP values for window sizes 1, 3, 5...19 for all models transferred to secondary instrument configurations for ethanol.

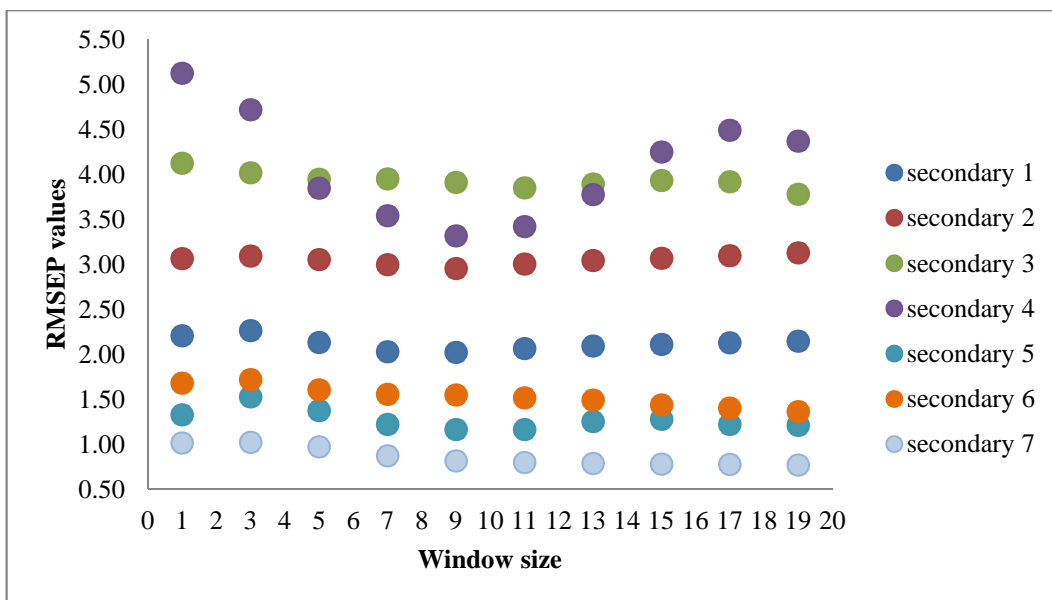


Figure 5.26: Plot of the mean RMSEP values for window sizes 1, 3, 5...19 for all models transferred to secondary instrument configurations for ethyl acetate.